NEW ROUTES TO FUNCTIONAL SILICONE ELASTOMERS THROUGH SULFUR CHEMISTRY

NEW ROUTES TO FUNCTIONAL SILICONE ELASTOMERS THROUGH SULFUR CHEMISTRY

By

SIJIA ZHENG,

M.Eng. (Zhejiang University, China) 2015

A Thesis

Submitted to the School of Graduate Studies

In Partial Fulfillment of the Requirements for the Degree of

Doctor of Philosophy

Doctor of Philosophy (2020), McMaster University (Chemistry), Hamilton, Ontario

TITLE:

New Routes to Functional Silicone Elastomers Through Sulfur Chemistry

AUTHOR: Sijia Zheng,

M. Eng. (Zhejiang University)

SUPERVISOR: Dr. Michael A. Brook

NUMBER OF PAGES: xxiv, 215

Abstract

Silicones elastomers are widely used all over the world due to their unusual properties when compared to their carbon-based counterparts. Synthetic methods for their synthesis are still quite limited and the traditional silicone products are not able to completely meet the requirement for modern materials. Silicone elastomers with customized structures and with higher levels of sustainability will be the research focus for the development of next generation materials.

The element sulfur and its functional groups are growing players in modern polymer and materials science, since sulfur reactions are exceptionally versatile. The incorporation of sulfur reactions into the design and preparation of silicone materials can lead to silicones with unique properties for various research interests.

Initial exploration was focused on the creation of general and simple methods for 3D printing silicone elastomers using thiol-ene chemistry. However, silicone inks suitable for 3D printing are still quite limited. Photo-initiated thiol-ene chemistry was proposed to design a rapid cure silicone ink for extrusion 3D printing. Unlike other radical reactions, the relatively oxygen insensitive thiol-ene was able to provide the necessary rapid reaction rate and build up the necessary viscosity for practical printing in less than 2 seconds in the presence of air. Various customized silicone structures with different moduli were obtained with a relative fast printing speed.

The use of thiol oxidation reactions in the synthesis of silicone elastomers is also demonstrated in this thesis. Reductive cleavage of the resulting disulfide bridge was successfully performed with the presence of hydrosilane and $B(C_6F_5)_3$ catalyst. Herein, a synthetic method to reversible silicone elastomers based on the disulfide linkage is described. This method could be extended to cleave the disulfide and polysulfide linkage in used automotive rubber materials. Various kinds of sulfur-cured rubbers were successfully devulcanized to polymeric oil. This simple and efficient method could potentially offer a solution for the huge amount of tire waste produced every year.

Finally, a new method for preparing thermoplastic silicone elastomers with ionic linkages is reported. A novel dicarboxylic acid-modified silicone was synthesized though thiol-Michael additions. The resulting ionic crosslinked networks were built though the neutralization between carboxylic and amino silicone. Thermoplastic silicone elastomers with unique viscoelastic behavior can be obtained. In summary, the thesis demonstrates that sulfur chemistry is an exceptional synthetic tool for the silicone chemist.

Acknowledgements

Now I look back from my 4 years of PhD study, I cannot express how grateful I am. I would not be where I am without all the unselfish support from my supervisors, group members, friends, family, McMaster University, and CSC Chinese Scholarship, and many others.

First and foremost, I would like to thank my supervisor, Dr. Michael A. Brook. I really appreciate the opportunity that Mike offered to work in his lab after my tough beginning in Canada. I feel really lucky to have had such a supportive supervisor. Mike is super enthusiastic for chemistry and really creative in research. He is always able to look at the positive side of unexpected results and guide projects to a good direction. It was very motivating and inspiring to be under his supervision. He encouraged me to walk outside my comfort zone and learn to be a better chemist. In addition, Mike taught me about Canadian life and culture. There are many good memories that I will not forget, no matter where I go in the future. Thank you for being there all the time.

I would like to express my sincere gratitude to my committee members: Dr. Ravi Selvaganapathy and Dr. Kalai Saravanamuttu, for their guidance and advice on my projects. I appreciate the time you both took to be on my committee and for the help provided for research.

I would like to thank Michael Zlatin for his excellent research work and his help in the silicone 3D printing project. Michael is a really creative person with great passion for research. We became close friends when we worked together on this project.

I would like to thank all of the Brook group members. We have had so much fun together, which made the lab time enjoyable. I would particularly like to say a big thanks to Mengchen who is really a close friend and was a reliable workmate over these years. Without her input, the tire project would not have been possible. Thank you to Dan for giving helpful suggestions to the projects and always being there when I need help. Thank you to Alyssa for being the elder sister and taking care of the whole group all over the years, and Robert and Cody for being good friends. Thank you to our postdocs Miguel, Akop, especially Shuai for really helpful guidance on research and all those undergraduates (Anthony, Harry, Adrien, Emily, Andrew, Daniel) for being really helpful and generous when I needed a hand.

To Stuart, James, Darryl, Eric, Dialia from Dr. Andronov's group, thank you for all the training on the equipment and for problem shooting.

Thank you to my parents for rising up with all the love and support. For all those years, you always believed in me and helped me to be the best version of myself. You encouraged me to pursue my dream and were supportive all the time. There were tough times, but I always know I have both of you standing at my back. It is a special time that Covid-19 spread all over the world. I am really sorry that I made both of you worry so much about me again. I will take good care of myself and please take care of yourselves for me.

我想特别感谢我的父母。你们给予我生命并养育我长大，成才。 你们一直相信我，鼓励我追求梦想。是你们的爱和支持让我在困难面前不曾退缩，勇往直前。在新冠疫情肆虐的这个特殊的时期，身在海外的我又让你们担心了。我的内心非常的愧疚。我会照顾好自己，健康的回到你们身边，也请你们千万要保重身体。

Finally, I would like to thank my boyfriend, Lingqi Huang. Thank you for your company during all my graduate studies. You are always understanding and patient when I was being negative. I am so lucky to have you in my life.

Table of Contents

Abstract iv
Acknowledgements vi
List of Tables xv
List of Figures xvi
List of Abbreviations and Symbols xxiii
1 Chapter 1: Introduction 1
1.1 Silicones 1
1.1.1 Si-O Bonds, Silicones, and Their Distinctive Properties 1
1.1.2 Traditional Preparative Methods in Silicone Chemistry 2
1.1.2.1 Traditional Synthesis Strategies for Silicone Fluids 2
1.1.2.2 Traditional Synthesis Strategies for Silicone Elastomers 4
1.1.3 Research Frontiers for Silicone Synthesis 7
1.1.4 Remaining Challenges and Opportunities 9
1.2 Sulfur Chemistry in the Organic World 10
1.2.1 Thiol-ene Radical Reactions 11
1.2.2 Thiol-Michael Additions 12
1.2.3 Thiol Oxidation 14
1.2.3.1 Disulfide Formation - Cross-linking 14
1.2.3.2 Other Oxidation States 14
1.2.4 Disulfide and Polysulfide Reduction 15
1.2.5 Other Relevant Sulfur Chemistry 16
1.3 Sulfur Chemistry in the Silicone World 17
1.3.1 Pioneering Studies on Small Molecule Silanes 17
1.3.2 Sulfur-Containing Silicone Fluids 19
1.3.3 Sulfur-Containing Silicones with Well-defined Structures 22
1.3.4 Sulfur-Containing Silicone Elastomers 23
1.4 Thesis Objectives 23

1.4.1 Silicone Inks for 3D Printing 24
1.4.2 Redox Responsive Silicone Elastomers..25
1.4.3 Thermoplastic Silicone Elastomers..26
1.5 References..27
2 Chapter 2: 3D Printable, Rapid Cure Silicone Elastomers Prepared using Thiol-ene "Click" Chemistry 34
2.1 Abstract 34
2.2 Introduction..35
2.3 Results and Discussion 40
2.3.1 Influence of Photoinitiator Concentration on Reaction Rate.........41
2.3.2 Influence of Oxygen Quenching Effect on Reaction Rate............41
2.3.3 Influence of Matching Photoinitiator Absorption to the UV Wavelength on Reaction Rate...43
2.3.4 Influence of Stoichiometric Ratio of SH and C=C on the Conversion of Functional Groups 45
2.3.5 Influence of Irradiation Time and UV Intensity on the Conversion of Functional Groups 45
2.3.6 Strategy of Adjusting Mechanical Properties 47
2.3.6.1 Influence of Cross-linker Functionality 47
2.3.6.2 Influence of Chain-extender 48
2.3.7 Highly Stretchable Formulation and Adhesion.............................51
2.3.8 Tolerance to Fumed Silica 52
2.3.9 Printed Structures..54
2.3.9.1 Demonstration of Extrusion Printing using Low Viscosity Inks ... .54
2.3.9.2 Printing of High Aspect Ratio Structures 55
2.3.9.3 Printing using Discontinuous Flow..56
2.3.9.4 Printing Overhanging Structures..57
2.3.9.5 Multi Ink Printing 58

2.4 Conclusions 61
2.5 Experimental Section 62
2.5.1 Materials 62
2.5.2 Methods...63
2.5.3 Synthesis of PDMS Thin Films 64
2.5.4 Synthesis of PDMS Elastomers 65
2.5.5 Preparation of Multi-moduli Materials 65
2.5.6 Preparation of UV Curable Thiol-ene Inks for 3D Printing 66
2.5.7 Printer Design 66
2.5.8 Printing of a Cube 68
2.5.9 Printing of a Cylinder...69
2.5.10 Printing of "McMaster" Sign 69
2.5.11 Printing of a Hemisphere 70
2.5.12 Printing of Multi-ink Cylinders 70
2.6 References..71
Supporting Information...73
3 Chapter 3: Reversible Redox Cross-linking of Thiopropylsilicones 78
3.1 Abstract 78
3.2 Introduction..79
3.3 Experimental Section 82
3.3.1 Materials 82
3.3.2 Methods...83
3.3.3 Oxidation of Dodecanethiol, a Model Compound 84
3.3.4 NaOCl Disulfide Oxidation 85
3.3.5 Reductive Cleavage of RS-SR 86
3.3.6 Silicone Elastomers, Foams and Films: General Procedures.........87
3.3.7 Cleavage of Oxidatively Cured Elastomers, Followed by Recrosslinking...88
3.3.8 Cleavage of Oxidatively Cured Silicone Foams 90

3.3.9 Surface Modification of S-S Crosslinked Silicone Elastomers 90
3.3.10 Freeze Drying and Rehydration of Foams 91
3.4 Results and Discussion 91
3.4.1 Model Reaction: Oxidation of 1-Dodecanethiol with NaOCl 91
3.4.2 Redox Elastomers: Oxidative Cure to Give Disulfide Linked Silicone Elastomers..92
3.4.3 Redox Elastomers: Reductive Cleavage of Silicone Elastomers with Hydrosilanes 93
3.4.4 Redox Foams: Oxidative Cure to Give Silicone Foams 95
3.4.5 Redox Foams: Cleavage of Silicone Foam with Hydrosilanes......96
3.4.6 Benefits of Overoxidation: Controlling Surface Hydrophilicity of Elastomers and Controlling Foam Structure...99
3.4.7 Rehydration of Foams...102
3.5 Conclusions...103
3.6 References...104
Supporting Information...108
4 Chapter 4: Dissolving Used Rubber Tires 115
4.1 Abstract...115
4.2 Introduction...116
4.3 Results and Discussion 119
4.3.1 Model Reductions of Dibenzyl Disulfide and Tetrasulfide 119
4.3.2 Reduction of Used Automotive Rubbers 120
4.4 Experimental...129
4.4.1 Materials 129
4.4.2 Methods..131
4.4.3 Preparation of Dibenzyl Tetrasulfide..135
4.4.4 Dibenzyl Disulfide Reduction using Bis(trimethylsiloxy)methylsilane ([SiH]/[SS]=2:1, Molar Ratio between Hydrosilane and Disulfide)...135

4.4.5 Titration of Disulfides to Establish Relative Reactivity of Functional Groups 136
4.4.6 Reduction of Rubbers: General Procedure 136
4.4.7 Reduction with Inexpensive Tetramethyldisiloxane M^HM^H........137
4.4.8 Desilylation of Product Polymeric Oils to Give 11 137
4.4.9 Crosslinking of Recovered Oils 138
4.4.9.1 Oxidative Coupling of Thiols Using Iodine............................138
4.4.9.2 Preparation of Toy Tire using a Peroxide Initiator (Figure 4.4) 138
4.5 Conclusions...142
4.6 References..143
Supporting Information...146
5 Chapter 5: Thermoplastic Silicone Elastomers Based on Gemini Ionic Crosslinks 167
5.1 Abstract..167
5.2 Introduction...168
5.3 Experimental Section...173
5.3.1 Materials 173
5.3.2 Methods..174
5.3.3 Synthesis of Gemini Acid (**G-COOH**) Silicones **G-COOH-14**, **G-COOH-4**, **G-COOH-2**...177
5.3.4 General Synthesis of Ionically Crosslinked Elastomers 178
5.3.5 Preparation of Samples for Self-healing Tensile Test at Elevated Temperatures..179
5.3.6 General Synthesis of Ionic Elastomer with SiO_2 Filler 180
5.3.7 General Synthesis of Hydrosilylation-cured Elastomers 180
5.4 Results and Discussion 182
Mechanical Properties - Products as a Function of NH_x/COOH Ratio 184
5.4.1.1 Gemini Acid + Mono Amine 1:1 Equivalent..........................184

5.4.1.2 Gemini Acid+ Gemini Amine 1:1 Equivalent 185
5.4.1.3 Gemini Acid + Gemini Amine at Different Ratios COOH/NH_x ... .186
5.4.1.4 Effect of Crosslink Density..190
5.4.2 Improving Mechanical Properties - Silica Fillers 192
5.4.3 Thermoplasticity 193
5.4.4 Thermal Stability 195
5.4.5 Viscoelastic Properties - Self-healing...197
5.4.6 Viscoelastic Properties - Time Dependent Mechanical Properties.... 201
5.5 Conclusions...203
5.6 References...205
Supporting Information...208
6 Chapter 6: General Conclusions...211

List of Tables

Chapter 2: 3D Printable, Rapid Cure Silicone Elastomers Prepared using Thiol-ene "Click" Chemistry

Table S2.1 Influence of catalyst concentration and oxygen inhibition on reaction time. 74
Table S2.2 Influence of and UV intensity and irradiation time on degree of cure.[a] 75
Table S2.3 Formulations for silicone elastomers with different modulus.[a] 76
Table S2.4 Reagents used to study the tolerance of fumed silica.[a] 77
Table S2.5 Optimized formulations for 3D printing inks.[a] 77

Chapter 3: Reversible Redox Cross-linking of Thiopropylsilicones

Table 3.1 Oxidation of 1-Dodecanethiol by NaOCl. 86
Table 3.2 Reduction[a] of didodecyl disulfide (RS-SR) by hydrosilanes. 87
Table 3.3 Preparation of disulfide-crosslinked silicone elastomers with different crosslink densities by oxidation with $PhI(OAc)_2$. 95
Table 3.4 Silicone foams and films by oxidation of thiopropylsilicone with NaOCl.[a] 97

Chapter 4: Dissolving Used Rubber Tires

Table 4.1 Constituents in rubber starting materials. 121
Table 4.2 Efficiency of reductive silylation of sulfur-crosslinked rubbers.[a] 123
Table 4.3 Depolymerization efficiency of organic elastomers by hydrosilanes.[a] 140
Table S4.1 Reactivity comparison using dibenzyl sulfide **1** and bis(trimethylsiloxy)methylsilane. 150
Table S4.2 Integration data used to plot Figure 4.2. 151
Table S4.3 Rubber components characterized by TGA profile. 154
Table S4.4 Decrosslinking of bulk rubber; effect of multiple repetitions. 160
Table S4.5 GPC data of recovered organic oil. 162
Table S4.6 Recrosslinking of recovered organic oil **8** with residual solid as reinforcing agent. .. 166

Chapter 5: Thermoplastic Silicone Elastomers Based on Gemini Ionic Crosslinks

Table 5.1 Formulations for ionic crosslinked silicone elastomers. 179
Table 5.2 Formulations for silica filled ionic crosslinked silicone elastomers and silica filled hydrosilylation cured control. 182
Table 5.3 Summary of mechanical properties of ionic crosslinked silicone elastomers. 193
Table 5.4 Self-healing ability of **G-COOH-14** + **G-NH$_x$-4** at 80 °C for various time periods. ... 201

List of Figures

Chapter 1: Introduction

Figure 1.1 Chemical structure of poly(dimethylsiloxane). 2
Figure 1.2 Conventional equilibrium preparation method for silicone fluids. 4
Figure 1.3 Strategies for synthesizing functionalized silicones. FG = functional groups. 4
Figure 1.4 Reaction schemes showing traditional methods for making silicone elastomers. (a) Pt-catalyzed hydrosilylation (b) Room temperature vulcanization (c) High temperature vulcanization. 5
Figure 1.5 Reaction schemes of Piers-Rubinsztajn reaction. 7
Figure 1.6 A reaction scheme showing use of the Piers-Rubinsztajn reaction to synthesize aryl-rich silicones. 8
Figure 1.7 Piers-Rubinsztajn reactions leading to either silicone foams or elastomers. 8
Figure 1.8 Synthesis of branched silicones starting from dendrons with alternating PR and hydrosilylation reactions.[41] 9
Figure 1.9 General thiol-ene polymerization reactions. 12
Figure 1.10 Mechanism for the base-catalyzed thiol-Michael addition.[46] 13
Figure 1.11 Stepwise oxidation of thiols. 15
Figure 1.12 Toolbox for all kinds of thiol-based reactions. 17
Figure 1.13 Reductive silylation of sulfur-based coupling agents by using hydrosiloxane $HSiMe(OSiMe_3)_2$. 19
Figure 1.14 Synthetic routes for pendant sulfide-modified silicone fluids. 20
Figure 1.15 Traditional synthetic route for thiol-functionalized silicone oil. 20
Figure 1.16 Synthetic routes for (a) thiol-modified cyclosiloxanes, (b) terminal sulfide-modified silicone fluids, (c) pendent sulfide-modified silicone fluids. 21
Figure 1.17 Synthetic routes for pendent sulfide-modified silicone fluid with well-defined structures under mild conditions. 22
Figure 1.18 Synthetic routes for well-defined, dendron-branched silicone surfactants. 22
Figure 1.19 Reaction scheme of crosslinking thiol-PDMS via dithioacetal linkages using aromatic aldehydes. 23

Chapter 2: 3D Printable, Rapid Cure Silicone Elastomers Prepared using Thiol-ene "Click" Chemistry

Figure 2.1 Pt-catalyzed hydrosilylation cure. 37

Figure 2.2 Silicone networks prepared by thiol-ene reaction. 38
Figure 2.3 Facile functionalization of PDMS elastomer surfaces using thiol-ene click chemistry. 39
Figure 2.4 Strategy of adjusting mechanical properties.. 40
Figure 2.5 Oxygen-scavenging mechanism of radicals. 42
Figure 2.6 Reaction time of thin films with different DHMP concentrations. 42
Figure 2.7 Reaction times of thin films with 5 mol% DHMP when different light sources were applied. 44
Figure 2.8 Reaction rates under various initiation systems. 44
Figure 2.9 Conversion of vinyl functional groups at different irradiation time............................... 46
Figure 2.10 Impact of UV intensity on the conversion of vinyl groups. 47
Figure 2.11 Crosslink density changes with different crosslinker. 48
Figure 2.12 (a) Young's modulus, and; (b) Shore OO hardness changes with an increase in the concentration of CL2 (SMS-992) in the formulation. 48
Figure 2.13 Crosslink density changes with the addition of chain-extender (SMS-022). 49
Figure 2.14 (a) Young's modulus, (b) Shore OO hardness changes with an increase in the concentration of chain-extender (SMS-022) in the formulation. 50
Figure 2.15 Deformation of different layers under tensile (a) and compression (b,c) force. 51
Figure 2.16 Snapshots of tensile test (a) 0% strain, (b) 600% strain, (c) after break, (d) stress-strain curve of multi-materials sample... 52
Figure 2.17 Optical properties of samples with different AEROSIL-150 concentration (a) 0 wt% (b) 5 wt%, (c) 10 wt%. (d) tensile test with different AEROSIL-150 concentrations. 53
Figure 2.18 (a) A cube generated during the printing process. (b) The coded path used for the print. (c) The printed cube. (d) Demonstration of the elasticity of the cube. (e) Fractured cube after compression test. 55
Figure 2.19 (a) A 50 layer helical cylinder object made from V21H ink (b) The toolpath for the print, with dimensions. (c) Z cross section of the cylinder, showing 50 layers merged together. (d) Print of text 'McMaster'. Each letter represents 30 layers of V31H ink. 57
Figure 2.20 (a) A hollow hemisphere was printed without use of support material; the rapid curing rate of the ink was enough to form the overhanging angles in place (the 90° cut was introduced for clarity). (b) The flexibility of the as printed hemisphere is demonstrated. (c,d) Non-stop printing with ink changes; V35H is red and V31H is blue. (e) Silicone parts printed with three different inks. 59
Figure 2.21 Illustration of the 3D printer. (a) Full view of the printer. (b) CAD model of the printhead consisting of the 3 ink reservoirs, attached to a common extrusion needle using a 3-way junction. (c) A zoom into the printing area, showing the arrangement of the lightguide tips, shadow mask, needle,

and the resulting shadow pattern. A UV lamp (Omnicure S1000, vendor) along with two light guides (positioned 4 cm away from the tip and at ~45° to the substrate) provided the illumination (~100 W in the 300-400 nm wavelength) to initiate crosslinking of the extruded material. 67

Figure 2.23 (a) The 'McMaster' sign printed in silicone elastomer. (b) The gcode illustration; printing moves are in green, while rapid non-printing moves are in red. The rapid moves are absent from the resulting print. 69

Chapter 3: Reversible Redox Cross-linking of Thiopropylsilicones

Figure 3.1 (a) Thiol oxidation and disulfide reduction with dodecanethiol/disulfide. (b) Preparation of elastomers using an organic soluble ($PhI(OAc)_2$) oxidant and silicone foam by using aqueous oxidants (NaOCl). (c) Using overoxidation to control hydrophilicity of the surface or bulk material. 94

Figure 3.2 (a) Silicone elastomer was swelled in toluene before reduction. (b) Reaction mixture after 30 minutes. (c) Recovered oil after solvents were evaporated. (d) Re-crosslinked silicone elastomers. Silicone foams prepared by oxidizing thiopropylsilicone oils with 1.2 equiv. of NaOCl solution, aqueous fraction in the foam (e) 24 wt%; (f) 52 wt%; (g) 70 wt%. (h) Disulfide-linked silicone foams swollen in toluene. (i) Reaction mixture after 30 minutes. (j) Recovered oil after solvents were evaporated. (k) Recrosslinked silicone foam. 98

Figure 3.3 Contact angle of silicone foams prepared with different concentration of bleach. (a) SH/NaOCl=1/0.6; (b) SH/NaOCl=1/1.2; (c) SH/NaOCl=1/1.8; (d) SH/NaOCl=1/3.6; (e) SH/NaOCl=1/4.8; (f) SH/NaOCl=1/6.9. Oxidative surface modification of disulfide-linked silicone elastomer. (g) Unmodified disulfide elastomer. Table 3.3, Entry 3. (h) After soaking in a concentrated NaOCl solution (1.85mmol/ml) for 5 days... 100

Figure 3.4 Microscope photos of silicone foams (a) SH/NaOCl=1/0.6; (b) SH/NaOCl=1/1.2; (c) SH/NaOCl=1/1.8; (d) SH/NaOCl=1/3.6; (e) SH/NaOCl=1/4.8; (f) SH/NaOCl=1/6.9; the x axis for the inset is the diameter of the pore size (0-240 μm); the y axis for the inset is the count number of the pores (0-90). Size bar = 200 μm. (g) Silicone gel created from hypochlorite and thiopropylsilicones. (h) Silicone foam after freeze drying. (i) Rehydration of the dry silicone foam with colored water. (j) The hydrated foam after 24h. The blue food coloring dye in the water solution was bleached by the residual NaOCl trapped in the foam. 101

Figure S 3.1 ^1H NMR of (a) 1-dodecanethiol, (b) dodecyl sulfide product from oxidation of dodecanethiol, and (c) dodecyl sulfonate (in $CDCl_3$ and DMSO-d_6, respectively)....................... 110

Figure S3.2 ^1H NMR of disulfide products (in $CDCl_3$). It is noted that a small amount of thiosulfonate (RSO_2SR)[38] and sulfonyl chloride (RSO_2Cl)[39] intermediates (> 3.0 ppm) were observed when excess oxidant was applied. 111

Figure S3.3 Hydrolysis of S-Si bonds in disilylation process. 112

Figure S3.4 ^{1}H NMR spectrum before (a) and after (b) treating sodium 1-decanesulfonate with 10 equiv. pentamethyldisiloxane and $B(C_6F_5)_3$. The identical spectra before and after reaction indicated no reaction occurred during this process. 112
Figure S3.5 ^{1}H NMR spectrum of silicone foam prepared with 0.6 equivalent NaOCl. The foam was crushed into small pieces and swelled in $CDCl_3$ to obtain as ^{1}H NMR spectrum. 113
Figure S3.6 ^{1}H NMR spectrum of thiopropylsilicone starting materials SMS 042, 4-6% SH (blue), recovered oil from first reduction reaction of silicone elastomer (red), and recovered oil from the reduction of the elastomer formed after the first iteration (green).. 114
Figure S3.7 ^{1}H NMR spectrum of thiopropyl silicone starting material SMS 042, 4-6% SH (blue), recovered oil from reduction of bleach cure foam reaction (red). 114

Chapter 4: Dissolving Used Rubber Tires

Figure 4.1 Selected examples of $B(C_6F_5)_3$-catalyzed reduction by SiH groups. (a) carbonyl reduction to silyl ethers; (b) silyl ether reduction to alkanes (Piers-Rubinsztajn); (c) aromatic thioacetal cleavage to alkanes; (d) disulfide cleavage to silyl thio ethers (this work); (e) reduction of thiols to silyl thio ethers; (f) silyl thiol ether formation from oligosulfides, and, (g) Si-S cleavage using acid or fluoride catalysis. 118
Figure 4.2 (a) Disulfide conversion in benzyl disulfide system versus [SiH]/[SS] using $MD^{H}M$. (b) Polysulfide conversion in benzyl tetrasulfide system versus [SiH]/[SSSS] using $MD^{H}M$............ 120
Figure 4.3 (a) Section of snow tire tread cross-section, unreacted. (b) reductive dispersion using **7** and 10wt% BCF after 6 days. (c) metal wires that self-affixed to the magnetic stir bar. (d) Shrunken sections after reaction. (e) Inorganic and unreacted rubber constituents isolated by gravity filtration. (f) Product silyl-protected thiolated organic oils **8** in toluene (56% yield; note: the recovered oil may be a darker color, depending on starting material and the specific reaction (Figure S4.7). (g) Reductive silylation (a→ d,e,f). (h) Cleavage of SiS bonds. (i) Oxidative coupling produces elastomers crosslinked by disulfides. (j) Radicals form elastomers from alkene-containing oils. Steps i and j can optionally use recovered inorganic constituents as reinforcing agents in the elastomers. 126
Figure 4.4 (a) The right front tire was removed from a toy car. (b) A silicone mold of the tire. (c) Organic oil **8** was prepared by reduction of truck tire tread (Sailun, IR/NR) with hydrosilane **7**. (d) Silicone mold filled with 0.707g **8** + 1wt% BPO + 0.3010g residual solid. (e) New tire after curing. (f) Tire replacement. (g) The residual solid during the preparation of **8** could be included in the pre-elastomer formulation. (h) Close up showing: i) the original tire, ii) tire made without additional inorganic excipients **13**, and iii) tire including inorganic excipients. 129
Figure 4.5 (a-c) A commercial snow tire was cut into (d) sidewall and tread sections using a reciprocating saw with blade designed for cutting metal. (e) tread 1.200 × 1.519 × 1.125 cm. (f)

sidewall cut into 1.595 × 1.427 × 0.6096 cm. These samples were subjected to 'bulk reduction' of their as-cut shape. (g) For other reductions, the rubbers were chopped into fine pieces after cooling with liquid nitrogen and (h) powdered using coffee grinder (KitchenAid). 131

Figure S4.1 Benzyl disulfide reaction with MD^HM monitored by ^1H NMR (during the titration, small quantities of solvent remained in the sample; peaks at1.5 and 2.3 ppm reflect the presence of water and toluene, respectively.). 151

Figure S4.2 Benzyl tetrasulfide reaction with MD^HM monitored by ^1H NMR 152

Figure S4.3 (a) Sailun Truck tread 2. (b) Sectioning the external, road contacting section with a reciprocating saw to give Truck tread 2. 152

Figure S4.4 Particle size of ground rubber (inner tube) crumb. 153

Figure S4.5 The ^{13}C HR-MAS NMR of different rubber samples. 154

Figure S4.6 The thermogravimetric analysis curves (a) and differential thermal analysis curves (b) of different rubber samples. 154

Figure S4.7 Sequence of conversion of starting rubber samples to organic oils and residual powers (shown for inner tube rubber). Note: the turbidity of the recovered oil can vary depending on batch and on starting material; oil on the right is from a batch of car snow tire tread. 156

Figure S4.8 Visible differences in the reaction processes as a function of reduction efficiency. . 156

Figure S4.9 Determination of organic polymer fraction using TGA, shown for the inner tube.... 157

Figure S4.10 Thermogravimetric analysis (TGA) of powder (red) or coupon (blue) inner tube after reduction. 157

Figure S4.11 Thermogravimetric analysis (TGA) of different rubber samples. Before (black line) and after reduction (red line). 158

Figure S4.12 Thermogravimetric analysis (TGA) of (a) tread (snow tire) and (b) Side wall (snow tire). Original starting bulk rubber (black, Figure 4.3a), residual bulk rubber (Figure 4.3d) after reduction (blue), and residual powder (Figure 4.3e) collected after reduction (red). 159

Figure S4.13 Thermogravimetric analysis (TGA) of (a) inner tube and (b) truck tread-1 (right) samples with different scales (small = 300 mg; large = 2000 mg). 159

Figure S4.14 Thermogravimetric analysis (TGA) of (a) truck tread samples with (red) or without (black) Soxhlet extraction. (b) Crumb-2 sample after multiple reduction steps. 161

Figure S4.15 ^1H NMR of recovered organic liquids. 162

Figure S4.16 GPC data of recovered organic oil with two molecular populations. 163

Figure S4.17 Inner tube reduction after 18 h at 100 °C with different hydrosilanes. (a) $Me_3Si(OSiMeH)_nSiMe_3$ **9**; (b) $HMe_2SiOSiMe_2H$ **10**. 163

Figure S4.18 Time lapse photos of rubber reduction and dissolution. 164

Figure S4.19 Shrinkage of bulk rubber after 1 reduction cycle (a) snow tire tread; (b) snow tire sidewall; (c) bulk rubber bicycle tire. 165
Figure S4.20 ^1H NMR showing loss of silicone groups from the organic polymers after utilizing TBAF. 165
Figure S4.21 (a) The crosslinked elastomer **16** formed by iodine reoxidation of thiols in **8**. (b) The picture of 0.1 g **17**, swollen in 10 ml hexane after 1h sonication. 166

Chapter 5: Thermoplastic Silicone Elastomers Based on Gemini Ionic Crosslinks

Figure 5.1 Preparation of Gemini acid silicones using thiol-Michael additions and then ionic crosslinked silicone elastomers. 185
Figure 5.2 Rheology curve for **G-COOH-2** + **M-NH$_2$-4**, COOH/NH$_x$ =1:1. 185
Figure 5.3 Different type of linkages could exist in the network when acid is in excess: (a) Gemini linkages with sol carboxysilicones, (b) single ionic linkages; or base is in excess: (c) Gemini linkages with sol aminoalkylsilicones, (d) single ionic linkages. 187
Figure 5.4 Rheology curve as a factor of temperature. (a) **G-COOH-2** + **G-NH$_x$-4**, COOH:NH$_x$ =2:1, (b) **G-COOH-2** + **G-NH$_x$-4**, COOH:NH$_x$ =1:2. 189
Figure 5.5 Young's modulus of **G-COOH-2** + **G-NH$_x$-14** series (black) and **G-COOH-2** + **G-NH$_x$-4** series (gray). 190
Figure 5.6 Tensile curves for PDMS elastomers with covalent linkages (hydrosilylation cure control, solid lines) and ionically linked elastomers (dashed lines). Different amounts of silica fillers (Aerosil-150) were added. The tensile speed for ionic elastomers and hydrosilylation cure elastomers were 500 mm/min and 10mm min^{-1}, respectively. 192
Figure 5.7 Rheology curve as a factor of temperature. (**G-COOH-2** + **G-NH$_x$-4**, COOH/NH$_x$ =1:1). 194
Figure 5.8 Pictures showing thermoplasticity. (a) **G-COOH-2** + **G-NH$_X$-14** elastomer was crashed into small pieces (b) The elastomer crumbs were remolded to give a new elastomer (the 90° lines on the elastomer were from a wrinkle from the Teflon sheet lined on the mold, not a crack). 195
Figure 5.9 (a) Stress-strain curves for **G-COOH-14** + **G-NH$_x$-4** elastomer stretched at 10 mm/min, 100 mm/min, and 500 mm/min. The sample could not extended to break at 10mm/min speed, since the length was beyond the test limit of the instrument. (b) Schematic behavior of ionic silicone elastomer under different stretching rate. (c) TGA curves of **G-COOH-14** oil, ionic crosslinked elastomer **G-COOH-14** + **G-NH$_x$-4**, COOH:NH$_x$=1:1 elastomer. 197
Figure 5.10 Optical microscopic images of a cut healed at room temperature. (a) **G-COOH-2** + **G-NH$_x$-4** (b) **G-COOH-4** + **G-NH$_x$-4** (c) **G-COOH-14** + **G-NH$_x$-4**. 200
Figure S5.1 FT-IR spectra of **G-COOH-2** (black), **G-COOH-4** (rad), **G-COOH-14** (blue). 208

Figure S5.2 Viscosity of thioalkylsilicone oil with different thiol concentrations and maleic acid-modified silicone oil with different maleic acid graft densities..209
Figure S5.3 Tensile curves with different COOH/NH_x. **G-COOH-14** + **G-NH_x-4** series. 209
Figure S5.4 Optical microscopic images of a scratch on **G-COOH-14** + **G-NH_x-4** healed at room temperature for 7 days. 210

Chapter 6: General Conclusions

Figure 6.1 Thesis scope of using sulfur chemistry to make silicone materials..............................215

List of Abbreviations and Symbols

BCF	Tris(pentafluorophenyl)borane
BD	Butadiene rubber
BPO	Benzoyl peroxide
CQ	Camphorquinone
cSt	Centistokes
D_3	Hexamethylcyclotrisiloxane
D_4	Octamethylcyclotetrasiloxane
D_5	Decamethylcyclopentasiloxane
DHMP	2-Hydroxy-2-methyl-propiophenone
DSC	Differential scanning calorimetry
DTA	Differential thermal analysis
EDB	Ethyl 4-(dimethylamino) benzoate
EPDM	Ethylene propylene diene terpolymer
FT-IR	Fourier-transform infrared spectroscopy
G’	Storage modulus (elastic modulus)
G’’	Loss modulus (viscous modulus)
GC-MS	Gas chromatography - mass spectrometry
LC-MS	Liquid chromatography - mass spectrometry
GPC	Gel permeation chromatography
NR	Natural rubber
NMR	Nuclear magnetic resonance

MW	Molecular weight
IIR	Isobutene isoprene
IR	Isoprene rubber
TBAF	Tetrabutylammonium fluoride trihydrate
TGA	Thermogravimetric analysis
Tg	Glass - transition temperature
TPO-L	2,4,6-trimethylbenzoylphenyl phosphinate
PDI	Polydispersity index
PDMS	Polydimethylsiloxane
Pt	Platinum
Psi	Pound force per square inch
THF	Tetrahydrofuran
UV	Ultraviolet

1 Chapter 1: Introduction

1.1 Silicones

1.1.1 Si-O Bonds, Silicones, and Their Distinctive Properties

Silicones, originally discovered in the 1920's by Kipping,[1] have become irreplaceable polymer materials that are used all over the world. Their extensive applications range from daily necessities, such as seals for kitchen appliances, wire coatings, bath or car sealants[2] to high end products like implantable devices, contact lenses, sealants for aerospace, etc.[3-5] Billions of kilograms of silicones are produced and sold in the market every year. The popularity of the silicone materials comes from their unique properties that cannot be achieved by carbon-based competitor.[6]

Silicone's unique features originate from their chemical structures. Silicone polymers are based on repeating units of -RR'SiO-; the most commonly used, commercial silicone is referred to as poly(dimethylsiloxane) (PDMS) as shown in Figure 1.1.[7] The bond energy of the siloxane bond (Si-O) is 549 kJ/mol while the C-C bond strength is, comparatively, only 334 kJ/mol.[8] As a result, siloxane bonds show better heat and chemical stability than C-C bonds; silicone rubber shows far better performance than organic polymers in terms of heat stability.[9] In the absence of acid or base, the degradation of silicone is not observed below 350 °C.[10] In addition, the strong but flexible Si-O-Si bond give silicones special weatherability. Silicone rubber is quite stable under exposure to rain and UV light.[11] The Si-O-Si bond is quite flexible due to larger bond lengths and bond angles, when compared to carbon-based polymers. The *C-C-C* bond length is 1.54 Å with the bond angle of 109°, while *Si-O*-Si has a bond length of 1.63 Å and a bond angle is around 145°;[12-13] the bending and torsional force constants are very low. As a consequence, the glass transition temperature (Tg) of silicone is low (~ -120 °C)[14] and provides excellent resistance to cold temperatures. At low temperatures (e.g., even at -20 °C), organic rubbers turn brittle while silicones can remain elastic. Moreover, the methyl groups on the PDMS back bone are able to rotate freely and shield the Si-O chain. This characteristic gives silicone unique interfacial behavior such as water repellency.[15] Some other intrinsic properties of silicone such as excellent gas and vapor permeability have also been investigated[16] and an example for relevant applications is contact lenses.[17-18]

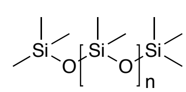

Figure 1.1 Chemical structure of poly(dimethylsiloxane).

1.1.2 Traditional Preparative Methods in Silicone Chemistry

Although silicones are widely used in industry, the chemical processes used in silicone chemistry are still rather limited.

1.1.2.1 Traditional Synthesis Strategies for Silicone Fluids

The conventional way of making silicone oil involves an acid or base-catalyzed equilibration reaction with octamethylcyclotetrasiloxane (D_4) (Figure 1.2).[19] The molecular weight is controlled by the stoichiometry of end capping groups (disiloxane, MM) to -Si-O- units. Although this reaction is very easy to perform, there are several disadvantages. As an equilibration reaction, the polydispersity of the product is high and, in addition, about 15% of cyclic starting materials remain after reaction because of the ring chain equilibrium.[20]

Another, less commonly used method to prepare silicone oil is through a kinetically controlled mechanism. An anionic polymerization process is normally initiated by an anionic initiator (e.g., butyllithium). The ring-opening polymerization of hexamethylcyclotrisiloxane (D_3) leads to silicones with narrow dispersity.[21] As with most other anionic polymerization methods, the reaction requires a clean system and must be performed under an inert atmosphere, since the propagating anion is easily quenched by impurities.[22] When doing silicone chemistry, as we can see from the preparation methods, one chemical property that one must pay special attention to is the sensitivity of silicones to acid as well as base. Under strong acidic or basic conditions, the silicone backbone will depolymerize.

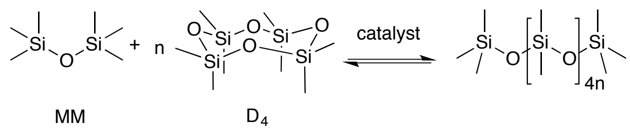

Figure 1.2 Conventional equilibrium preparation method for silicone fluids.

Silicone oils that bear functional groups are normally made by one of two strategies. First, as shown in Figure 1.3a, instead of using unfunctionalized D_4 in an equilibration process, a functional group-substituted D_4 can be used (e.g., D_4^H). The substitution degree of the final product may be controlled by the ratio of functionalized/unfunctionalized cyclic starting materials. The other common strategy used to make functional silicones uses the hydrosilylation reaction.[23] Methylhydrosiloxanes are readily available starting materials. By reacting Si-H with a C=C group that also holds the target organic functional group, silicone polymers with interesting chemical structure can be prepared and then used for further manipulation (Figure 1.3b).

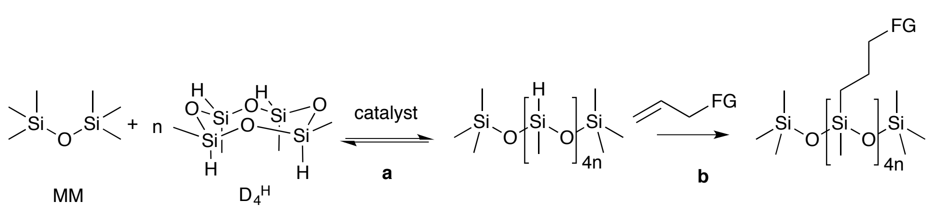

Figure 1.3 Strategies for synthesizing functionalized silicones. FG = functional groups.

1.1.2.2 Traditional Synthesis Strategies for Silicone Elastomers

There are three traditional methods to cure silicone fluids into elastomers.[24-26] (1) Pt-cure hydrosilylation (Figure 1.4a): In this case, hydrosilylation is promoted between Si-H and vinyl silicones by Speier's catalyst or Karstedt's catalyst. (2) Room temperature vulcanization (RTV) (Figure 1.4b): The reaction proceeds by reacting alkoxy-functional silanes with silanol-containing silicones. The catalysts include acids, bases, organtin or titanium-based catalysts. Ambient moisture is always used as co-catalyst for these processes. (3) High temperature vulcanization (HTV) (Figure 1.4c): This process occurs though radical pathways using radical initiators (e.g., peroxides).

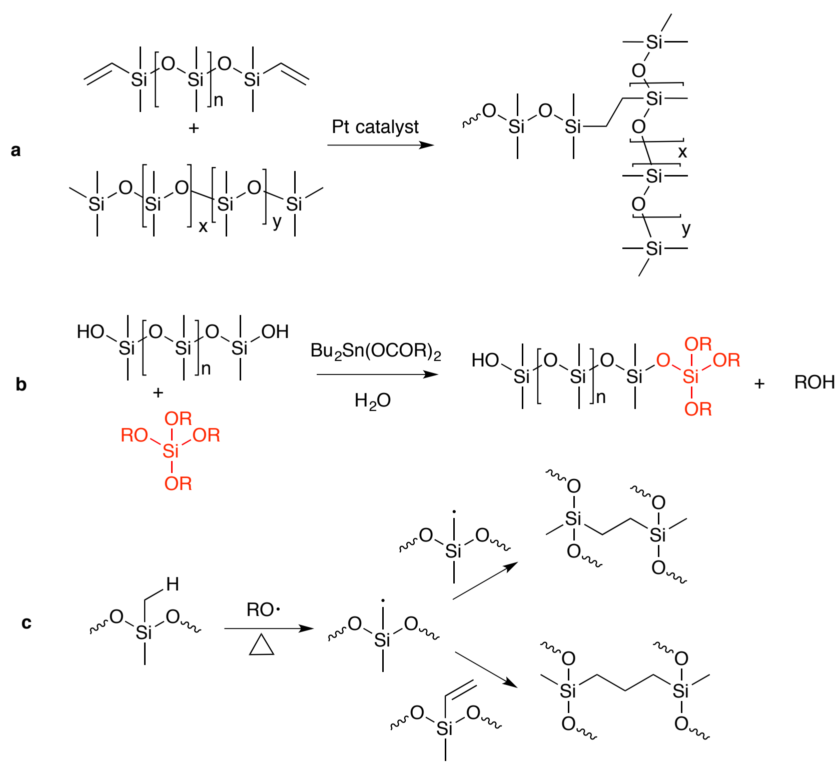

Figure 1.4 Reaction schemes showing traditional methods for making silicone elastomers. (a) Pt-catalyzed hydrosilylation (b) Room temperature vulcanization (c) High temperature vulcanization.

The hydrosilylation/addition reaction is considered to be the gold standard for silicone elastomer preparation and is the commonly used chemistry for commercial silicone kits sold by various venders. Among them, Sylgard 184 from Dow is a silicone elastomer that is used extensively in academic and industrial fields.[27-28] In addition to the ability to easily control the reaction, the product elastomers are considered safe for humans and are used as health care products with confidence. However, a disadvantage is that the process involves platinum catalyst. Since platinum is readily coordinates with nucleophiles (e.g., S, N ligands), attempts to use this chemistry in systems that contain sulfur and/or amine groups may fail.[25, 29] Moreover, residual platinum remains trapped in the material, which can cause the material to yellow over time.

Room temperature vulcanization (RTV) silicone is also widely used.[30-32] The reaction is catalyzed by an organotin catalyst, which is considered as toxic.[33] Alternative catalysts have proven elusive. Therefore, these products are commonly used in the area that does not have direct contact with human (e.g., bathtub sealant, sealant in automobile industry).

High temperature vulcanization (HTV) involves a curing process initiated by a radical initiator. Radicals can abstract a H from the methyl groups of dimethylsilicones to produce $SiCH_2^{\bullet}$ and two $SiCH_2^{\bullet}$ can couple together to produce a two-carbon bridge. With the vinyl silicones, $SiCH_2^{\bullet}$ is able to add across the double bond, resulting a 3-carbon bridge. Reactions undertaken also in the presence of vinylsilicones can occur at a lower temperature. HTV silicone are designed for the processing methods and equipment of the rubber industry. The vulcanization of the HTV silicones is usually carried out in unpressurized hot air ovens.[34] In a more recent example of elastomer formation that does not require a catalyst, Si-H functionalized silicones could be cured into elastomers in air at 250 °C though a radical mechanism (first step: RR'R''SiH + O_2 + MeSi-silicone → RR'R''SiO-CH_2Si-silicone + oxygen species).[24]

1.1.3 Research Frontiers for Silicone Synthesis

The Piers-Rubinsztajn reaction (PR) is a novel method to make silicone fluids and elastomers. This reaction involved a alkoxysilane and hydrosilane.[35] The mechanism involves coordination of Si-H groups with the catalyst $B(C_6F_5)_3$, followed by nucleophilic attack at Si, and concomitant formation of a siloxane bond, releasing an alkane byproduct. This reaction was first reported by Piers and co-workers[36] and Rubinsztajn did pioneering work to use this reaction to make linear silicone polymers (Figure 1.5).[37] In our lab, extensive research has been done to explore the potential application of PR reactions in the silicone field.[19]

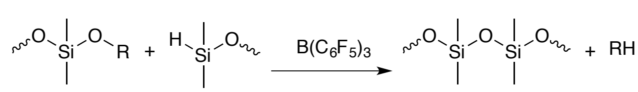

Figure 1.5 Reaction schemes of Piers-Rubinsztajn reaction.

PR reactions were used as an alternative method to incorporate interesting functional groups onto silicone backbones. Aryl-rich silicones are, historically, hard to make due to their unusual properties. The equilibrium between arylsilicone cyclics/linear polymers lies to the cyclic side. Therefore, it is not a perfect way to make silicones with high aryl content though traditional equilibration reactions. An alternative method was proposed by Schneider et al.[38] By reacting Si-H silicone with aryl phenyl ethers though a PR reaction, aryl-rich silicones were successfully synthesized (Figure 1.6). Similarly, natural products with phenyl ethers (e.g., eugenol) could also be a good source for silicone oils bearing phenyl groups.[39]

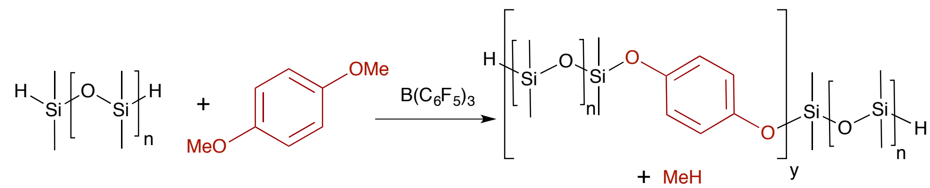

Figure 1.6 A reaction scheme showing use of the Piers-Rubinsztajn reaction to synthesize aryl-rich silicones.

Low density silicone foams may be made through PR reactions, as the byproduct of PR reaction is an alkane that can act as a blowing agent. The foam morphology is readily controlled by optimizing the reaction cure rate vs bubble formation rate. When solvents were added to the system to reduce the viscosity, bubble-free elastomers could be produced, as shown in Figure 1.7.[19, 40]

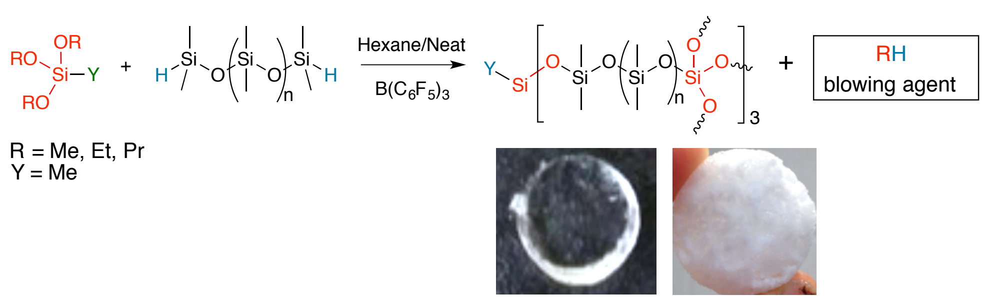

Figure 1.7 Piers-Rubinsztajn reactions leading to either silicone foams or elastomers.

The PR reaction has also been used as a versatile method to synthesize silicone molecules with well-defined 3D structures. By alternating the use of the hydrosilylation and PR reactions, dendrimeric silicones with different 3D structures were synthesized (Figure 1.8).[41] Since the topic is beyond the scope of this thesis, further details will not be provided.

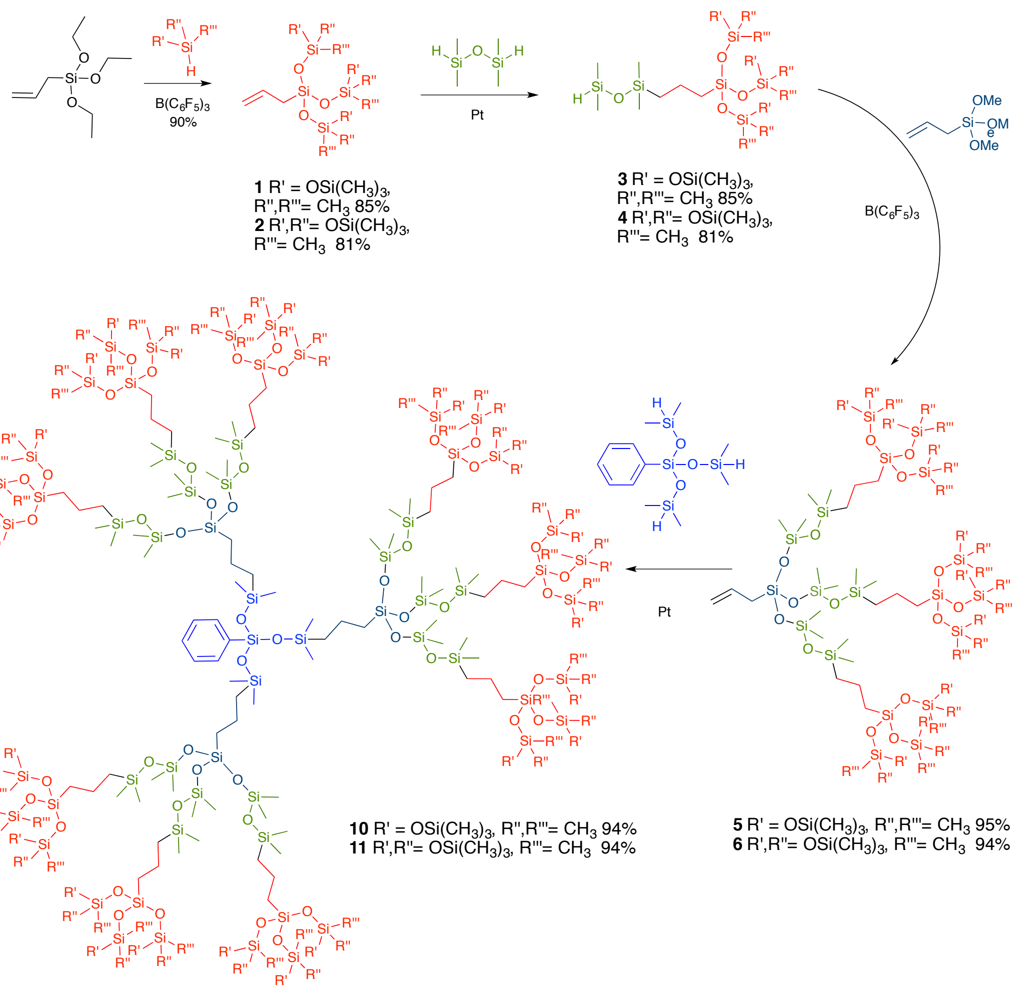

Figure 1.8 Synthesis of branched silicones starting from dendrons with alternating PR and hydrosilylation reactions.[41]

1.1.4 Remaining Challenges and Opportunities

As has been described above, the strategies used to prepare silicone fluids and elastomers are rather limited and, all too often, the classical reactions have restrictions or drawbacks that hold back their further development. For example, both RTV and hydrosilylation reactions involve metal catalysts that can be toxic (tin), or sensitive to S, N, H_2O, and expensive (platinum); HTV requires high temperatures. The PR reaction produces gas as a byproduct and a lot of manipulation in formulation is therefore necessary when the target is a bubble free elastomer.

In this thesis, I have examined the possibility of combining traditional organic chemistry with the silicone world. In principle, the world of organic chemistry can be used, at least in part, as a toolbox for further modification of silicone polymers. Special interest was given to sulfur-based chemistry, since sulfur has a broad organic chemistry and its reactivity can be adjusted by manipulating its oxidation/valence state. Various sulfur-based reactions are summarized in the following section.

1.2 Sulfur Chemistry in the Organic World

Sulfur and its functional groups are playing an increasingly important role in synthesis, polymerizations, and polymer modifications.[42-44] This is due to the variety of sulfur reactions available, versatile reactivity of sulfur-based functional groups, as well as many other benefits, such as high efficiency processes under mild conditions.

Although sulfur chemistry is a well-established field, many sulfur reactions have only been recognized and exploited within polymer chemistry in the last 10 years;

the utility of sulfur has potential in all science and engineering fields (chemical, biological, physical, materials and engineering, etc.). Pioneering studies of sulfur-containing reactions has been previously summarized in various in-depth reviews.[45-47] In particular, Mutlu et al.[42] provides an overview of the development of sulfur reactions used in the last 5 years; a book was recently written exploring sulfur-based reactions and their successful applications in a wide range of topics.[48]

In this thesis, we are exploring the possibility of using some of those sulfur reactions in the silicone world. Research spanning sulfur reactions including thiol-ene, thiol-Michael addition, thiol oxidation, and disulfide and polysulfide reduction cleavage are all well studied. We propose their utilization with silicones in applications ranging from silicone 3D printing, silicone elastomer with reversible crosslinks, and synthetic rubber recycling.

1.2.1 Thiol-ene Radical Reactions

Thiol-ene reactions are addition reactions that occur between molecules possessing alkenes and thiols, using a radical chain mechanism Figure 1.9. Typically, thiol-ene reactions are initiated by light, thermal initiators (e.g., peroxides AIBN), or other systems that generate radicals; commonly used initiation system and their efficiencies were well studied by Uygun et al.[49] The reaction of enes and thiols was first observed in 1905[50] and; in the 1930s, the radical mechanism was first proposed.[51] However, commercial applications for thiol-ene polymers were not developed until the very recent decades due to dominant commercial acrylate systems. In 1990s, due to the toxicological concerns over acrylate monomers, the thiol-ene reaction was examined with renewed interest.[52]

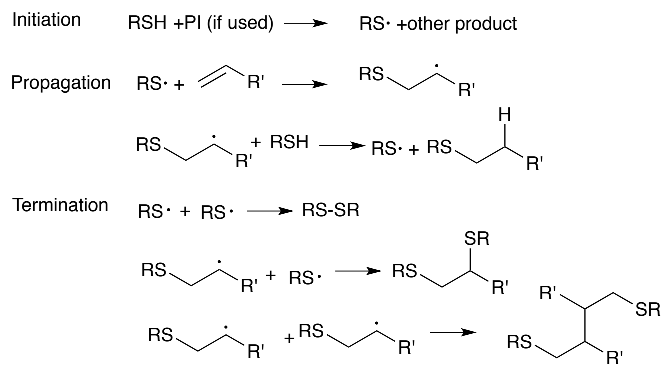

Figure 1.9 General thiol-ene polymerization reactions.

Thiol-ene reactions exhibit characteristics that address the drawbacks of most photopolymerization systems. Thiol-ene radical reactions are easy to perform, occur rapidly in high yields, are relatively tolerant to oxygen, and exhibit few or no side products.[53] These unique properties led to continued interest and development in thiol-ene radial chemistry. Followed by the first review published in 1993, the potential application of using thiol-ene in various materials science has been continuously explored as summarized in several reviews,[53-54] indicating the resurgence of overall interest in thiol-ene radical chemistry.

1.2.2 Thiol-Michael Additions

A reaction analogous to the thiol-ene radical reaction involves ionic addition of thiols to electron deficient C=C double bonds (Figure 1.10). This process is normally initiated by base (e.g., triethylamine, imidazole) or a nucleophile (e.g., trialkylphosphine). The accepted mechanism for thiol-Michael additions is shown in Figure 1.10. A thiolate is generated by base abstraction. The nucleophilic thiolate anion then attacks the electrophilic C=C, resulting in the formation of a stabilized carbanion. Proton abstraction yields the thiol-Michael product. Thiol-Michael reactions are typically cleaner, with fewer by-product, when compared to normal radical pathways.[55] Besides, for certain alkenes, such as acrylates, the thiol-Michael is more selective than thiol-ene radical reactions, since the homopolymerization of acrylates would occur competitively under radical conditions.[53]

Figure 1.10 Mechanism for the base-catalyzed thiol-Michael addition.[46]

As was discussed above, the nature of the thiol-ene reaction provides for an interesting scenario: the separate utilization of both electron-rich enes (radical), and electron-poor enes (Michael addition). That is, use of thiol-radical and thiol-Michael addition reactions may be considered to be a complementary strategy for linking various thiol compounds with very useful and readily available organic substrates containing double bond(s).

1.2.3 Thiol Oxidation

1.2.3.1 Disulfide Formation - Cross-linking

The oxidative coupling reaction of thiols that generates disulfide products has been recognized since the 1940s. Such chemistry is commonly seen in nature through the disulfide bonds between cysteine moieties that act to stabilize protein structures. The reactions usually take place in the presence various kinds of oxidation reagents, such as oxygen, iodine, hydrogen peroxides,[56] sodium hypochlorite,[57] and dimethyl sulfoxide,[58] and, in vivo, glutathione.[59]

Use of the disulfide bond in materials research is attractive because of its reversibility in response to diverse stimuli, including light or heat, redox conditions, thiol nucleophiles, etc. Because of the dynamic properties of the disulfide bond, materials with disulfide linkages have been used as self-healing,[60] adaptable materials.[61] In particular, polymer hydrogels based on this functional group are potential candidates for biomedical applications (e.g., drug delivery) as they may undergo programmed degradation using redox conditions, for example, with glutathione.

1.2.3.2 Other Oxidation States

The oxidation of thiols can afford many products, including disulfides (RSSR), sulfenic (RSOH), sulfinic (RSO_2H), and sulfonic (RSO_3H) products; full oxidation leads eventually to sulfates.[56] The oxidation of thiols usually proceeds in a stepwise fashion, generating a disulfide product initially, then on to sulfinic acids, etc., and finally sulfonic acid Figure 1.11. Strong powerful oxidants or vigorous conditions carry a desired disulfide through processes b,c to a sulfonic acid, the final product of oxidation (Figure 1.11).

$$2RSH \xrightarrow{a} RSSR \xrightarrow{b} \text{Intermediates} \xrightarrow{c} 2RSO_3H$$

Figure 1.11 Stepwise oxidation of thiols.

However, among the oxidation products, some are so reactive that their existence is only putative, for example, sulfenic acid. As noted in a recently published review,[62] these oxidation reactions are common reactions, but have historically been very difficult to study.

1.2.4 Disulfide and Polysulfide Reduction

Many materials contain S-S bonds, both natural materials (e.g., proteins) and synthetic polymers (e.g., natural and synthetic rubbers). As mentioned above, since S-S bonds are redox responsive, highly polarizable and present dynamic covalent property. A literature survey[43] shows there is a continuously growing interest in introducing high SS content into polymers for various research targets. In the following section, we will discuss the cleavage of disulfide and polysulfide bonds by reduction methods.

Disulfides are normally quite easy to reduce to thiols. The traditional reducing reagents to cleave -S-S- bonds are thiols, metal sulfides,[63] $LiAlH_4$,[64] or phosphines.[65] Disulfides can also be cleaved by amines,[66] yielding thiols. More recently, as the part of developments in biochemistry, other reducing agents have come to be used. Among them dithiothreitol – Cleland's reagent - is a mild and widely used reagent. The application of some other reagents like mercaptoethanol and thioglycolic acid have also been seen.[67-68]

As with oxidation reactions, reducing agents must be selected for a specific scenario. For example, $LiAlH_4$ is a strong reducing agent that is able to reduce bond disulfides and polysulfides. For example, for systems with $-NO_2$ groups, $LiAlH_4$ would not be a good choice since it will reduce nitro group to NH_2 as well.[69] A more selective reducing agent is required in that situation.

1.2.5 Other Relevant Sulfur Chemistry

We note that there are many useful sulfur-based reactions and an exhaustive examination of the chemistry goes beyond the framework of the present thesis. For example, there are still many other useful thiol-based reactions (Figure 1.12): thiol-alkynes reactions though radical chemistry, thiol-isocyanate reactions, thiol-S_N2 ring opening of epoxides, and thiol S_N2 nucleophilic substitution with halogens, etc., that could be exploited. In sum, efficient sulfur reactions open all kinds of potential applications for the preparation of small and polymeric molecules, for materials, and for surface modification.[46, 53, 70-71]

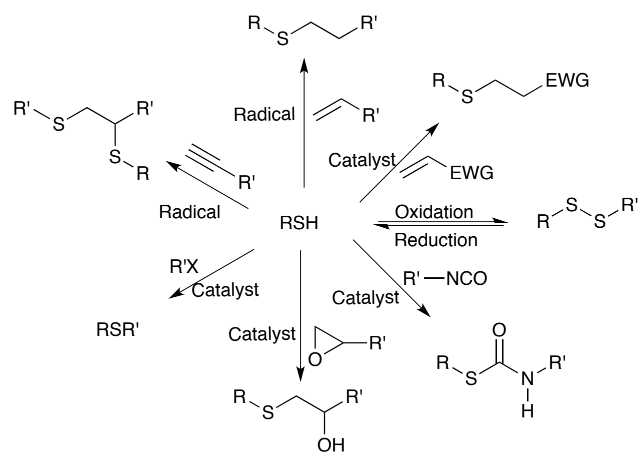

Figure 1.12 Toolbox for all kinds of thiol-based reactions.

1.3 Sulfur Chemistry in the Silicone World

As discussed above, sulfur-based chemistry is not new, but its application in organic, materials and polymer chemistry has undergone a resurgence in the last decades. Likewise, the application of the sulfur reaction in organosilicon chemistry has been relatively minimal as well.

1.3.1 Pioneering Studies on Small Molecule Silanes

Early studies using sulfur chemistry in organosilicon chemistry start around the 1950s. Burkhard demonstrated their work of reacting vinyltrimethylsilane and allylsilanes through thiol-ene reactions with yields ranging from 18-63%.[72] The Si-C bond was not affected by the presence of sulfur. Their work with thiols involved molecules that also contained functional groups like (COOH or COOR), which shows the tolerance of the reaction to potentially sensitive groups. Muller and Kunze did the first mechanistic study of thiol-ene reactions in silicone polymers in

1996.[73] The reactivity of various C=C bond (vinyl, vinyloxy, allyl, norbornenyl, etc.) under radical photopolymerization conditions with thiosilicone oils was investigated.

Bis(trimethylsilyl) sulfide (TMS-S-TMS) has been widely used in synthesis as a reducing agent, sulfur transfer agent, and silylating reagent.[74] The reagent is prepared by reacting trimethylsilyl chloride with sodium sulfide.[75] Bis(trimethylsilyl) sulfide can transform alcohols, acid, and amines into their silylated counterparts.[76] Those transformations show the affinity of silicon for oxygen.[8] The compound is exceptionally unstable towards hydrolysis.[75]

A model study of the reduction of commercial sulfur-silane coupling agents by hydrosilanes in the presence of $B(C_6F_5)_3$ was recently performed by our group member Mengchen Liao.[77] It was observed that when the thiol coupling agent $(EtO)_3Si(CH_2)_3SH$ **1** was titrated with 1 equivalent of $HSiMe(OSiMe_3)_2$ **4**, SH groups reacted faster than SiOEt, leading first to the silyl thioether **6** and eventually, with the excess of hydrosilane, all alkoxy groups reacted though the Piers-Rubinsztajn pathway. Analogous outcomes were observed when the reductions were repeated with analogous disulfide **2** or tetrasulfide coupling agents **3**. With the addition of $HSiMe(OSiMe_3)_2$, S-S bonds were preferentially cleaved over the Si-OEt groups (thus, relative reaction rates are S-H > S-S > Si-OR). Complex mixtures resulted until excess reducing agent was added, at which point the identical product **7** was formed from all three sulfur-silane coupling agents (Figure 1.13).

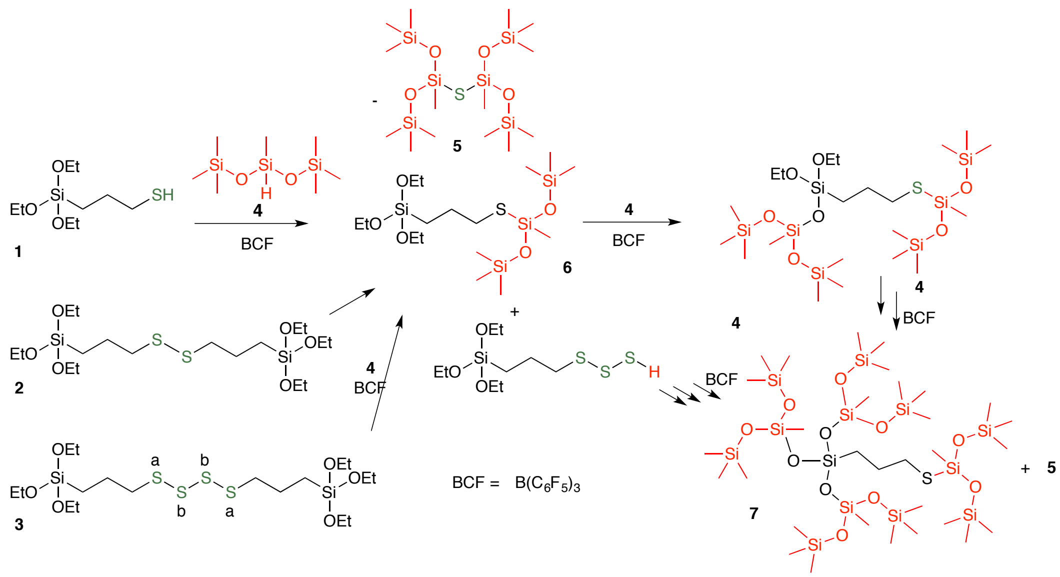

Figure 1.13 Reductive silylation of sulfur-based coupling agents by using hydrosiloxane $HSiMe(OSiMe_3)_2$.

1.3.2 Sulfur-Containing Silicone Fluids

Apart from use of the reaction for small molecules, the first attempt to use thiol-ene reactions in silicone polymers was not reported until the late 1990s. Sulfur-containing siloxane copolymers with organic sulfide pendent groups attracted early research interest, since these groups undergo interesting chemical transformations. Besides, since sulfur atoms have strong affinity for metal ions, sulfur-containing siloxane copolymers could be good candidates for selective sorbents, membranes, or metal adhesives. In 1996, pendent sulfide silicones were successfully synthesized by Chojnowski using a two-step strategy (Figure 1.14).[78] The cyclic siloxane (D_2D^{vinyl}) readily reacted with thiols, followed by the ring opening polymerization to generate sulfide-modified silicone oil. Alternatively, the cyclic siloxane (D_2D^{vinyl}) could be polymerized first and then the thiol-ene could be used to modify the side chain of vinyl-containing silicone. The desired sulfide derivatives were successfully made by both synthetic routes.

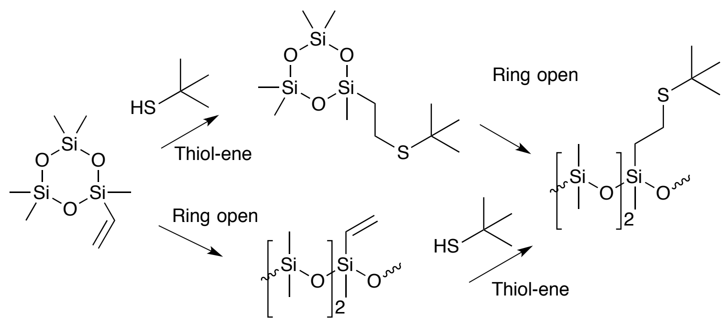

Figure 1.14 Synthetic routes for pendant sulfide-modified silicone fluids.

Polysiloxanes with thiol functional groups could be used as starting materials subject to further modification using organic synthesis, since thiol groups can react with almost all kinds of vinyl compounds via thiol-ene or thiol-Michael reactions. That is, various kinds of functional groups could be attached to thiol-functionalized polysiloxanes through a vinyl linkage for different research interests. The traditional way of synthesizing polysiloxanes with pendent thiol groups involves the acid-catalyzed hydrolysis reaction of thiodialkyloxysilanes with D_4 or dialkyloxysilanes (Figure 1.15).

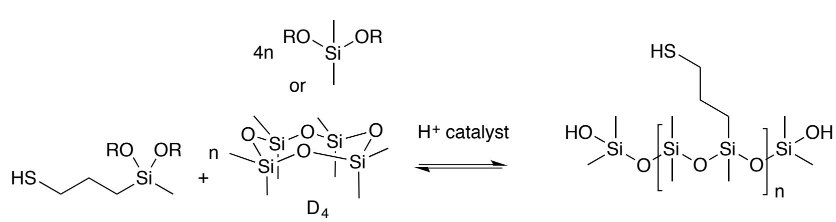

Figure 1.15 Traditional synthetic route for thiol-functionalized silicone oil.

The drawbacks of the traditional approach are, first, the molecular weight of the product is relatively low and, second, polysiloxanes with terminal thiol groups cannot be prepared. Perju[79] demonstrated a synthetic strategy for making thiol-modified cyclosiloxanes, and pendant and telechelic thiol silicones. When cyclic siloxane (D^{vinyl}_4) reacts with thioacetic acid via UV radical thiol-ene reaction, the resulting thioester is able to be reduced to thiol with $LiAlH_4$ (Figure 1.16).[80] In their work, it was also shown that, by using the same strategy, both pendant and telechelic thiol silicones could be synthesized starting from pendant and telechelic vinyl silicones.

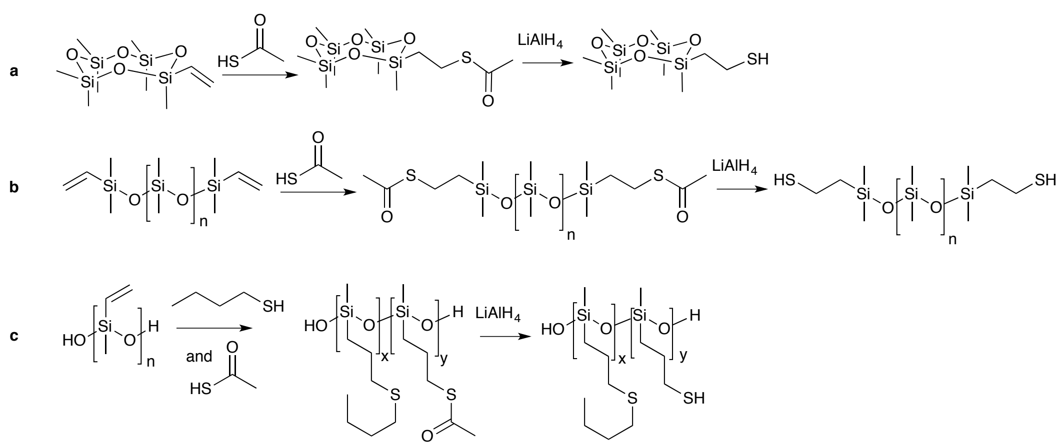

Figure 1.16 Synthetic routes for (a) thiol-modified cyclosiloxanes, (b) terminal sulfide-modified silicone fluids, (c) pendent sulfide-modified silicone fluids.

Although this method shows better control of the structure over the traditional equilibrium process, this method still has some issues like the need for the aggressive reducing agent $LiAlH_4$. We are currently examining the PR reaction as a route to well-defined thiol-functionalized silicone oils (Figure 1.17).

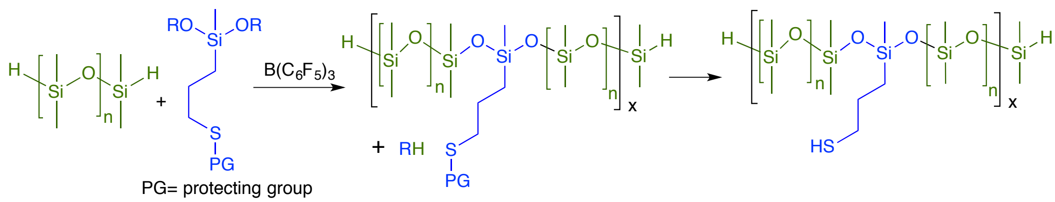

Figure 1.17 Synthetic routes for pendent sulfide-modified silicone fluid with well-defined structures under mild conditions.

1.3.3 Sulfur-Containing Silicones with Well-defined Structures

In 2011, our group reported a synthetic route for silicone surfactant with well-defined structures.[80] The synthesis of well-defined silicone-based surfactants has been a long-standing challenge, due to the instability of silicones towards acid or base; selective synthetic routes need to be developed. Dendron-branched silicone surfactants were designed and successfully synthesised though thiol-ene chemistry by Keddie. Pure silicone dendrons were first synthesized by the PR reaction. Alkoxysilanes react with vinyl-functionalized hydrosilanes with the presents of $B(C_6F_5)_3$. The hydrophilic poly(ethylene glycol) (PEG) with different molecular weights was then attached though UV initiated thiol-ene reaction (Figure 1.18).

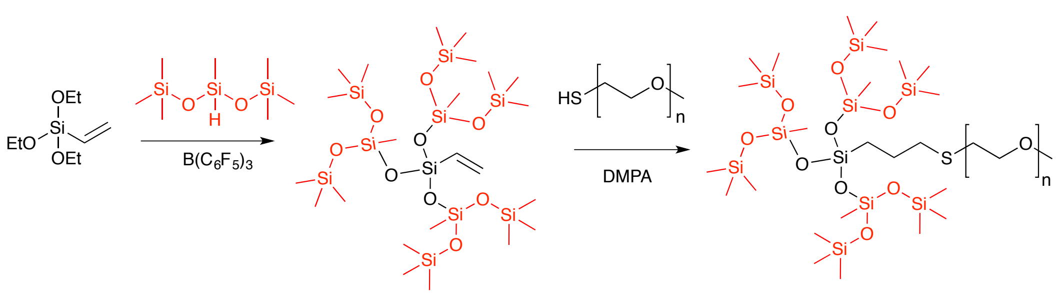

Figure 1.18 Synthetic routes for well-defined, dendron-branched silicone surfactants.

1.3.4 Sulfur-Containing Silicone Elastomers

Silicone elastomers can also be prepared though sulfur chemistry. In recent years, various research attempts have been conducted to explore new curing methods that avoid using heavy metals for environmental and cost reasons.[40, 81-83] Fatona[84] demonstrated his work of establishing dithioacetal silicone networks by thiol-modified silicone and aromatic aldehydes (Figure 1.19). The mechanical property of the product can be readily turned by controlling the chemical or physical linkages.

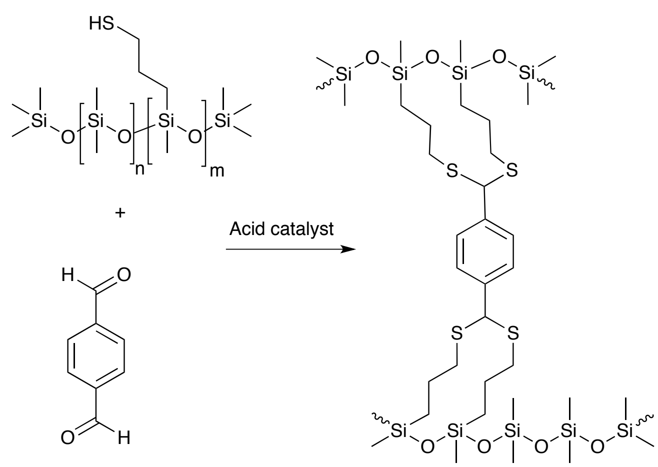

Figure 1.19 Reaction scheme of crosslinking thiol-PDMS via dithioacetal linkages using aromatic aldehydes.

1.4 Thesis Objectives

The main purpose of this thesis was to take advantage of sulfur reactions and unique properties of the resulting linkages to develop new silicone elastomers for different research interests.

1.4.1 Silicone Inks for 3D Printing

Silicone materials were widely used in a lot of areas due to the properties mentioned above. Nowadays, there rises an increasing demand for silicone materials with customized structures along with the development of 3D printing technology. Although 3D printing method has been successfully used to print a lot of thermoplastic materials,[85] 3D printing with silicone materials is a lot more challenging. Silicones are fluids at room temperature and, therefore, cannot simply be heated up to a high temperature above the melting point and printed as the thermoplastics or metals are.[86] They must be cured into thermosets. To date, silicone structures prepared by extrusion based 3D printing are mainly Pt-catalyzed hydrosilylation reaction (Figure 1.4a) with large initial viscosity.[87-88] The disadvantages of the traditional process include: (1) The printing efficiency was low since hydrosilylation is a relatively slow reaction. (2) As large viscosity was required to remain the shape before curing, complicated processing method for ink degassing and dispensing were required. (3) There are restrictions of printed products (e.g., printed parts only have a single modulus). (4) Other environmental and cost drawbacks related to metal catalysts. Methods to print objects with multiple materials, allowing mixed moduli or other properties, are barely reported in literatures.

In Chapter 2, we explored the possibility of using photoinduced thiol-ene click chemistry as an efficient method to produce crosslinked networks. This design is reasoned by the fact that the rate of radical thiol-ene reaction is rapid when triggered by UV light. [73] The rapid reaction rate matches the requirement for extrusion based 3d printing of silicone materials with low initial ink viscosity. Besides, compared to traditional radical chemistry, thiol-ene click chemistry is less sensitive to ambient oxygen or water which allows robust printing environment.[89]

1.4.2 Redox Responsive Silicone Elastomers

Glutathione (GSH) and oxidized glutathione (GSSG) is known to be the main redox buffer for cells in vivo.[90] In recent years, with improved in-depth understanding of the development and formation of tumors, it has been reported that the tumor microenvironment exhibits high levels of reduced glutathione (GSH).[91] Tremendous research has been done to develop target drug delivery systems based on the disulfide linkage where those disulfide linkages could be reduced in vivo to release drug for tumor treatment.[92] Inspired by the redox process in living cells, we discuss the incorporation of thiol-disulfide redox pairs in the silicone network in chapter 3. The disulfide linked silicone network is able to be established by oxidation of thiopropylsilicones. The reduction of disulfide linkages reproduces the thiol silicone starting materials. The reversible linkages could reduce the amount of used waste, which matches the concept of improving materials sustainability.

Chapter 3 established a method of cleavage disulfide linkages by using hydrosilane with the presents of $B(C_6F_5)_3$ catalyst. In chapter 4, the method was adopted to cleave the disulfide and polysulfide linkages in used rubber tires. The research mainly focused on converting the used rubber tire back into uncrosslinked polymeric oils that can be further processed to new elastomers.[93] If successful, the research could possibly have huge impact on the large amount of tire waste produced annually[94] and addressing the related environmental issues.

1.4.3 Thermoplastic Silicone Elastomers

Besides reversible bonds based on dynamic chemical linkage, silicone elastomer based on physical linkage was also explored in this thesis. Utilizing the physical interactions of the polymers can lead to smart materials with unique mechanical properties. A variety of molecular interactions (e.g., dynamic covalent bonds,[95] hydrogen bonding,[96-97] aromatic association,[98] electrostatic interactions,[99-100] and metal-ligand coordination[101]) can be used to control reversibility. In most of these cases, those physical crosslinks can be overcome thermally, leading to thermoplastic materials that allows recycling of fabricated products and results in a great reduction of wastes. The traditional thermoplastic silicone materials are silicone polyurethane copolymers that the polyurethane segment provide the physical linkages at room temperature.[102] A research survey shows there was not a lot of work related to thermoplastic silicone based on purely silicone component. It is definitely an area need further exploration.

In chapter 5, research was focused on creating ionic crosslinked thermoplastic silicone elastomers. The synthetic route of grafting the thiol silicone with maleic acid though thiol-Michael pathway was proposed. The ionic linkages were built by neutralization of the acidic silicone with amino silicone.

1.5 References

1. Vyle, L. R.; Kipping, F. S., CCCLVII.—Organic Derivatives of Silicon. Part XXXI. Action of Mercuric Oxide on Diaryldichlorosilicanes. *J. Chem. Soc., Trans.* **1924,** *125* (0), 2616-2622.
2. Dietlein, J. E.; Kamis, R. P.; Klosowski, J. M. Silicone Sealants. US4978706A, 1990.
3. Kim, S. H.; Moon, J.-H.; Kim, J. H.; Jeong, S. M.; Lee, S.-H., Flexible, Stretchable and Implantable PDMS Encapsulated Cable for Implantable Medical Device. *Biomed. Eng. Lett.* **2011,** *1* (3), 199.
4. Banea, M. D.; da Silva, L. F. M., Static and Fatigue Behaviour of Room Temperature Vulcanising Silicone Adhesives for High Temperature Aerospace Applications. *Materialwiss. Werkstofftech.* **2010,** *41* (5), 325-335.
5. Mower, T. M., Thermomechanical Behavior of Aerospace-grade RTV (Silicone Adhesive). *Int. J. Adhes. Adhes.* **2018,** *87*, 64-72.
6. Brook, M. A., Silicones. In *Silicon in Organic, Organometallic, and Polymer Chemistry*, Jhon Wiley & Sons, INC: 1999; pp 256-298.
7. *Linear Poly(dimethyldisiloxane)* Joint Assessment of Commodity Chemicals: 1994; Vol. 26.
8. Brook, M. A., Atomic and Molecular Properties of Silicon. In *Silicon in Organic, Organometallic, and Polymer Chemistry*, Jhon Wiley & Sons, INC: 1999; pp 27-38.
9. Noll, W., Chapter 9 - Properties of Technical Products. In *Chemistry and Technology of Silicones*, Noll, W., Ed. Academic Press: 1968; pp 437-530.
10. Kopylov, V. M.; Kovyazin, V. A.; Kostyleva, E. I.; Fedorov, A. Y.; Kovyazin, A. V., The Thermal Stabilisation and Ceramifying of Silicone Rubbers. *Int. Polymer Sci. Tech.* **2016,** *43*, T33-T40.
11. Ghanbari-Siahkali, A.; Mitra, S.; Kingshott, P.; Almdal, K.; Bloch, C.; Rehmeier, H. K., Investigation of the Hydrothermal Stability of Cross-linked Liquid Silicone Rubber (LSR). *Polym. Degrad. Stab.* **2005,** *90* (3), 471-480.
12. Hanifeh, M.; Zandi, M.; Shokrollahi, P.; Atai, M.; Ghafarzadeh, E.; Askari, F., Compositional Design and Taguchi Optimization of Hardness Properties in Silicone-based Ocular Lenses. *Prog. Biomater.* **2017,** *6* (3), 67-74.
13. Mark, J. E., Silicon-Containing Polymers. In *Silicon-Based Polymer Science*, American Chemical Society: 1989; Vol. 224, pp 47-68.
14. McKeen, L. W., 13 - Elastomers and Rubbers. In *Film Properties of Plastics and Elastomers (Fourth Edition)*, McKeen, L. W., Ed. William Andrew Publishing: 2017; pp 419-448.
15. Owen, M. J., The Surface Activity of Silicones: A Short Review. *Ind. Eng. Chem. Prod. Res. Dev.* **1980,** *19* (1), 97-103.
16. Cannon, P.; St. Pierre, L. E.; Miller, A. A., Solubilities of Hydrogen and Oxygen in Polydimethylsiloxanes. *J. Chem. Eng. Data* **1960,** *5* (2), 236-236.

17. Lin, C.-H.; Yeh, Y.-H.; Lin, W.-C.; Yang, M.-C., Novel Silicone Hydrogel Based on PDMS and PEGMA for Contact Lens Application. *Colloids Surf. B* **2014,** *123*.
18. Keir, N.; Jones, L., Wettability and Silicone Hydrogel Lenses: A Review. *Eye Contact Lens* **2013,** *39* (1), 100-108.
19. Brook, M. A., New Control Over Silicone Synthesis using SiH Chemistry: The Piers–Rubinsztajn Reaction. *Chem. Eur. J* **2018,** *24* (34), 8458-8469.
20. Wright, P. V.; Semlyen, J. A., Equilibrium Ring Concentrations and the Statistical Conformations of Polymer Chains: Part 3. Substituent Effects in Polysiloxane Systems. *Polymer* **1970,** *11* (9), 462-471.
21. Goff, J.; Kimble, E.; Arkles, B., Living Polymerization Routes to Siloxane Macromers and Higher Order Silicone Structures. In *Progress in Silicones and Silicone-Modified Materials*, American Chemical Society: 2013; Vol. 1154, pp 59-78.
22. Orofino, T. A.; Wenger, F., The Effect of Impurities on the Molecular Weight Distributions of Anionic Polymers. *The Journal of Chemical Physics* **1961,** *35* (2), 532-538.
23. Marciniec, B., Functionalisation and Cross-Linking of Organosilicon Polymers. In *Hydrosilylation: A Comprehensive Review on Recent Advances*, Marciniec, B., Ed. Springer Netherlands: Dordrecht, 2009; pp 159-189.
24. Wong, M.; Schneider, A.; Lu, G.; Chen, Y.; Brook, M., Autoxidation: Catalyst-Free Route to Silicone Rubbers by Crosslinking Si-H Functional Groups. *Green Chem.* **2019,** *21*.
25. Madsen, F. B.; Yu, L.; Skov, A. L., Self-Healing, High-Permittivity Silicone Dielectric Elastomer. *ACS Macro Lett.* **2016,** *5* (11), 1196-1200.
26. Shit, S. C.; Shah, P., A Review on Silicone Rubber. *Natl Acad Sci Lett.* **2013,** *36* (4), 355-365.
27. Johnston, I. D.; McCluskey, D. K.; Tan, C. K. L.; Tracey, M. C., Mechanical Characterization of Bulk Sylgard 184 for Microfluidics and Microengineering. *J. Micromech. Microeng* **2014,** *24* (3), 035017.
28. Qin, D.; Xia, Y.; Whitesides, G. M., Soft Lithography for Micro- and Nanoscale Patterning. *Nat. Protoc.* **2010,** *5* (3), 491-502.
29. Brook, M. A., Formation of Si-C Bonds: The Synthesis of Functional Organosilanes. In *Silicon in Organic, Organometallic, and Polymer Chemistry*, Jhon Wiley & Sons, INC: 1999; pp 381- 458.
30. Siderakis, K.; Pylarinos, D., Room Temperature Vulcanized Silicone Rubber Coatings: Application in High Voltage Substations. *Concise Encyclopedia of High Performance Silicones* **2014**, 1-17.
31. Wang, J.; Feng, L.; Chao, X.; Feng, Y., Performance of Room Temperature Vulcanized (RTV) Silicone Rubber-Based Composites: DBDPO/RTV and DBDPE/Sb2O3/RTV. *Polym. Plast. Technol. Eng.* **2012,** *51* (12), 1245-1250.
32. Scholz, M.; Meyer, J.; Wissler, G. RTV Two-Component Silicone Rubber. US8338528B2, 2007.

33. Cervantes, J.; Zárraga, R.; Salazar‐Hernández, C., Organotin Catalysts in Organosilicon Chemistry. *Appl. Organomet. Chem.* **2012,** *26*.
34. Moretto, H.-H.; Schulze, M.; Wagner, G., Silicones. *Ullmann's Encyclopedia of Industrial Chemistry* **2000**.
35. Brook, M. A.; Grande, J. B.; Ganachaud, F., New Synthetic Strategies for Structured Silicones Using $B(C_6F_5)_3$. In *Silicon Polymers*, Muzafarov, A. M., Ed. Springer Berlin Heidelberg: Berlin, Heidelberg, 2011; pp 161-183.
36. Parks, D. J.; Piers, W. E., Tris(pentafluorophenyl)boron-Catalyzed Hydrosilation of Aromatic Aldehydes, Ketones, and Esters. *J. Am. Chem. Soc.* **1996,** *118* (39), 9440-9441.
37. Rubinsztajn, S.; Cella, J. A., A New Polycondensation Process for the Preparation of Polysiloxane Copolymers. *Macromolecules* **2005,** *38* (4), 1061-1063.
38. Schneider, A. F.; Laidley, E.; Brook, M. A., Facile Synthesis of Cx(AB)yCx Triblock Silicone Copolymers Utilizing Moisture Mediated Living-End Chain Extension. *Macromol. Chem. Phys.* **2019,** *220* (8), 1800575.
39. Laengert, S. E.; Schneider, A. F.; Lovinger, E.; Chen, Y.; Brook, M. A., Cover Picture: Sequential Functionalization of a Natural Crosslinker Leads to Designer Silicone Networks (Chem. Asian J. 11/2017). *Chem. Asian J.* **2017,** *12* (11), 1121-1121.
40. Fawcett, A. S.; Grande, J. B.; Brook, M. A., Rapid, Metal-free Room Temperature Vulcanization Produces Silicone Elastomers. *J. Polym. Sci., Part A: Polym. Chem.* **2013,** *51* (3), 644-652.
41. Zheng, S.; Liang, S.; Chen, Y.; Brook, M. A., Hyperbranched Silicone MDTQ Tack Promoters. *Molecules* **2019,** *24* (22), 4133.
42. Mutlu, H.; Ceper, E. B.; Li, X.; Yang, J.; Dong, W.; Ozmen, M. M.; Theato, P., Sulfur Chemistry in Polymer and Materials Science. *Macromol. Rapid Commun.* **2019,** *40* (1), 1800650.
43. Worthington, M. J. H.; Kucera, R. L.; Chalker, J. M., Green Chemistry and Polymers Made from Sulfur. *Green Chem.* **2017,** *19* (12), 2748-2761.
44. Kleine, T. S.; Glass, R. S.; Lichtenberger, D. L.; Mackay, M. E.; Char, K.; Norwood, R. A.; Pyun, J., 100th Anniversary of Macromolecular Science Viewpoint: High Refractive Index Polymers from Elemental Sulfur for Infrared Thermal Imaging and Optics. *ACS Macro Lett.* **2020,** *9* (2), 245-259.
45. Vo, C. D.; Kilcher, G.; Tirelli, N., Polymers and Sulfur: What are Organic Polysulfides Good For? Preparative Strategies and Biological Applications. *Macromol. Rapid Commun.* **2009,** *30* (4‐5), 299-315.
46. Hoyle, C. E.; Lowe, A. B.; Bowman, C. N., Thiol-click Chemistry: a Multifaceted Toolbox for Small Molecule and Polymer Synthesis. *Chem. Soc. Rev.* **2010,** *39* (4), 1355-1387.
47. Lowe, A. B., Thiol-yne 'Click'/Coupling Chemistry and Recent Applications in Polymer and Materials Synthesis and Modification. *Polymer* **2014,** *55* (22), 5517-5549.

48. Lowe, A. B.; Bowman, C. N., *Thiol-X Chemistries in Polymer and Materials Science*. Royal Society of Chemistry: 2013; p 001-317.
49. Uygun, M.; Tasdelen, M. A.; Yagci, Y., Influence of Type of Initiation on Thiol-Ene Click Chemistry. *Macromol. Chem. Phys.* **2010,** *211* (1), 103-110.
50. Posner, T., Beiträge zur Kenntniss der ungesättigten Verbindungen. II. Ueber die Addition von Mercaptanen an ungesättigte Kohlenwasserstoffe. *Berichte der deutschen chemischen Gesellschaft* **1905,** *38* (1), 646-657.
51. Kharasch, M. S.; May, E. M.; Mayo, F. R., The Peroxide Effect in The Addition of Reagents to Unsaturated Compounds XVIII. The Addtition and Substitution of Bisulfite. *J. Org. Chem.* **1938,** *03* (2), 175-192.
52. Cramer, N. B.; Bowman, C. N., CHAPTER 1 Thiol-ene and Thiol-yne Chemistry in Ideal Network Synthesis. In *Thiol-X Chemistries in Polymer and Materials Science*, The Royal Society of Chemistry: 2013; pp 1-27.
53. Hoyle, C. E.; Bowman, C. N., Thiol-ene click chemistry. *Angew. Chem. Int. Ed.* **2010,** *49* (9), 1540-73.
54. Hoyle, C. E.; Lee, T. Y.; Roper, T., Thiol-enes: Chemistry of the Past with Promise for the Future. *J. Polym. Sci., Part A: Polym. Chem.* **2004,** *42* (21), 5301-5338.
55. Sun, Y.; Liu, H.; Cheng, L.; Zhu, S.; Cai, C.; Yang, T.; Yang, L.; Ding, P., Thiol Michael Addition Reaction: a Facile Tool for Introducing Peptides into Polymer-Based Gene Delivery Systems. *Polym. Int.* **2017,** *67* (1), 25-31.
56. Chauvin, J.-P. R.; Pratt, D. A., On the Reactions of Thiols, Sulfenic Acids, and Sulfinic Acids with Hydrogen Peroxide. *Angew. Chem. Int. Ed.* **2017,** *56* (22), 6255-6259.
57. Hashemi, M.; Rahimi, A.; Karimi-Jaberi, Z., Sodium Hypochlorite/Montmorillonite K10: An Effective Oxidant for the Oxidation of Thiols to Disulfides. *Lett. Org. Chem.* **2005,** *2*, 485-486.
58. Goethals, E. J.; Sillis, C., Oxidation of Dithiols to Polydisulfides by Means of Dimethylsulfoxide. *Die Makromolekulare Chemie* **1968,** *119* (1), 249-251.
59. Bardwell, J. C.; Lee, J. O.; Jander, G.; Martin, N.; Belin, D.; Beckwith, J., A Pathway for Disulfide Bond Formation in Vivo. *Proc. Natl. Acad. Sci.* **1993,** *90* (3), 1038.
60. Yu, K.; Xin, A.; Du, H.; Li, Y.; Wang, Q., Additive Manufacturing of Self-healing Elastomers. *NPG Asia Mater.* **2019,** *11* (1), 7.
61. Fairbanks, B. D.; Singh, S. P.; Bowman, C. N.; Anseth, K. S., Photodegradable, Photoadaptable Hydrogels via Radical-Mediated Disulfide Fragmentation Reaction. *Macromolecules* **2011,** *44* (8), 2444-2450.
62. Schilter, D., Thiol Oxidation: A Slippery Slope. *Nat. Rev. Chem.* **2017,** *1*, 0013.
63. Fettes, E. M.; Mark, H., Cleavage of Disulfide Polymers. I. By Inorganic Sulfides. *J. Appl. Polym. Sci.* **1961,** *5* (13), 7-15.
64. Studebaker, M. L., Lithium Aluminum Hydride Analysis of Sulfur-Cured Vulcanizates. *Rubber Chem. Technol.* **1970,** *43* (3), 624-650.

65. Overman, L. E.; O'Connor, E. M., Nucleophilic Cleavage of the Sulfur-sulfur Bond by Phosphorus Nucleophiles. IV. Kinetic Study of the Reduction of Alkyl Disulfides with Triphenylphosphine and Water. *J. Am. Chem. Soc.* **1976,** *98* (3), 771-775.
66. Walvekar, R.; Afiq, Z. M.; Ramarad, S.; Khalid, S., Devulcanization of Waste Tire Rubber Using Amine Based Solvents and Ultrasonic Energy. *MATEC Web Conf.* **2018,** *152*.
67. Katchalski, E.; Benjamin, G. S.; Gross, V., The Availability of the Disulfide Bonds of Human and Bovine Serum Albumin and of Bovine γ-Globulin to Reduction by Thioglycolic Acid. *J. Am. Chem. Soc.* **1957,** *79* (15), 4096-4099.
68. Hermanson, G. T., Chapter 2 - Functional Targets for Bioconjugation. In *Bioconjugate Techniques (Third Edition)*, Hermanson, G. T., Ed. Academic Press: Boston, 2013; pp 127-228.
69. Field, L., Disulfide and Polysulfide. In *Organic Chemistry of Sulfur* Oae, S., Ed. New York, 1977; Vol. Chpater 7.
70. Lowe, A. B., Thiol–ene "Click" Reactions and Recent Applications in Polymer and Materials Synthesis: a First Update. *Polym. Chem.* **2014,** *5* (17), 4820-4870.
71. Devatha P.Nair, M. P. s., Shunsuke Chatani,Tao Gong,Weixian Xi,Christopher R. Fenoli, and Christopher N. Bowman,, The Thiol-Michael Addition Click Reaction: A Powerful and Widely Used Tool in Materials Chemistry. *Chem. Mater.* **2014,** *26*, 724-744.
72. Burkhard, C. A., The Reaction of Mercaptans with Alkenyl Silanes. *J. Am. Chem. Soc.* **1950,** *72* (3), 1078-1080.
73. Kunze, U. M. a. A., Photocrosslinking of Silicones. Part 13. Photoinduced Thiol-ene Crosslinking of Modified Silicones *Pure Appl. Chem. A* **1996,** *33* (4), 439-457.
74. Hwu, J.; Lin, C. F.; Tsay, S. C., Hexamethyldisilathiane in Novel Chemical Transformations: Concept of "Counterattack Reagent". *ChemInform* **2005,** *36*.
75. So, J.-H.; Boudjouk, P.; Hong, H. H.; Weber, W. P., Hexamethyldisilathiane. *Inorg. Synth.* **1992**, 30-32.
76. Matulenko, M. A., Bis(trimethylsilyl) Sulfide. In *Reagents for Silicon-Mediated Organic Synthesis*, Fuchs, P. L., Ed. 2011; p 83.
77. Liao, M.; Brook, M., Boron Catalyzed Disulfide Cleavage Study Using Hydrosilane. *Angew. Chem. Int. Ed.* **2020,** *n/a* (n/a), To be submitted.
78. Rózga-Wijas, K.; Chojnowski, J.; Zundel, T.; Boileau, S., Controlled Synthesis of Siloxane Copolymers Having an Organosulfur Group by Polymerization of Cyclotrisiloxanes with Mixed Units. *Macromolecules* **1996,** *29* (8), 2711-2720.
79. Perju, E.; Dünki, S. J.; Opris, D. M., A Versatile Synthetic Path to Thiol Containing Polysiloxanes. *J. Polym. Sci., Part A: Polym. Chem.* **2016,** *54* (18), 2940-2948.

80. Keddie, D. J.; Grande, J. B.; Gonzaga, F.; Brook, M. A.; Dargaville, T. R., Amphiphilic Silicone Architectures via Anaerobic Thiol-Ene Chemistry. *Org. Lett.* **2011,** *13* (22), 6006-6009.
81. Rambarran, T.; Gonzaga, F.; Brook, M. A.; Lasowski, F.; Sheardown, H., Amphiphilic Thermoset Elastomers from Metal-free, Click Crosslinking of PEG-Grafted Silicone Surfactants. *J. Polym. Sci., Part A: Polym. Chem.* **2015,** *53* (9), 1082-1093.
82. Bui, R.; Brook, M. A., Dynamic Covalent Schiff-Base Silicone Polymers and Elastomers. *Polymer* **2019,** *160*, 282-290.
83. Liao, M.; Schneider, A.; Laengert, S.; Gale, C.; Chen, Y.; Brook, M., Living Synthesis of Silicone Polymers Controlled by Humidity. *Eur. Polym. J.* **2018,** *107*.
84. Fatona, A.; Moran-Mirabal, J.; Brook, M. A., Controlling Silicone Networks using Dithioacetal Crosslinks. *Polym. Chem.* **2019,** *10* (2), 219-227.
85. Wang, X.; Jiang, M.; Zhou, Z.; Gou, J.; Hui, D., 3D printing of Polymer Matrix Composites: A Review and Prospective. *Compos. B. Eng.* **2017,** *110*, 442-458.
86. Roh, S.; Parekh, D. P.; Bharti, B.; Stoyanov, S. D.; Velev, O. D., 3D Printing by Multiphase Silicone/Water Capillary Inks. *Adv. Mater.* **2017,** *29* (30), 1701554.
87. Wehner, M.; Truby, R. L.; Fitzgerald, D. J.; Mosadegh, B.; Whitesides, G. M.; Lewis, J. A.; Wood, R. J., An Integrated Design and Fabrication Strategy for Entirely Soft, Autonomous Robots. *Nature* **2016,** *536* (7617), 451-455.
88. Qin, Z.; Compton, B. G.; Lewis, J. A.; Buehler, M. J., Structural Optimization of 3D-printed Synthetic Spider Webs for High Strength. *Nat. Commun.* **2015,** *6* (1), 7038.
89. Nagarjuna, R.; Saifullah, M. S. M.; Ganesan, R., Oxygen Insensitive Thiol–ene Photo-click Chemistry for Direct Imprint Lithography of Oxides. *RSC Adv.* **2018,** *8* (21), 11403-11411.
90. Chakravarthi, S.; Jessop, C. E.; Bulleid, N. J., The Role of Glutathione in Disulphide Bond Formation and Endoplasmic Reticulum Generated Cxidative Stress. *EMBO Rep* **2006,** *7* (3), 271-275.
91. Taketa, K.; Ichikawa, E.; Umetsu, K.; Suzuki, T., Allomyrina Dichotoma Lectin-nonreactive α-Fetoprotein in Hepatocellular Carcinoma and Other Tumors: Comparison with Ricinus Communis Agglutinin-I. *Cancer Lett.* **1986,** *31* (3), 325-331.
92. Chang, S.; Wang, Y.; Zhang, T.; Pu, X.; Zong, L.; Zhu, H.; Zhao, L.; Feng, B., Redox-Responsive Disulfide Bond-Bridged mPEG-PBLA Prodrug Micelles for Enhanced Paclitaxel Biosafety and Antitumor Efficacy. *Front. Oncol.* **2019,** *9*, 823.
93. Zheng, S.; Liao, M.; Chen, Y.; Brook, M. A., Dissolving Used Rubber Tires. *Green Chem.* **2020,** *22*, 94-102.
94. World Tires (http://www.freedoniagroup.com/industry-study/world-tires-3357.htm). *Freedonia Group* **2015,** *Industry Study 3357*.
95. Nasresfahani, A.; Zelisko, P. M., Synthesis of a Self-healing Siloxane-based Elastomer Cross-linked via a Furan-modified Polyhedral Oligomeric

Silsesquioxane: Investigation of a Thermally Reversible Silicon-based Cross-link. *Polym. Chem.* **2017,** *8* (19), 2942-2952.
96. Wittenberg, E.; Meyer, A.; Eggers, S.; Abetz, V., Hydrogen Bonding and Thermoplastic Elastomers - a Nice Couple with Temperature-Adjustable Mechanical Properties. *Soft Matter* **2018,** *14* (14), 2701-2711.
97. Prisacariu, C.; Scortanu, E.; Agapie, B., Effect of the Hydrogen Bonding on the Inelasticity of Thermoplastic Polyurethane Elastomers. *J. Ind. Eng. Chem.* **2013,** *19* (1), 113-119.
98. Park, S.-A.; Jeon, H.; Kim, H.; Shin, S.-H.; Choy, S.; Hwang, D. S.; Koo, J. M.; Jegal, J.; Hwang, S. Y.; Park, J.; Oh, D. X., Sustainable and Recyclable Super Engineering Thermoplastic from Biorenewable Monomer. *Nat. Commun.* **2019,** *10* (1), 2601.
99. Antony, P.; De, S. K., Ionic Thermoplastic Elastomers: A Review. *J. Macromol. Sci. Polymer. Rev.* **2001,** *41* (1-2), 41-77.
100. Rousseaux, D. D. J.; Drooghaag, X.; Sclavons, M.; Godard, P.; Carlier, V.; Marchand-Brynaert, J., Polypropylene Ionic Thermoplastic Elastomers: Synthesis and Properties. *Polym. Degrad. Stab.* **2010,** *95* (3), 363-368.
101. Wang, W.; Zhang, J.; Jiang, F.; Wang, X.; Wang, Z., Reprocessable Supramolecular Thermoplastic BAB-Type Triblock Copolymer Elastomers with Enhanced Tensile Strength and Toughness via Metal-Ligand Coordination. *ACS Appl. Polym. Mater.* **2019,** *1* (3), 571-583.
102. Stricher, A. M.; Rinaldi, R. G.; Barrès, C.; Ganachaud, F.; Chazeau, L., How I Met Your Elastomers: from Network Topology to Mechanical Behaviours of Conventional Silicone Materials. *RSC Adv.* **2015,** *5* (66), 53713-53725.

2 Chapter 2: 3D Printable, Rapid Cure Silicone Elastomers Prepared using Thiol-ene "Click" Chemistry

2.1 Abstract

Silicone elastomers are of commercial interest in a number of areas because of their distinctive properties. 3D printing (additive manufacturing) is becoming advantageous over conventional technologies for the fabrication of sophisticated structures. Current printing technologies for silicones are limited to extrusion of premixed uncured elastomers, which can be challenged by limitations of pot life. In our research, we are exploring the possibility of using photoinduced thiol-ene click chemistry as an efficient method to produce crosslinked networks[1] and examine their potential for use in 3D printing application. Polydimethylsiloxane (PDMS) inks were formulated using a combination of chain-extender, cross-linker and base polymer. The ratio of chain-extender and catalyst was varied for certain inks to achieve a fast reaction and affect the hardness of the printed structures. Results show that this procedure allows for very fast cure times (<20 s) under UV radiation. The ability to print different types of multimoduli silicones will be presented.

2.2 Introduction

Polysiloxanes known as “silicones”, have received wide spread attention due to their unique properties, including low toxicity, good thermal stability, optical transparency and high permeation to oxygen, etc.[2] Furthermore, with the increasing industrial demand for functional polysiloxanes, precise fabrication of complex polymers with well-defined silicone-containing structures has been widely studied[3] to broaden the application of silicone materials in the fields of nanothechnology[4] and bioscience.[5] The ability to integrate both structure and function within manufactured silicone elastomers is the next frontier in this field.[6] To move beyond prototyping, new manufacture methods are required.

Additive manufacturing (AM), known as 3D printing, has gained great interest in recent years, as it allows the creation of complex 3D geometries with delicate and customized structures. A variety of printing technologies have been established that are capable of printing objects in three dimensions. For example, 3D-printing by fused deposition modeling (FDM) is widely used, in which thermoplastic polymer filaments are employed as inks.[7] Along with FDM technology, some light-based technology have attracted interest in recent years. In selective laser sintering (SLS) of polymeric powders, a laser light is used to fuse polymer particles in a powder bed.[8] Among those technologies, extrusion-based, direct ink writing is considered a low cost, high throughput additive manufacturing technique. In the light of this consideration, we proposed an extrusion based, UV curable method, in which a photocurable liquid polymer is deposited and crosslinked by an external UV light source as soon as it flows out of the nozzle during the printing process.

To date, 3D printing method has been successfully used in the fabrication of functional devices such as wearable sensors[9], soft robots[10], 3D tissue[11], hydrogel[12], microfluidic devices[13-14], etc. However, 3D printing with silicone materials has not been possible. In part, this is due to their low Tg.[15] Silicones are fluids at room temperature and, therefore, cannot simply be heated up to a high temperature above the melting point and printed as the thermoplastics or metals are. They must be cured into thermosets. To date, silicone structures prepared by with silicones are mainly extrusion-based printing methods. Wacker Chemie AG[16] reported a method to prepare 3D print silicone elastomers using a hydrosilylation reaction for cure (Figure 2.1). Methylhydrosiloxane-dimethylsiloxane copolymers were cured with vinyldimethylsiloxy-terminated PDMS, using a UV-activated platinum catalyst: trimethyl(methylcyclopentadienyl) platinum. A 3 hour vacuum process is required to remove the negative influence of oxygen prior to starting the printing. Hinton et al.[17] reported development of a method to 3D print PDMS elastomers in a hydrophilic support bath. In this a platinum catalyst based silicone (PDMS – polydimethylsiloxanes), Sylgard 184 (Dow Corning), was used and a relatively long curing time (72 h) was required. Since metal catalysts were involved in these processes, they may be disadvantageous on the basis of cost or for environmental reasons. Furthermore, in these approaches, only a single material with a single modulus was printed. Methods to print objects with multiple materials, allowing mixed moduli or other properties, are barely reported in literature.

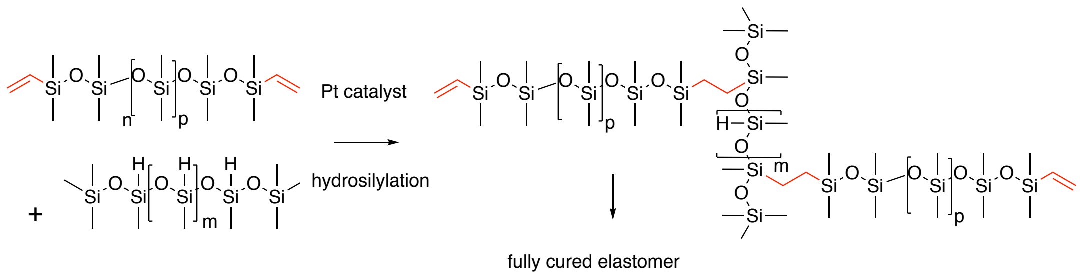

Figure 2.1 Pt-catalyzed hydrosilylation cure.

It was therefore the aim of this study to develop metal-free silicone inks for 3D printing. The goal was to achieve a rapid curing time, as this feature would efficiently shorten printing period and improve fidelity of final products. Also, exquisite control over network structure is desired to give final products with reproducible and adjustable hardness.

There are several methods available for the synthesis of silicone elastomers, the most common of these are high-temperature radical cure, room-temperature vulcanization, platinum-catalyzed hydrosilylation and Piers-Rubinsztajn cure.[2] However, each of these processes has its own disadvantages for 3D printing. For example, high-temperature radical cure is not very convenient (cure would require temperatures in excess of 100 °C), while the room temperature moisture cure is too slow for 3D printing. With respect to rapid Piers-Rubinsztajn cure, it can be difficult to control the process to give reproducible bubble free networks and extreme attention should be given to managing the flammable alkane by product.[18]

In our research, we are exploring the possibility of using photoinduced thiol-ene click chemistry as an efficient method to produce crosslinked networks (Figure 2.2). The reaction of thiols with alkenes provides many of the attractive attributes for the cross-linking of silicone materials.[19] First, it can achieve quantitative yields with a rapid reaction rate.[20] Second, compared to traditional radical chemistry, thiol-ene click chemistry is less sensitive to ambient oxygen or water, requiring essentially no degassing procedures. Due to the high oxygen permeability of silicones, this feature of thiol-ene cure provides a huge advantage by avoiding the long vacuum process needed to remove oxygen from traditional inks before printing. Third, the polymerization process is triggered by UV light,[21] therefore, allowing localized polymerization. Finally, no expensive and toxic metal catalysts are required, allowing the manufacture of implantable devices.

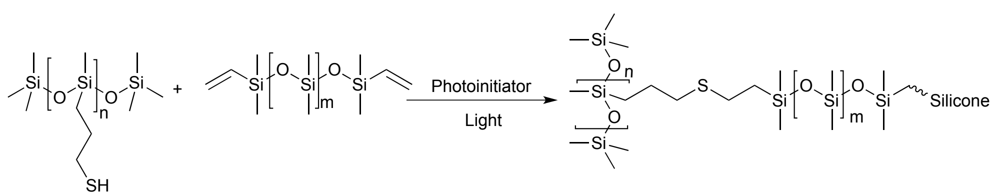

Figure 2.2 Silicone networks prepared by thiol-ene reaction.

Since early 1900s, the thiol-ene reaction have been studied and applied to many fields[16, 22-23], however, its application in silicone chemistry has only rarely been reported. In a former work, our group described a method to functionalize PDMS elastomer surfaces by thiol-ene chemistry (Figure 2.3). The resulting products are ready to be applied in the field of biological and pharmaceutical application.[24]

Muller and Kunze[25] investigated the crosslinking kinetics of ene-terminated silicones (vinyl, vinyloxy, allyl, norbornenyl, etc.) with siloxanes containing pendant thiol groups. An ultrafast reaction rate could be achieved even in the presence of oxygen. Berg and coworkers[26] showed a method to prepare low modulus, dry silicone-gel materials through thiol-ene cure. Recently, Nguyen et al.[27] demonstrated an approach to thiol-ene based crosslinking of silicone elastomers for biomedical applications. In their work, a thiol-functional silicone homopolymer was crosslinked with vinyl-terminated siloxanes. Biocompatibility of the resulting products was examined. So far, there is still a lack of understanding of how to control thiol-ene cure network structure and its impact on mechanical properties. Thiol-ene cure silicone inks for 3D printing have not been reported up to date as far as we can determine.

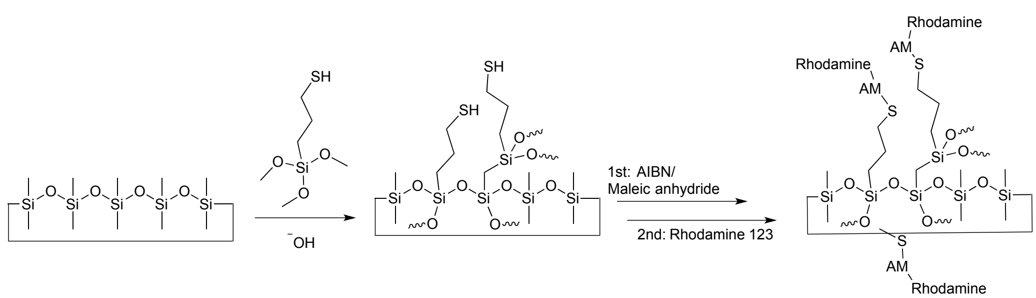

Figure 2.3 Facile functionalization of PDMS elastomer surfaces using thiol–ene click chemistry.

In this report, we have examined the applicability of thiol-ene reaction as a synthetic route to silicone elastomer. α,ω-Vinyl-terminated PDMS were crosslinked with thiol-functional silicone copolymers using UV light. The reaction rates were examined as a function of light sources, photoinitiator type, reagent concentrations and the impact of oxygen inhibition. In addition, the ability to adjust the mechanical properties of silicone elastomers by use of thiol-functional PDMS chain-extenders and different functionality cross-linkers was studied (Figure 2.4). Finally, two optimized cross-linking formulations were prepared to yield the desired 3D silicone structures with both low and high cross-link densities.

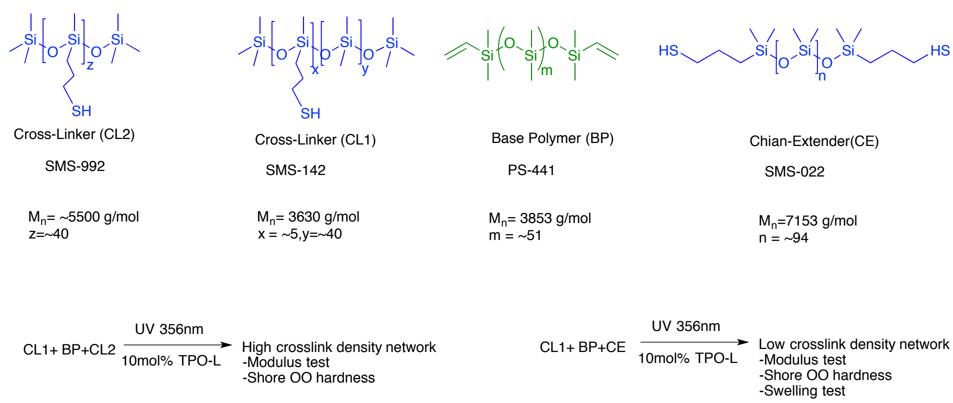

Figure 2.4 Strategy of adjusting mechanical properties.

2.3 Results and Discussion

Thiol-functional silicones were allowed to react with vinyl-terminated silicones in the presence of photoinitiators to give silicone elastomers. The rates of the reactions depended on a variety of factors including initiator concentration and oxygen, each of which will be discussed in turn.

2.3.1 Influence of Photoinitiator Concentration on Reaction Rate

Initially, the photoinitiated thiol-ene reaction was initiated using 0.1 mol% catalyst. The reaction took about 50 seconds to give complete cure. As would be expected, increasing the catalyst concentration led to a significant decrease in reaction time. For example, using 5mol% DHMP instead of 0.1 mol% catalyst decreased the reaction time from 50s to 30s (Table S2.1:**3,1**). This exceptionally rapid cure rate facilitates the potential application of this reaction in the 3D printing field. Further manipulation of photoinitiator concentration was examined. Results show that photoinitiator loading higher than 10 mol% seems not provide further improvement in reducing the reaction time. That could be explained by the mechanism of thiol-ene chemistry. Once there were enough radicals produced, the initiation step was no longer the rate limiting step in the process and the total reaction rate depended on propagation.

2.3.2 Influence of Oxygen Quenching Effect on Reaction Rate

Free radical chemistry suffers from the effects of the presence oxygen in the coating and at the surface of the printed object during cure by quenching the excited state of photoinitiator and scavenging the radicals (Figure 2.5). This was found to be particularly problematic for low viscosity inks that are very susceptible to oxygen diffusion into the ink, the cure speed is strongly influenced by oxygen.[28] It was observed that the surface of the film was always the last to cure. If we limit the oxygen concentration on the surface, a very low concentration of photoinitiator could provide excellent cure performance (Figure 2.6). Of course, for 3D printing, it is not practical to isolate the object being printed from air. These studies were undertaken to allow an understanding of the degree to which oxygen could compromise cure.

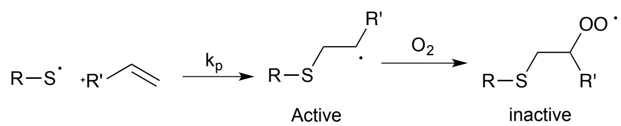

Figure 2.5 Oxygen-scavenging mechanism of radicals.

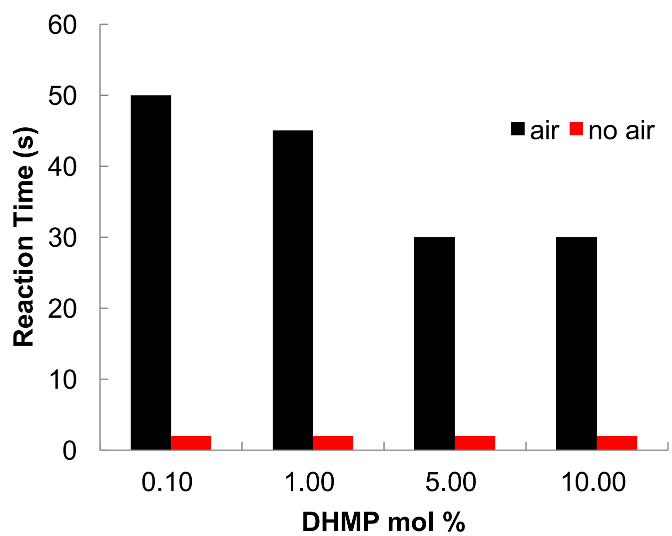

*Light source: UV 254 nm

Figure 2.6 Reaction time of thin films with different DHMP concentrations.

2.3.3 Influence of Matching Photoinitiator Absorption to the UV Wavelength on Reaction Rate

Formulations with 5mol% DHMP photoinitiator - a compound designed to fragment at 254 nm - demonstrate that if 365 nm UV light was instead applied, the reaction time was prolonged from 30 s to 300 s. This could be explained by the absorption pattern of DHMP. DHMP has a strong absorption in the shortwave UV around 230-270 nm that provides a fast initiation using 254 nm UV and a weak absorption at longer wavelengths up to 365 nm that the 365 nm UV lamp provides leading only to slow cure. However, the poor absorption behavior at other wavelength limits the ability of this photoinitiator to initiate reactions when either white light or blue light LED were applied (Figure 2.7). Therefore, matching photoinitiator absorption to the UV wavelength can be considered as an important factor in high-speed photopolymerization. Figure 2.8 demonstrates this effect with three pairs of photoinitiators and light sources. Each photoinitiator was reported to have a strong absorption at the wavelength applied. Therefore, our initial studies were undertaken with UV light. However, as we progress towards practical 3D printing we will revisit the choice of catalyst in the hope of transitioning away from UV. As shown in Figure 2.8, the fastest reaction rate achieved was 20 s with 10mol% TPO-L and 365 nm UV light. In the following study, this condition was applied exclusively unless otherwise specified.

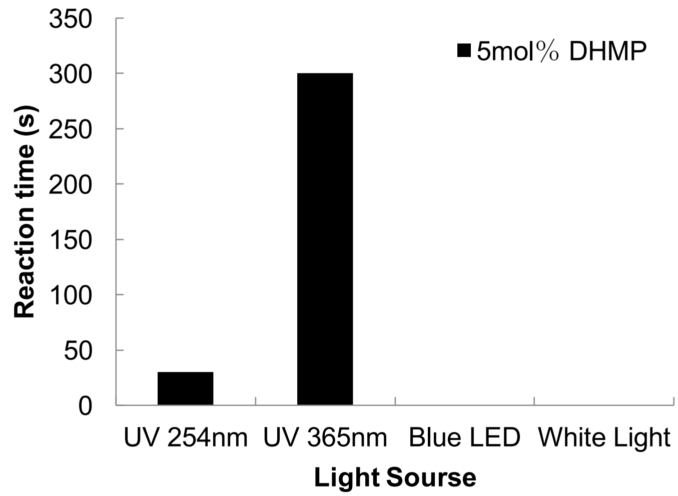

Figure 2.7 Reaction times of thin films with 5 mol% DHMP when different light sources were applied.

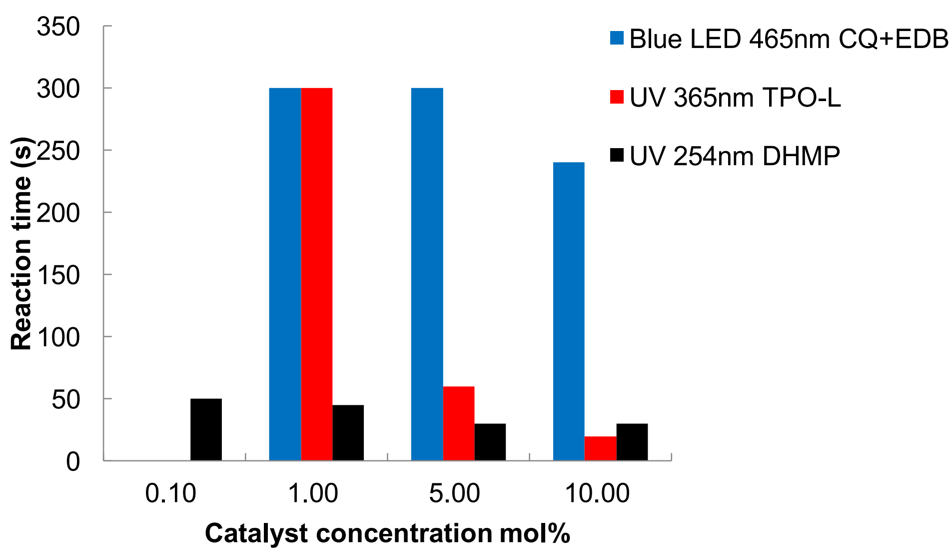

Figure 2.8 Reaction rates under various initiation systems.

2.3.4 Influence of Stoichiometric Ratio of SH and C=C on the Conversion of Functional Groups

During our initial study, we noticed that with a balanced stoichiometric ratio of functional groups, the surface of resulting elastomer was always tacky, especially when a high molecular weight base polymer was used. This phenomenon could be significantly improved by adding an excess of thiol PDMS. The study of the influence of the functional groups ratio **17**, **18** shows the full conversion of vinyl group the final crosslinked network does not occur at a balanced stoichiometry but instead at stoichiometric ratios higher than unity. This result indicates the imperfection of networks formed from vinyl: thiol ratios of 1:1. This could be attributed to an oxygen inhibition effect. In the thiol-ene reaction mechanism, a carbon radical is transferred to thiol group by hydrogen-abstraction process. The efficiency of his process must be related to the thiol concentration. With a lower thiol content, the carbon radical is more likely to be quenched by oxygen or coupling together, leading to a termination of the process.

2.3.5 Influence of Irradiation Time and UV Intensity on the Conversion of Functional Groups

The reaction kinetics of the crosslinking process was shown in Figure 2.9. A very fast initial reaction rate suggests it could be useful for 3D printing. At times less than 10 s, 50% of the vinyl groups had already been consumed, leading to a rapid increase in viscosity; the complete conversion of vinyl groups occurred within 1 minute. This should facilitate the printing process by holding the shape of printed parts before full crosslink and suggests the possibility of printing low viscosity inks.

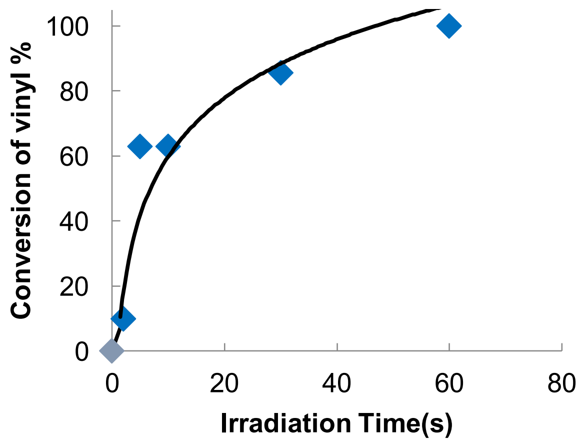

Figure 2.9 Conversion of vinyl functional groups at different irradiation time.

Since the photoinitiator is activated by UV light, it is necessary to study the influence of light intensity on the crosslinking process. With increasing UV intensity, reaction rates exhibited a significant initial increase then followed by a plateau (Figure 2.10). This strong dependence of reaction rates was a result of the larger number of photoinitiators excited at higher UV intensities. However, when the UV intensity was higher than 3.98 W/cm^2, the initiation step was no longer the rate limiting step in the process and the total reaction rate depended on propagation.

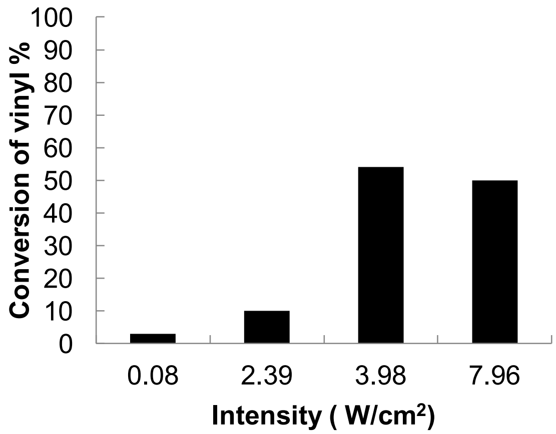

Figure 2.10 Impact of UV intensity on the conversion of vinyl groups.

2.3.6 Strategy of Adjusting Mechanical Properties

The mechanical properties were associated with the crosslink density and could be optimized by adjusting the structure of network. Harder materials formed when shorter silicone chains were found between each crosslink site. In this study, we are using two methods to control that: one involves varying the functionality of cross-linkers and the other is adding chain-extenders.

2.3.6.1 Influence of Cross-linker Functionality

Crosslinker functionality plays a critical role in elastomer crosslink density. Elastomers with higher moduli were expected when homopolymer crosslinkers were used. In our study, two kinds of thiol-functional PDMS crosslinker were studied (SMS-142 CL1, SMS-992 CL2, Figure 2.11). Unexpectedly, after an initial increase in moduli, the mechanical properties of elastomers started to decrease with an increase in CL2 concentration (Figure 2.12). This trend can be verified by Shore OO hardness data (Figure 2.12b). This phenomenon is most likely caused by the steric effects of homopolymer CL2. The decrease of moduli was result from the decrease of conversion.

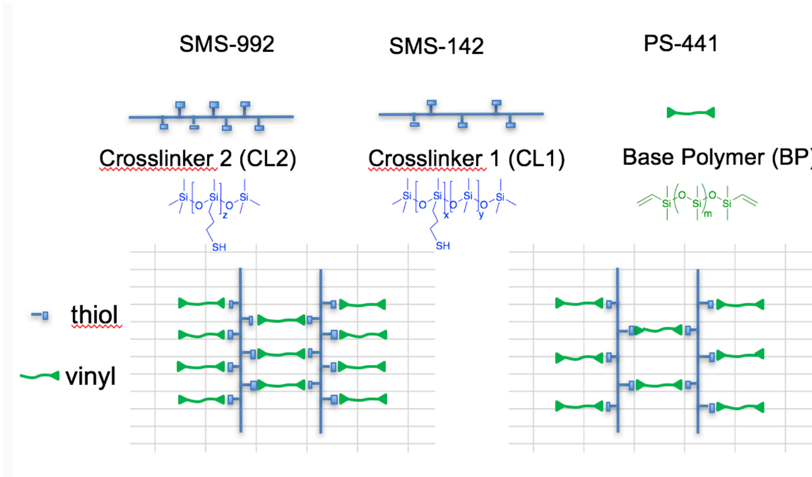

Figure 2.11 Crosslink density changes with different crosslinker.

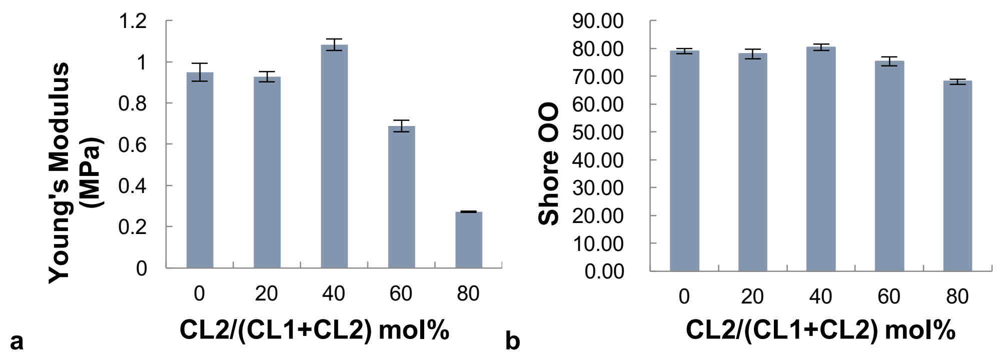

Figure 2.12 (a) Young's modulus, and; (b) Shore OO hardness changes with an increase in the concentration of CL2 (SMS-992) in the formulation.

2.3.6.2 Influence of Chain-extender

The traditional route to obtain low crosslink density materials uses vinyl-terminated PDMS spacers with different molecular weights. Silicone oils with higher molecular weight always present higher viscosities that could potentially cause mixing problems in 3D printing. In our research, an alternative route to prepare hardness tunable silicone elastomers with viscosity matched components was developed.

Two kinds of thiol-functional PDMS with similar viscosities (100 cSt) were used (SMS-142, SMS-022, Figure 2.13). SMS-142 acted as cross-linker in formulations to provide the necessary crosslink sites. The main purpose for SMS-022 was to extend the chain length of the vinyl-terminated PDMS spacer. An increase in chain-extender (SMS-022) concentration results in longer spacers and fewer crosslink sites, ultimately leading to more elastomeric and less brittle materials (Figure 2.13).

This was evident in the modulus of elastomers with different chain-extender concentration (Figure 2.14a), as well as the Shore OO hardness (Figure 2.14b). As the degree of crosslink decreased, softer elastomers were produced.

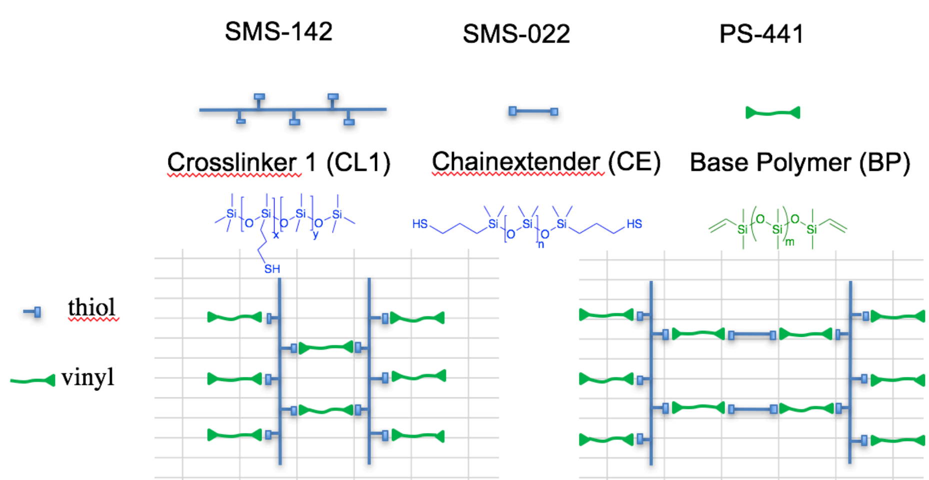

Figure 2.13 Crosslink density changes with the addition of chain-extender (SMS-022).

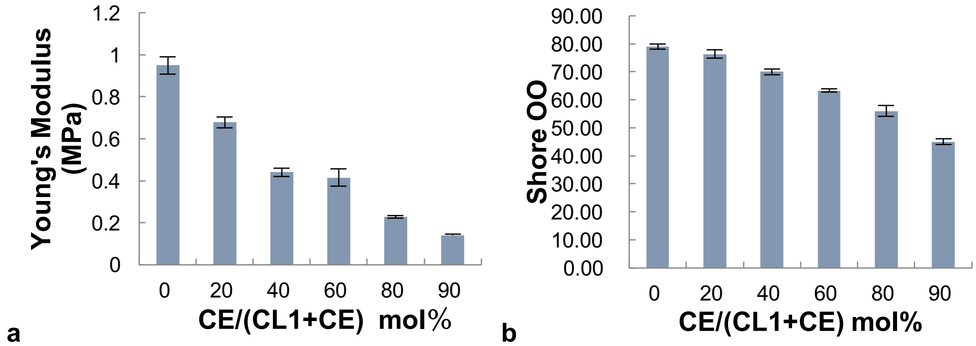

Figure 2.14 (a) Young's modulus, (b) Shore OO hardness changes with an increase in the concentration of chain-extender (SMS-022) in the formulation.

The combination of materials with different elastic properties led to non-homogeneous deformation phenomena that are exhibited in response to compressive forces. Figure 2.15 demonstrates the uneven deformation between different layers when compression force was applied. Similarly, an anisotropic material can be easily designed by the combination of materials with different moduli. Figure 2.15 shows the direction dependent elastic modulus of the multi-materials structure. The ability to control deformation over a wide range simply by tuning the formulation, thus, the elastic modulus and non-homogeneous deformation opens new opportunities for using such materials for various applications.

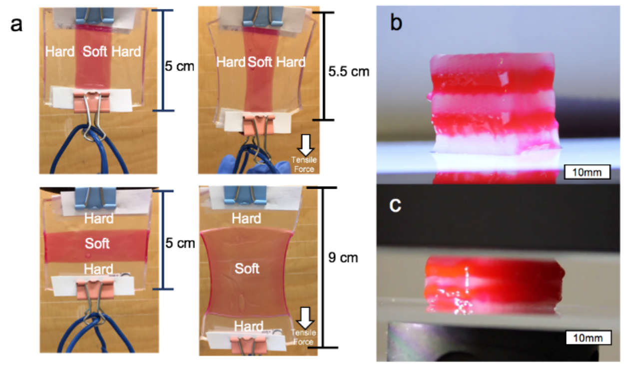

Figure 2.15 Deformation of different layers under tensile (a) and compression (b,c) force.

2.3.7 Highly Stretchable Formulation and Adhesion

A highly elastic behavior of the long chain-based polymer with a CL1- CE mixing ratio of 40:60 mol% is presented in Figure 2.16. It was observed that an increase of the chain length of base polymer not only leads to the decrease in Young's modulus from 0.414 ± 0.041 MPa to 0.051 ± 0.003 MPa (Table S2.3:**36,40**), but also significantly increases the elongation at break. The multi-layered elastomers can be stretched by up to 600%, which is around three times the elongation at break of commercial UV curable elastomers.[10] Figure 2.16 shows snapshots of a tensile test; a reasonable adhesion between different materials was observed. The intrinsic failure happened at stress 90 KPa before adhesion failure occurs.

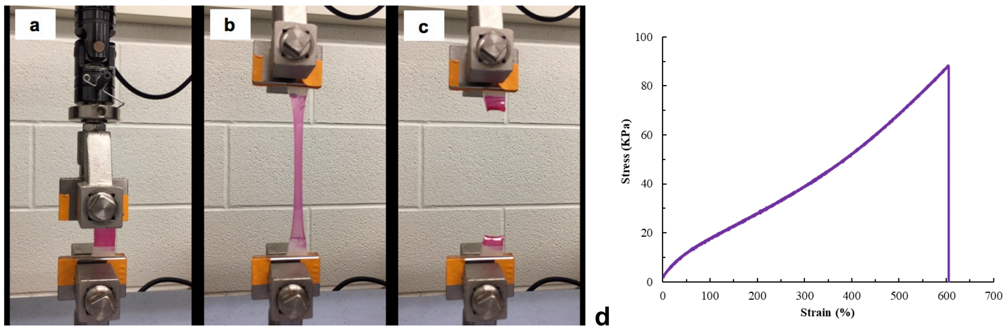

Figure 2.16 Snapshots of tensile test (a) 0% strain, (b) 600% strain, (c) after break, (d) stress-strain curve of multi-materials sample.

2.3.8 Tolerance to Fumed Silica

Silica is widely used as reinforce agent in PDMS formulations. In some cases, 20-30 wt% (or more) of fumed silica is added to improve mechanical properties. As shown in Figure 2.17, the optical property change as a function of silica concentration is very obvious: additional silica leads to loss of transparency. Besides, fillers also absorb light in the UV spectrum, particularly at the shorter wavelengths.[28] Thus, the adverse effect on the curing process in that UV absorption by silica needed to be studied.

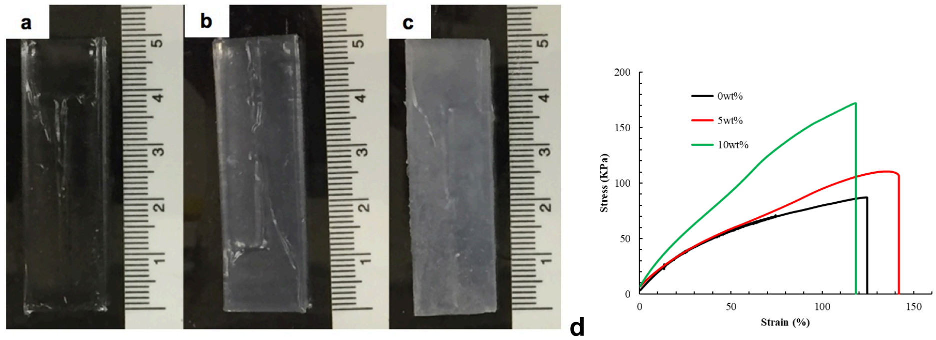

Figure 2.17 Optical properties of samples with different AEROSIL-150 concentration (a) 0 wt% (b) 5 wt%, (c) 10 wt%. (d) tensile test with different AEROSIL-150 concentrations.

The mechanical properties of fumed silica-reinforced elastomers were examined to demonstrate the influence of silica on the curing process. Higher mechanical properties should be expected as the result of the additional silica as reinforcing filler. However, if the curing process is inhibited by UV absorption of the filler, a decrease in mechanical properties will result from a lower crosslink density. The results of tensile test (Figure 2.17d, Table S2.4) show that break stress of elastomers increases with increasing concentration of silica in formulation. Note that with respect to break strain, a decrease in the trend was observed following the initial increase. This phenomenon is more likely caused by aggregation of fillers, leading to defects in microstructure. Thus, the presence of silica is highly compatible with this system providing the concentration is not too high.

2.3.9 Printed Structures

2.3.9.1 Demonstration of Extrusion Printing using Low Viscosity Inks

A simple cube structure with raster filling was used to show the feasibility of printing low viscosity inks by extrusion using the custom designed printer (Figure 2.18a, Figure 2.21). The results of printing (Figure 2.18) show that 3D structures (and voids) with good definition can be printed with these inks. The printed cube had a dimension of (19.6 mm (X) × 19.1 mm (Y) × 19.8 mm (Z)). The crosslinking of the ink under the UV illumination was fast, ensuring that the definition of the written pattern was maintained. The fast polymerization of the silicone led to line patterns with gaps between traces. The adhesion between the layers was found to be strong and the printed material was elastic as shown in Figure 2.18d.

Compression testing to failure was performed on the printed structure; the printed cube was able to withstand up to 200 N. The failure occurred along the edge of the cube, which is typical of bulk material failure rather than loss of adhesion between the layers (Figure 2.18e) This demonstrates that the ink and the printing process used produce structures that are mechanically similar to cast or injection molded structures.

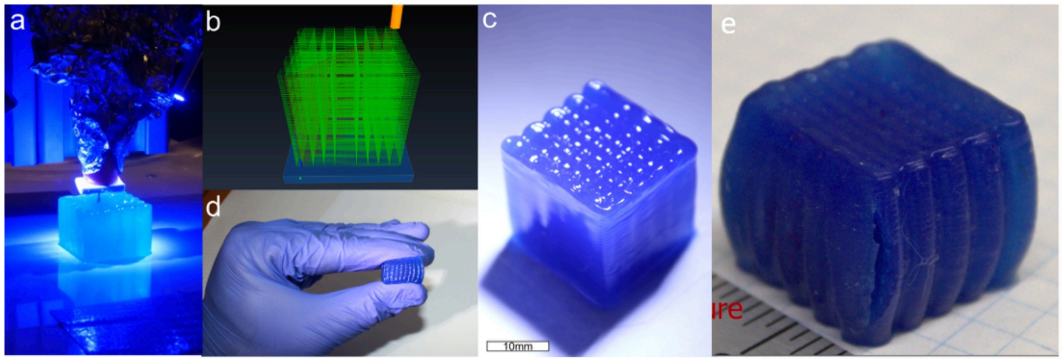

Figure 2.18 (a) A cube generated during the printing process. (b) The coded path used for the print. (c) The printed cube. (d) Demonstration of the elasticity of the cube. (e) Fractured cube after compression test.

2.3.9.2 Printing of High Aspect Ratio Structures

High viscosity silicone inks are normally used for 3D printing primarily because they can hold the shape of the print prior to cure. Low viscosity inks on the other hand are prone to dripping, spreading, or slumping upon contact with the printed part unless they are cured essentially instantaneously. In order to demonstrate that the low viscosity inks developed here can cure rapidly and retain their shape, a high aspect ratio cylindrical structure was printed (Figure 2.19).

The printed part as shown in Figure 2.19a had a diameter of 20.9 mm and a height of 20.8 mm and contained no voids or cavities. The thickness of the traced path was found to be 1.9 ± 0.1 mm, as shown in cross-section in Figure 2.19c, and was very consistent through the height of the structure, unlike high viscosity inks which create voids, cavities, and irregularities,[9] demonstrating the uniformity of the printing process. The aspect ratio of the printed structure was thus 10:1. This experiment demonstrates that the thiol-ene inks cure sufficiently fast that a second layer can be printed and cured on top of an already printed one within 3.7 s. The cross-section of the printed part in Figure 2.19c shows no voids or cavities between stacked traces, making for the smooth interface that is crucial to produce good mechanical properties for the printed part. Finally, it also demonstrates that the process is scalable and can be used to print high aspect ratio structures that are tall as long as the structural properties of the design allow the part to stay rigid during the printing process.

2.3.9.3 Printing using Discontinuous Flow

Conventional 3D printing using a positive displacement pump[6] is suitable for continuous printing but is difficult to use when discontinuous flow is needed. Use of pneumatic pressure allows precise stop and go operation to control the flow through the nozzle. We demonstrate the usefulness of the pneumatic control system by printing discrete features such as a 3D 'McMaster' sign without dripping, as shown in Figure 2.19d.

The printed part as shown in Figure 2.19d demonstrates that clean unconnected structures can be accurately printed in the discrete regions where the letters occur with little to no ink in the regions where the pressure was removed. Figure 2.22b shows the rapid moves in red and the printing moves in green in the design file.

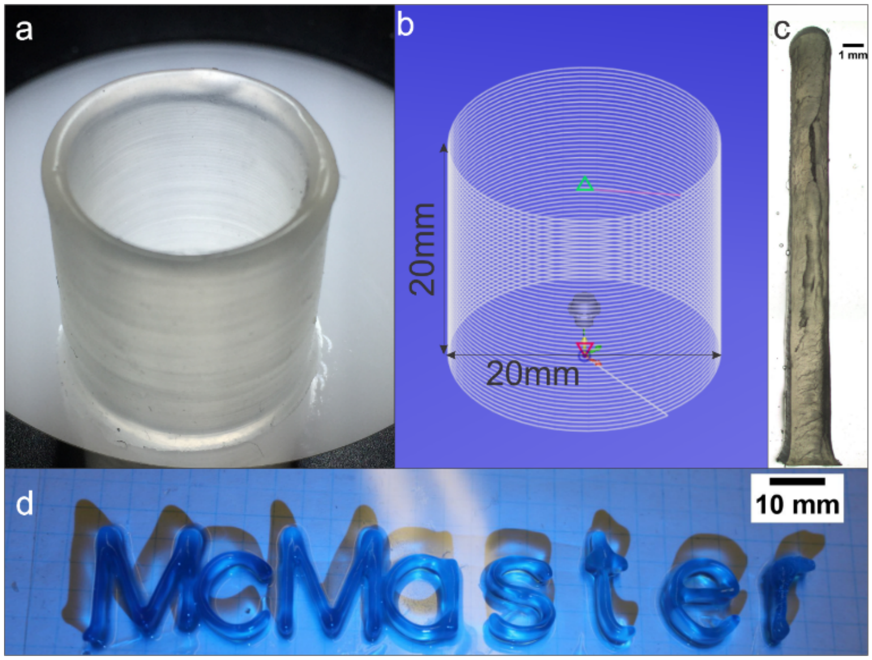

Figure 2.19 (a) A 50 layer helical cylinder object made from V21H ink (b) The toolpath for the print, with dimensions. (c) Z cross section of the cylinder, showing 50 layers merged together. (d) Print of text 'McMaster'. Each letter represents 30 layers of V31H ink.

2.3.9.4 Printing Overhanging Structures

Printing overhanging structures by extrusion printing can be quite challenging especially when low viscosity inks are used. The fast curing of thiol-ene cure inks provides the ability to print such structures without the use of sacrificial supports. For example, a hollow hemisphere structure was printed, with a diameter of 30 mm and a helical tool path with XY layers and layer spacing of 1.5°.

The printed part (Figure 2.20a) demonstrates that overhanging structures such as those that have a gradual curvature are readily printed using the fast curing inks. The dimensions of the design and the printed part match closely. The printed part was also found to be highly flexible as shown in Figure 2.20b and did not break apart even after extensive deformation.

2.3.9.5 Multi Ink Printing

The custom printhead developed here allows switching between different inks so that parts with different compositions, colors or mechanical properties can be printed. Note that multiple modulus objects cannot be prepared using with competing technologies such as DLP printing. The priming volume of the print head nozzle is currently 130 μl. Therefore, in order to change the ink, this volume of the ink already present in the printhead must be exhausted before the next ink can be extruded.

This mode of operation was shown by printing a cylinder consisting of alternate layers of two different inks (V31H blue, V35H red). The total print time was 3.4 minutes, which was comparable to the printing of a similar cylinder using a single ink (3.15 minutes). The printed structure shown in Figure 2.20c,d demonstrates that multi-ink printing using this mode is feasible and that the algorithm smoothly transitions from one ink to another to reproduce the designed alternate ink layers. Mechanical testing of the printed pattern showed that the layers were well bonded with each other; there was no delamination of the layers upon mechanical deformation.

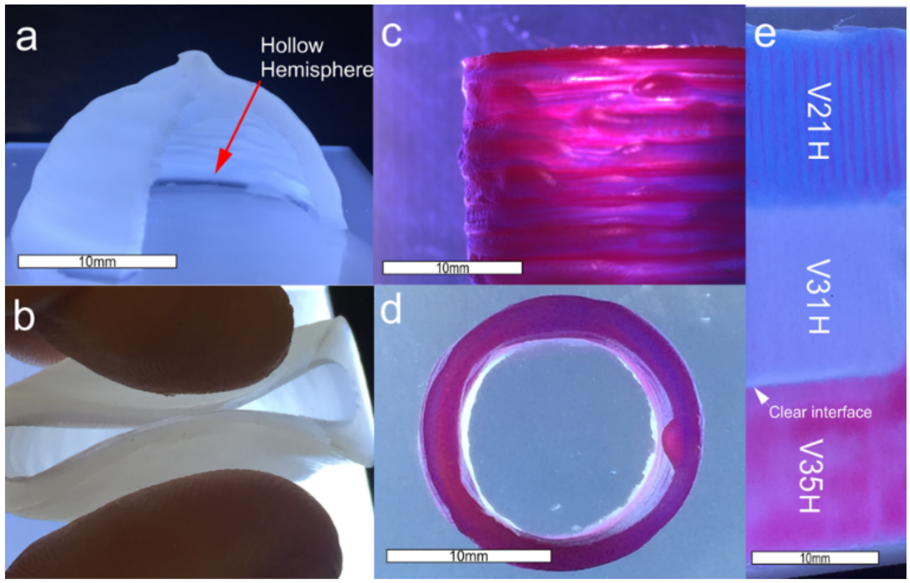

Figure 2.20 (a) A hollow hemisphere was printed without use of support material; the rapid curing rate of the ink was enough to form the overhanging angles in place (the 90° cut was introduced for clarity). (b) The flexibility of the as printed hemisphere is demonstrated. (c,d) Non-stop printing with ink changes; V35H is red and V31H is blue. (e) Silicone parts printed with three different inks.

Another mode of operation, which is useful when rapid transition of ink is not needed, allows all the regions in a single layer consisting of one ink to be printed first, followed by moving the printhead to a purge station to clear the printhead of the previous ink and then filling it with the next ink and resuming printing. This mode does not require anticipation of the ink in the tool path ahead of time and therefore the control algorithm is simpler. However, the time to print is extended by the number of ink switches and the time required for each switch. And of course, the process makes less efficient use of ink. This mode of operation was demonstrated by printing a slab of silicone consisting of three regions each consisting of a single ink. The V21H (blue), V31H (white), V35H (red) inks were used in the respective ink reservoirs and extruded through a 25G needle to print a

3-layer part (18 mm (X) × 45 mm (Y) × 2 mm (Z)). The reservoirs were pneumatically actuated for a given ink to extrude using a pressure of 207 kPa (30 psi). The total printing time was ~ 10 minutes, which included 9 ink changes with each of the ink changes taking 30 s to purge and refill the needle with the new ink. The printed part (Figure 2.20e) demonstrates that this mode was also suitable for printing certain designs that have large areas composed of a single ink. The ink changes and the switching times were larger in this mode.

Silicone elastomers have utility in a broad range of technical applications. 3D printing of silicone elastomers for these applications has been typically limited to extrusion of one part (one modulus) materials, or two part very high viscosity pre-elastomers leading, in most cases, to objects of a single modulus. The current work exhibits several advantages, particularly for soft elastomeric materials and gels, as a consequence of the use of low viscosity materials and of rapid cure. Elastomers of a different modulus are prepared by mixing, in different ratios, only two preformulated inks. Extrusion is delivered by low pressure devices that are readily controlled both for ink switching and for multi-element objects, without dripping during printing. In the latter case, rapid cure avoids the use of support material yet permits excellent adhesion between printed layers of the device, which may be differentiated by color or other constituents and modulus; slumping is not problematic.

2.4 Conclusions

A method based on efficient, rapid, and orthogonal thiol-ene reactions was developed for the synthesis of sulfur-containing silicone elastomers with varied and controlled mechanical properties. The approach above exhibits a variety of benefits. First, it avoids the use of the metal catalysts such as platinum or tin used in traditional processes, which may be disadvantageous for reasons of price or of potential toxicity. Second, the rapid reaction rate at room temperature even in the presence of oxygen makes it extremely suitable for 3D printing applications where the fidelity of products and print time are highly reliant on crosslink speed. Third, the use of light permits reactions directed to certain loci, unlike most thermal processes. Finally, the process allows elastomers with different physical and other properties to be readily prepared by manipulating ratios of chain-extender in the formula without the need for support materials. The low viscosity inks and the process are eminently suitable for 3D printing of soft silicone elastomers (Shore OO range). Multimaterials (3 different inks) were programmed to undergo, on demand, rapid printing of high aspect ratio, complex single printed part structures without need for supporting materials in some cases. This relied on efficient printing of low viscosity inks, and facile pressure driven switching from one ink to another. Synchronous control of the printer and multi-ink deposition was demonstrated. The printer technology is scalable to as many inks as required and can also be adapted for other polymer families with ease. In the future work, the resolution of the printed silicone parts will be investigated. The incorporation of microfluidic mixer printhead is another important development that needs to be made in order to achieve continues hardness change on fly. Moreover, the hardness of the current formulation falls in the range of Shore OO (11.0-79.0). The effect of the reinforcing agent on the transparency, curing degree, and mechanical properties needs to be well studied.

2.5 Experimental Section

2.5.1 Materials

Mercapto-functional silicones: 2-3% (mercaptopropyl)methylsiloxane-dimethylsiloxane copolymer (SMS-022, 100cSt, Lot#:4A-22039), 13-17% (mercaptopropyl)methylsiloxane-dimethylsiloxane copolymer (SMS-142, 100-200cSt, Lot#: 7J-31570), (mercaptopropyl)methylsiloxane homopolymer (SMS-992, 75-150cSt, Lot#: 8I-33907) were purchased from Gelest. Vinyl-functional silicones: α,ω-vinyl-terminated poly(dimethylsiloxane) copolymer (PS-441, MW 3853 g/mol, 100cSt, Lot#: 70532), α,ω-vinyl-terminated poly(dimethylsiloxane) copolymer (DMS-V31, DMS-V35 with molecular weights of 21497, 42303 g/mol, Lot#: 3B-19891, 8F-33461) were purchased from Petrarch Systems and Gelest respectively. Silicone oils: Decamethylcyclopentasiloxane (D_5, $(Me_2SiO)_5$) was purchased from Gelest. Photoinitiator TPO-L was received as a gift from IGM resins, Inc. 2-Hydroxy-2-methyl-propiophenone (DHMP), camphorquinone (CQ) and ethyl 4-(dimethylamino)benzoate (EDB) were purchased from Sigma-Aldrich.

Red Silc Pig silicone pigment was purchased from Smooth-On. Aerosil 150 was purchased from Evonic industries. All materials were used as received.

2.5.2 Methods

The molecular weights and conversion of functional groups were calculated from NMR spectra. NMR spectra were recorded using a Bruker Avance 600. The light source used in this work produces 365 nm UV light in high intensity (100 watt, Black-Ray B-100SP, 1.27 W/cm^2). 254 nm UV light was given produced using UV bulb. A blue LED array was used to give 465 nm light. The light source we used in 3D printing was Omnicure S1000 (100 watt, intensity :0 - 7.96 W/cm^2, major wavelength: 365 nm.

Shore OO durometers (Rex Gauge Company, Inc. U.S.) were used to characterize the hardness of the elastomers. The thickness of the sample for measurement is about 5 mm. The moduli of elastomers were determined using a MECH-1 micromechanical system (Biomomentum Instruments). All measurements were conducted at 22 °C and in triplicate, with error bars representing the standard deviation of the replicate measurements.

The tensile strength of silica/silicone elastomers was determined by a Universal Test System (INSTRON 3366, 50 N load cell). Rectangular samples (5cm × 1.5cm × 1.5mm) were prepared. The addition of small amounts of D_5 was required in some formulations to adjust the viscosities, thereby allowing for a homogeneous dispersion of reinforcing silica. After mixing in as planetary centrifugal mixer

(FlackTek Inc), samples were cast in mold and crosslinked with UV light (365 nm). The elastomers were put into 75 °C oven for 12 h to remove D_5 by evaporation. During tensile tests, the ends of the elastomers were clamped with grips, and then stretched using a crosshead speed of 5 mm/min. The dimensions (thickness and width) of tested elastomer specimens were measured with an electronic digital micrometer (Mitutoyo, Japan) at three random positions.

2.5.3 Synthesis of PDMS Thin Films

In a typical synthesis (shown for 3,850 MW PS-441 with SMS-142, 1:1 equiv. vinyl:SH, Table S2.1:**1**), PS-441 (0.5 g, 0.26 mmol), SMS-992 (0.21 g, 0.26mmol SH), 0.85 μl DHMP 50mg/ml stock solution (0.1 mol%, 0.026 mmol) were placed in a 25 ml glass vial. The content was stirred gently until a homogenous mixture was produced.

For films produced in air, 10 μl of the mixed silicone derivative and photoinitiator were placed on a glass slide. UV (254 nm) light was applied immediately. The resulting sample thickness was about 250 μm. Reaction time refers to the time from initially applying UV light to the time when a piece of cured film has been fully produced - such films were no longer tacky on the surface. All measurements were performed at least 3 times to ensure the reproducibility of the results (Table S2.1).

Alternatively, 10 μl of mixture was taken into glass slide and covered with thin quartz cover glass (Chemglass). The oxygen concentration was reduced using this approach. Immediately after, this glass slide was irradiated by UV (254 nm) light.

Reaction time refers to the time from applying UV (254 nm) light to the time the cover slide was stick. All the measurements were done in triplicate.

2.5.4 Synthesis of PDMS Elastomers

In a typical synthesis (shown for 3,859 MW PS-441 with SMS-142, 1:1.4 equiv. vinyl:SH, Table S2.3:**28**), PS-441 (2.0 g, 1.04 mmol vinyl), SMS-992 (0.133 g, 1.04 mmol SH), TPO-L (32.8 mg, 0.104 mmol) were placed in a 25 ml glass vial. The contents were stirred until a homogenous mixture was produced. The mixture (2 ml) was placed in a syringe that was used to inject the pre-cured materials into a 12-well plate that had been lined with Teflon. The PDMS elastomers could be formed by exposure to UV (365 nm) light for 10 min.

2.5.5 Preparation of Multi-moduli Materials

Sample for compression measurements (Figure 2.15) was prepared by adding mixture **33** (2 ml) in a 1.5 cm × 1.5 cm × 5 cm Teflon-lined mold. UV(365nm) light was applied for 10min to cure the elastomer. Red Silc Pig silicone pigment was added to **38** as a color modifier. That mixture (2 ml) was added on top of the initial layer. Again, 10 min UV (365 nm) was applied to cure the sample.

By alternating dispensing uncured materials and then exposing them to UV (365nm) light, a 5.0 cm × 5.0 cm × 0.1 cm multi-material sheet was prepared (Figure 2.18). The mixture **39** (3 ml) and **40** (3 ml) were added in 5 cm x 5 cm x 1 cm mold, which was divided into three parts. The barrier in each part was removed carefully. UV (365 nm) was applied for 10 min to cure the sample.

2.5.6 Preparation of UV Curable Thiol-ene Inks for 3D Printing

Three PDMS inks (Table S2.5) were formulated using PS-441, DMS V31, DMS V35 and thiol-functional PDMS. AEROSIL-150 (2 wt%) was added to increase the viscosity of the uncured ink, and to reinforce the resulting elastomer. Silc Pig silicone pigment was added to inks as color modifier. Each ink was prepared by adding one component at a time, proceeding from left to right in Table S2.5. After addition of all components, the inks were mixed in a planetary centrifugal mixer (FlackTek Inc) at 3000 rpm for 5 min.

2.5.7 Printer Design

A custom-made 3D printer was designed to extrusion-print these inks. The printer (shown in Figure 2.21) consisted of a number of components including a XYZ positioner, a multimaterial printhead, a UV illumination system, a pneumatic control system and an integrated computer control to synchronize the movement of the printhead with the pneumatic system.

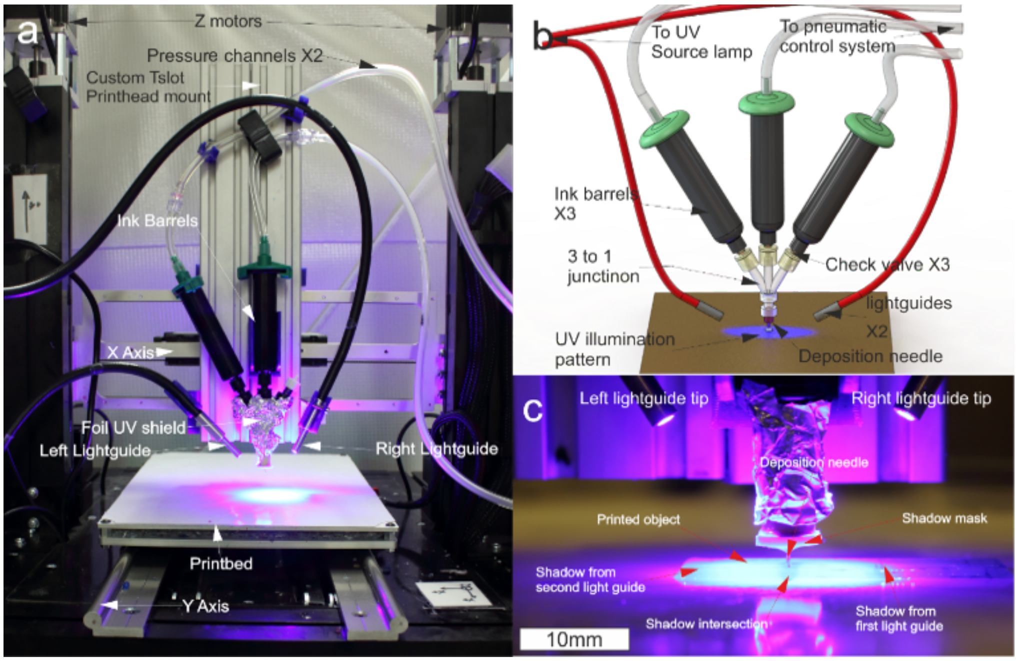

Figure 2.21 Illustration of the 3D printer. (a) Full view of the printer. (b) CAD model of the printhead consisting of the 3 ink reservoirs, attached to a common extrusion needle using a 3-way junction. (c) A zoom into the printing area, showing the arrangement of the lightguide tips, shadow mask, needle, and the resulting shadow pattern. A UV lamp (Omnicure S1000, vendor) along with two light guides (positioned 4cm away from the tip and at ~45° to the substrate) provided the illumination (~100 W in the 300-400 nm wavelength) to initiate crosslinking of the extruded material.

Flow from the reservoirs was controlled using pneumatic lines that applied a dynamic pressure head on them. In order to print a particular ink, its reservoir was pressurized while the other reservoirs were maintained at atmospheric pressure. A pressure control system consisting of a pressure source (620 kPa (90 psi)) with switchable solenoid valves was used to dynamically control the pressure on the reservoirs. The reservoirs were connected to the extrusion nozzle (blunt tip 413 µm, 22 Ga or 25 Ga needle) through a 3 to 1 flow mixer that merges the output of the reservoirs. The priming volume of the flow combiner was 130 µl, which determined the response time of the material switching, as well as the speed of the solenoid valve.

A single nozzle design was chosen rather than the multi nozzle design that is conventionally used for multimaterial printing, as the inks used are fast curing and UV sensitive. As is shown below, switching inks is straightforward. Reflection of UV light from the part or the substrate can easily cure material at the tip of other nozzles that are idling, leading to clogging and print failure in a multinozzle configuration. By contrast, in the case of the single nozzle, the material through the nozzle flows continuously while the UV light is on, thereby avoiding cross-linking and subsequent clogging of the needle.

2.5.8 Printing of a Cube

The cube (Figure 2.18, 19 mm (X) × 19 mm (Y) × 19.8 mm (Z) in the toolpath dimension) was printed using a V31H-based ink (and irradiation time 10 min.

Table S2.5) with a blue pigment additive (Smooth-On, Inc.) for easy visualization. An effective print rate of 4 $\mu l \cdot s^{-1}$ feed rate of 750 $mm \cdot min^{-1}$ with a tool path that consisted of 65 layers of overlay raster patterns in X and Y with 2 mm spacing between traces, and 0.3 mm layer spacing (Z) was used. The total print time was 34 minutes. The UV light intensity was set at ~ 95 W, the light guides were positioned 3.5 cm from the needle tip and at 45° to the plane, yielding 17 W cm^{-2} on average.

2.5.9 Printing of a Cylinder

The helical cylinder in Figure 5a, was printed using a V21H-based ink. The V21H ink (Table S6) was extruded through a 22 Ga needle tip using a pneumatic pressure of 24 kPa (3.5 psi), which produced a flow rate of 12.7 $\mu l \cdot s^{-1}$ while a helical tool path of 50 layers was traced. The designed dimensions of the cylinder were 20 mm in diameter and 20 mm in height encoded in a single width helix. The total time for the print was 3.15 minutes, which corresponds to 3.7 s per layer.

2.5.10 Printing of "McMaster" Sign

The V31H ink with a blue color additive (Smooth-On, Inc.) was extruded through a 25 Ga needle using 620 kPa pressure, which yielded a flow rate of 9 $\mu l \cdot s^{-1}$ when the pressure was on. The tool path spanned dimensions of 136 mm (X) × 54 mm (Y) × 4.7 mm (Z) and was divided into 30 layers with the layer spacing of 0.15 mm. The print process is shown in the supplementary information video SV4; the total print time was 18 min.

Figure 2.22 (a) The 'McMaster' sign printed in silicone elastomer. (b) The gcode illustration; printing moves are in green, while rapid non-printing moves are in red. The rapid moves are absent from the resulting print.

2.5.11 Printing of a Hemisphere

The V21H ink was used for printing with the same conditions as for the cylinder (24 kPa (3.5 psi), 12.7 $\mu l \cdot s^{-1}$). The time for printing the 60 helical layers was 220 s and the thickness of the structure was found to be 2.0 mm. The printed object is shown in Figure 6a.

2.5.12 Printing of Multi-ink Cylinders

In this design, the cylinder had a diameter of 15 mm and a height of 18.9 mm. Each layer was designed to be 0.35 mm in height and 54 such layers constituted the entire structure. This structure was printed using V31H and V35H inks (Table S2.5) extruded through a 25 Ga needle by applying 207 kPa (30 psi) to both the ink chambers to produces flow rates of ~1.5 $\mu l\ s^{-1}$ for V31H and ~1.5 $\mu l\ s^{-1}$ for V35H in a continuous manner; the ink was switched smoothly.

2.6 References

1. Cole, M. A.; Bowman, C. N., Synthesis and Characterization of Thiol–ene Functionalized Siloxanes and Evaluation of Their Crosslinked Network Properties. *J. Polym. Sci., Part A: Polym. Chem.* **2012,** *50* (20), 4325-4333.
2. Brook, M. A., *Silicon in Organic, Organometallic, and Polymer Chemistry*. Jhon Wiley & Sons, INC: 1999.
3. J. Chojnowski, M. C., Synthesis of Linear Polysiloxanes In *Silicon-Containing Polymers*, Springer Netherlands: 2000; pp 3-41.
4. Gross, P. G.; Kartalov, E. P.; Scherer, A.; Weiner, L. P., Applications of Microfluidics for Neuronal Studie*s. J. Neurol. Sci.* **2007***, 252* (2), 135-143.
5. Marie–Claire Be´ langer, Y. M., Hemocompatibility, Biocompatibility, Inflammatory and in Vivo Studies of Primary Reference Materials Low-Density Polyethylene and Polydimethylsiloxane: A Review. *J. Biomed. Mater. Res.* **2001,** *58* (5), 467-477.
6. Hardin, J. O.; Ober, T. J.; Valentine, A. D.; Lewis, J. A., Microfluidic Printheads for Multimaterial 3D Printing of Viscoelastic Inks. *Adv. Mater.* **2015,** *27* (21), 3279-3284.
7. Griffini, G.; Invernizzi, M.; Levi, M.; Natale, G.; Postiglione, G.; Turri, S., 3D-printable CFR Polymer Composites with Dual-cure Sequential IPNs. *Polymer* **2016,** *91*, 174-179.
8. Truby, R. L.; Lewis, J. A., Printing Soft Matter in Three Dimensions. *Nature* **2016,** *540* (7633), 371-378.
9. Muth, J. T.; Vogt, D. M.; Truby, R. L.; Menguc, Y.; Kolesky, D. B.; Wood, R. J.; Lewis, J. A., Embedded 3D printing of Strain Sensors within Highly Stretchable Elastomers. *Adv. Mater.* **2014,** *26* (36), 6307-6312.
10. Patel, D. K.; Sakhaei, A. H.; Layani, M.; Zhang, B.; Ge, Q.; Magdassi, S., Highly Stretchable and UV Curable Elastomers for Digital Light Processing Based 3D Printing. *Adv. Mater.* **2017,** *29*, 1606000.
11. Lauridsen, H.; Hansen, K.; Norgard, M. O.; Wang, T.; Pedersen, M., From Tissue to Silicon to Plastic: Three-dimensional Printing in Comparative Anatomy and Physiology. *R. Soc. Open Sci.* **2016,** *3* (3), 150643.
12. Stefan Baudis, D. B., Marica Markovic, Peter Gruber, Aleksandr Ovsianikov, Robert Liska, Modular Material System for the Microfabrication of Biocompatible Hydrogels Based on Thiol–Ene-Modified Poly(vinyl alcohol). *J. Polym. Sci. A Polym. Chem.* **2016,** *54*.
13. Au, A. K.; Huynh, W.; Horowitz, L. F.; Folch, A., 3D-Printed Microfluidics. *Angew. Chem.* **2016,** *55* (12), 3862-3881.

14. Rajendra, V.; Sicard, C.; Brennan, J. D.; Brook, M. A., Printing Silicone-based Hydrophobic Barriers on Paper for Microfluidic Assays using Low-cost Ink jet Printers. *The Analyst* **2014,** *139* (24), 6361-6365.
15. *Interim Report January-June 2015:3D Printing with Silicones*; Wacker Chemie AG: 2015; pp 5-10.
16. Selbertinger E., Achenbach F., Pachaly B., Method for Producing Silicone Elastomer Parts. *US patent* US20170312981A1. 2016.
17. Thomas J. Hinton, A. H., Kira Pusch, Andrew Lee, and Adam W. Feinberg, 3D Printing PDMS Elastomer in a Hydrophilic Support Bath via Freeform Reversible Embedding. *ACS Biomater. Sci. Eng.* **2016,** *2* (10), 1781-1786.
18. Grande, J. B.; Fawcett, A. S.; McLaughlin, A. J.; Gonzaga, F.; Bender, T. P.; Brook, M. A., Anhydrous Formation of Foamed Silicone Elastomers using the Piers–Rubinsztajn Reaction. *Polymer* **2012,** *53* (15), 3135-3142.
19. Hoyle, C. E.; Bowman, C. N., Thiol-ene Click Chemistry. *Angew. Chem.* **2010,** *49* (9), 1540-73.
20. Zonca, M. R.; Falk, B.; Crivello, J. V., LED-Induced Thiol-ene Photopolymerizations. *J. Maromol. Sci. A* **2004**, *41* (7), 741-756.
21. Uygun, M.; Tasdelen, M. A.; Yagci, Y., Influence of Type of Initiation on Thiol-Ene Click Chemistry. *Macromol. Chem. Phys.* **2010,** *211* (1), 103-110.
22. Hoyle, C. E.; Lee, T. Y.; Roper, T., Thiol-enes: Chemistry of the Past with Promise for the Future. *J. Polym. Sci., Part A: Polym. Chem.* **2004,** *42* (21), 5301-5338.
23. Devatha P.Nair, M. P. s., Shunsuke Chatani,Tao Gong,Weixian Xi,Christopher R. Fenoli, and Christopher N. Bowman,, The Thiol-Michael Addition Click Reaction: A Powerful and Widely Used Tool in Materials Chemistry. *Chem. Mater.* **2014,** *26*, 724-744.
24. Zhang, J.; Chen, Y.; Brook, M. A., Facile Functionalization of PDMS Elastomer Surfaces using Thiol-ene Click Chemistry. *Langmuir* **2013,** *29* (40), 12432-12442.
25. Kunze, U. M. a. A., Photocrosslinking of Silicones. Part 13. Photoinduced Thiol-ene Crosslinking of Modified Silicones *Pure Appl. Chem. A* **1996,** *33* (4), 439-457.
26. Otto van den Berg, L.-T. T. N., Roberto F. A. Teixeira, Fabienne Goethals, Ceren Özdilek, Stephane Berghmans, and Filip E. Du Prez, Low Modulus Dry Silicone-Gel Materials by Photoinduced Thiol−Ene Chemistry. *Macromolecules* **2014,** *26*, 724-744.
27. Nguyen, K. D. Q.; Megone, W. V.; Kong, D.; Gautrot, J. E., Ultrafast Diffusion-Controlled Thiol–ene Based Crosslinking of Silicone Elastomers with Tailored Mechanical Properties for Biomedical Applications. *Polym. Chem.* **2016,** *7* (33), 5281-5293.
28. Green, W. A., *Industrial Photoinitiators a Technical Guide* 2010.

.

Supporting Information

3D printable, Rapid Cure Silicone Elastomers Prepared using Thiol-ene "Click" Chemistry

Sijia Zheng,[a] Michael Zlatin,[b] Ponnambalam Ravi Selvaganapathy,[b] and Michael A. Brook[a]*

[a] Department of Chemistry and Chemical Biology, McMaster University, 1280 Main St. West, L8S 4M1, Ontario, Canada.

[b] Department of Mechanical Engineering, McMaster University, 1280 Main St. West, L8S 4M1, Ontario, Canada

* Corresponding author. Tel.: +1-905-525-9140; fax:+1 -905 522-2509; e-mail: mabrook@mcmaster.ca.

Table S2.1 Influence of catalyst concentration and oxygen inhibition on reaction time.

Exp #	PS-441 MW(g)	SMS-142 (g)	Photoinitiator (mol%)	Light source	Stoichiometry (vinyl:SH)	Reaction Time (s)	
						In air	No air
1	3,850(0.50)	0.21	DHMP (0.1)	UV (254nm)	1:1.4	50	2
2	3,850(0.50)	0.21	DHMP (1.0)	UV (254nm)	1:1.4	45	2
3	3,850(0.50)	0.21	DHMP (5.0)	UV (254nm)	1:1.4	30	2
4	3,850(0.50)	0.21	DHMP (10.0)	UV (254nm)	1:1.4	30	2
5	3,850(0.50)	0.21	TPO-L (0.1)	UV (365nm)	1:1.4	-[a]	10
6	3,850(0.50)	0.21	TPO-L (1.0)	UV (365nm)	1:1.4	300	5
7	3,850(0.50)	0.21	TPO-L (5.0)	UV (365nm)	1:1.4	60	2
8	3,850(0.50)	0.21	TPO-L (10.0)	UV (365nm)	1:1.4	20	2
9	3,850(0.50)	0.21	TPO-L (17.0)	UV (365nm)	1:1.4	20	2
10	3,850(0.50)	0.21	CQ+EDB (0.1)	Blue LED (465nm)	1:1.4	-[a]	60
11	3,850(0.50)	0.21	CQ+EDB (1.0)	Blue LED (465nm)	1:1.4	300	60
12	3,850(0.50)	0.21	CQ+EDB (5.0)	Blue LED (465nm)	1:1.4	300	60
13	3,850(0.50)	0.21	CQ+EDB (10.0)	Blue LED (465nm)	1:1.4	240	30
14	3,850(0.50)	0.21	DHMP (5.0)	UV (365nm)	1:1.4	300	-
15	3,850(0.50)	0.21	DHMP (5.0)	Blue LED (465nm)	1:1.4	-[a]	-
16	3,850(0.50)	0.21	DHMP (5.0)	White light	1:1.4	-[a]	-

[a] Materials did not cure in 10min.

Table S2.2 Influence of and UV intensity and irradiation time on degree of cure.[a]

Exp #	PS-441 MW(g)	SMS-142 (g)	Photoinitiator (mol%)	Light intensity (UV 365nm) W/cm^2	Irradiation time (s)	Stoichio-metry (vinyl:SH)	Conversion of vinyl group mol%
17	3,850(0.50)	0.15	TPO-L (10.0)	1.27	600	1:1	39
18	3,850(0.50)	0.21	TPO-L (10.0)	1.27	600	1:1.4	100
19	3,850(0.50)	0.21	TPO-L (10.0)	2.39	0	1:1.4	0
20	3,850(0.50)	0.21	TPO-L (10.0)	2.39	2	1:1.4	10
21	3,850(0.50)	0.21	TPO-L (10.0)	2.39	5	1:1.4	63
22	3,850(0.50)	0.21	TPO-L (10.0)	2.39	10	1:1.4	63
23	3,850(0.50)	0.21	TPO-L (10.0)	2.39	30	1:1.4	86
24	3,850(0.50)	0.21	TPO-L (10.0)	2.39	60	1:1.4	100
25	3,850(0.50)	0.21	TPO-L (10.0)	0.08	2	1:1.4	3
26	3,850(0.50)	0.21	TPO-L (10.0)	3.98	2	1:1.4	54
27	3,850(0.50)	0.21	TPO-L (10.0)	7.96	2	1:1.4	50

[a] Elastomer thickness: 0.6 mm

Table S2.3 Formulations for silicone elastomers with different modulus.[a]

	Parameters						Outcomes [c]	
Exp #	BP MW(g)	SMS-142 mol% (g)	SMS-992 mol% (g)	SMS-022 mol% (g)	Stoichio-metry (vinyl:SH)	TPO-L mol% (mg)	Shore OO	Young's Modulus (MPa)
28	3,850(2.00)	0(0.000)	100(0.133)	0(0.000)	1:1.4	10.0(32.8)	-[b]	-[b]
29	3,850(2.00)	20(0.171)	80(0.106)	0(0.000)	1:1.4	10.0(32.8)	68.0±1.0	0.273±0.002
30	3,850(2.00)	40(0.342)	60(0.080)	0(0.000)	1:1.4	10.0(32.8)	75.0±1.5	0.688±0.028
31	3,850(2.00)	60(0.513)	40(0.053)	0(0.000)	1:1.4	10.0(32.8)	80.3±1.2	1.081±0.028
32	3,850(2.00)	80(0.684)	20(0.027)	0(0.000)	1:1.4	10.0(32.8)	78.0±1.7	0.927±0.025
33	3,850(2.00)	100(0.854)	0(0.000)	0(0.000)	1:1.4	10.0(32.8)	79.0±0.8	0.949±0.042
34	3,850(2.00)	80(0.768)	0(0.000)	20(0.816)	1:1.4	10.0(32.8)	76.3±1.3	0.679±0.026
35	3,850(2.00)	60(0.576)	0(0.000)	40(1.936)	1:1.4	10.0(32.8)	70.0±0.8	0.440±0.020
36	3,850(2.00)	40(0.344)	0(0.000)	60(2.165)	1:1.4	10.0(32.8)	63.3±0.5	0.414±0.041
37	3,850(2.00)	20(0.172)	0(0.000)	80(2.898)	1:1.4	10.0(32.8)	56.0±1.6	0.228±0.005
38	3,850(2.00)	10(0.086)	0(0.000)	90(3.260)	1:1.4	10.0(32.8)	45.0 ±1.0	0.139 ±0.005
39	42.300(2.00)	100(0.0766)	0(0.000)	0(0.000)	1:1.4	10.0(2.98)[d]	62.3 ±0.5	0.285 ±0.017
40	42.300(2.00)	40(0.0308)	0(0.000)	60(0.0394)	1:1.4	10.0(2.98)[d]	11.0 ±0.8	0.051±0.003

[a] Light source: 365 nm UV, 1.27 W/cm^2 and irradiation time 10min; [b] Material did not cure in 10 min; [c] Sample thickness 5 mm

Table S2.4 Reagents used to study the tolerance of fumed silica.[a]

	Parameters					Outcomes	
Exp #	BP MW(g)	SMS-142 (g)	D_5 (ml)	TPO-L mol% (mg)	AEROSIL-150 wt%(g)	Break Stress (KPa)	Break Strain%
41	21,500(2.00)	0.15	3.0	10.0(5.88)	0(0.00)	87.03	124.61
42	21,500(2.00)	0.15	3.0	10.0(5.88)	5(0.10)	104.35	142.25
43	21,500(2.00)	0.15	3.0	10.0(5.88)	10(0.20)	171.98	118.41

[a] Light source: 365 nm UV, 1.27 W/cm^2 and irradiation time 10 min.

Table S2.5 Optimized formulations for 3D printing inks.[a]

Inks	Vinyl terminated silicone MW(g)	SMS-142 mol% (g)	SMS-022 mol% (g)	AEROSIL-150 wt%(g)
V21H	3,850 (10.00)	100 (4.20)	0 (0.00)	2 (0.37)
V31H	21,500 (10.00)	100 (0.75)	0 (0.00)	0 (0.00)
V31S	21,500 (10.00)	40 (0.30)	60 (1.65)	0 (0.00)
V35H	42,300 (10.00)	100 (0.38)	0 (0.00)	0 (0.00)

[a] Stoichiometry (vinyl/SH) =1:1.4, TPO-L 10 mol% (164 mg). Light source: Black-Ray B-100SP, 365 nm UV, 1.27 W/cm^2.

3 Chapter 3: Reversible Redox Cross-linking of Thiopropylsilicones

3.1 Abstract

Silicone elastomers can be reversibly cured and uncrosslinked using redox conditions. Thiopropyl-modified silicones were oxidized to elastomers with disulfide crosslinks using organosoluble oxidants such as $PhI(OAc)_2$. As with any elastomer, mechanical properties could be tuned by varying crosslink density. Uncrosslinking back to the same thiopropyl-modified silicones involved reductive S-S bridge cleavage using a Piers-Rubinsztajn reaction with hydrosilanes catalyzed by $B(C_6F_5)_3$; $HSiMe_2OSiMe_3$ was identified as a convenient reducing agent. The initially formed silicone-$(CH_2)_3S$-$SiMe_2OSiMe_3$ products needed deprotection with water in isopropanol/water to completely regenerate the thiopropylsilicones. This oxidation/reduction crosslinking/uncrosslinking cycle was practiced thrice, with essentially no change in the Young's moduli of the elastomers, or ^1H NMR spectra of the uncrosslinked fluids after reduction. Oxidation of thiopropylsilicones with aqueous bleach led instead to elastomeric foams, the pore sizes of which depended on the relative concentration of the bleach and total water/silicone ratio. At higher bleach concentrations, crosslinking via disulfide formation was accompanied by (over)oxidation to give some sulfonate groups that stabilized the internal pore

surface area. Dried foams could be used as storage vehicles for bleach, that was regenerated upon rehydration.

3.2 Introduction

Smart polymeric materials that can respond to a variety of stimuli (light, pH, temperature, redox reaction, electric fields or redox conditions, etc.) are attracting increasing attention.[1-3] One subset of these, materials that respond to redox conditions, have been examined for their utility in drug delivery,[4] reversible adhesives,[5] color-tunable materials for liquid crystal display,[6] etc. The use of redox chemistry as a trigger is appealing because it can be initiated electrically, or by using inorganic or organic oxidant/reductant pairs, including with biological systems. Reaction conditions are often mild.[7-9]

Extensive studies have been done to explore which molecular motifs have accessible and practicable redox properties; classic chemical examples include ferrocene, viologen, tetrathiafulvalene, naphthalene diimide, oligothiophene, disulfides, and tris(bipyridine)ruthenium.[8] Among these, disulfide/thiol pairs have long been highlighted because of their importance in biological processes. As is widely known, the glutathione (GSH) - glutathione disulfide redox couple plays an essential role in maintaining the redox potentials in the extracellular and intracellular media[10] and, moreover, is an important process for the formation/degradation of tertiary structure in proteins.[11] The ability to exploit the dynamic covalent features of disulfides has been extensively summarized in seminal reviews.[4, 12-13]

Only the reduction of disulfide linkages is typically used in the material design of redox sensitive polymers. Disulfide linkages are typically present in polymer networks from the incorporation of disulfide-containing monomers.[14-15] For example, Alyar et al[16] synthesized disulfide-containing acrylamide hydrogels by the radical polymerization of *N*,*N′*-bis(acryloyl)cysteamine with acrylamide. This hydrogel was readily reduced to water soluble thiol-containing copolymers by dithiothreitol; the materials were proposed to be employed in ophthalmological applications. Other disulfide-containing polymers have been reduced by agents including glutathione, dithiothreitol, and tris(2-carboxyethyl)phosphine, all of which require only mild reaction conditions. The relatively high cost of these reducing agents can restrict their application. In previous work, we reported a versatile, inexpensive method to reduce organic disulfide bonds with hydrosilanes.[17] We were interested to apply this method reversibly in redox sensitive silicone polymer networks.

The reverse reaction, oxidation of thiols, has been investigated much less frequently in polymer science. Oxidation reactions of thiol to disulfide conventionally involve metal-containing oxidants or catalysts, including Pd,[18] Fe,[19-20] Cu, Al, etc. Metal-free oxidation reagents that will oxidize thiols to disulfides include oxygen, iodine, sodium hypochlorite bleach, hydrogen peroxide,[21] and dimethyl sulfoxide,[22] among others. These reagents can suffer from disadvantages such as availability, difficult work-up, long reaction times, harsh reaction conditions, and/or toxicity.[23] Green methods for thiol oxidation are continually being developed as part of an increasing focus on sustainability. In a very relevant example, Abdel-Mohsen et al.[24] reported a new method for the oxidation of thiols to disulfides by oxygen in air using laccase as the catalyst. This process can achieve yields in up to 95% under mild conditions.

Silicones are an irreplaceable class of polymer materials due to their unique properties when compared to their carbon-based counterparts, which include thermal and chemical resistance, high oxygen, vapor permeability, weatherablity, etc.[25] They are highly stable to oxidation and UV radiation and, therefore, are used as seals for kitchen appliances and in aerospace, as wire coatings, and domes on LEDs.[26] However, silicones are rendered redox sensitive by the incorporation of organic groups, including allyl groups,[27] alcohols and thiols.

In the interest of developing green(er) silicone elastomers that can be reprocessed in the absence of metal oxidants or reductants, and inspired by the reversible redox processes that occur in living cells, we have examined the reactivity of thiol/disulfide couples within silicone networks. We report the use of various oxidants to facilitate the oxidation of thiopropylsilicones to elastomers, and the complementary reduction of those elastomers back to silicone oils. The synthetic processes, the properties of the elastomers in both foam and elastomer form, and the efficiency with which the processes can be reversibly practiced are examined in detail.

3.3 Experimental Section

3.3.1 Materials

2-3% (mercaptopropyl)methylsiloxane-dimethylsiloxane copolymer (SMS-022, Lot# 9B-35147, MW: 6000-8000 g/mol, viscosity: 120-180 cSt), 4-6% (mercaptopropyl)methylsiloxane-dimethylsiloxane copolymer (SMS-042, Lot# 8I-13501, MW: 6000-8000 g/mol, viscosity: 120-170 cSt), 13-17% (mercaptopropyl)methylsiloxane-dimethylsiloxane copolymer (SMS 142, Lot# 9H-36436, MW: 3000-4000 g/mol, viscosity: 100-200 cSt) were purchased from Gelest. Pentamethyldisiloxane (Penta-H) was purchased from Gelest and used after drying over molecular sieves overnight. Diacetoxyiodo benzene (Sigma-Aldrich), sodium hypochlorite solution (available chlorine 10-15%) and 1-dodecanethiol (Sigma-Aldrich), potassium iodide (Fisher Scientific), hydrochloric acid (Caledon Laboratory), sodium thiosulfate (Chem-Impex), and potato starch (EMD) were used as received. Blue food dye (for baking, McCormick) was purchased from a local grocery store. Solvents were purchased from Caledon Laboratories and used after drying over activated alumina. $B(C_6F_5)_3$ catalyst was prepared by a Grignard reaction following a literature procedure;[28] we acknowledge with gratitude Prof. David Emslie, McMaster University, for providing this sample. Deuterated NMR solvents were obtained from Cambridge Isotope Laboratories.

3.3.2 Methods

^{1}H NMR spectra were recorded on a Bruker Avance 600 MHz nuclear magnetic resonance spectrometer using deuterated solvents chloroform-*d* and dimethyl sulfoxide-d_6. The proton impurity of the deuterated solvent was calibrated to 7.26 ppm $CDCl_3$ and 2.50 ppm for DMSO.

The disulfide product of the model compound 1-dodecanethiol was characterized by GC/MS using an Agilent 6890N gas chromatograph (Santa Clara, CA, USA) coupled to an Agilent 5973 mass selective detector (MSD) run in EI mode. The sodium 1-dodecanesulfonate product was characterized by ESI-MS (Exactive Plus Orbitrap, Thermo Scientific, Waltham, Massachusetts).

The Young's moduli of rubber samples were determined using a MACH-1 micromechanical system (Biomomentum Instruments) with a 0.500 mm hemispherical indenter radius, and Poisson ratio of 0.5. All measurements were conducted at 22 °C and in triplicate, with error bars representing the standard deviation of the replicate measurements.

The pore size of sodium hypochlorite-cured foams were determined from photographs obtained with a Nikon Eclipse LV100 upright epifluorescence microscope; a 10X magnification lens was used. The pore diameters of 100 randomly chosen pores were analyzed by image J.

The contact angle of the silicone films was taken using an OCA 20 Future Digital Scientific system (Garden City, NY). 18.2 MΩ cm^{-1} water (3 µl of A10-Merck-Millipore system, Darmstadt, Germany) was placed onto PDMS films surfaces and digital images were acquired within 1 min.

3.3.3 Oxidation of Dodecanethiol, a Model Compound

The conditions for oxidation of 1-dodecanethiol are given in Figure 3.1a. The general experimental procedure is as follows. 1-Dodecanethiol (1.0g, 1.183ml, 5 mmol) was added to a 100ml round-bottomed flask to which was added diluted NaOCl solution (Table 3.1). The mixture was vigorously stirred for 18 h at room temperature. After reaction, hexanes (30ml) was added to extract unreacted products from the aqueous phase. The polar product sodium 1-dodecanesulfonate was observed as a precipitate from the hexanes phase. The hexanes phase was centrifuged (Thermo Electron, 4000 rpm) and the solids were washed with 3 x 10 ml hexanes to permit isolation of sodium 1-dodecanesulfonate (Table 3.1).

^{1}H NMR (600 MHz, DMSO-d_6) δ 0.86 (t, J = 6.8 Hz, 3H), 1.24 (d, J = 4.7 Hz, 18H), 1.53 (s, 2H), 2.29 - 2.37 (m, 2H). Low resolution mass spectrometry electrospray, negative ion mode): m/z 251.2 (M+1, 5), 250.2 (15), 249.2 (M-1, 100), 79.9 (10).

The nonpolar supernatants were combined and solvents were removed by rotary evaporation. The didodecyl disulfide product was examined using ^{1}H NMR, GC-MS.

^{1}H NMR (600 MHz, chloroform-*d*) δ 0.88 (t, *J* = 7.0 Hz, 3H), 1.19 - 1.42 (m, 19H), 1.61 (p, *J* = 7.3 Hz, 2H), 2.51 (q, *J* = 7.4 Hz, 2H). GC-MS, $C_{24}H_{50}S_2$, m/z 402 (60), 234(30), 201 (35), 97 (20), 85 (40), 71 (60), 57 (100).

3.3.4 NaOCl Disulfide Oxidation

Thiols were first oxidized to disulfides, which may undergo further oxidization. The oxidation of didodecyl disulfide with concentrated NaOCl was examined (SS/NaOCl = 1/13.8). White waxy didodecyl disulfide (0.5 g. 1.25 mmol) was added to a 50 ml round-bottomed flask, followed by undiluted NaOCl solution (concentration:1.84 mmol/ml, 9.2 ml, 16.9 mmol). The mixture was stirred vigorously using a magnetic stirrer at RT for 24h. After reaction, hexanes (~20ml) were added to extract products from the aqueous phase. The polar product sodium 1-dodecanesulfonate was observed as a precipitate from the hexanes phase. The hexanes phase was centrifuged (ThermoElectron, 4000 rpm) and the solids were washed with 3 x 5ml hexanes to permit isolation of sodium 1-dodecanesulfonate.

The results showed that the oxidation of disulfide to sulfonate was not efficient. Even with high concentrations of sodium hypochlorite solution, oxidative cleavage of the disulfide linkage occurred only in low yield to give sodium 1-dodecanesulfonate (0.024 g, 2.3%), even after 24 h.

Table 3.1 Oxidation of 1-Dodecanethiol by NaOCl.

Dodecane-thiol g (mmol)	Bleach concentration (mmol/ml)	Bleach volume (ml)	Stoichiometric ratio [SH]/[NaOCl]	Didodecyl-disulfide yield [a] [%]	Sodium 1-dodecane sulfonate yield [b] [%]
1.0 (5)	1.29	2.3	1:0.6	95	1.3
1.0 (5)	0.16	18.4	1:0.6	96	0.7
1.0 (5)	0.32	18.4	1:1.2	96	2
1.0 (5)	0.48	18.4	1:1.8	83	6
1.0 (5)	0.97	18.4	1:3.6	63*	17
1.0 (5)	1.29	18.4	1:4.8	42*	47
1.0 (5)	1.85	18.4	1:6.9	47*	50
0.5(2.5)[c]	1.85	25	1:18.8	15*	73

[a] Yield after removal of the sulfonate (*there are still traces of other oxidized species, as shown by ^1H NMR) (Figure S3.2).
[b] Isolated yields are reported.
[c] The thiol was added dropwise into a vigorously stirred, concentrated NaOCl solution.

3.3.5 Reductive Cleavage of RS-SR

The general reduction procedure was as follows: To a pre-dried 100 ml round-bottomed flask was added didodecyl disulfide (0.3 g, 0.75 mmol) and pentamethyldisiloxane (0.11 g, 0.89 mmol) in dry toluene (10 ml) as solvent. Freshly prepared $B(C_6F_5)_3$ stock solution was added (0.182 ml, 0.0178 mmol) after the starting materials had dissolved. After 3 h, the reaction was quenched by the addition of neutral alumina (~ 0.5 g). The reaction mixture, which contained silylated thiols (silyl thio ethers), was then filtered through a layer of Celite using a sintered glass funnel. The solution was concentrated using rotary evaporation.

Hydrolyses of the S-Si compounds to thiols were carried out by stirring the product in isopropanol/H_2O (80/20 v/v, in 5 ml) overnight, followed by purging with N_2. S-

Si cleavage was shown by the disappearance of peaks near 0 ppm in the ^{1}H NMR (Figure S3.3, Table 3.2).

Table 3.2 Reduction[a] of didodecyl disulfide (RS-SR) by hydrosilanes

RS-SR mg (mmol)	Penta-H ml (mmol)	SiH/SS	Yield [%][b]
300 (0.75)	0.173 (0.89)	1.2/1	50[c]
300 (0.75)	0.346 (1.78)	2.4/1	100

[a] Reaction conditions: 2 mol% $B(C_6F_5)_3$/SiH, 3 h, RT.
[b] NMR yield.
[c] The remaining material was starting didodecyl disulfide.

3.3.6 Silicone Elastomers, Foams and Films: General Procedures

Silicone elastomers: Details for the preparation of silicone elastomers by the oxidation of thiopropyl silicone oils are listed in Table 3.3. The general experimental procedure is as follows: thiopropyl-functionalized silicone SMS 042 (0.35 g, 0.17 mmol SH) or, in one case, SMS 022 (0.15 g, 0.04 mmol SH), was added to a polypropylene cup to which was added $PhI(OAc)_2$ solution (30 mg/ml, 30/70 v/v THF/ethyl acetate). The mixture was rapidly stirred and gelation occurred quickly (~10 s). The gel was left in a fumehood overnight to permit complete cure; the solvent used to dissolve the oxidant evaporated during this time to give transparent silicone elastomers.

Elastic foams: The formulations used for oxidative conversion of thiopropylsilicones into foams are given in Table 3.4. The general experimental procedure is as follows: thiopropyl-functional silicone SMS 042 (1.0 g, 0.49 mmol) was added to a well of a 12-well plate, to which was added the diluted NaOCl solution. Then the mixture was rapidly stirred and the content emulsified (~ 1 min); gelation occurred within ~ 5 min (the mixture would not flow when turn the plate was turned upside down). Then the reaction was left to undergo completion overnight.

Thin Foam Films: To more easily examine the morphology of the foam structures, foamed films (thickness: 200 μm) were prepared using the same formulation as the elastic foams. Once the thiopropyl-functionalized silicone and NaOCl solution mixture had emulsified, the emulsion was spread onto a PTFE substrate using a film applicator (Elcometer 3540/1 Four-Sided Film Applicator, 200 μm edge). The film was allowed to cure at RT for 48 h after which images were taken using a microscope (Nikon Eclipse LV100). ImageJ was used to analyze the average pore size of the films (100 pores were picked randomly).

3.3.7 Cleavage of Oxidatively Cured Elastomers, Followed by Recrosslinking

Silicone elastomers (2.0 g) were prepared by oxidizing thiopropyl-functionalized silicones with $PhI(OAc)_2$ as described above.

Oxidative Crosslinking: SMS 042 (2.0 g, 0.98 mmol of SH) was mixed rapidly with $PhI(OAc)_2$ solution (5.2 ml, 30 mg/ml in 30/70 v/v THF/ethyl acetate solution, 0.48 mmol). The mixture was quickly mixed and the gelation occurred ~ 10s after mixing. The gel was allowed to cure and dry overnight. Reductive Cleavage: To a dried 50 ml round-bottomed flask were added a silicone elastomer (2.0 g), pentamethyldisiloxane (279 μm, 1.45 mmol) and toluene (5ml), followed by

$B(C_6F_5)_3$ stock solution (0.0145 mmol, 1mol% vs Si-H). After the addition of catalyst, the solid elastomer began to fall apart within ~1 h. The reaction mixture was allowed to react for another 2 h in RT before neutral alumina (~0.5 g) was added to quench the catalyst. The reaction mixture was then filtered through a sintered glass filter funnel with a layer of Celite and the filtrate concentrated using rotary evaporation.

Desilylation: The desilylation process was performed by adding IPA/H_2O solution (5ml, IPA/H_2O 80/20 v/v) to the recovered oil and stirring for 18 h at room temperature. After the IPA was evaporated by rotary evaporation, hexane (~10 ml) was added to extract the recovered thiopropylsilicone oil. The hexane layer was separated by separatory funnel and sodium sulfate (~1 g) was added to dry the hexane solution. The sodium sulfate was then removed by filtration through a Buchner funnel and the solvent was removed by rotary evaporation. Yield 89%, 1.7754g (^{1}H NMR is shown in Figure S3.6).

Second Iteration: A new elastomer was prepared by oxidizing the thiopropylsilicone oil recovered above. Recovered silicone oil (0.5 g, 0.25 mmol of SH) was mixed rapidly with $PhI(OAc)_2$ solution (1.3 ml, 30 mg/ml in 30/70 v/v THF/ethyl acetate solution, 0.12 mmol). After rapid mixing, the mixture gelled (~10s). The mixture was allowed to cure and dry overnight and the Young's modulus was measured (Figure 3.3). An additional reduction/oxidation cycle was performed using the same protocol.

3.3.8 Cleavage of Oxidatively Cured Silicone Foams

Oxidatively cured foams were first prepared for reductive cleavage following the procedures above. Thiopropyl-functionalized silicone SMS 042 (1.0 g, 0.49 mmol of SH) was mixed rapidly with 1.9 ml diluted NaOCl solution (concentration: 0.23 mmol/ml, 0.44 mmol), then the emulsified mixture allowed to fully cure for 48 h. Three pieces of silicone foam were prepared for the subsequent reduction reaction. The cured wet foam was ground into crumbs (approximately 2-3 mm in diameter) using a mortar and pestle and purified by Soxhlet extraction with isopropanol over 24 h to remove water and other excipients. The extracted foam was dried at 60 °C in a vacuum oven for 48h (pressure: 25 mmHg). To a dried 50 ml round-bottomed flask, were added a silicone foam in crumb form (2.0 g), pentamethyldisiloxane (560 µm, 2.9 mmol) and toluene (5 ml), followed by $B(C_6F_5)_3$ solution (3 mol% vs SiH) was required for full cleavage of the foam). The mixture was allowed to react for 3 h in RT before neutral alumina (~0.5 g) was added to quench the catalyst. The reaction mixture was then filtered through a sintered glass filter funnel with a layer of Celite and the filtrate concentrated using rotary evaporation. The same desilylation process was performed using IPA/H_2O (80/20 v/v) as described above (for the ^{1}H NMR see Figure S3.7).

3.3.9 Surface Modification of S-S Crosslinked Silicone Elastomers

A silicone elastomer (0.5 g) was prepared by oxidizing thiopropyl silicone with $PhI(OAc)_2$. Thiopropyl-functionalized silicone SMS 042 (0.5 g, 0.25 mmol) was mixed rapidly with $PhI(OAc)_2$ solution (1.3 ml, 30mg/ml in 30/70 v/v THF/ethyl acetate solution, 0.125 mmol). After the mixture was cured and allowed to dry overnight, the product elastomer (0.5 g) was allowed to soak in concentrated NaOCl solution (1.85 mmol/ml) for 5 days. The elastomer was washed with DI water and dried in room temperature and contact angle measurements was made using imageJ (Figure 3.3g h).

3.3.10 Freeze Drying and Rehydration of Foams

Foams were prepared using bleach as described above (Table 3.4 Entry 4 and 9) and freeze dried using a VirTis BenchTop Pro Freeze Dryer for 3 days at -87 ◦C (Pressure: 37 mTorr). The freeze dried were then rehydrated in colored water (containing ~5 drops blue food coloring in 500 ml water, Figure 3.4g-j) for 24h. The rehydrated elastomers were wiped by Kimwipes. The mass of elastomers was recorded both before W_{dry} and after rehydration (W_{wet}). The water absorption was calculated: $(W_{wet}- W_{dry})/ W_{dry}$. The bleach in the rehydrated foam oxidized the blue food coloring.

3.4 Results and Discussion

3.4.1 Model Reaction: Oxidation of 1-Dodecanethiol with NaOCl

The oxidation of thiols can afford a variety of products ranging from the least oxidized – disulfides – to more highly oxidized sulfonic acids.[29] Prior to working with silicone elastomers, reaction conditions were optimized with the model compound 1-dodecanethiol. Conversion to the disulfide could be induced with dilute bleach (Figure 3.1a i); a small amount (0.7 %) of overoxidation byproduct sodium 1-dodecanesulfonate was observed by ESI and NMR (Figure S 3.1c). When more concentrated bleach was used, both disulfides and sulfonic acids were formed [S-S]/[SO_3^-] 15/73 (Figure 3.1a ii,Table 3.1); it was not possible in our hands to prepare the sulfonic acid exclusively. Finally, reductive cleavage of the disulfide product under Piers-Rubinsztajn conditions[30] – hydrosilane and $B(C_6F_5)_3$ catalyst – led to efficient recovery of the thiol starting material, initially protected as a silylsulfide. It has previously been reported that the hydrolysis of Si-S bonds is very facile, based on observations with $Me_3SiSSiMe_3$.[31] However, it was necessary to hydrolyze the SSi products in water/IPA overnight[17, 32] to produce the thiol (Figure 3.1a ii, iii, Figure S3.3, Figure S3.4).

3.4.2 Redox Elastomers: Oxidative Cure to Give Disulfide Linked Silicone Elastomers

Analogous protocols were used to prepare and then uncrosslink silicone elastomers (Figure 3.1b). Initially, to avoid two phase reactions (e.g., between bleach and silicone), the organic oxidant $PhI(OAc)_2$ was used to oxidatively crosslink thiopropylsilicones; this compound completely converts 4-chlorothiophenol into its disulfide product within 5 minutes at room temperature.[33] The mixture of thiopropyl-modified silicone oil and $PhI(OAc)_2$ solution gelled within 10s, indicating the efficient formation of disulfide linkages. After the solvents (required to solubilize the oxidant) were allowed to evaporate overnight, a transparent silicone elastomer formed. The crosslink density of the resulting disulfide elastomer, as reflected by the Young's modulus, could be easily tuned either by controlling the density of thiopropyl groups in the silicone oil starting materials, or the amount of chain-extender (SMS 022) added (Table 3.3).

3.4.3 Redox Elastomers: Reductive Cleavage of Silicone Elastomers with Hydrosilanes

Disulfide-linked silicone elastomers were successfully cleaved using pentamethyldisiloxane in the presence of $B(C_6F_5)_3$ concentration (1mol% vs SiH). Successful cleavage could be seen by the conversion of solid elastomers into fluids (Figure 3.2a to b, c); the ^{1}H NMR spectra of the recovered oils were identical to the thiopropyl silicone starting materials (Figure S3.6).

The iterative crosslinking/decrosslinking process was reproduced three times to ensure the oxidation/reduction cycle was robust. The elastomer Figure 3.2d) was reduced using with the same protocol reported above to make thiopropyl silicone oil (^{1}H NMR shown in Figure S3.6). The successful recovery of the thiopropylsilicone oil from reduction of an elastomer was demonstrated by using the recovered thiopropylsilicones to make new elastomers. The oxidation/reduction process was practiced twice more. As shown in Table 3.3, the elastomer made from a second and third iterations showed a similar Young's moduli to the original elastomer.

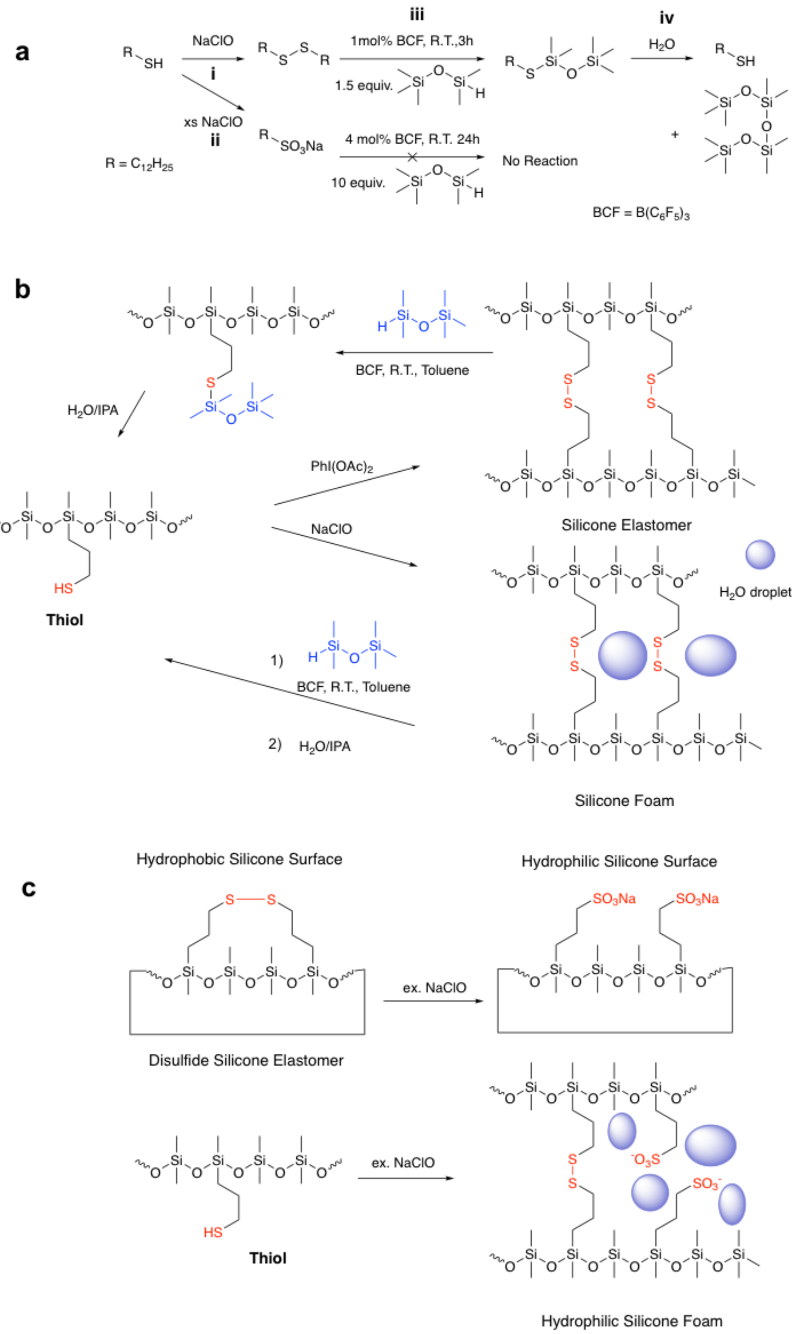

Figure 3.1 (a) Thiol oxidation and disulfide reduction with dodecanethiol/disulfide. (b) Preparation of elastomers using an organic soluble ($PhI(OAc)_2$) oxidant and silicone foam by using aqueous oxidants (NaOCl). (c) Using overoxidation to control hydrophilicity of the surface or bulk material.

Table 3.3 Preparation of disulfide-crosslinked silicone elastomers with different crosslink densities by oxidation with $PhI(OAc)_2$.

Entry 1 2 3 4

Entry	SMS 142 13-17 mol% SH(g)	SMS 042 4-6 mo% SH(g)	SMS 022 2-3 mol% SH(g)	$PhI(OAc)_2$[b] (g)	SS concentration in elastomer mmol/g	Young Modulus (MPa)
1	-	0.35	0.15	0.0343	0.21	0.047±0.001
2	-	0.4	0.1	0.0350	0.22	0.211±0.005
3		0.5		0.0380	0.24	0.242±0.011
4	0.1	0.4	-	0.0894	0.37	0.384±0.011
Iterative oxidation (SS formation) and PR cleavage)						
5	-	0.5[c]	-	0.0380	0.24	0.242±0.011
6	-	0.5[c]	-	0.0380	0.24	0.250±0.089
7	-	0.5[c]	-	0.0380	0.24	0.230±0.073

[a] Chain extender: pendent thiopropyl silicone oil with average two SH function groups on every chain. [b] The oxidant was dissolved in 30/70 v/v THF/ethyl acetate solution. 0.5 equiv. of $PhI(OAc)_2$ vis SH was added. Iterative processes: [c] First formed elastomer. [d] Elastomer made from recovered oil after reduction of first formed elastomer. [e] Elastomer made from recovered oil after second formed elastomer.

3.4.4 Redox Foams: Oxidative Cure to Give Silicone Foams

Silicones are notoriously insoluble in water. However, it was rather easy to disperse thiopropylsilicones into aqueous bleach. Milky emulsions formed within ~1 minute by mixing with a spatula (~ 200 rpm) that cured into shape-holding hydrogel within 5 minutes; full cure required ~18 h. Unlike the model compound, where 0.6 equivalent of NaOCl was sufficient for convert thiols to disulfide product, a slightly higher amount of NaOCl was required for full consumption of thiols. The stoichiometric deviation from the model study is probably a consequence of low mobility of functional groups when locked in the polymer network. After the reaction was complete, the foam was kept at room temperature. As can be seen in Table 3.4, it was possible to control the Young's moduli of the silicone foams simply by controlling the NaOCl concentration; the hardest materials were achieved when a near stoichiometric quantity of bleach to SH groups was added (as shown in Figure S3.5, the ^{1}H NMR of a swelled silicone elastomer prepared using 0.6 equivalent NaOCl still showed peaks associated with residual starting material). The foam density could be easily tailored by the volume ratio of silicone to NaOCl solution; foams containing 24-70 wt% water content were successfully prepared (Table 3.4, Figure 3.2e-g).

3.4.5 Redox Foams: Cleavage of Silicone Foam with Hydrosilanes

The ability to convert NaOCl cured silicone foam back to oils was also examined by reductive cleavage of the disulfide linkage. The silicone foam prepared was initially purified by Soxhlet extraction using IPA to remove any the residual oxidant and water.[34] After drying in a 60 °C oven for 48 h the foam was successfully converted to oils, but higher concentrations of $B(C_6F_5)_3$ (3 mol% vs SiH) were required for foams than elastomers. Although a liquid formed, it was slightly opaque because it contained both free thiols and a small amount of sulfonate groups (Figure 3.2i).

Table 3.4 Silicone foams and films by oxidation of thiopropylsilicone with NaOCl.[a]

Entry	Bleach concentration[b] (mmol/ml)	SH/oxidizing agent Stoichiometric ratio	Volume of bleach (ml)	Water Content wt%	Young's Modulus[c] (MPa)
1	0.16	1:0.6	1.853	65	-[d]
2	1.85	1:1.2	0.315	24	0.283±0.013
3	0.54	1:1.2	1.065	52	0.351±0.020
4	0.32	1:1.2	1.853	65	0.151±0.001
5	0.25	1:1.2	2.315	70	0.206±0.005
6	0.48	1:1.8	1.853	65	0.205±0.007
7	0.97	1:3.6	1.853	65	0.183±0.004
8	1.29	1:4.8	1.853	65	0.139±0.002
9	1.85	1:6.9	1.853	65	0.114±0.007
10	0.32	1:1.2	0.926	65	0.137± 0.013

[a] For entries 1-9, the starting silicone oil SMS 042 4-6 mol%SH (7000 g/mmol) 1 g (0.49 mmol SH). For entry 10, recovered thiol silicone oil after reduce Entry 4 (0.5g. 0.25 mmol of SH).
[b] NaOCl (11.5wt%) solution, diluted by different amounts of water.
[c] Young's modulus was measured 48h after the foam was made.
[d] The foam was too soft to test (<0.05 MPa, lower than test minimum limit).
[e] PDMS-SH was recovered after reduction of the material by hydrosilane with the present of $B(C_6F_5)_3$ catalyst.

As with the elastomers, the oxidation/reduction process could be practiced iteratively. A new silicone foam prepared in a second iteration from oils arising from the first iteration had a similar Young's modulus (0.14 MPa for the foam prepared from recovered oil vs 0.15 MPa for foam made from virgin starting materials, Figure 3.2h-k).

The need for higher concentrations of $B(C_6F_5)_3$ and Si-H reagents to reduce the foam, compared to the elastomer, may be due to the existence of a small amount of overoxidation products besides sulfonate (Figure S3.2), That is, the aqueous process is more difficult to control. As Porwal and coworker demonstrated, sulfoxides and sulfones may be reduced to sulfides with 10 equiv. of hydrosilane and 10mol% $B(C_6F_5)_3$ concentration.[35] While sulfonate groups cannot be reduced under the conditions we applied during foam reduction, other functional groups with higher sulfur oxidation states may be reduced by these harsher conditions (higher $B(C_6F_5)_3$ and Si-H concentration).

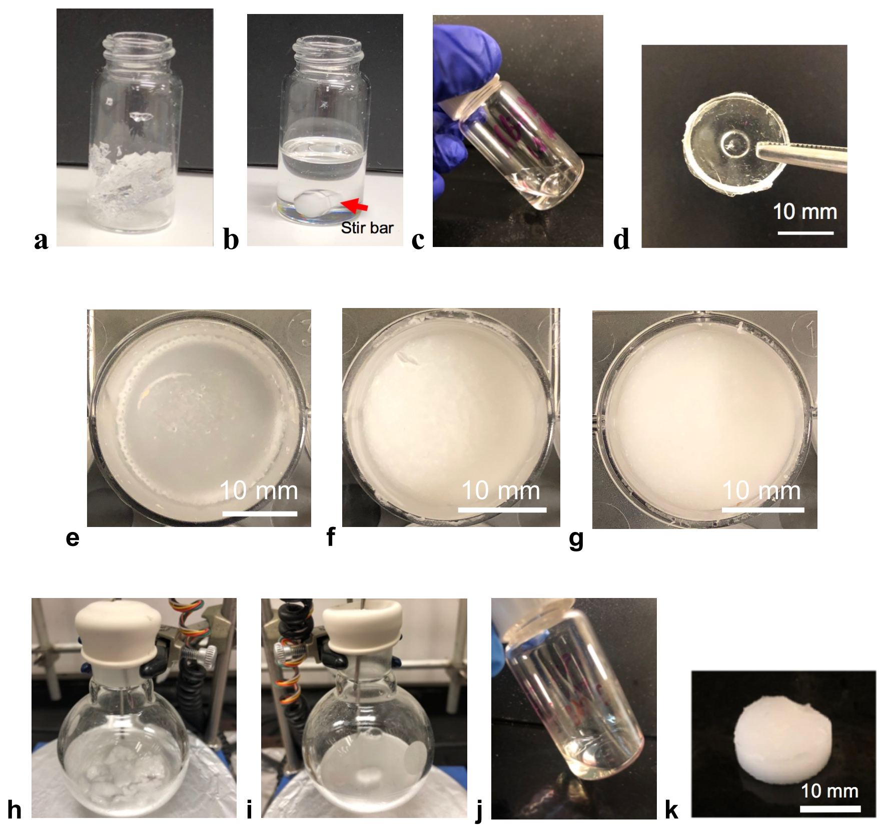

Figure 3.2 (a) Silicone elastomer was swelled in toluene before reduction. (b) Reaction mixture after 30 minutes. (c) Recovered oil after solvents were evaporated. (d) Re-crosslinked silicone elastomers. Silicone foams prepared by oxidizing thiopropylsilicone oils with 1.2 equiv. of NaOCl solution, aqueous fraction in the foam (e) 24 wt%; (f) 52 wt%; (g) 70 wt%. (h) Disulfide-linked silicone foams swollen in toluene. (i) Reaction mixture after 30 minutes. (j) Recovered oil after solvents were evaporated. (k) Recrosslinked silicone foam.

3.4.6 Benefits of Overoxidation: Controlling Surface Hydrophilicity of Elastomers and Controlling Foam Structure

Pure silicone elastomers have sessile water drop contact angles >100°.[36] Foams prepared with higher bleach concentrations had a greater extent of surface oxidation, as shown from the lower static water droplet contact angles (Figure 3.3a-f). This is consistent with an increase in the fraction of thiol groups that were oxidized to sulfonate (note: the film made by SH/NaOCl=1/0.6 (Figure 3.3a) was exceptional, exhibiting a decrease in contact angle from 109° to 102°. This increase wettability is probably a consequence of surface roughness as shown in microscope picture (Figure 3.4a).

Analogous oxidation of a preformed disulfide-crosslinked silicone elastomer using NaOCl solution also led to surface oxidation of sulfur moieties, as shown by the decrease of contact angle from 107° for the unmodified disulfide silicone to 58° for the surface modified one (Figure 3.3h vs g). In this case, only the surface is oxidized, unlike the foam that will also be oxidized on the internal pore surfaces.

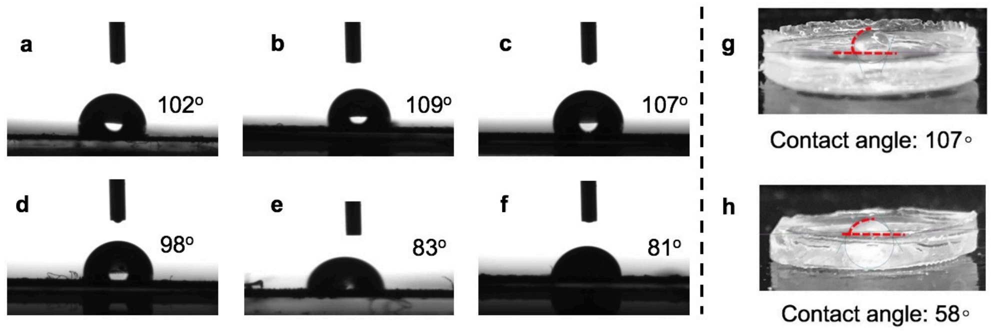

Figure 3.3 Contact angle of silicone foams prepared with different concentration of bleach. (a) SH/NaOCl=1/0.6; (b) SH/NaOCl=1/1.2; (c) SH/NaOCl=1/1.8; (d) SH/NaOCl=1/3.6; (e) SH/NaOCl=1/4.8; (f) SH/NaOCl=1/6.9. Oxidative surface modification of disulfide-linked silicone elastomer. (g) Unmodified disulfide elastomer. Table 3.3, Entry 3. (h) After soaking in a concentrated NaOCl solution (1.85mmol/ml) for 5 days.

The analogous introduction of hydrophilic groups on the silicone backbone will convey changes to the properties of the bulk materials. In the case of foams, the change of hydrophilicity with increasing levels of oxidation manifested as a larger number of small pores in the foam, which reflects a larger hydrophilic surface area. As shown in Figure 3.4a-f, the pore size of the crosslinked foams decreased from 82 to 8.6μm with more bleach leading to a higher internal concentration of SO_3^- groups.

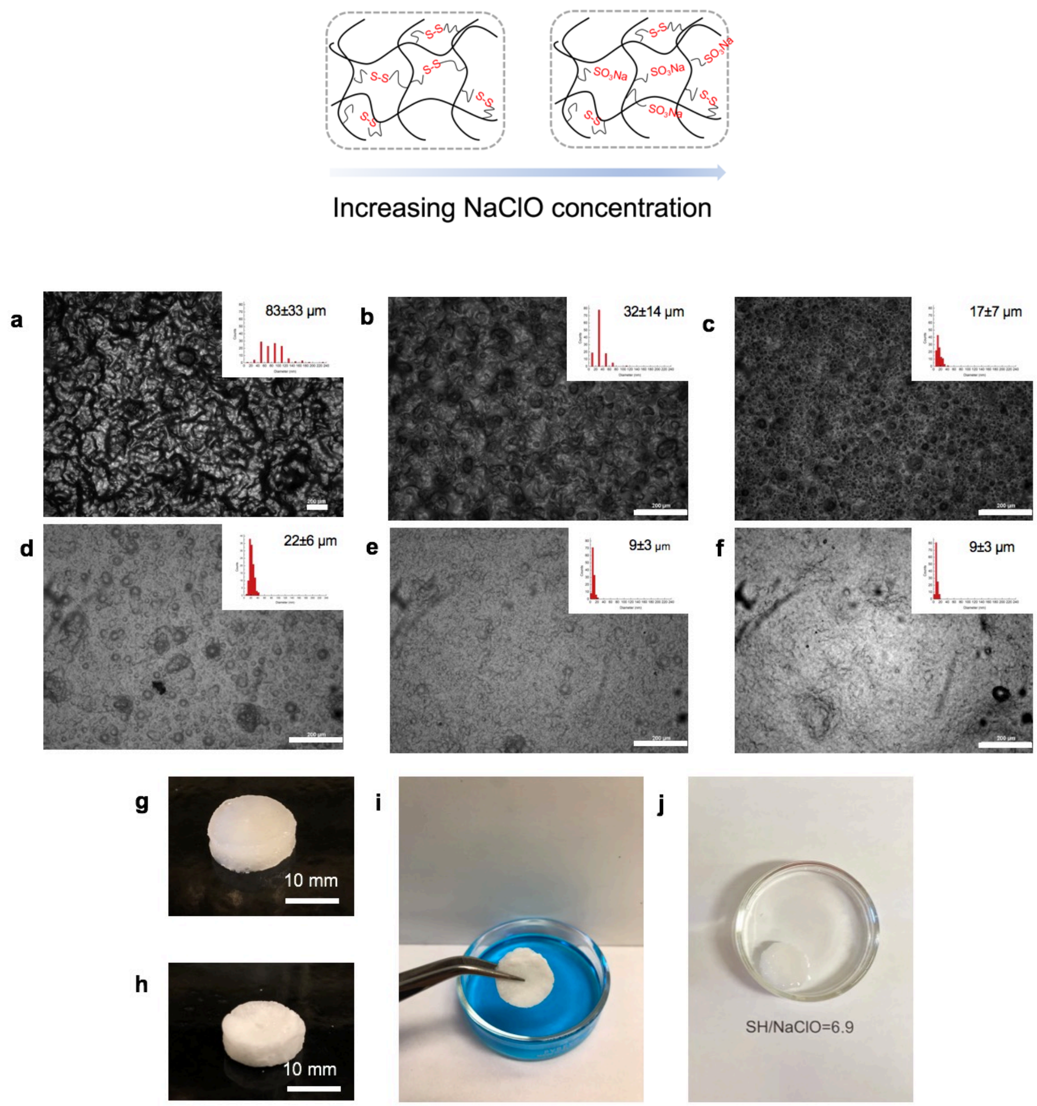

Figure 3.4 Microscope photos of silicone foams (a) SH/NaOCl=1/0.6; (b) SH/NaOCl=1/1.2; (c) SH/NaOCl=1/1.8; (d) SH/NaOCl=1/3.6; (e) SH/NaOCl=1/4.8; (f) SH/NaOCl=1/6.9; the x axis for the inset is the diameter of the pore size (0-240 µm); the y axis for the inset is the count number of the pores (0-90). Size bar=200 µm. (g) Silicone gel created from hypochlorite and thiopropylsilicones. (h) Silicone foam after freeze drying. (i) Rehydration of the dry silicone foam with colored water. (j) The hydrated foam after 24h. The blue food coloring dye in the water solution was bleached by the residual NaOCl trapped in the foam.

3.4.7 Rehydration of Foams

The equilibrium amount of water in the foams was measured after 24 hours. The sample with the highest concentration of SO_3^- absorbed the most water (148 wt % over 24 h), while foams with lower [SO_3^-] absorbed considerably less (25 wt % over 24 h). From these data, it is clear that these reactions permit the design of hydrophilic silicone foams. Surprisingly, any excess sodium hypochlorite present in the foam remains active even after the sample was freeze dried for 3 days and then rehydrated; its ability to bleach the blue food coloring after rehydration is shown in Figure 3.4i→j. This opens the potential utility of these foams as delivery vehicles for bleach in application such as eczema treatment, bleaching, deodorizing, etc., where bleach must be stored for extended periods of time.

The synthetic flexibility demonstrated in biology with the thiol/disulfide redox couple is mimicked in the silicone elastomers described above. Organic oxidation cleanly converts thiopropyl oils into elastomers under mild conditions. Aqueous oxidation leads instead to silicone foams, the porosity of which depends on both the quantity of oxidant and of water. Overoxidation to form sulfonates can be utilized to increase the internal surface area in foams, or to decrease the water contact angle of elastomeric surfaces. Both elastomers and elastomeric foams can be reduced to silyl-protected thiopropylsilicones oils using Piers-Rubinsztajn conditions. The oxidation/reduction cycle can be repeated several times.

3.5 Conclusions

Thiol groups are easily oxidized by various oxidants. In this work, redox reversible silicone foams and elastomers were created based on the ease of disulfide formation and cleavage. Commercial thiol-functionalized silicones were crosslinked by aqueous oxidants (NaOCl) or organo-soluble oxidants (hypervalent iodine; $PhI(OAc)_2$) to give silicone foams or elastomers, respectively. The resulting disulfide linkages in silicone foams or elastomers were successfully reduced back to thiol-functionalized silicone oils by hydrosilanes in the presence of $B(C_6F_5)_3$; the thiol/disulfide processes could be performed several times. Partial overoxidation of the sulfur-containing elastomer, which generates sulfonates or other species, could be avoided by careful control of the quantity of oxidants. However, the process can be profitably used to achieve other objectives. Thus, overoxidation of thiopropylsilicones with bleach, in the absence of additional surfactants or catalysts, led to elastomeric foams with up to 70% water content. The morphology (bubble size and density) and crosslink density of the foams can be easily controlled by the concentration of NaOCl solution utilized for oxidation. Hydrophilic silicone elastomers could be alternatively prepared by interfacial oxidative cleavage of disulfide linkages at the elastomer surface.

3.6 References

1. Wells, C. M.; Harris, M.; Choi, L.; Murali, V. P.; Guerra, F. D.; Jennings, J. A., Stimuli-Responsive Drug Release from Smart Polymers. *J. Funct. Biomater.* **2019,** *10* (3), 34.

2. Ganesh, V. A.; Baji, A.; Ramakrishna, S., Smart Functional Polymers – a New Route towards Creating a Sustainable Environment. *RSC Adv.* **2014,** *4* (95), 53352-53364.

3. Wei, M.; Gao, Y.; Li, X.; Serpe, M. J., Stimuli-responsive Polymers and their Applications. *Polym. Chem.* **2017,** *8* (1), 127-143.

4. Zhang, X.; Han, L.; Liu, M.; Wang, K.; Tao, L.; Wan, Q.; Wei, Y., Recent Progress and Advances in Redox-responsive Polymers as Controlled Delivery Nanoplatforms. *Mater. Chem. Front.* **2017,** *1* (5), 807-822.

5. Ahn, Y.; Jang, Y.; Selvapalam, N.; Yun, G.; Kim, K., Supramolecular Velcro for Reversible Underwater Adhesion. *Angew. Chem. Int. Ed.* **2013,** *52* (11), 3140-3144.

6. Nucara, L.; Greco, F.; Mattoli, V., Electrically Responsive Photonic Crystals: a Review. *J. Mater. Chem. C* **2015,** *3* (33), 8449-8467.

7. Connelly, N. G.; Geiger, W. E., Chemical Redox Agents for Organometallic Chemistry. *Chem. Rev.* **1996,** *96* (2), 877-910.

8. Fukino, T.; Yamagishi, H.; Aida, T., Redox-Responsive Molecular Systems and Materials. *Adv. Mater.* **2017,** *29* (25), 1603888.

9. Huo, M.; Yuan, J.; Tao, L.; Wei, Y., Redox-responsive Polymers for Drug Delivery: from Molecular Design to Applications. *Polym. Chem.* **2014,** *5* (5), 1519-1528.

10. Schafer, F. Q.; Buettner, G. R., Redox Environment of the Cell as Viewed Through the Redox State of the Glutathione Disulfide/Glutathione Couple. *Free Radical Biol. Med.* **2001,** *30* (11), 1191-1212.

11. Okumura, M.; Saiki, M.; Yamaguchi, H.; Hidaka, Y., Acceleration of Disulfide-coupled Protein Folding using Glutathione Derivatives. *FEBS J.* **2011,** *278* (7), 1137-1144.

12. Guo, X.; Cheng, Y.; Zhao, X.; Luo, Y.; Chen, J.; Yuan, W.-E., Advances in Redox-responsive Drug Delivery Systems of Tumor Microenvironment. *J. Nanobiotechnology* **2018,** *16* (1), 74.

13. Liu, L.; Liu, P., Synthesis Strategies for Disulfide Bond-containing Polymer-based Drug Delivery System for Reduction-responsive Controlled Release. *Front. Mater. Sci.* **2015,** *9* (3), 211-226.
14. Meng, F.; Hennink, W. E.; Zhong, Z., Reduction-sensitive Polymers and Bioconjugates for Biomedical Applications. *Biomaterials* **2009,** *30* (12), 2180-2198.
15. Gyarmati, B.; Némethy, Á.; Szilágyi, A., Reversible Disulphide Formation in Polymer Networks: A Versatile Functional Group from Synthesis to Applications. *Eur. Polym. J.* **2013,** *49* (6), 1268-1286.
16. Aliyar, H. A.; Hamilton, P. D.; Ravi, N., Refilling of Ocular Lens Capsule with Copolymeric Hydrogel Containing Reversible Disulfide. *Biomacromolecules* **2005,** *6* (1), 204-211.
17. Zheng, S.; Liao, M.; Chen, Y.; Brook, M. A., Dissolving Used Rubber Tires. *Green Chem.* **2020,** *22*, 94-102.
18. Laps, S.; Sun, H.; Kamnesky, G.; Brik, A., Palladium-Mediated Direct Disulfide Bond Formation in Proteins Containing S-Acetamidomethyl-cysteine under Aqueous Conditions. *Angew. Chem. Int. Ed.* **2019,** *58* (17), 5729-5733.
19. Dhakshinamoorthy, A.; Alvaro, M.; Garcia, H., Aerobic Oxidation of Thiols to Disulfides using Iron Metal–organic Frameworks as Solid Redox Catalysts. *Chem. Commun.* **2010,** *46* (35), 6476-6478.
20. Kamada, J.; Koynov, K.; Corten, C.; Juhari, A.; Yoon, J. A.; Urban, M. W.; Balazs, A. C.; Matyjaszewski, K., Redox Responsive Behavior of Thiol/Disulfide-Functionalized Star Polymers Synthesized via Atom Transfer Radical Polymerization. *Macromolecules* **2010,** *43* (9), 4133-4139.
21. Chauvin, J.-P. R.; Pratt, D. A., On the Reactions of Thiols, Sulfenic Acids, and Sulfinic Acids with Hydrogen Peroxide. *Angew. Chem. Int. Ed.* **2017,** *56* (22), 6255-6259.
22. Goethals, E. J.; Sillis, C., Oxidation of Dithiols to Polydisulfides by Means of Dimethylsulfoxide. *Makromol. Chem.* **1968,** *119* (1), 249-251.
23. Hashemi, M.; Rahimi, A.; Karimi-Jaberi, Z., Sodium Hypochlorite/Montmorillonite K10: An Effective Oxidant for the Oxidation of Thiols to Disulfides. *Lett. Org. Chem.* **2005,** *2*, 485-486.
24. Abdel-Mohsen, H. T.; Sudheendran, K.; Conrad, J.; Beifuss, U., Synthesis of Disulfides by Laccase-catalyzed Oxidative Coupling of Heterocyclic Thiols. *Green Chem.* **2013,** *15* (6), 1490-1495.

25. Shit, S. C.; Shah, P., A Review on Silicone Rubber. *Natl. Acad. Sci. Lett.* **2013,** *36* (4), 355-365.
26. Brook, M. A., *Silicon in Organic, Organometallic, and Polymer Chemistry*. John Wiley & Sons, Inc: 1999.
27. Congiusta, C.; Granleese, J.; Graiver, D.; Hoffman, L.; Mathew, S.; Clarke, D.; Johnston, M.; Clarke, S., Novel Grafting onto Silica via Aldehyde Functionality. *Silicon* **2009,** *1*, 29-36.
28. Beckett, M. A.; Brassington, D. S.; Coles, S. J.; Hursthouse, M. B., Lewis Acidity of Tris(pentafluorophenyl) borane: Crystal and Molecular Structure of $B(C_6F_5)_3$. $OPEt_3$. *Inorg. Chem. Commun.* **2000,** *3* (10), 530-533.
29. Schilter, D., Thiol Oxidation: A Slippery Slope. *Nat. Rev. Chem.* **2017,** *1*, 0013.
30. Liao, M.; Schneider, A.; Laengert, S.; Gale, C.; Chen, Y.; Brook, M., Living Synthesis of Silicone Polymers Controlled by Humidity. *Eur. Polym. J.* **2018,** *107*.
31. So, J.-H.; Boudjouk, P.; Hong, H. H.; Weber, W. P., Hexamethyldisilathiane. *Inorg. Synth.* **1992,** *29*, 30-32.
32. Grande, J. B.; Thompson, D. B.; Gonzaga, F.; Brook, M. A., Testing the Functional Tolerance of the Piers–Rubinsztajn Reaction: a New Strategy for Functional Silicones. *Chem. Commun.* **2010,** *46* (27), 4988-4990.
33. Rattanangkool, E.; Krailat, W.; Vilaivan, T.; Phuwapraisirisan, P.; Sukwattanasinitt, M.; Wacharasindhu, S., Hypervalent Iodine(III)-Promoted Metal-Free S–H Activation: An Approach for the Construction of S–S, S–N, and S–C Bonds. *Eur. J. Org. Chem.* **2014,** *2014* (22), 4795-4804.
34. Schneider, A. F.; Chen, Y.; Brook, M. A., Trace Water Affects Tris(pentafluorophenyl)borane Catalytic Activity in the Piers–Rubinsztajn Reaction. *Dalton Trans.* **2019**.
35. Porwal, D.; Oestreich, M., $B(C_6F_5)_3$-Catalyzed Reduction of Sulfoxides and Sulfones to Sulfides with Hydrosilanes. *Synthesis* **2017,** *49*.
36. Roucoules, V.; Ponche, A.; Geissler, A.; Siffer, F.; Vidal, L.; Ollivier, S.; Vallat, M. F.; Marie, P.; Voegel, J. C.; Schaaf, P.; Hemmerlé, J., Changes in Silicon Elastomeric Surface Properties under Stretching Induced by Three Surface Treatments. *Langmuir* **2007,** *23* (26), 13136-13145.
37. Qin, G. F.; Li, Z. Y.; Chen, X. D.; Russell, A. B., An Experimental Study of an NaOCl Generator for Anti-microbial Applications in the Food Industry. *J. Food Eng.* **2002,** *54* (2), 111-118.

38. M R McNeil, N.; McDonnell, C.; Hambrook, M.; G Back, T., Oxidation of Disulfides to Thiolsulfinates with Hydrogen Peroxide and a Cyclic Seleninate Ester Catalyst. *Molecules (Basel, Switzerland)* **2015,** *20*, 10748-62.
39. Madabhushi, S.; Jillella, R.; Sriramoju, V.; Singh, R., Oxyhalogenation of Thiols and Disulfides into Sulfonyl Chlorides/Bromides using Oxone-KX (X = Cl or Br) in Water. *Green Chem.* **2014,** *16* (6), 3125-3131.

Supporting Information

Reversible Redox Cross-linking of Thiopropylsilicones

Sijia Zheng, Michael A. Brook*

Department of Chemistry and Chemical Biology, McMaster University, 1280 Main St. West, Ontario, Canada, L8S 4M1.

Quantification of sodium hypochlorite solutions

The concentration of sodium hypochlorite, the active ingredient in commercial bleach (Sigma-Aldrich) was determined by a redox titration with standardized thiosulfate solution using starch-iodine indicator.[37] Before the titration, the density of the bleach solution was measured by weighting the mass of 1ml solution. The density of the solution was measured as 1.206 g/ml and this value was used for the calculation.

The sodium hypochlorite solution (5 ml) was diluted 50-fold with a clean 250 ml volumetric flask. 5 ml of the diluted sodium hypochlorite solution was delivered into a 250 ml Erlenmeyer flask by a volumetric pipet. The solution in the Erlenmeyer flask was further diluted with 15 ml of distilled water and acidified with 2M HCl solution (20 ml). An excess of potassium iodide solution (20 ml, concentration: 10wt% solution, 13.4 mmol) was added to reduce ClO^-, resulting in the formation of an equivalent amount of thiiodide, which was titrated with the standard solution of sodium thiosulfate (0.26 M): $Na_2S_2O_3$ and iodide ion and dithionate ions are formed as the products. Potato starch solution (2 ml, concentration: 2 wt% solution) was the indicator used in this titration. The volume of consumed standard sodium thiosulfate solution (0.26 M) was recorded: The disappearance of the blue starch–triiodide complex marks the end point. The general scheme is summarized as follows:

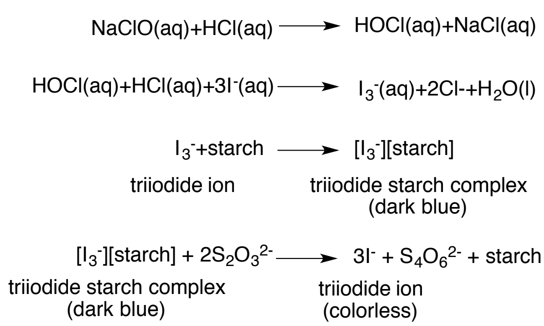

The titration process was performed for three times.

$$\text{Mass\% of NaOCl} =$$

$$\frac{\frac{1}{2} * [Na_2S_2O_3] * \text{Voulme of } Na_2S_2O_3 \text{ in titration} * 50 * \text{molar mass of NaOCl}}{\text{density of bleach} * \text{volume of undiluted bleach}} * 100$$

Where the molar mass of $[Na_2S_2O_3]$ =0.26 M, NaOCl = 74.5 g/mol, density of bleach = 1.206 g/ml, volume of undiluted bleach = 5 ml.

The average mass% of NaOCl from experiment is 11.51% ± 0.46% (the label indicated available chlorine 10-15%).

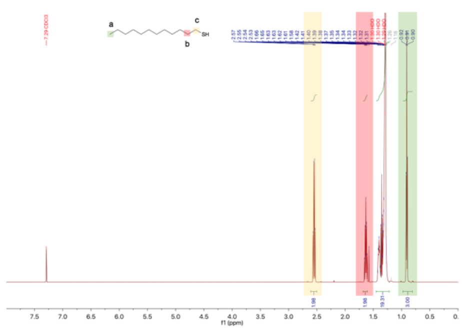

a

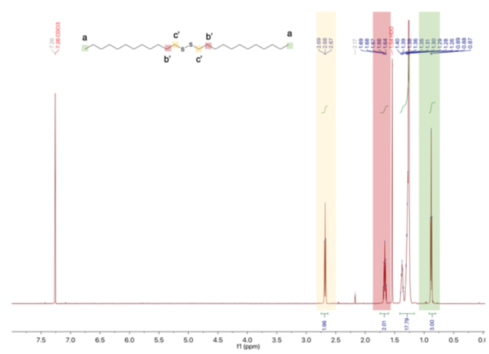

b

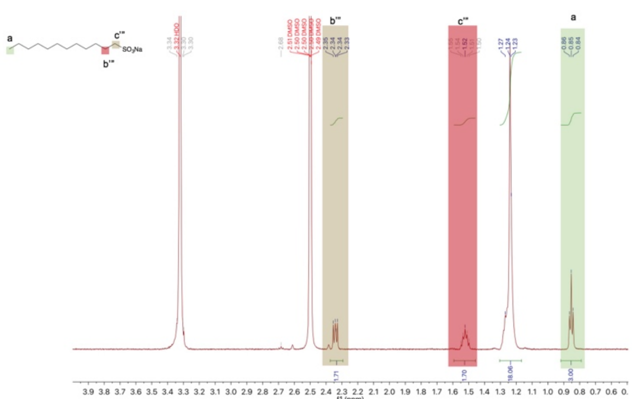

c

Figure S 3.1 ^{1}H NMR of (a) 1-dodecanethiol, (b) dodecyl sulfide product from oxidation of dodecanethiol, and (c) dodecyl sulfonate (in $CDCl_3$ and DMSO-d_6, respectively)

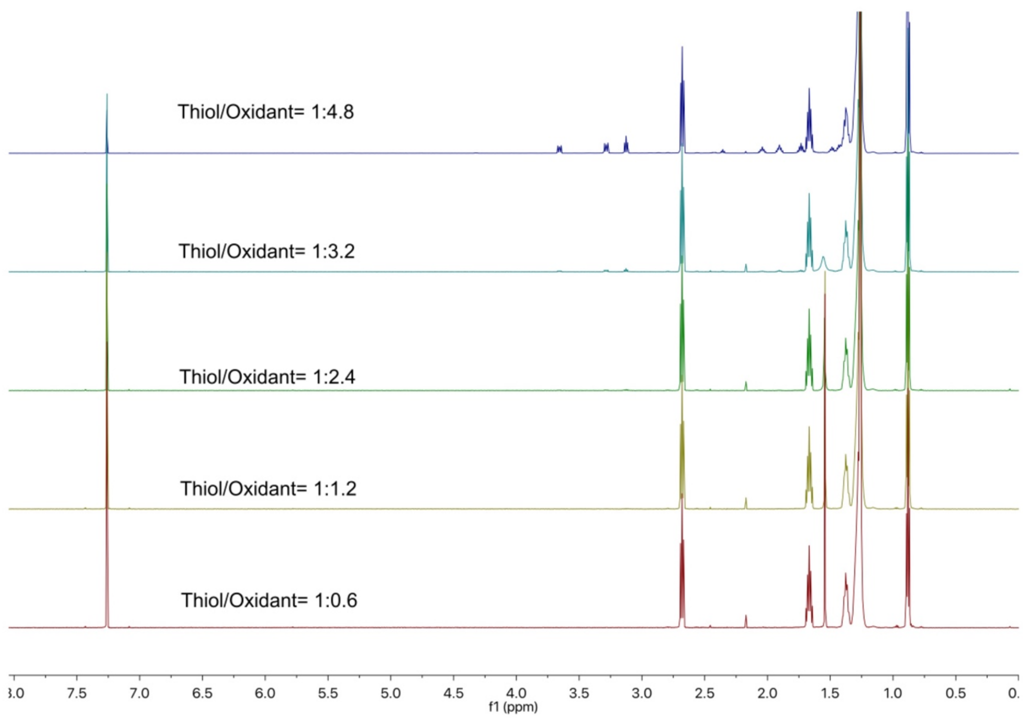

Figure S3.2 ^{1}H NMR of disulfide products (in $CDCl_3$). It is noted that a small amount of thiosulfonate (RSO_2SR)[38] and sulfonyl chloride (RSO_2Cl)[39] intermediates (> 3.0 ppm) were observed when excess oxidant was applied.

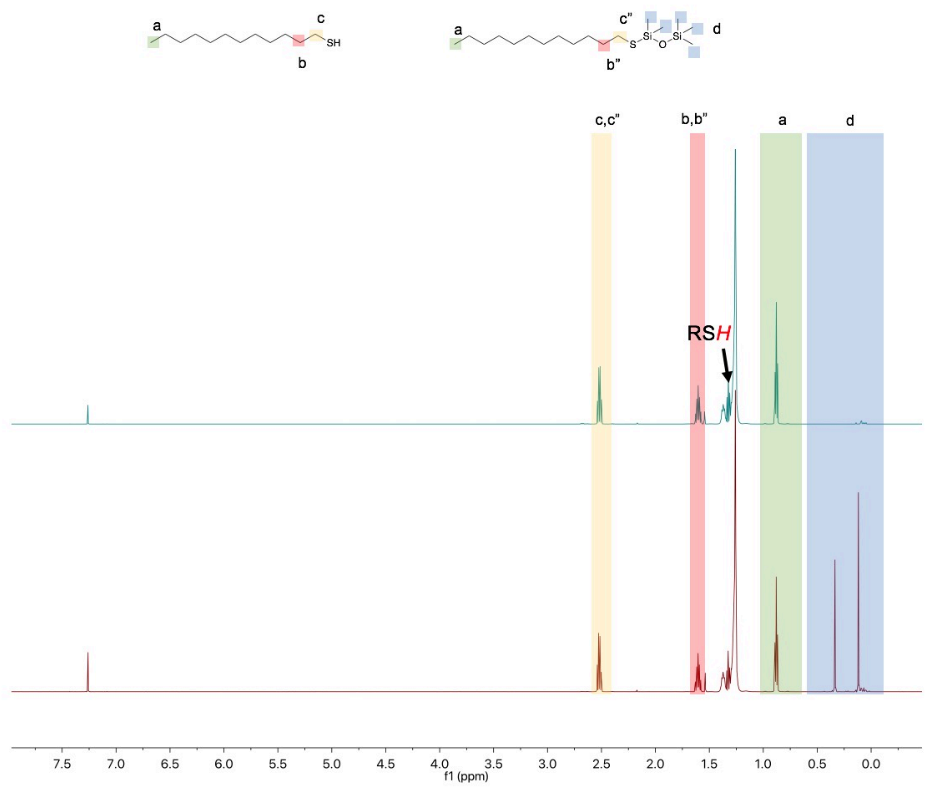

Figure S3.3 Hydrolysis of S-Si bonds in disilylation process.

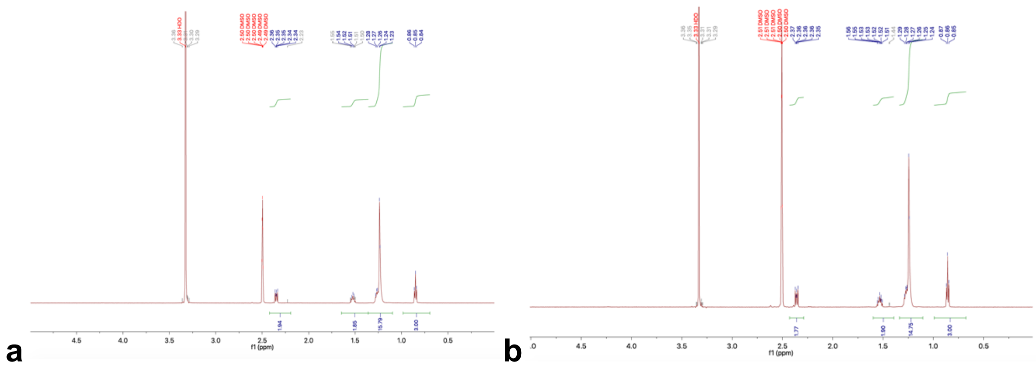

Figure S3.4 ^{1}H NMR spectrum before (a) and after (b) treating sodium 1-decanesulfonate with 10 equiv. pentamethyldisiloxane and $B(C_6F_5)_3$. The identical spectra before and after reaction indicated no reaction occurred during this process.

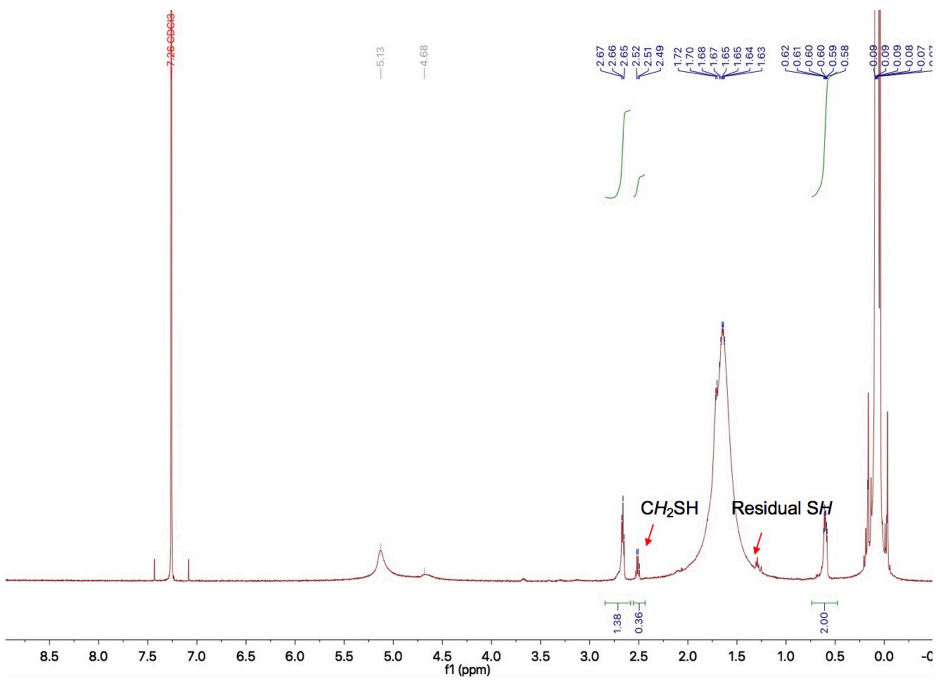

Figure S3.5 ^{1}H NMR spectrum of silicone foam prepared with 0.6 equivalent NaOCl. The foam was crushed into small pieces and swelled in $CDCl_3$ to obtain as ^{1}H NMR spectrum.

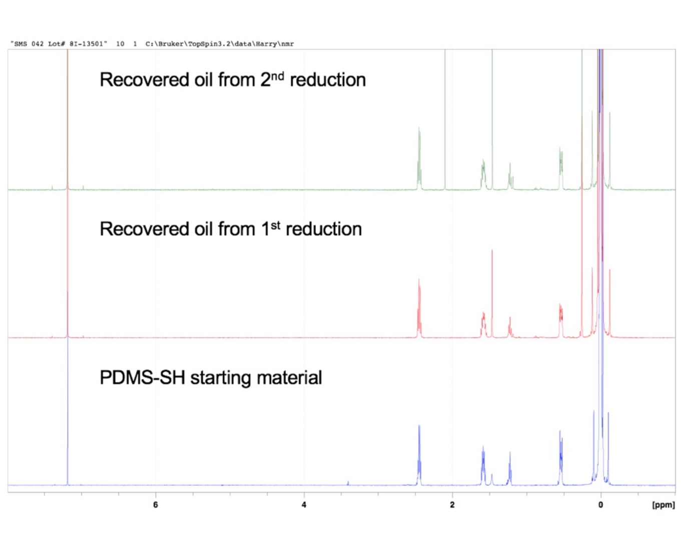

Figure S3.6 ^{1}H NMR spectrum of thiopropylsilicone starting materials SMS 042, 4-6% SH (blue), recovered oil from first reduction reaction of silicone elastomer (red), and recovered oil from the reduction of the elastomer formed after the first iteration (green).

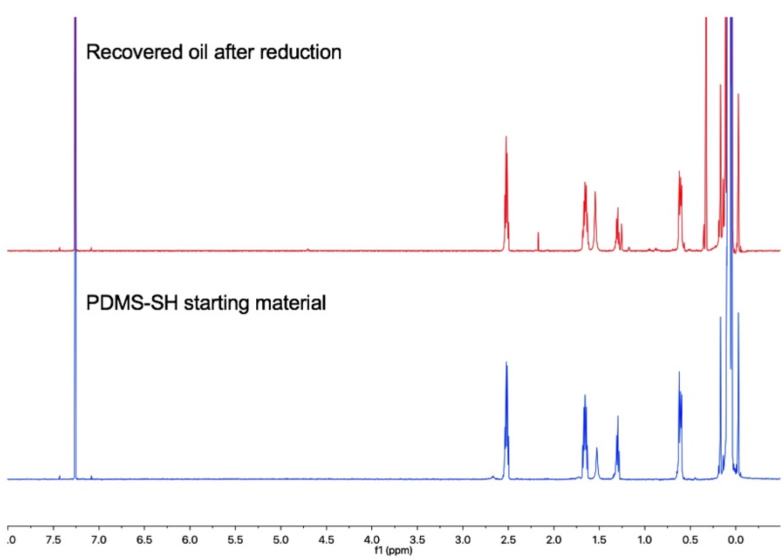

Figure S3.7 ^{1}H NMR spectrum of thiopropyl silicone starting material SMS 042, 4-6% SH (blue), recovered oil from reduction of bleach cure foam reaction (red).

4 Chapter 4: Dissolving Used Rubber Tires

4.1 Abstract

Used automobile tires present an enormous environmental burden. Efficient methods for degradation of the sulfur crosslinks in organic elastomers have proven elusive. We show that the reductive silylation of RS-SR bonds to silyl thio ethers $RSSiR''_3$ in up to 90% yield using a variety of hydrosilicones occurs in an open vessel in the presence of <1mol% $B(C_6F_5)_3$ for model compounds. Sulfur-cured automotive rubber required 10wt% catalyst for efficient sulfide cleavage. At temperatures ranging from room temperature to 100 °C recoveries of organic polymers as oils from tires using this one step process ranged from 56% for complex mixtures of rubber crumb from ground tires to 93% for butyl rubber (bicycle inner tubes; 87% yield at 100 °C over 30 minutes). After removal of inorganic materials by simple filtration, the recovered polymeric oils were radically or oxidatively crosslinked to generate new elastomers that can be optionally reinforced with the solids recovered in the initial reduction procedure. This mild process constitutes a facile route to reutilize the organic polymers found in automobile and other sulfur-crosslinked rubbers.

4.2 Introduction

The radically induced[1] vulcanization of alkene-containing hydrocarbon polymers, reported by Goodyear in 1844,[2] is a technological advancement that remains an integral part of modern life; the sales of automobile tires prepared using this process are expected to reach 3 billion units in 2019.[3] The elastomer products, crosslinked with sulfur oligomers, are incredibly robust products, which pose a major challenge; they are far too stable to be readily recycled.

Automobile tires exemplify polymers derived from fossil fuels that are destined for a single use. Used tires constitute a significant environmental burden, particularly because of the scale of production.[4] In large part, used tires are simply placed in stockpiles,[5] from which leaching into the environment of their many (toxic) constituents occurs.[6] Dangerous, highly polluting, difficult-to-arrest tire fires at such storage facilities are not uncommon.[7]

Some automotive rubber is exploited as fuel in the cement industry; capturing the SO_2 produced during combustion may be problematic. Some tires are turned into crumb and used as fillers,[8] for example, in asphalt, cement or turf replacements from which, however, leaching of contaminants may still occur.[9] There is a longstanding need to recover the organic materials from tires for sustainable reuse. Although the S-S bond strength is only ~280 $kJ \cdot mol^{-1}$,[10] practicable processes for S-S cleavage in vulcanized tires have not been reported. Aggressive chemical approaches, for example, reactive reduction with $LiAlH_4$[11-12] or amines,[13] have not proven commercially viable. Reuse strategies for automotive rubbers therefore typically involve energetically intensive, relatively inefficient, pyrolytic conversion into fuel gas, low grade carbon black and other low value materials.[14] The world is in dire need of new efficient methods for recycling waste tire rubber, especially in ways that allow the recovery and reuse of the basic building blocks.

The weak Si-H bond in hydrosilanes makes them excellent reducing agents, particularly when strong Si-heteroatom bonds are formed in the process.[15] Thus, reductive hydrolysis/alcoholysis[16] and C=O hydrosilylation,[17] among others, are efficient processes. Key to the work described here is the Lewis acid-catalyzed (typically $B(C_6F_5)_3$ = BCF) reduction of carbonyls (Figure 4.1a), ethers, silanols, alkoxysilanes (the Piers-Rubinsztajn reaction[18-20] Figure 4.1b), benzylic sulfides, and thioacetals (Figure 4.1c) using HSi functional groups.[21] These reactions are normally easy to control, often work at room temperature, and the main experimental issues are associated with managing the co-products when they are flammable gases, including hydrogen or alkanes.

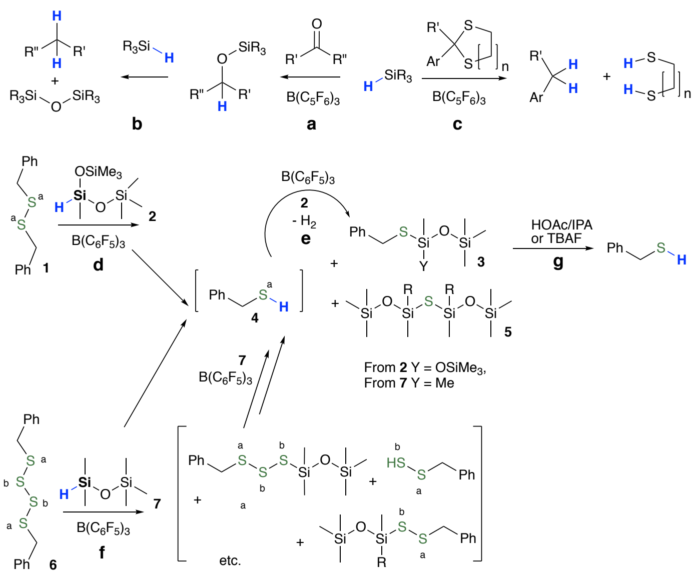

Figure 4.1 Selected examples of $B(C_6F_5)_3$-catalyzed reduction by SiH groups. (a) carbonyl reduction to silyl ethers; (b) silyl ether reduction to alkanes (Piers-Rubinsztajn); (c) aromatic thioacetal cleavage to alkanes; (d) disulfide cleavage to silyl thio ethers (this work); (e) reduction of thiols to silyl thio ethers; (f) silyl thiol ether formation from oligosulfides, and, (g) Si-S cleavage using acid or fluoride catalysis.

We report that, with catalysis by $B(C_6F_5)_3$, hydrosilanes will effectively reduce the S-S bonds of model organic disulfides, tetrasulfides and, more importantly, complex sulfur-crosslinked solid automotive rubbers in the forms of bicycle inner tubes, solid tires or tire crumb in good to excellent yield. The products are polymeric, silyl-protected thiolated organic oils that are readily separated from the accompanying, unreactive solids, such as fillers, fiber and metal reinforcements, pigments, etc. simply by filtration or centrifugation. The products – sulfur-containing polymeric oils – may be converted back into (reinforced) rubbers using simple oxidative or radical processes.

4.3 Results and Discussion

4.3.1 Model Reductions of Dibenzyl Disulfide and Tetrasulfide

Model reductions of dibenzyl disulfide **1** (n=1) were undertaken using bis(trimethylsiloxy)methylsilane **2** ($HSiMe(OSiMe_3)_2$, MD^HM) (the common nomenclature used for silicones is Q: $SiO_{4/2}$; T: $MeSiO_{3/2}$; D: $MeSiO_{2/2}$ and M: Me_3SiO~) as reducing agent in the presence of BCF (Figure 4.1d,e, Figure 4.2, Table S4.1, Figure S4.1, ESI†). With less than one equivalent of hydrosiloxane, residual starting material and only product **3** were recovered, demonstrating that the reaction of SiH with S-H, e.g., in compound **4**, is faster than that with S-S bonds. The complete reduction of **1** → **3** required 2 equiv. of the hydrosiloxane and occurred in 90% yield using only 0.8 mol%BCF; the other sulfur-based product **5** was removed under reduced pressure. Reduction of the analogous tetrasulfide **6** to **3** using $HSiMe_2OSiMe_3$ **7** required five equivalents of MD^HM and demonstrated that both C-$\mathbf{S^a}$-$\mathbf{S^a}$ and S^a-$\mathbf{S^b}$-$\mathbf{S^b}$ linkages undergo efficient reductive silylation (Figure 4.1f, Figure 4.2, Figure S4.2, ESI†).

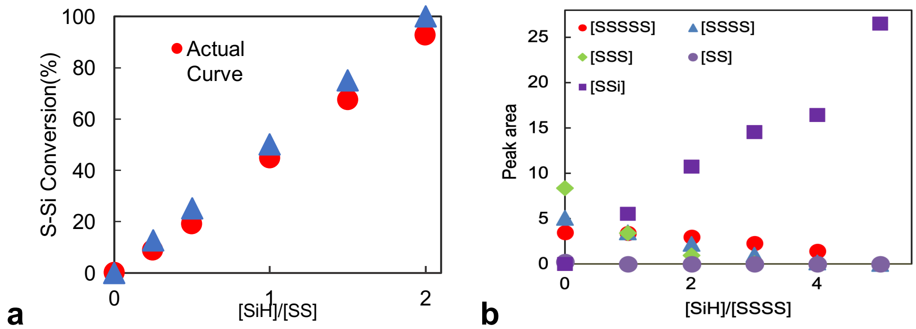

Figure 4.2 (a) Disulfide conversion in benzyl disulfide system versus [SiH]/[SS] using $MD^{H}M$. (b) Polysulfide conversion in benzyl tetrasulfide system versus [SiH]/[SSSS] using $MD^{H}M$.

4.3.2 Reduction of Used Automotive Rubbers

Automotive tires contain a complex variety of constituents, including (spent) catalysts for their formation, antioxidants, colorants, particulate reinforcing agents like carbon black and/or organosulfur-modified silica, and fibrous reinforcing agents including nylon cord and woven steel.[14] Holding together this complex assortment of excipients is the sulfur-crosslinked elastomer. We reasoned that the (oligo)sulfide linkages in rubber tires could be reductively cleaved using hydrosilanes in analogy to the reactions with the oligosulfide model compounds (Figure 4.1d-f).

Scrap rubber from automobile tires is available in large quantity in the form of ‘rubber crumb’. It is formed by shredding tires from multiple sources to remove metal wires and polyester cord and grinding the resulting product to various crumb sizes. The typical organic constituents in crumb mixtures include isobutene isoprene (IIR), butadiene rubber (BR), styrene-butadiene rubber (SBR), isoprene rubber (IR) and natural rubber (NR). Thermal degradation profiles allow one to determine the constitution of sulfur-crosslinked elastomers; depending on their structure, the polymers degrade between 300 - 485 °C;[22-23] (Figure S4.5, Figure S4.6, Table S4.3) while inorganic carbon (carbon black) thermally decomposes from 560 - 800 °C in oxygen.[24] In the rubbers tested, the organic rubber content was approximately 60wt% (Table 4.2, Figure S4.11).

Table 4.1 Constituents in rubber starting materials.

Rubber	Rubber constituents[a]	Components		
		Organic %	Carbon black %	Other solids %
EPDM	EPDM	55.1	26.4	18.5
Inner Tube		61.1	33.0	5.9
Truck tread-1	IR/NR	62.2	28.4	9.4
Truck tread-2	IR/NR	65.0	23.0	12.0
Tread (Snow tire)	IR/NR+BR	63.0	22.9	14.1
Side wall (Snow tire)	IIR+IR/NR+BR	59.4	22.2	18.4
Crumb-1	BR+EPDM	47.6	44.6	8.8
Crumb-2	IIR+PBD	61.6	31.5	6.9

[a] EPDM terpolymer of ethylene, propylene and diene, IR/NR isoprene rubber / nature rubber, IIR isobutene isoprene rubber, BR butadiene rubber. Constituents were determined by a combination of TGA, which showed separate decomposition temperatures for IIR and IR/NR, and ^{1}H NMR.

Two separate sources of commercial crumb were compared for their reactivity under the reducing silylation conditions. Much more BCF catalyst (10 wt% compared to the rubber starting material) was required to achieve reasonable yields of reduction with rubbers than with the model compounds (<1 mol%), which is not surprising given the complexity of the mixed rubber starting materials and the fact that they have been exposed to degradation and various environments during use.

With **7** as reducing agent, organic oils were recovered in 36% yield from one crumb rubber source and a moderate 56% yield from another (2 lots, Figure 4.3g). Use of second and third reduction steps with fresh catalyst and hydrosilane significantly improved overall conversion of elastomer to oils (steps 1) 56% → 2) +29.6% → 3) +2.5% (total 88% organic recovery - the inorganic constituents were removed by centrifugal separation (Table 4.2, Table 4.3, Figure S4.14). In retrospect, in a practical sense, only the improvement in overall efficiency of the second step could be justified. The reduction process was readily visible by eye, as black dispersions were converted to yellow oils (Figure 4.3b⟶f,g, Figure S4.7, Figure S4.8, ESI†).

Improved recoveries of organic polymers were observed with single composition rubbers. For example, about 60% of an EPDM elastomer (ethylene propylene diene terpolymer, 'pond liner') was converted to a soluble oil using reductive silylation with **7** and $B(C_6F_5)_3$ in toluene at 60 °C. Automotive rubbers were efficiently reduced to oils in one step in yields ranging from 52-93%. These included: IIR from a (used) bicycle inner tube; IR/NR from the outermost section of truck tire tread; a mixture of IIR, IR/NR and BR from a snow tire side wall; and IR/NR, BR from a snow tire tread (Table 4.2, Table 4.3). The process is easily seen from the reduction of a bulk section of snow tire tread (Figure 4.3a). Shortly after the reduction reaction started, the reinforcing steel wires separated from the bulk rubber and were collected on the magnetic stir bar (Figure 4.3c); accompanied by particulate formation to give a black dispersion (Figure 4.3b) – the bulk rubber underwent shrinkage, but not complete disintegration (Figure 4.3d, Figure S4.19). Filtration allowed separation of a black solid mass comprised primarily of inorganic excipients and a yellow solution of silylated organic oils in toluene (Figure 4.3e,f, Figure S4.7,Figure S4.18).

Table 4.2 Efficiency of reductive silylation of sulfur-crosslinked rubbers.[a]

Rubber	Rubber constituents[b]	Starting Components			Yield %[c]
		Organic %	Carbon black %	Other solids %	Organic oil
Crumb-1	BR+IR/NR+ EPDM	47.6	44.6	8.8	35.8
Crumb-2	IIR+BR	61.6	31.5	6.9	56.2
repeat process with 1st product					85.8
repeat process with 2nd product					88.3[d]
EPDM	EPDM	55.1	26.4	18.5	60.4
Inner Tube	IIR	61.1	33.0	5.9	92.9
	100 °C 30 min[e]				87.0
Truck Tread[f]	IR/NR	65.0	23.0	12.0	89.8
Tread (Snow tire)[g]	IR/NR+BR	63.0	22.9	14.1	51.8
Side Wall (Snow tire)	IIR+IR/NR+BR	59.4	22.2	18.4	53.8

[a] Experimental conditions: rubber (300 mg); $B(C_6F_5)_3$ (30 mg, 10wt%), 12 ml toluene **7** (1.5 ml) at 60 °C for 48 h. [b] Constituents were determined by a combination of TGA, which showed separate decomposition temperatures for IIR and IR/NR, and ^1H NMR. EPDM = terpolymer of ethylene, propylene and diene, IR/NR isoprene rubber or natural rubber, IIR isobutene isoprene rubber, BR butadiene rubber. [c] Organic yield = (Total Organic-Recovered Organic)/Total Organic * 100. Organic composition established using TGA (Figure S4.6, Figure S4.9, Figure S4.11, Table S4.3, Table 4.1). [d] Cumulative yield for 3 process steps. [e] Process utilized hydrosilicone **10** (1.5 ml) at 100 °C for 30 min. [f] External road

contacting component only. [g] Cross-section of entire tread from core to external surface.

Oligosulfides were converted into silyl thiol ethers during reduction (Figure 4.3g, Figure S4.7). Therefore, the residual solids and recovered non-volatile liquids often exhibited a weight gain when compared to the starting rubber mass (Table S4.4). The product oils **8** (Figure 4.3, for ^{1}H NMR data, see Figure S4.15) typically exhibited a bimodal distribution of molecular weight, with a low fraction centered near 10,000 $g \cdot mol^{-1}$ and a broad peak centered near 1 million $g\ mol^{-1}$ (Table S4.5 , Figure S4.16).

Several factors were manipulated to improve the efficiency of the reduction process. Commercial hydrosilicones that vary in the density of SiH groups are readily available. Model studies on the reduction of the organic sulfides or automotive rubbers were undertaken with **10** or **7**, respectively, because the use of small molecules facilitated the characterization of the reaction products. Either compound is too expensive for practical use. Attempts to facilitate the reduction of rubbers with the inexpensive, high SiH density polymer $Me_3Si(OSiMeH)_nSiMe_3$ **9** were unsuccessful (Figure S4.17) because the silicone product of the reduction is a network polymer, which led to the formation of intractable tars. By contrast, the use of inexpensive, high SiH density $HMe_2SiOSiMe_2H$ **10** led to efficacious, rapid reduction of rubbers (Table 4.2, Table 4.3, Figure S4.17).

Unlike the model compounds above, relatively large quantities of the BCF catalyst, 10 wt% against the rubber, were required for the reduction of rubbers to occur efficiently. Pre-swelling the rubber in commonly used organic solvents like acetone,[25] or an initial Soxhlet extraction using acetone to remove potential catalyst inhibitors, e.g., amines, free sulfur, acetone soluble colorants, antioxidants, processing rubber additives, etc., did not appreciably increase either the rate or the yield of the reduction process (Table 4.3, Figure S4.14). We continue to work on process optimization to reduce the quantities of catalyst required.

Several other factors were found to the affect the efficiency of the reduction of rubbers, including the surface area, process temperature and reducing agent. Unsurprisingly, the reduction of bulk elastomers, including cylindrical sections of bicycle inner tube (diameter ~16.9 mm, thickness ~0.82 mm, IIR, Figure S4.7), and a cross-section of an automobile snow tire (IR/NR + BR, Figure 4.3), were slow to occur and low yielding at 60 °C using **7** (Table 4.3). In both cases, the objects underwent significant shrinkage (Figure S4.19), and exhibited an increased crosslink density, as shown by an increase in Young's modulus (Table S4.4), but maintained their shape. Cryogenic grinding of the starting rubbers to increase rubber surface area (to particle size ~ 330 μm, Figure S4.4) led to significant enhancements in yield; an increase from 52 to 93% was observed in the case of the inner tube (IIR, Table 4.3).

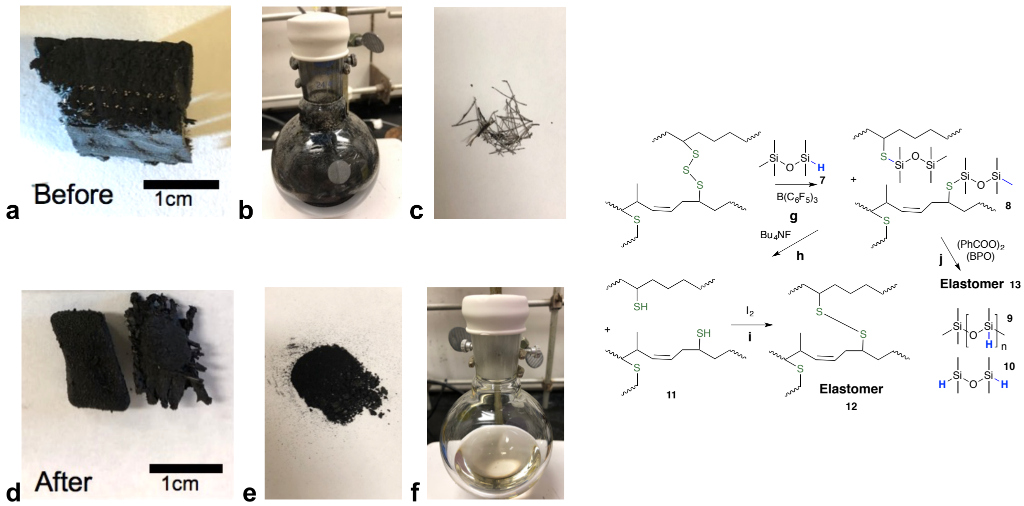

Figure 4.3 (a) Section of snow tire tread cross-section, unreacted. (b) reductive dispersion using **7** and 10wt% BCF after 6 days. (c) metal wires that self-affixed to the magnetic stir bar. (d) Shrunken sections after reaction. (e) Inorganic and unreacted rubber constituents isolated by gravity filtration. (f) Product silyl-protected thiolated organic oils **8** in toluene (56% yield; note: the recovered oil may be a darker color, depending on starting material and the specific reaction (Figure S4.7). (g) Reductive silylation (a→ d,e,f). (h) Cleavage of SiS bonds. (i) Oxidative coupling produces elastomers crosslinked by disulfides. (j) Radicals form elastomers from alkene-containing oils. Steps i and j can optionally use recovered inorganic constituents as reinforcing agents in the elastomers.

The tire reductive silylation studies were initially undertaken using relatively mild temperatures because literature suggests that the $B(C_6F_5)_3$ catalyst undergoes degradation at temperatures above 80 °C in the presence of moisture.[26] Current studies with rubber reduction, however, showed this not to be problematic. A 93% yield of recovered organic polymer (IIR from inner tube) was achieved at 100 °C after 18 hours using **10**, but an 87% yield had already been achieved in the first 30 minutes (Table 4.3). This result suggests that reduction processes at 100 °C or higher could be adapted to a continuous process.

Initial studies for reusing/re-crosslinking the recovered oil focused initially on the regeneration of thiols from silyl thio ethers. There are few reports of the reactivity of Si-S compounds. Me_3Si-S-$SiMe_3$ is very labile, undergoing rapid degradation simply in the presence of water (vapor) to form H_2S and Me_3SiOH.[27] By contrast, the hydrolysis of silicone-based thio ethers was much less facile. Alcoholysis of **3** (Figure 4.1g) yielded 12% product only once acetic acid was added to isopropanol solutions (the less sterically hindered thio ether $PhCH_2SSiMe_2OSiMe_3$ underwent rapid, quantitative cleavage under the same conditions). The silylated polymeric oils derived from elastomers **8** were yet less reactive. It was necessary to use more aggressive nucleophiles for silicon, such as Bu_4NF[28] to regenerate the silyl free thiols **11** (Figure 4.3h, Figure S4.20).

Once cleaved, the freed thiols on the organic polymers could be crosslinked into a new elastomer **12** by oxidative coupling using iodine in isopropyl alcohol[29] (Figure 4.3i, Figure S4.21). However, it was also discovered that, if silylated polymers **8** were derived from IR/NR or BR and possessed residual alkenes, re-crosslinking did not require the removal of the silyl groups; simply adding a radical initiator such as benzoyl peroxide (BPO) and heating led to new elastomers **13** (Figure 4.3j).

The ability to create new elastomers from the recovered polymeric oils was demonstrated by creating a new automotive tire (for a child's toy) using **8**. A mold of the tire was made in silicone rubber (Figure 4.4a,b). Silylated oil **8** derived from IR/NR (tire tread) was placed in the mold in the presence of BPO and heated to give a new, soft elastomer (Figure 4.4b+c ➛ e,f durometer Shore OO 68, Table S4.6). Adding to **8** the inorganic excipients (recovered from the production of **8**, Figure 4.4h), and then curing oxidatively, led to harder, more brittle elastomers (Shore A 91; original rubber Shore A 60).

Reductive silylation processes have shown synthetic merit in many arenas. The relatively weak SiH bond,[30] particularly in the in the presence of $B(C_6F_5)_3$ and related Lewis acids, readily reduces a variety of bonds[15] driven, in large part, by the thermodynamic benefit of forming Si-heteroatom bonds (heteroatom=O, N, S, etc.).[31] We have demonstrated that this type of process works effectively with S-S bonds to form thio silyl ethers. The key finding of this work is that, in addition to clean model compounds, the process works with complex and dirty samples – used automotive tires – to convert sulfur-cured elastomers into polymeric oils in up to ~90% yield. The process can be rendered practicable at temperatures as low as 100 °C and the product oils can find new utility in elastomeric objects using at least two different cure modes. We are currently establishing the quality of elastomers that can be produced from different used tire feedstocks. The recovered inorganic mass can also be repurposed as a filler in those new elastomers. Thus, reductive silylation provides a new opportunity to find commercial value in materials that are environmentally problematic. It is not possible to effectively 'reuse' automotive rubber, but reductive silylation is worthy of consideration as a strategy for recycling and reuse.

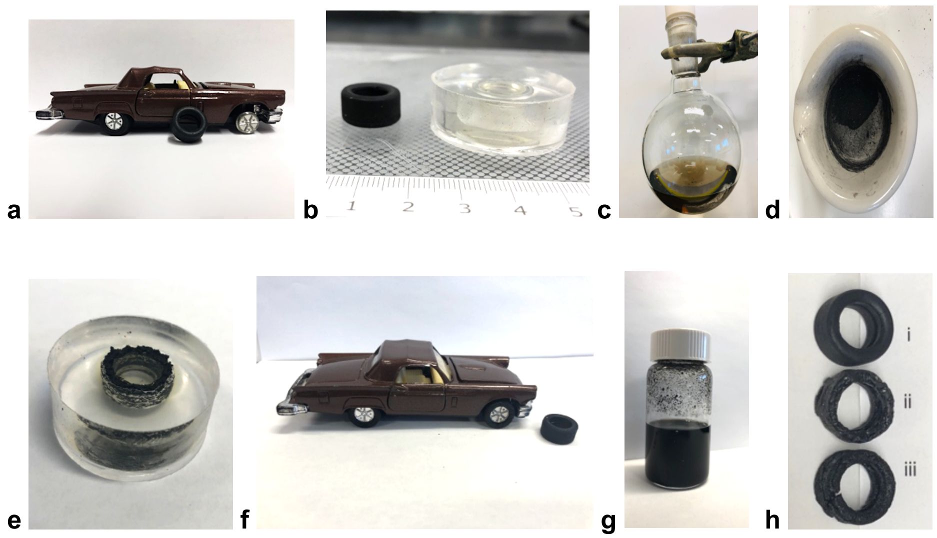

Figure 4.4 (a) The right front tire was removed from a toy car. (b) A silicone mold of the tire. (c) Organic oil **8** was prepared by reduction of truck tire tread (Sailun, IR/NR) with hydrosilane **7**. (d) Silicone mold filled with 0.707g **8** + 1wt% BPO + 0.3010g residual solid. (e) New tire after curing. (f) Tire replacement. (g) The residual solid during the preparation of **8** could be included in the pre-elastomer formulation. (h) Close up showing: i) the original tire, ii) tire made without additional inorganic excipients **13**, and iii) tire including inorganic excipients.

4.4 Experimental

4.4.1 Materials

Pentamethyldisiloxane **7**, bis(trimethylsiloxy)methylsilane ($HSiMe(OSiMe_3)_2$, MD^HM) **2**, tetramethyldisiloxane ($HMe_2SiOSiMe_2H$, M^HM^H) **10**, ($Me_3Si(OSiMeH)_nOSiMe_3$, $MD^H{}_nM$) **9**, were purchased from Gelest and used after drying over molecular sieves overnight. Dibenzyl disulfide, benzyl bromide, tetrabutylammonium fluoride trihydrate (TBAF), and iodine (I_2) were obtained from Sigma Aldrich and used as received. Benzoyl peroxide (BPO) was purchased from BDH. Sodium tetrasulfide was purchased from Dojindo. $B(C_6F_5)_3$ (BCF) was prepared by Grignard reaction following a literature procedure;[32] we acknowledge with gratitude Prof. David Emslie, McMaster University, for providing this sample. Rubber samples: bicycle inner tube (Chaoyang 700×38/45C bicycle inner tube, China), EPDM (pond liner, purchased at a local garden centre, producer unknown), Crumb-1 (Als-RC, Amazon, Canada), Crumb-2 (Canadian Eco Rubber Ltd., Emterra, Canada), were used as received. Truck tread 1: a piece of truck tread, not part of a complete tire, was found at a local garbage dump (origin unknown). Truck tread 2: (Sailun 225/70R19.5). In both cases, samples were cut only from the external, road contacting tread part (Figure S4.3); both rubbers were based on polyisoprene. The tread and side wall samples – cross-sections – were cut from different parts of a used car tire (snow tire, Cooper 185/65R4, Figure 4.5). Naphthalene (internal standard) was purchased from Fisher. Toluene (solvent) received from Caledon (HPLC grade) was dried over activated alumina before use. Deuterated NMR solvents were obtained from Cambridge Isotope Laboratories. Glass apparatus were dried overnight at 120 °C and cooled under a dry nitrogen atmosphere for 30 min prior to use.

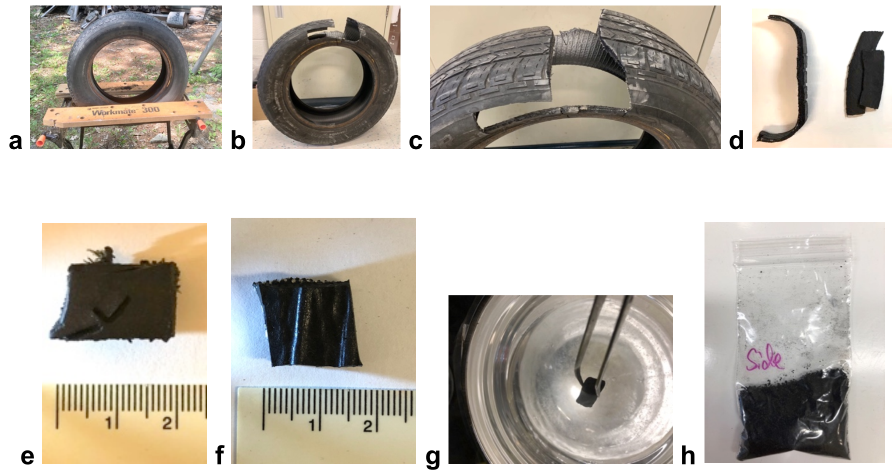

Figure 4.5 (a-c) A commercial snow tire was cut into (d) sidewall and tread sections using a reciprocating saw with blade designed for cutting metal. (e) tread 1.200 × 1.519 × 1.125 cm. (f) sidewall cut into 1.595 × 1.427 × 0.6096 cm. These samples were subjected to 'bulk reduction' of their as-cut shape. (g) For other reductions, the rubbers were chopped into fine pieces after cooling with liquid nitrogen and (h) powdered using coffee grinder (KitchenAid).

4.4.2 Methods

NMR: ^{1}H, ^{13}C and ^{29}Si NMR spectra were recorded on a Bruker Avance 600 MHz nuclear magnetic resonance spectrometer using deuterated solvents chloroform-*d* and actone-d_6. For ^{29}Si NMR, chromium(III) acetylacetonate was used as paramagnetic relaxation agent.

GC-MS: analyses were performed using an Agilent 6890N gas chromatograph (Santa Clara, CA, USA), equipped with a DB-17ht column (30 m × 0.25 mm i.d. x 0.15 µm film, J&W Scientific) and a retention gap (deactivated fused silica, 5 m x 0.53 mm i.d.), and coupled to an Agilent 5973 MSD single quadruple mass spectrometer. One microliter of sample was injected using an Agilent 7683 autosampler in splitless mode. The injector temperature was 250 °C and carrier gas (helium) flow was 1.1 ml/min. The transfer line was 280 °C and the MS source temperature was 230 °C. The column temperature started at 50 °C and was increased to 300 °C at 8 °C /min, then held at 300 °C for 15 min to give a total run time of 46.25 min. Full scan mass spectra between m/z 50 and 800 mass units were acquired after a solvent delay of 8 min.

LC-MS: analyses were undertaken using an Agilent Technologies 1200 LC coupled to an Agilent 6550 QTOF mass spectrometer. An injection volume of 2 µl was separated on a Phenomenex Luna C18(2) (150 mm×2.0 mm, 3 µm) column with 100 Å pore size (Phenomenex, CA, USA). The mobile phases were LC-MS-grade 45/55 water/methanol with 0.5% acetic acid (A) and methanol with 0.5% acetic acid (B) at a flow rate of 300 µl/min. The column temperature was maintained at 40 °C, and the autosampler storage tray was set at 10 °C. The mobile phase gradient eluted isocratically with 10% B for 1.0 min followed by a gradient to 100% B over 17 min. The gradient was maintained at 100 % B for 2 min and decreased to 10 % B over 0.1 min. The gradient was then followed by a 5 min re-equilibration prior to the next injection. The total time for an HPLC run was 25 min.

The MS parameters (for LC-MS) chosen were as follows: ESI, gas temperature at 225 °C, drying gas at 13 L/min, nebulizer pressure at 20 psi, sheath gas temperature at 400 °C, sheath gas flow at 12 L/min, VCap at 3500 V, Nozzle Voltage at 1000 V, fragmentor at 375 V, and Oct 1 RF Vpp at 750 V. The data were acquired in electrospray positive mode from m/z 50 to 1000 at a scan rate of 1.5 Hz. The mass was auto recalibrated using reference lock mass from Agilent ESI-T Tuning Mix (for Ion Trap).

GPC: Molecular weight of recovered organic oil and polydispersity index (PDI) were estimated from gel permeation chromatography (GPC) using a Waters 2695 Separations Module equipped with a Waters 2996 photodiode array detector, a Waters 2414 refractive-index detector, and two Jordi Labs Jordi Gel DVB columns. Polystyrene standards were used for calibration, and THF was used as the eluent at a flow rate of 1.0 ml min^{-1}.

The polymer constituents of rubber samples were estimated from carbon high-resolution magic angle spinning (^{13}C HR-MAS) NMR spectroscopy (Figure S4.5).
TGA: Thermogravimetric analysis (TGA) according to ASTM D 6370-99 (American Society for Testing and Materials) was used to measure the organic carbon (polymer), carbon black content and inorganic residue of the component.[24] A small amount of test sample (2 to 5 mg) was placed into the alumina pan of the calibrated Thermogravimetric Analyzer (Mettler Toledo TGA/DSC 3+). A 100 cm^3 min^{-1} argon purge was applied and the furnace was heated from 50 °C to 560 °C at 10 °C·min^{-1}. Then, the furnace was cooled to 300 °C and the purge gas was changed to air at 100 cm^3·min^{-1}. The temperature was allowed to equilibrate for 2 min before the furnace was heated to 800 °C at 10 °C min^{-1}.

The constituents of sulfur-cured rubbers have well-defined thermal decomposition profiles (Table S4.3). Within the thermal decomposition range of the organic polymers, there are further distinctions. TGA and DTA data (Figure S4.6) show the constituents of the rubber samples tested (Table 4.2).

Young's modulus: The Young's moduli of rubber samples were determined using a MACH-1 micromechanical system (Biomomentum Instruments) with a 0.500 mm hemispherical indenter radius, and Poisson ratio of 0.3. All measurements were conducted at 22 °C and in triplicate, with error bars representing the standard deviation of the replicate measurements.

Preparation of powdered rubber: Raw rubber samples of different shapes and sizes were obtained. The rubber crumb samples were of broad dispersity, with average particles sizes of 1.30±0.09 mm for Crumb-1 and 2.14±0.06 mm for Crumb-2. As noted above, more efficient reduction occurred with higher surface area samples. A cryogenic grinding progress was used to obtain rubber powder samples with homogeneous particle sizes for comparable experiments. Liquid nitrogen was employed to cool the rubber samples below their glass transition temperature before they were pulverized with a coffee grinder (KitchenAid) to give powders with an average particle size of ~330 mm (Figure 4.5g i, Figure S4.4).

4.4.3 Preparation of Dibenzyl Tetrasulfide

To a pre-dried 200 ml round-bottomed flask purged with dry N_2 were added sodium tetrasulfide (0.098 g, 0.562 mmol), benzyl bromide (0.209 g, 1.22 mmol) and dry THF (50 ml, 44.45 g, 0.616 mol) as solvent. The mixture was stirred for 23 d and collected by vacuum filtration. The mixture was purified using column chromatography; the low polarity impurity (S_8) was removed using hexanes, after which the elution solvent was switched to dichloromethane, to give a yield of 77% (137 mg, based on the different sulfides found in the product. Note: it was not possible to detect tetrasulfide or higher polysulfide linkages in the GC-MS, which may be due to thermal degradation of polysulfide bond (when n>3).[33,34]

^{1}H NMR (600 MHz, acetone-d_6): δ 3.72 (s, 0.11H), 4.11 (s, 2.02H), 4.24 (s, 1.20H), 4.30 (s, 0.67H), 7.28-7.40 (m, 9.21H) ppm. ^{13}C NMR (600 MHz, acetone-d_6): δ 29.85, 43.55, 43.99, 44.54, 128.36, 129.42, 130.33, 137.54, 137.80 ppm. GC-MS $C_{14}H_{14}S_2$, MW:246: [M^+-1] = 65.2 (18), 77.2 (8), 91.1 (90), 121.1 (5), 181.2 (18), 246.1 (20); S_8, MW:256: [M^+-1] = 64.1 (100), 77.1 (7), 91.1 (66), 127.9 (60), 160.0 (66), 191.9 (53), 207.1 (5), 223.9 (7), 255.8 (98), 315.1 (5). $C_{14}H_{14}S_3$, MW:278: [M^+-1] = 65.2 (13), 77.1 (3), 91.2 (100), 123.1 (3), 181.2 (2), 213.1 (56), 278.1 (13).

4.4.4 Dibenzyl Disulfide Reduction using Bis(trimethylsiloxy)methylsilane ([SiH]/[SS]=2:1, Molar Ratio between Hydrosilane and Disulfide)

To a pre-dried 200 ml round-bottomed flask purged with dry N_2 gas, was added dibenzyl disulfide (0.50 g, 2.04 mmol) and bis(trimethylsiloxy)methylsilane (0.91 g, 4.09 mmol) together with dry DCM (3.81 g, 44.86 mmol) as solvent. Freshly prepared $B(C_6F_5)_3$ stock solution was added (0.167 ml, 0.0326 mmol) after 5 min stirring. The total reaction time was 3 h, then the reaction was quenched by adding neutral alumina. Each datapoint in Figure 4.2 was obtained using the identical reaction protocol, only changing the ratio of hydrosilane to disulfide [SiH]/[SS] (Table S4.1).

4.4.5 Titration of Disulfides to Establish Relative Reactivity of Functional Groups

Conversion in the reaction was shown by peak area of the hydrogens on the carbon adjacent to the disulfide bond (-C**H₂**SS) in ^{1}H NMR, which was plotted against different ratios of hydrosilane (Si**H**) to disulfide. Analogous techniques were used to follow the reduction of the tetrasulfide (Figure 4.2).

4.4.6 Reduction of Rubbers: General Procedure

The reaction conditions for the reduction of rubber powder are given in Table 4.2, Table 4.3. The general experimental procedure is as follows. The cryogenically ground rubber powder was allowed to swell in dry toluene (12 ml) for 30 min.

Pentamethyldisiloxane **7** was added to the reaction mixture. The stock catalyst solution was added to initiate the reaction. The suspension was heated in a 60 °C oil bath for 48 h. The residual undissolved rubber powder was washed with toluene and separated by centrifugation (Eppendorf, Centrifuge 5424, at 12000 rpm for 20 min). The extraction process was repeated twice to completely remove soluble compounds. The supernatants were mixed, and the solvents were removed by rotary evaporation. Any residual (organic) volatiles were removed under a stream of N_2

over 24 h. The recovered organic liquid was characterized by NMR. The recovered rubber powders were dried at 100 °C overnight and then examined by TGA. The bulk sample were reduced by the similar protocol and more details were provided in SI.

4.4.7 Reduction with Inexpensive Tetramethyldisiloxane M^HM^H

Cryogenically ground inner tube powder (300 mg) was placed in dry toluene (12 ml), followed by tetramethyldisiloxane M^HM^H (1.5 ml, 8.5 mmol). The stock catalyst solution (600 μL, stock catalyst concentration: 50 mg/ml in toluene, catalyst concentration in reaction: 10wt%/ inner tube) was added immediately afterwards to initiate the reaction. The suspension was heated in a preheated 100 °C oil bath for 30 min. The reaction flask was put into a room temperature water bath to quench the reaction and followed by a separation process using the same protocol stated in the former paragraph. The organic yield was 87%.

4.4.8 Desilylation of Product Polymeric Oils to Give 11

The silylated organic oil **8** (based tire tread, derived from IR/NR, 0.50 g) was desilylated by treatment with TBAF solution (0.5 g TBAF, 1.92 mmol TBAF, dissolved in 10 ml THF containing 0.1ml methanol) for 24 h at 80 °C. The solvent and siloxane fragments were removed by using a rotary evaporator, followed by kugelrohr distillation; loss of silicone was clearly seen in the ^{1}H NMR (200 °C, 3h,Figure S4.20)

4.4.9 Crosslinking of Recovered Oils

4.4.9.1 Oxidative Coupling of Thiols Using Iodine

The desilyated organic oil **11** (derived from truck tread IR/NR, 0.2g) was allowed to react with an iodine solution (50 mM dissolved in 1/1 v/v toluene/isopropanol) for 12h at room temperature. Solvents associated with the resulting elastomer **12** were removed under a stream of N_2 over 12 h (Figure S4.21a). Crosslinking was confirmed using a swelling test. Compound **12** (0.1g) was swelled in 10ml of hexane; the degree of swelling was 209 wt %. The precursor oil **8** dissolved readily in hexane easily while **12** remained an elastomeric solid even after 1h sonication (Figure S4.21b).

4.4.9.2 Preparation of Toy Tire using a Peroxide Initiator (Figure 4.4)

A silicone mode was prepared with a two-part liquid component kit (Sylgard 184). Two components were mixed at the recommended ratio of 10 parts (10.0 g) base to 1 part curing agent (1.0 g). The mixing process was performed using a planetary centrifugal mixer (FlackTek Inc.) with a duration of 5 min at a speed of 3000 rpm. In order to fabricate bubble free elastomer, the mixed uncured PDMS was thoroughly degassed in a vacuum desiccator at low pressure for 30 min.

The right front tire of a toy car was removed from the toy and placed in the degassed, uncured mixture. The mixture was cured in an 80 ^{o}C oven overnight. The tire was removed from the cured mold.

Used rubber powder from the truck tread (Sailun) (2.0 g) was reduced by pentamethyldisiloxane **7** in a 100 °C oil bath for 18 h to give a polymeric oil **8** (81.5% yield). Solvents in the supernatants, after centrifugation, were removed by rotary evaporation; any residual volatiles and silicone by-products were removed using a stream of N_2 over 24 h. The oil was accompanied by residual undissolved rubber powder that was washed with toluene and separated by centrifugation (Eppendorf, Centrifuge 5424, at 12000 rpm for 20 min), dried an 80 ^{o}C oven for 18h, and ground into powder using a mortar and pestle (Figure 4.4d).

The silylated organic oil **8** from the former step (comprised of IR/NR derivatives, 0.707 g) was dissolved in hexanes (10 ml), benzoyl peroxide (BPO, 0.01 g, 1wt%, 0.0413 mmol) and, optionally, ground residual inorganic solids (from the preparation of **8**, 0.3010 g), were added sequentially and mixed to give a homogeneous dispersion. After the solvent was removed by rotary evaporation, the mixture was placed in the silicone mold and degassed under vacuum in a dessicator for 30 min. The curing process was performed at 100 ^{o}C for 18 h. The formulations for rubber with different residual solid are listed in Table S4.6.

Table 4.3 Depolymerization efficiency of organic elastomers by hydrosilanes.[a]

Starting rubber components[b]					Parameters		Results	
Sample (mg)		Form	Organic (mg)	Inorganic[c] (mg)	Hydrosilanes (ml)	Temperature (°C) & Time (h)	Organic yield[d] (%)	Residual solid[e] (mg)
Crumb 1 (300)		powder	143	157	**7** (1.5)	60/48	35.8	206.7
Crumb 2	First[g]	powder	185	115	**7** (1.5)	60/48	56.2	182.9
	Second[g]	powder	80.9	102	**7** (1.5)	60/48	85.8	74.0
	Third[g]	powder	26.3	47.7	**7** (1.5)	60/48	88.3	64.0
EPDM (300)		powder	165	135	**7** (1.5)	60/48	60.4	162.0
Inner Tube (300)		coupon	183	117	**7** (1.5)	60/48	62.4	49.0+118.0[f]
Inner Tube (300)		powder	183	117	**7** (1.5)	60/48	92.9	112.7
Inner Tube (2000)		powder	1222	778	**7** (10.0)	60/48	89.1	821.0
Inner tube (300)		powder[h]	183	117	**7** (1.5)	100/0.5	79.0	150.0
Inner tube (300)		powder[h]	183	117	**7** (1.5)	100/2	80.3	143.4
Inner tube (300)		powder[h]	183	117	**7** (1.5)	100/4	81.5	142.3
Inner tube (300)		powder[h]	183	117	**7** (1.5)	100/10	85.0	122.0
Inner tube (300)		powder[h]	183	117	M^HM^H (1.5)	100/0.5	87.0	151.0
Inner tube (300)		powder[i]	183	117	M^HM^H (1.5)	100/0.5	85.0	151.0
Truck Tread 1 (300)		powder	187	113	**7** (1.5)	60/48	88.3	109.5

Truck Tread 1 (300)	powder (Soxhlet)	175	125	**7** (1.5)	60/48	87.6	115.1
Truck Tread 1(2000)	powder	1244	756	**7** (10.0)	60/48	84.6	861.0
Truck Tread 2 (300)	powder	195	105	**7** (1.5)	60/48	89.8	109.0
Tread (snow tire) (300)	powder	189	111	**7** (1.5)	60/48	51.8	180.0
Side wall (snow tire) (300)	powder	178	122	**7** (1.5)	60/48	53.8	183.0

[a] Experimental conditions: $B(C_6F_5)_3$/ Rubber = 10wt%, 12 ml toluene. [b] Based on TGA. [c] Includes carbon black and thermally stable inorganic moieties. [d] Fraction of available elastomer converted into organic soluble oils. [e] Residual solid contains carbon black, inorganics and residual polymeric rubber. [f] 49.0 mg of residual powder and 188mg of residual coupon still containing elastomer (Figure S4.10). [g] Process for degradation of Crumb-2 using multiple reduction cycles; 169.0 mg of starting material were used in the 2nd reduction and 65.0 mg in the 3rd (Figure S4.14b). [h] The rubber powder was allowed to swell in reaction mixture for 3h before adding $B(C_6F_5)_3$ catalyst. i Catalyst solution was added immediately after addition of hydrosilane.

4.5 Conclusions

Utilization of the reactions described here to create polymeric oils by the reductive silylation of used automotive rubbers, and subsequent oxidation to new elastomers, permits the completion of a full cycle of use for these organic materials. Mild, efficient reduction of S-S bonds of organic disulfides, including those found in used, sulfur-cured rubbers permits the formation of silylated polymers **8** – already in 87% yield at 100 °C within 30 minutes – that can be separated from the inorganic constituents. Radical cure of the oils if alkenes are present, or following desilylation, oxidative cure of thiolated polymers leads to new elastomers **12**, **13** that, optionally, can be reinforced by the inorganic constituents recovered during the reduction process. The practice of this recycling process has the potential to reduce the environmental impact of used, sulfur-crosslinked elastomer.

4.6 References

1. Coran, A. Y., Chapter 7 - Vulcanization. In *The Science and Technology of Rubber (Fourth Edition)*, Mark, J. E.; Erman, B.; Roland, C. M., Eds. Academic Press: Boston, 2013; pp 337-381.
2. Goodyear, C., Improvement in India-Rubber Fabrics. *US Patent 3633* **1844**.
3. World Tires (http://www.freedoniagroup.com/industry-study/world-tires-3357.htm). *Freedonia Group* **2015,** *Industry Study 3357*.
4. Evans, J. J., Rubber Tire Leachates in the Aquatic Environment. *Rev. Environ. Contam. Toxicol.* **1997,** *151*, 67-115.
5. Stevenson, K.; Stallwood, B.; Hart, A. G., Tire Rubber Recycling and Bioremediation: A Review. *Biorem. J.* **2008,** *12* (1), 1-11.
6. Liu, X.; Wang, J.; Gheni, A.; ElGawady, M. A., Reduced Zinc Leaching from Scrap Tire during Pavement Applications. *Waste Manage. (Oxford)* **2018,** *81*, 53-60.
7. Singh, A.; Spak, S. N.; Stone, E. A.; Downard, J.; Bullard, R. L.; Pooley, M.; Kostle, P. A.; Mainprize, M. W.; Wichman, M. D.; Peters, T. M.; Beardsley, D.; Stanier, C. O., Uncontrolled Combustion of Shredded Tires in a Landfill – Part 2: Population Exposure, Public Health Response, and an Air Quality Index for Urban Fires. *Atmos. Environ.* **2015,** *104*, 273-283.
8. *Rubber Recycling: Challenges and Developments*. RSC: 2019.
9. Cheng, H.; Hu, Y.; Reinhard, M., Environmental and Health Impacts of Artificial Turf: A Review. *Environ. Sci. Technol.* **2014,** *48* (4), 2114-2129.
10. Ochmann, M.; Hussain, A.; von Ahnen, I.; Cordones, A. A.; Hong, K.; Lee, J. H.; Ma, R.; Adamczyk, K.; Kim, T. K.; Schoenlein, R. W.; Vendrell, O.; Huse, N., UV-Photochemistry of the Disulfide Bond: Evolution of Early Photoproducts from Picosecond X-ray Absorption Spectroscopy at the Sulfur K-Edge. *J. Am. Chem. Soc.* **2018,** *140* (21), 6554-6561.
11. Studebaker, M. L.; Nabors, L. G., Sulfur Group Analyses in Natural Rubber Vulcanizates. *Rubber Chem. Technol.* **1959,** *32* (4), 941-961.
12. Studebaker, M. L., Lithium Aluminum Hydride Analysis of Sulfur-Cured Vulcanizates. *Rubber Chem. Technol.* **1970,** *43* (3), 624-650.
13. Walvekar, R.; Afiq, Z. M.; Ramarad, S.; Khalid, S., Devulcanization of Waste Tire Rubber Using Amine Based Solvents and Ultrasonic Energy. *MATEC Web Conf.* **2018,** *152*.
14. Czajczyńska, D.; Krzyżyńska, R.; Jouhara, H.; Spencer, N., Use of Pyrolytic Gas from Waste Tire as a Fuel: A Review. *Energy* **2017,** *134*, 1121-1131.
15. Brook, M. A., Hydrosilanes as Reducing Agents. In *Silicon in Organic, Organometallic and Polymer Chemistry*, Wiley: New York, 2000; pp 171-188.
16. Lukevics, E.; Dzintara, M., The Alcoholysis of Hydrosilanes. *J. Organomet. Chem.* **1985,** *295* (3), 265-315.

17. MarcIniec, B.; Gulinski, J.; Urbaniak, W.; Kornetka, Z. W., *Comprehensive Handbook on Hydrosilylation Chemistry*. Pergamon: Oxford, 1992.
18. Brook, M. A., New Control Over Silicone Synthesis using SiH Chemistry: The Piers–Rubinsztajn Reaction. *Chem. Eur. J* **2018,** *24* (34), 8458-8469.
19. Gevorgyan, V.; Rubin, M.; Liu, J. X.; Yamamoto, Y., A Direct Reduction of Aliphatic Aldehyde, Acyl Chloride, Ester, and Carboxylic Functions into a Methyl Group. *J. Org. Chem.* **2001,** *66* (5), 1672-1675.
20. Parks, D. J.; Piers, W. E., Tris(pentafluorophenyl)boron-catalyzed Hydrosilation of Aromatic Aldehydes, Ketones, and Esters. *J. Am. Chem. Soc.* **1996,** *118* (39), 9440-9441.
21. Saito, K.; Kondo, K.; Akiyama, T., $B(C_6F_5)_3$-Catalyzed Hydrodesulfurization Using Hydrosilanes – Metal-Free Reduction of Sulfides. *Org. Lett.* **2015,** *17* (13), 3366-3369.
22. Jakab, E.; Omastová, M., Thermal Decomposition of Polyolefin/Carbon Black Composites. *J. Anal. Appl. Pyrolysis* **2005,** *74* (1), 204-214.
23. Brazier, D. W.; Nickel, G. H., Thermoanalytical Methods in Vulcanizate Analysis II. Derivative Thermogravimetric Analysis. *Rubber Chem. Technol.* **1975,** *48* (4), 661-677.
24. Standard Test Method for Rubber - Compositional Analysis by Thermogravimetry (TGA). *ASTM* **2014,** *D6370-99*.
25. Standard Test Methods for Rubber Products - Chemical Analysis. *ASTM* **2002,** *D 297–93*.
26. Piers, W. E., The Chemistry of Perfluoroaryl Boranes. *Adv. Organomet. Chem.* **2005,** *52*, 1-77.
27. So, J.-H.; Boudjouk, P.; Hong, H. H.; Weber, W. P., Hexamethyldisilathiane. *Inorg. Synth.* **1992,** *29*, 30-32.
28. Crouch, R. D., Recent Advances in Silyl Protection of Alcohols. *Synth. Commun.* **2013,** *43* (17), 2265-2279.
29. Zeynizadeh, B., Oxidative Coupling of Thiols to Disulfides with Iodine in Wet Acetonitrile. *J. Chem. Res.* **2002,** *2002* (11), 564-566.
30. Oestreich, M.; Hermeke, J.; Mohr, J., A Unified Survey of Si–H and H–H Bond Activation Catalysed by Electron-Deficient Boranes. *Chem. Soc. Rev.* **2015,** *44* (8), 2202-2220.
31. Fernández-Alvarez, F. J.; Aitani, A. M.; Oro, L. A., Homogeneous Catalytic Reduction of CO_2 with Hydrosilanes. *Catal. Sci. Technol.* **2014,** *4* (3), 611-624.
32. Beckett, M. A.; Brassington, D. S.; Coles, S. J.; Hursthouse, M. B., Lewis Acidity of Tris(pentafluorophenyl) Borane: Crystal and Molecular Structure of $B(C_6F_5)_3$. $OPEt_3$. *Inorg. Chem. Commun.* **2000,** *3* (10), 530-533.
33. Akbulut, H.; Yamada, S.; Endo, T., Preparation of a Zwitterionic Polymer Based on L-cysteine for Recovery Application of Precious Metals. *RSC Adv.* **2016,** *6* (110), 108689-108696.

34. Stensaas, K. L.; Brownell, A. S.; Ahuja, S.; Kaiser Harriss, J.; Herman, S. R., Competitive Oxidations of Dibenzyl Trisulfide vs. Substituted Aryl Polysulfides. *J. Sulfur Chem.* **2008,** *29* (3-4), 433-443.

Supporting Information

Dissolving Used Rubber Tires

Sijia Zheng, Mengchen Liao, Yang Chen, and Michael A. Brook*

Department of Chemistry and Chemical Biology, McMaster University, 1280 Main St. West, L8S 4M1, Ontario, Canada.

TABLE OF CONTENTS

ADDITIONAL GENRAL METHODS

Soxhlet extraction

Stock solutions

DISULFIDE AND TETRASULFIDE CHEMISTRY

Dibenzyl tetrasulfide titration using bis(trimethylsiloxy)methylsilane ([SiH]/[SS]=1:1)

Table S4.1 Reactivity comparison using dibenzyl sulfide **1** and bis(trimethylsiloxy)methylsilane. 150

Table S4.2 Integration data used to plot Figure 4.2. 151

Figure S 4.1 Benzyl disulfide reaction with MD^HM monitored by ^1H NMR (during the titration, small quantities of solvent remained in the sample; peaks at 1.5 and 2.3 ppm reflect the presence of water and toluene, respectively.). 151

Figure S4.2 Benzyl tetrasulfide reaction with MD^HM monitored by ^1H NMR. 152

RIBBER CHEMISTRY

Sample Preparation

Figure S4.3 (a) Sailun Truck tread 2. (b) Sectioning the external, road contacting section with a reciprocating saw to give Truck tread 2. 152

* Corresponding author. Tel.: +1-905-525-9140; fax:+1 -905 522-2509; e-mail: mabrook@mcmaster.ca.

Starting Material Characterization

Particle sizes

Figure S4.4 Particle size of ground rubber (inner tube) crumb 153

^{13}C HR-MAS NMR

Figure S4.5 The 13C HR-MAS NMR of different rubber samples 154

TGA of starting materials

Table S4.3 Rubber components characterized by TGA profile 154
Figure S4.6 The thermogravimetric analysis curves (a) and differential thermal analysis curves (b) of different rubber samples. 154

Reduction of Rubbers: General Procedure (with Powders or Coupons)

Bulk samples

Figure S4.7 Sequence of conversion of starting rubber samples to organic oils and residual powers (shown for inner tube rubber). Note: the turbidity of the recovered oil can vary depending on batch and on starting material; oil on the right is from a batch of car snow tire tread.. 156
Figure S4.8 Visible differences in the reaction processes as a function of reduction efficiency 156

Product characterization

TGA of reduced products

Figure S4.9 Determination of organic polymer fraction using TGA, shown for the inner tube. 157
Figure S4.10 Thermogravimetric analysis (TGA) of powder (red) or coupon (blue) inner tube after reduction. 157
Figure S4.11 Thermogravimetric analysis (TGA) of different rubber samples. Before (black line) and after reduction (red line).. 158
Figure S4.12 Thermogravimetric analysis (TGA) of (a) tread (snow tire) and (b) Side wall (snow tire). Original starting bulk rubber (black, Figure 4.3a), residual bulk rubber (Figure 4.3d) after reduction (blue), and residual powder (Figure 4.3e) collected after reduction (red)............. 159
Figure S4.13 Thermogravimetric analysis (TGA) of (a) inner tube and (b) truck tread-1 (right) samples with different scales (small = 300 mg; large = 2000 mg). 159

Extraction efficiency during repetitions

Table S4.4 Decrosslinking of bulk rubber; effect of multiple repetitions 160
Figure S4.14 Thermogravimetric analysis (TGA) of (a) truck tread samples with (red) or without (black) Soxhlet extraction. (b) Crumb-2 sample after multiple reduction steps.................... 161

NMR characterization of product polymer oils

Figure S4.15 ^{1}H NMR of recovered organic liquids.. 162

GPC (MW) characterization of product polymer oils

Table S4.5 GPC data of recovered organic oil 162
Figure S4.16 GPC data of recovered organic oil with two molecular populations. 163

Efficiency of reduction using other hydrosilicones

Figure S4.17 Inner tube reduction after 18h at 100 °C with different hydrosilanes. (a) $Me_3Si(OSiMeH)_nSiMe_3$ **9**; (b) $HMe_2SiOSiMe_2H$ **10**.. 163

Multiple Reductions with Bulk Rubber (analogous to the Inner Tube Experiments Shown in Table 4.2, Table 4.3)

Figure S4.18 Time lapse photos of rubber reduction and dissolution. 164
Figure S4.19 Shrinkage of bulk rubber after 1 reduction cycle (a) snow tire tread; (b) snow tire sidewall; (c) bulk rubber bicycle tire. 165

Preparation of New Elastomers

Desilylation

Figure S4.20 ^1H NMR showing loss of silicone groups from the organic polymers after utilizing TBAF. 165

New Elastomers

Figure S4.21 (a) The crosslinked elastomer **16** formed by iodine reoxidation of thiols in **8**. (b) The picture of 0.1 g **17**, swollen in 10 ml hexane after 1 h sonication. 166
Table S4.6 Recrosslinking of recovered organic oil **8** with residual solid as reinforcing agent (Figure 4.4). 166

ADDITIONAL GENERAL METHOS

Soxhlet extraction

Raw rubber samples may contain organic additives, including oil or other additives that could influence the reductive cleavage process. Therefore, in a control experiment, the extractable components were extracted prior to reduction. The most commonly used extraction solvent,[25] acetone, was used to remove resins, free sulfur, acetone soluble softeners and antioxidants, processing rubber additives, mineral oils, waxes, organic accelerators and their reactive products and fatty acids. The extraction procedure was as follows: 5.0 g raw truck tread-1 rubber powder was placed inside Whatman cellulose extraction thimble (33 mm×118 mm). The sample containing the thimble was extracted with 200ml refluxing acetone 56 °C for 72 h in a standard Soxhlet apparatus. After this purification, the sample was dried in 100 °C oven overnight. The weight of collected sample was 4.48 g.

Stock solutions

$B(C_6F_5)_3$: BCF was dissolved in dry toluene to prepare a stock solution (50mg ml^{-1}).

Stock solution of naphthalene in chloroform-*d*: solid naphthalene (4 mg, 0.031 mmol) was added to chloroform-*d* (2 ml, 3.0 g, 24.92 mmol) in a dried 20.0 ml glass vial.

DISULFIDE AND TETRASULFIDE CHEMISTRY

Dibenzyl tetrasulfide titration using bis(trimethylsiloxy)methylsilane ([SiH]/[SS]=1:1)

To a dried glass NMR tube (7×5 mm) purged with dry N_2 gas, dibenzyl tetrasulfide (0.055 g, 0.185 mmol, a mix of oligosulfides, see above) and bis(trimethylsiloxy)methylsilane (0.048 g, 0.216 mmol) were added together with chloroform-*d* stock solution (0.6 ml). Freshly prepared $B(C_6F_5)_3$ stock solution was added (0.023 ml, 0.0045 mmol) after 5 min sonication. Each point in Figure S4.2 was obtained by adding bis(trimethylsiloxy)methylsilane (0.048 g, 0.216 mmol) and $B(C_6F_5)_3$ stock solution (0.023 ml, 0.0045 mmol) in aliquots portion by portion with 3 h time interval between additions. The peak area of the hydrogens on the carbon adjacent to polysulfide bonds including pentasulfide (-C$\mathbf{H_2}$SSSSS), tetrasulfide (-C$\mathbf{H_2}$SSSS), trisulfide (-C$\mathbf{H_2}$SSS) and disulfide (-C$\mathbf{H_2}$SS) in ^{1}H NMR (Figure S4.2) were plotted against different ratio of hydrosilane (Si**H**) input (Figure S4.2).

Table S4.1 Reactivity comparison using dibenzyl sulfide **1** and bis(trimethylsiloxy)methylsilane **2**.

Ratio [SiH]/[SS]	**1** (g)	**2** (g)	DCM (g)	$B(C_6F_5)_3$ (ml)[a]
0.25	0.50	0.12	1.68	0.021
0.5	0.50	0.24	2.05	0.042
1	0.50	0.46	2.59	0.084
1.5	0.50	0.68	3.20	0.125
2	0.50	0.91	3.81	0.167

[a] 100 mg ml^{-1} $B(C_6F_5)_3$ stock solution

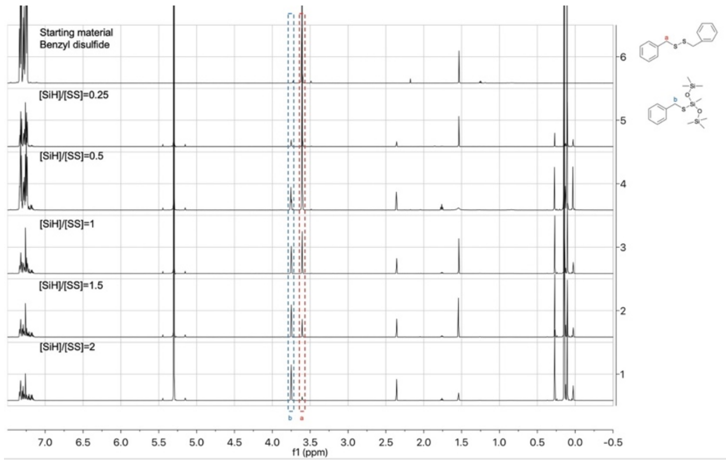

Figure S4.1 Benzyl disulfide reaction with MD^HM monitored by ^1H NMR (during the titration, small quantities of solvent remained in the sample; peaks at1.5 and 2.3 ppm reflect the presence of water and toluene, respectively.).

Table S4.2 Integration data used to plot Figure 4.2.

Ratio [SiH]/[SS]	**1** (g)	**2** (g)	DCM (g)	$B(C_6F_5)_3$ (ml)[a]
Figure 4.2a				
0.5	0.50	0.24	2.05	0.042
1	0.50	0.46	2.59	0.084
1.5	0.50	0.68	3.20	0.125
2	0.50	0.91	3.81	0.167
Figure 4.2b				
0.25	0.50	0.12	1.68	0.021
0.5	0.50	0.24	2.05	0.042
1	0.50	0.46	2.59	0.084
1.5	0.50	0.68	3.20	0.125
2	0.50	0.91	3.81	0.167

[a] 100 mg ml^{-1} $B(C_6F_5)_3$ stock solution

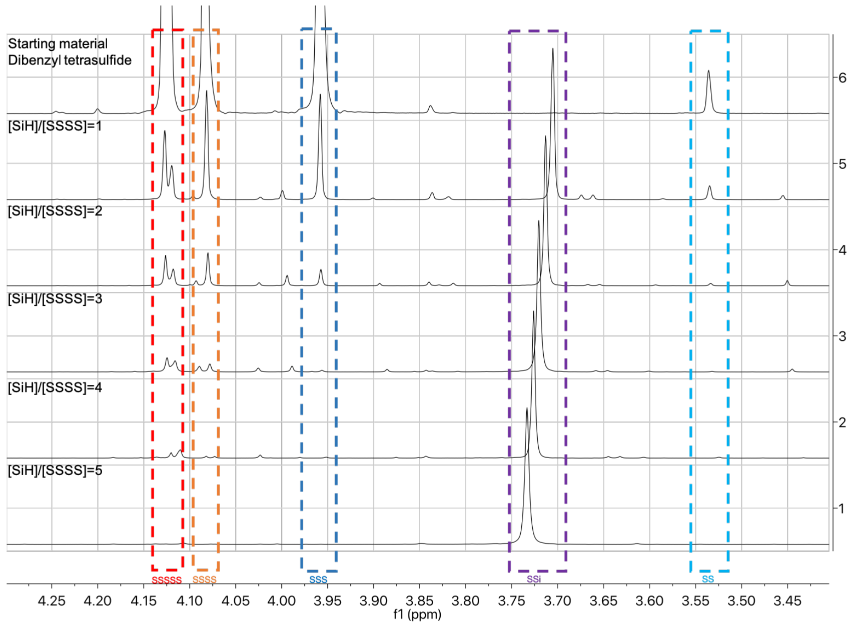

Figure S4.2 Benzyl tetrasulfide reaction with MD^{H}M monitored by ^{1}H NMR

RUBBRER CHEMISTRY

Sample Preparation

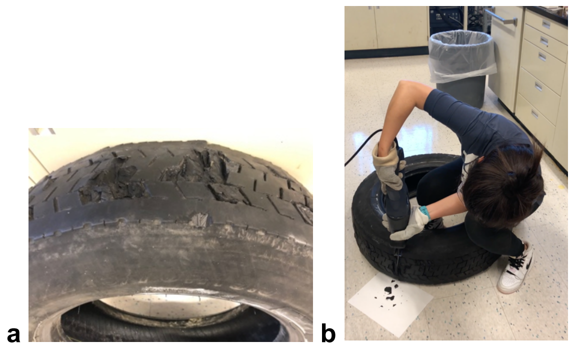

Figure S4.3 (a) Sailun Truck tread 2. (b) Sectioning the external, road contacting section with a reciprocating saw to give Truck tread 2.

Starting Material Characterization

Particle sizes

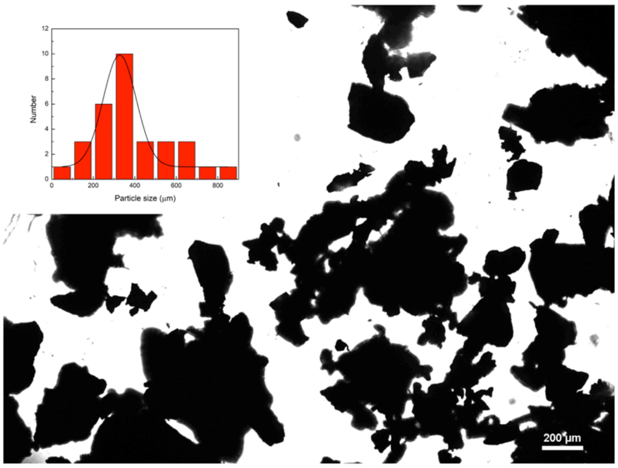

Figure S4.4 Particle size of ground rubber (inner tube) crumb.

^{13}C HR-MAS NMR

The polymer constituents of rubber samples were estimated from carbon high-resolution magic angle spinning (^{13}C HR-MAS) NMR spectroscopy. The dry rubber powder samples were weighed (～ 10 mg) and placed into a ^{13}C HR-MAS rotor and then inserted into the spectrometer. ^{13}C HR-MAS spectra were acquired using a Bruker Avance 850HD NMR spectrometer operating at 213.8 MHz for ^{13}C. Samples were typically spun at 8 kHz using a 4 mm ^{13}C HR-MAS probe (P/N 132955, S/N 0002) maintained at 25 °C. One-dimensional spectra were acquired using standard pulse-acquisition (Figure S4.5).

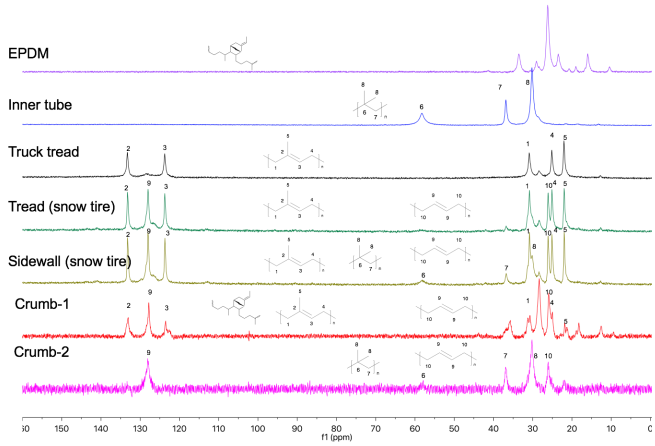

Figure S4.5 The ^{13}C HR-MAS NMR of different rubber samples.

TGA of starting materials

Table S4.3 Rubber components characterized by TGA profile

Component	% Mass Loss
Organic materials	50 °C to 550 °C (nitrogen)
Carbon black	560 °C to 800 °C (air)
Ash	Residue at 800 °C

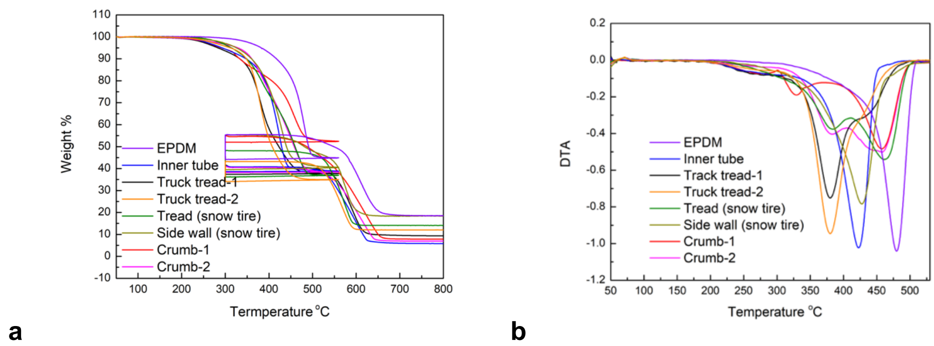

Figure S4.6 The thermogravimetric analysis curves (a) and differential thermal analysis curves (b) of different rubber samples.

Reduction of Rubbers: General Procedure (with Powders or Coupons)

Bulk samples

Bulk samples were cut directly from different parts of a car tire using a reciprocating saw (Figure S4.3). The experimental procedure for their reduction is as follows. The bulk piece of raw tread (cross-section, 2.083 g, ~1.200 cm × 1.519 cm × 1.125 cm, containing metal and fiber) was allowed to swell in dry toluene (80 ml) for 6h. Pentamethyldisiloxane (7.6 g, 51.35 mmol, 10 ml) was added to the reaction mixture. Several ceramic beads were added to increase shear force while stirring with a magnetic stirrer. BCF catalyst was added portion by portion each 24 h (6+2+2+2 wt% $B(C_6F_5)_3$). The reaction mixture was heated in a 60 °C oil bath for 6 d (Figure S4.18). The residual undissolved rubber bulk was washed with toluene and dried in a 100 °C oven. The suspension was centrifuged, then washed, and re-centrifuged (repeated twice). The supernatants were mixed, and the solvent was removed by rotary evaporation. The volatile organics were removed by blowing with a stream of N_2 for 48 h. The residual (now smaller, Figure S4.19 a) rubber bulk (0.460g, broken in two pieces: 0.675 cm × 1.331 cm × 0.445 cm, 0.754 cm × 0.937 cm × 0.340 cm) and powder (0.527 g) were separately examined using TGA (Figure S4.12a). The recovered organic liquid was characterized by NMR.

Powdered samples were reduced following the same protocol. Powders were prepared by cryogenic grinding as noted in the main text.

The calculations of yield and the appearance of the materials are shown in Figure S4.9 and Figure S4.19. The TGA data before and after reduction for the different rubbers may be found in (Figure S4.11). Increasing the scale from 300 to 2000 mg did not significantly change the efficiency of the process (Figure

S4.13). The effect of Soxhlet extraction was minor. Multiple reductions led to additional material, but with decreasing fractions of soluble oil produced (Figure S4.14, Table 4.2, Table 4.3).

The organic yields were calculated from TGA profiles:

$$\text{Organic Yield }\% = \frac{m_0 \times W_0 - m_i \times W_i}{m_0 \times W_0} \times 100$$

i.e., (Organic yield = (Total Organic-Recovered Organic)/Total Organic * 100)

Where m_0 is the mass of starting rubber and m_i is the mass of residual solid. W_0 is the organic weight % in starting rubber. W_i is the organic weight% in residual solid. Both W_0 and W_i is got from TGA.

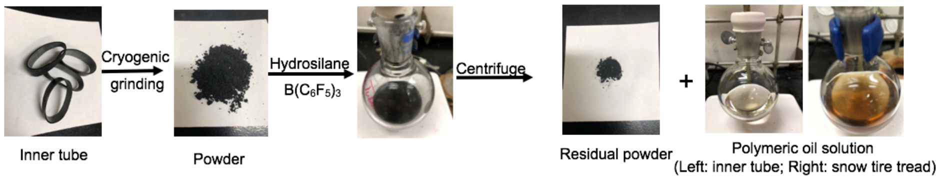

Figure S4.7 Sequence of conversion of starting rubber samples to organic oils and residual powers (shown for inner tube rubber). Note: the turbidity of the recovered oil can vary depending on batch and on starting material; oil on the right is from a batch of car snow tire tread.

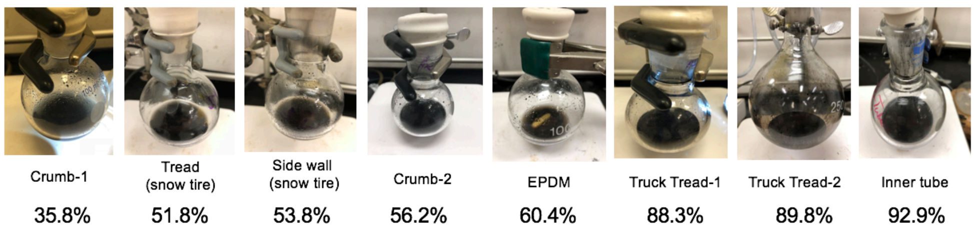

Figure S4.8 Visible differences in the reaction processes as a function of reduction efficiency.

Product characterization

TGA of reduced products

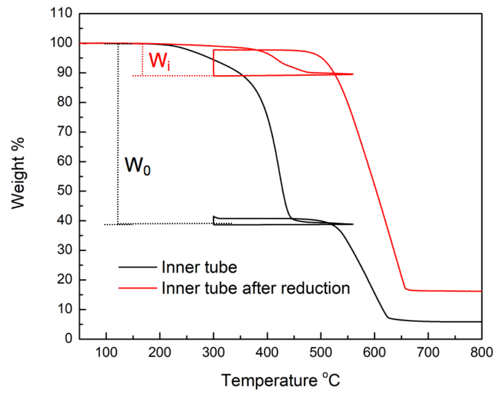

Figure S4.9 Determination of organic polymer fraction using TGA, shown for the inner tube.

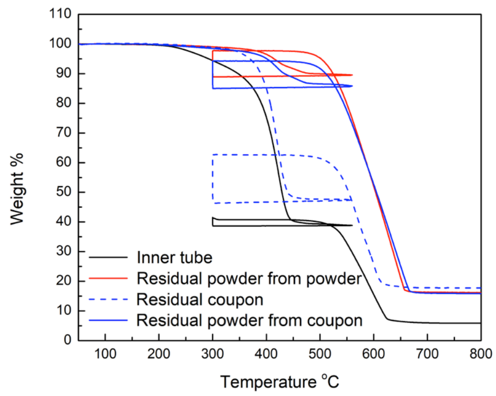

Figure S4.10 Thermogravimetric analysis (TGA) of powder (red) or coupon (blue) inner tube after reduction.

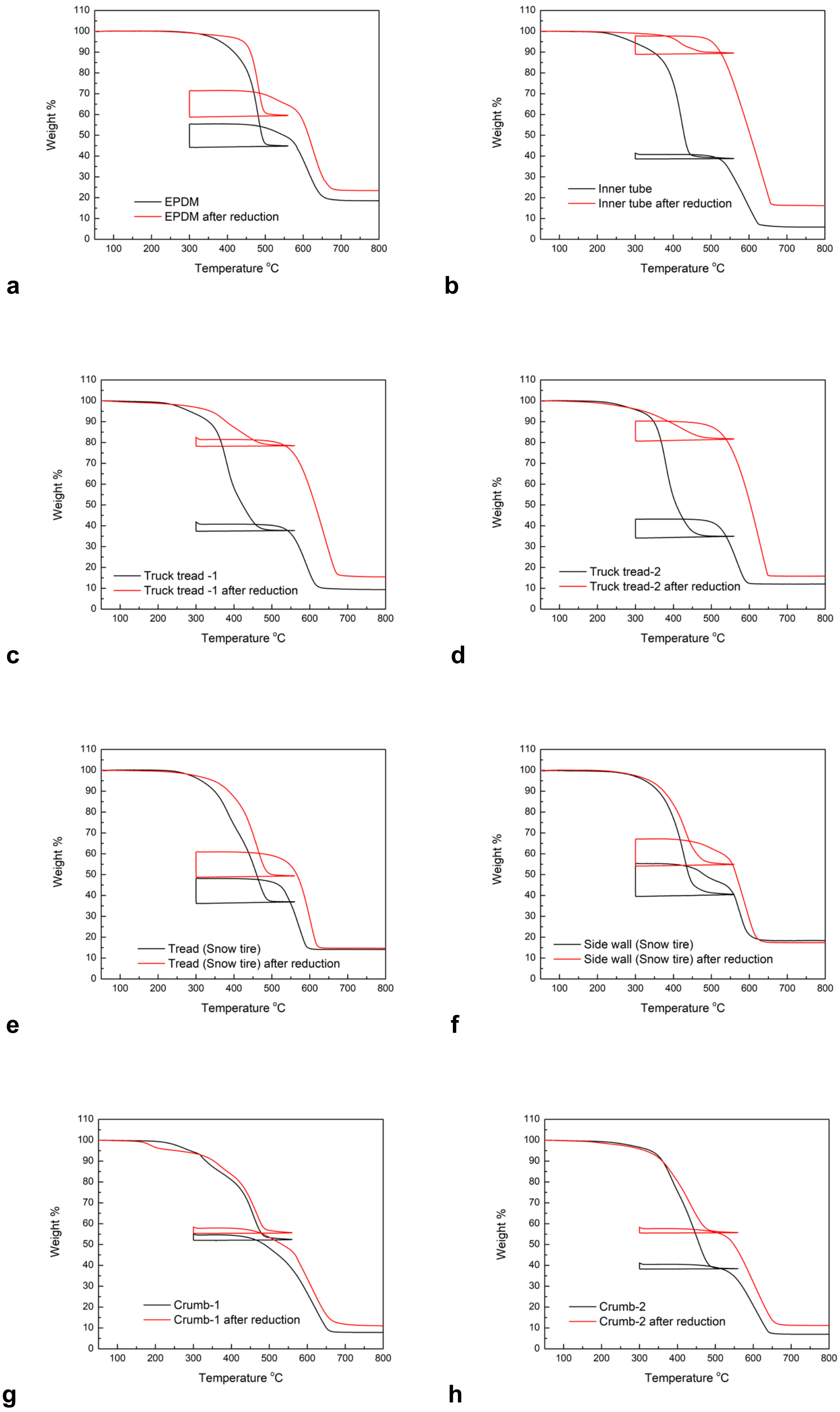

Figure S4.11 Thermogravimetric analysis (TGA) of different rubber samples. Before (black line) and after reduction (red line).

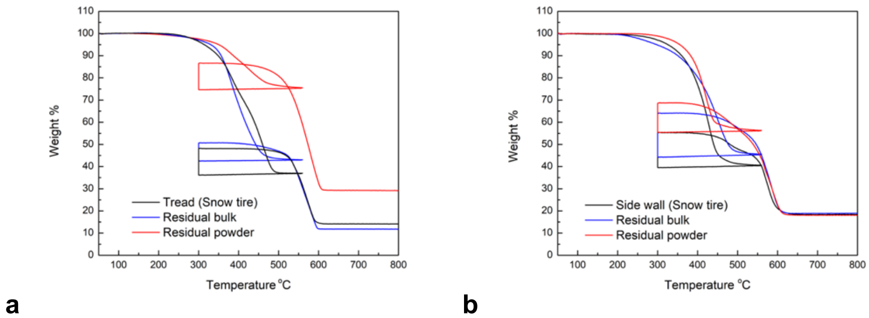

Figure S4.12 Thermogravimetric analysis (TGA) of (a) tread (snow tire) and (b) Side wall (snow tire). Original starting bulk rubber (black, Figure 4.3a), residual bulk rubber (Figure 4.3d) after reduction (blue), and residual powder (Figure 4.3e) collected after reduction (red).

Effect of Reaction Scale

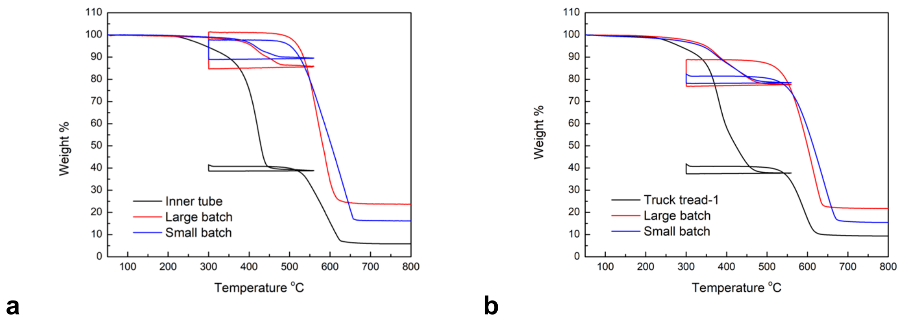

Figure S4.13 Thermogravimetric analysis (TGA) of (a) inner tube and (b) truck tread-1 (right) samples with different scales (small = 300 mg; large = 2000 mg).

Table S4.4 Decrosslinking of bulk rubber; effect of multiple repetitions.

Rubber type	Starting material Characteristics	Starting mass (mg)	**7** (ml)	Constitution of Residue				Recovered volatile liquid (mg)	Young's modulus of bulk Before/After (MPa)
				Bulk (mg)	Powder (mg)	Metal[d] (mg)	Total mass (mg)		
Side Wall	First (Bulk with fiber)[a]	1475	7.4	1197	48	0	1245	142	5.52±1.21/ 16.86±1.36
Side Wall[b]	Second (Powder, no metal or fiber)[c]	300	1.5	-	204	-	204	221	-
Tread	First (Bulk with metal and fiber)[a]	2083	10.0	460	527	294	1281	830	22.28±1.62/ 57.78±2.40
Tread[b]	Second (Powder, no metal or fiber)[c]	300	1.5	-	214	-	214	183	-

[a] Experimental conditions for the first reduction: BCF/ Rubber = 12 wt% (added portion by portion: 6+2+2+2), 6 days, 60 °C. [b] The residual bulk materials from the first reduction were ground into a powder prior to the second reduction. [c] Experimental conditions for the second reduction: BCF/ Rubber = 10wt% (added all at once), 48 h, 60 °C. [d] Note: Only metal was removed from the elastomer matrix in step 1; polymeric fiber; remained bound to the residual bulk solid.

Extraction Efficiency During Repetitions

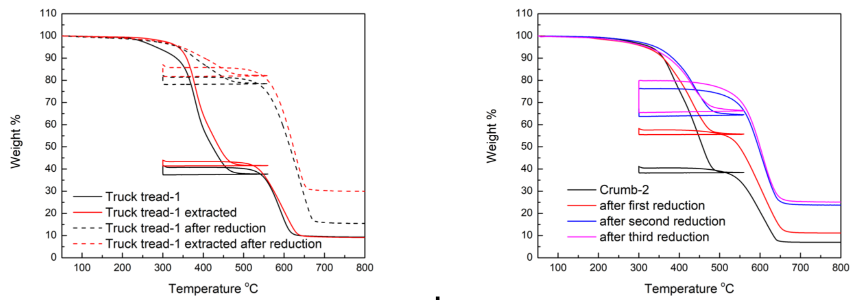

a b

Figure S4.14 Thermogravimetric analysis (TGA) of (a) truck tread samples with (red) or without (black) Soxhlet extraction. (b) Crumb-2 sample after multiple reduction steps.

NMR characterization of product polymer oils

The oils produced by the silylating reductions were characterized primarily by NMR. The signatures of the constituent polymers were readily identified. The geminal dimethyl groups on the backbone of polyisobutylene is particularly characteristic (Figure S4.15), as are backbone methyl groups from propylene and isoprene units. The constituent rubber components, as shown by NMR, are consistent with the TGA data on the starting elastomers (Figure S4.6). The molecular weights of these oils were in the 10000 g mol^{-1} range, with much higher fractions in some cases (Figure S4.16).

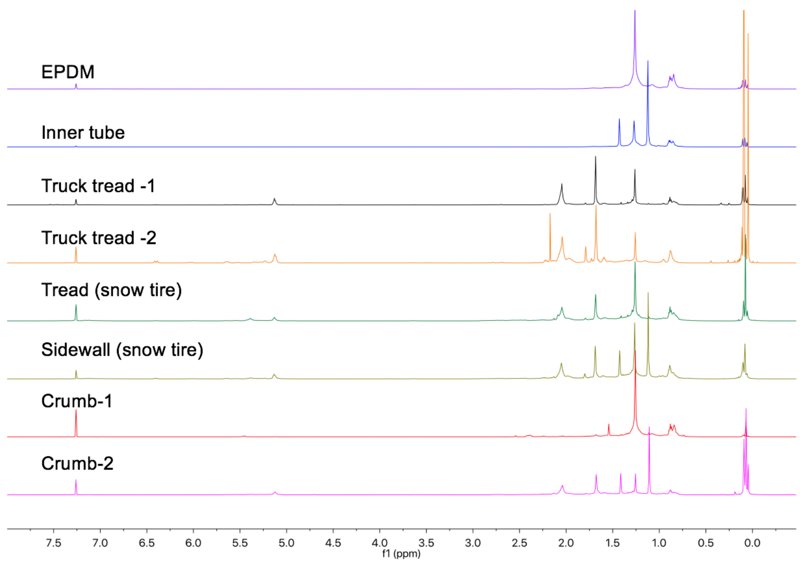

Figure S4.15 ^{1}H NMR of recovered organic liquids.

GPC (MW) characterization of product polymer oils

Table S4.5 GPC data of recovered organic oil.

Rubber sample	Components	Peak 1		Peak 2	
		Mw	PDI	Mw	PDI
EPDM	EPDM	-	-	6.54×10^{4}	1.39
Inner tube	PIB	1.1×10^{7}	1.12	7.9×10^{4}	2.50
Truck tread-1	IR/NR	0.8×10^{7}	1.25	2.02×10^{4}	2.05
Truck tread-2	IR/NR	-	-	6.63×10^{4}	1.95
Tread (snow tire)	IR/NR+BR	-	-	2.18×10^{4}	1.63
Side wall (snow tire)	IR/NR+IIR+BR	-	-	4.66×10^{4}	1.84
Crumb-1	BR+IR/NR+EPDM	-	-	6.13×10^{4}	2.11
Crumb-2	IIR+BR	1.42×10^{6}	1.18	4.18×10^{4}	2.39

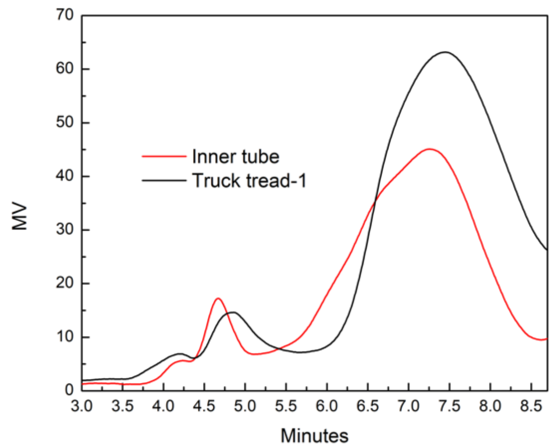

Figure S4.16 GPC data of recovered organic oil with two molecular populations.

Efficiency of reduction using other hydrosilicones

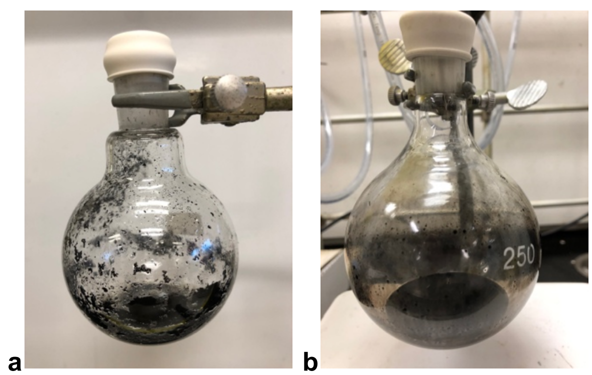

Figure S4.17 Inner tube reduction after 18 h at 100 °C with different hydrosilanes. (a) $Me_3Si(OSiMeH)_nSiMe_3$ **9**; (b) $HMe_2SiOSiMe_2H$ **10**.

Multiple Reductions with Bulk Rubber (analogous to the Inner Tube Experiments Shown in Table 4.2, Table 4.3)

It can be seen that shrinkage of the bulk elastomer occurs during the first reduction (Figure S4.18). The residual solid (300 mg) was ground cryogenically (under liq. N_2) and subjected to a secondary reduction using fresh catalyst (30 mg) and pentamethyldisiloxane (1.14 g, 1.5 ml). The reduction was carried out for 48 h in a 60 °C oil bath, followed with an additional wash sequence. The relative efficiency of reducing a powder vs bulk rubber (see previous section) is shown for the inner tube in Table 4.3.

A similar protocol was followed using a piece of sidewall (cross-section, 1.595 × 1.427 × 0.6096 cm, 1.475 g), which led to 1.427 × 1.409 × 0.549 cm). Sequential reactions showed that it was possible to capture additional depolymerized material in a second step, but it was not particularly efficient in bulk form (Table S4.4, Figure S4.12b).

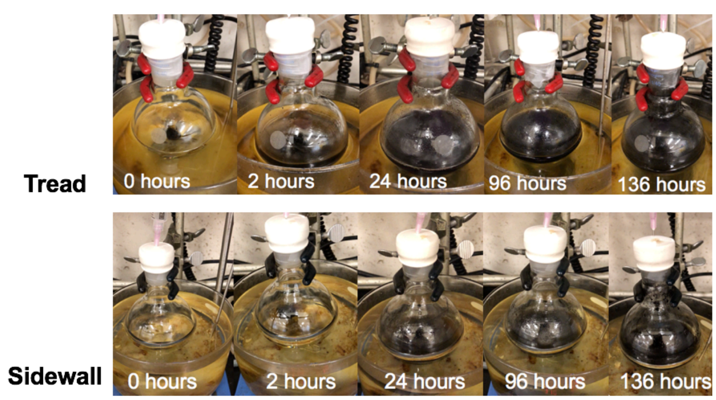

Figure S4.18 Time lapse photos of rubber reduction and dissolution.

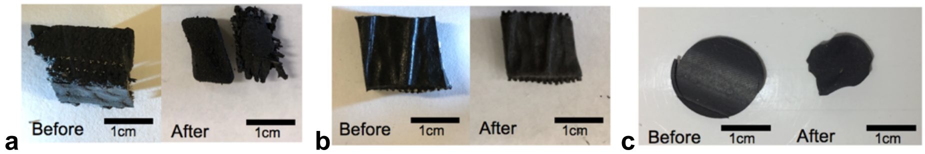

Figure S4.19 Shrinkage of bulk rubber after 1 reduction cycle (a) snow tire tread; (b) snow tire sidewall; (c) bulk rubber bicycle tire.

Preparation of New Elastomers

Desilylation

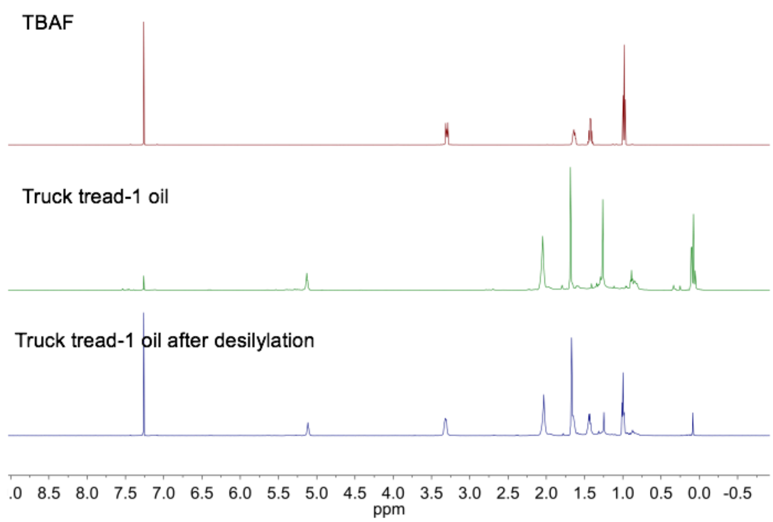

Figure S4.20 ^{1}H NMR showing loss of silicone groups from the organic polymers after utilizing TBAF.

New Elastomers

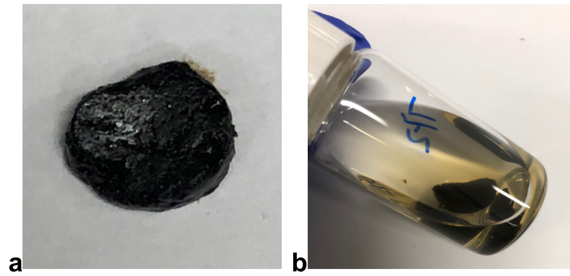

Figure S4.21 (a) The crosslinked elastomer **14** formed by iodine reoxidation of thiols in **8**. (b) The picture of 0.1 g **15**, swollen in 10 ml hexane after 1h sonication.

Table S4.6 Recrosslinking of recovered organic oil 8 with residual solid as reinforcing agent (Figure 4.4).

Organic oil **8** (Truck tire Sailun, g)	Ground residual solid (g)	BPO (g)	Hardness
1.000	0.000	0.010	68±3 (Shore OO)
0.700	0.300	0.010	91±4 (Shore A)

5 Chapter 5: Thermoplastic Silicone Elastomers Based on Gemini Ionic Crosslinks

5.1 Abstract

Traditional silicone elastomers are thermoset polymers with crosslink sites linked through covalent bonds. The benefits of silicone elastomers would be improved by the ability to reuse the materials. Here we report an ionically crosslinked thermoplastic, silicone material based on acid/base neutralization. Dicarboxylic acid silicones were prepared by the Michael addition to maleic acid of thiopropylsilicones. A range of materials was prepared by incorporating different concentrations of maleic acid on the silicone backbone. Gemini (double ionic) crosslink sites were established by neutralizing both COOH groups with β-diaminoethylsilicones. The combination of these two difunctional agents were synergistic; stronger mechanical properties were observed than for materials with analogous crosslink densities arising from monofunctional ions. The physical properties of the elastomers were dynamic. The ionic networks showed competitive mechanical strength to their covalently crosslinked counterparts under fast

deformation but exhibited much higher extension (>1200%) under slow deformation. The ionic interactions could be easily overcome thermally.

Keywords: Thermoplastic silicones, Gemini ionic crosslinks; dynamic tensile response

5.2 Introduction

Since the invention of radical-induced vulcanization of rubber by Goodyear in 1844,[1] elastomers have become an irreplaceable part of modern life. The normally used covalent crosslinks between polymer chains provide a variety of advantages including excellent toughness, high fracture strength and, most importantly, excellent elastic extension. These properties are easily tuned with crosslink density. However, highly crosslinked elastomers are strong but exhibit poor stretchability; these two properties are a trade-off.[2]

Silicones, a class of thermoset elastomers, are widely used because of their excellent dielectric properties, outstanding thermal stability, biocompatibility and high hydrophobicity.[3] Silicone elastomer networks are normally prepared by moisture cure (RTV), heat-activated radical cure (HTV) or transition metal-catalyzed hydrosilylation.[4] The stable covalent linkages created between different components provide thermoset networks with elastomeric mechanical properties. However, with the development of applications such as wearable devices and the rising desire for environmental sustainability, the demand for silicone elastomers has switched from exploiting their mechanical properties to the development of smarter materials that possess properties including self-healing, and that are re-usable, re-processable and recyclable.

Thermoplastic silicone elastomers are polymeric materials that possess both plastic and rubbery properties. Unlike conventional rubbers, they can be re-processed at high(er) temperatures. The major advantage of these materials is the sustainability that results from the ability to reuse/recycling of fabricated products. A variety of molecular interactions can be used to control the mechanical properties and degree of reversibility of thermoplastic elastomers, including dynamic covalent bonds,[5] hydrogen bonding,[6,7] aromatic association,[8] electrostatic interactions,[9,10] and metal-ligand coordination.[11] These physical crosslinks can be overcome thermally.

Some approaches to thermoplastic or self-healing silicone elastomers have been reported.[12,13] For example, a silicone-urea copolymer is a typical thermoplastic silicone elastomer comprised of PDMS segments and thermoplastic urethane groups.[14] The soft silicone segments have a glass transition temperature well below room temperature but the urethane segments aggregate to form distinct microphases and act as physical crosslinks. At high temperatures, the hard segments melt, allowing the copolymer to flow and to be processed like an ordinary thermoplastic.[15] Another silicone coating based on hydrogen bonding was recently demonstrated by Liu.[16] An aminosilicone was modified with 2-amino-4-hydroxy-6-methylpyrimidine (UPy). The hydrogen bonding provided by the UPy units self-assembled into a network.

Silicone materials with dynamic covalent bonding have also been described. A silicone vitrimer was reported by Stukenbroeker et al.[17] The dynamic network was built by crosslinking pendent aminosilicone oil with bis-vinylogous urethane crosslinker. The vinylogous urethane exchange reaction imbues the elastomer with thermally activated behavior such that the silicone materials were able to be reshaped at 100 °C. We recently reported that aminosilicones crosslinked by aromatic aldehydes – via Schiff-base links – exhibit self-healing properties.[13] Finally, transient polymer networks are readily generated by H-bonding reactions between sugars grafted into a silicone matrix.[18]

Ionic groups have also been used in the design of polymer materials due to their polarity and dynamic properties. Pioneering work describing the incorporation of ionic groups into silicone was reported by Skov et al.[19, 20] Self-healing dielectric elastomers were created from an interpenetrating polymer network based on the combination of a covalent crosslinked RTV cure network and an ionic network. The covalent network provided the required mechanical properties while the ionic network offered self-healing and required polarizability for their target dielectric properties. However, the permeant covalent network used in this case reduced the recyclability of the material. Silicones with crosslinking provided by purely ionic associations were described by Lu et al.[21] A supramolecular silicone elastomer was prepared by neutralizing aminosiloxanes with organic or inorganic acids to yield an ionic-association complex ("salt-forming vulcanization"). The crosslinking in this system was achieved by aggregation of ionic sites due to the phase separation,[21] and strong acids (H_2SO_4, HNO_3) or solid organic acids were favored. In addition, excess solid acid was added on purpose to improve mechanical properties via physical reinforcement. Recently, Shi et al[22] developed a thermoplastic silicone elastomer based on coulombic interactions between carboxylic acid groups on the polydimethylsiloxane (PDMS) side chains and commercially available ZnO;

crosslinking arose from metal oxide ion clusters. The obtained PDMS-g-COOH/ZnO composites exhibited self-healing and thermoplastic properties.

In the hope of developing more robust thermoplastic silicone elastomer networks, we have examined the use of higher order ionic association as a crosslinking motif, in analogy with the benefits that multiple hydrogen bonding motifs bring to elastomer properties.[16] Unlike traditional ionic linkages, a double crosslink – a Gemini ionic linkage – was introduced through use of silicone oil modified with succinic acid side groups. These were then crosslinked with ethylenediamine-modified silicones. The materials exhibit excellent mechanical properties at room temperature but are thermoplastic elastomers. Low crosslink density elastomers can spontaneously self-heal at room temperature; higher crosslinked materials required elevated temperatures to exhibit this property. The Gemini ionic crosslinked silicone elastomer exhibited very high extension with slow stretching rates but a strong, elastic response at a fast stretching speed.

5.3 Experimental Section

5.3.1 Materials

Thiopropylsilicones: 2-3% (mercaptopropyl)methylsiloxane-dimethylsiloxane copolymer (SMS-022, Lot# 9B-35147, MW: 6000-8000 g/mol, viscosity: 120-180 cSt), 4-6% (mercaptopropyl)methylsiloxane-dimethylsiloxane copolymer (SMS-042, Lot# 8I-13501, MW: 6000-8000 g/mol, viscosity: 120-170 cSt), 13-17% (mercaptopropyl)methylsiloxane-dimethylsiloxane copolymer (SMS 142, Lot# 9H-36436, MW: 3000-4000 g/mol, viscosity: 100-200 cSt); Aminosilicones: **Gemini amine-14 (G-NH_x-14):** 18-24% (aminoethylaminopropylmethylsiloxane)-dimethylsiloxane (AMS 2202, Lot# 1G-16149, viscosity: 300-500 cSt), **Gemini amine-4 (G-NH_x-4):** 2-4% (aminoethylaminopropylmethylsiloxane)-dimethylsiloxane (AMS 233, Lot# 4F-23054, viscosity: 900-1200 cSt), **Mono amine-4 (M-NH_2-4):** 4-5% aminopropylmethylsiloxane-dimethylsiloxane copolymer (AMS-152, Lot# 9H-36435, MW 7000 - 9000 g/mol,100-300 cSt); Hydride silicones: 4-6% hydromethylsiloxane-dimethylsiloxane copolymer (HMS 053, Lot# 6I-9487, MW 20000-25000 g/mol, viscosity: 750-1000 cSt) were purchased from Gelest. Vinyl silicones: α,ω-vinyl-terminated poly(dimethylsiloxane) copolymer (PS-441, Lot#: 70532, MW 3850 g/mol, viscosity: 100cSt) were purchased from Petrarch Systems. Maleic acid (BDH), hydrochloric acid (Caledon Laboratory), sodium sulfate (EMD Millipore Corporation), triethylamine (Sigma-Aldrich) were used as received. Silica Aerosil 150 was purchased from Evonik Industries. Solvents were purchased from Fisher Chemical. Deuterated NMR solvents were obtained from Cambridge Isotope Laboratories.

5.3.2 Methods

NMR Analysis: ^{1}H NMR spectra were recorded on a Bruker Avance 600MHz or Avance NEO 500 MHz nuclear magnetic resonance spectrometer using deuterated solvents chloroform-*d*. The proton impurity in the deuterated solvent was calibrated to 7.26 ppm $CDCl_3$.

Infrared Spectroscopy: Measurements were performed on a Thermo Scientific Nicolet 6700 FT-IR spectrometer equipped with a Smart iTX attenuated total reflectance (ATR) attachment.

Viscosity measurements were carried out on a TA Instruments Discovery HR-2 Hybrid Rheometer with a 40mm steel Peltier plate was used for low viscosity (<1Pa·s) thiopropylsilicone oil (SMS 022, SMS 042, SMS 142) and 20 mm plate was used to measure the more viscous maleic acid-modified thiopropylsilicone oils (**G-COOH-14**, **G-COOH-4**, **G-COOH-2**). The measurement was done at room temperature with the shear rate setting between 1 and 100 rad s^{-1}.

Gel temperature measurements: a TA Instruments HR-2 Rheometer equipped with a 20 mm plate was used. The gap between the two plates was set to 1000 μm for all experiments. Temperature dependent measurements were conducted between 25 and 80 °C using a heating or cooling ramp of 3 $K{\cdot}min^{-1}$. The oscillatory frequency of 10 rad s^{-1} and a strain of 0.1% was applied to obtain the dynamic viscosity as a function of temperature. The crossover point of G' and G" was defined as the gel point[23] and the temperature where G'=G" was defined as the gel temperature.

Thermogravimetric analysis (TGA): A small amount of test sample (2 to 5 mg) was placed into the alumina pan. The measurement was performed using a Thermogravimetric Analyzer (Mettler Toledo TGA/DSC 3+). A 20 cm^3 min^{-1} N_2 or air flow was applied and the furnace was heated from 50 to 800 °C at 10 °C min^{-1}.

The compression Young's modulus was measured using a MACH-1 micromechanical testing instrument (Biomomentum Instruments) equipped with a plate indenter (diameter:12.7 mm). The compression speed was 0.03 mm/s. The Young modulus was reported at 20% strain.

Tensile tests were performed on a tensile tester (Autograph AG-X, Shimadazu, USA) with a 500 N load cell; dog bone specimens were used for the test. The dimensional parameters for the neck of the specimens are as follows: gauge length ~45.00 mm; width:3 mm; thickness: 2 mm. Metal dog bone molds were used for high temperature self-healing tests. The geometry parameters for the metal dog bone mold neck were as follows: gauge length: ~20 mm; width:3 mm; thickness: 4 mm) and a tensile speed of 500 mm/min was used unless noted.

Room temperature self-healing tests: A sample film (thickness: 2mm) was cut though by scalpel to make a 1.5 cm length cut. The two parts of the sample film were placed in contact and were stored at room temperature for different time periods. The films were then examined under optical microscope (Nikon Eclipse LV100 upright epifluorescence microscope). A 4X magnification lens was used.

5.3.3 Synthesis of Gemini Acid (G-COOH) Silicones G-COOH-14， G-COOH-4，G-COOH-2

Shown for **Gemini acid-2 (G-COOH-2)**, the number refers to the mole% of the succinic acid modified siloxane unit vs the total number of siloxane unit (based on ^{1}H NMR; **G-COOH-2** therefore has 2% of the backbone monomers bearing the diacid and 98% Me_2SiO units). To a mixture of maleic acid (3.46 g, 0.029 mol), triethylamine (8.85 ml, 0.063 mol), and 2-3% (mercaptopropyl)methylsiloxane-dimethylsiloxane copolymer SMS 022 (50 g, 0.014 mol SH) was added isopropyl alcohol (100 ml). The reaction was allowed to stir at room temperature for 48 h; an initially opaque dispersion became a clear solution. The degree of conversion and completion of reaction were monitored by ^{1}H NMR. The workup consisted of removal of the solvent by rotary evaporator, acidification of the product with 1M HCl solution, extraction with ethyl acetate, followed by dehydration of the organic phase with sodium sulfate, followed by filtration. Residual solvent was removed under vacuum. The product was a clear, pale-yellow oil.

G-COOH-2: ^{1}H-NMR (500 MHz, chloroform-*d*, ppm) δ = 0.07 (297H, Si-CH_3), 0.61 (2H, Si-CH_2, 1.66 (2H, CH_2), 2.68 (2H, S-CH_2,1H, CH_2C=O), 2.99 (1H,

$CH_2C{=}O$), 3.63 (1H, S-CHC=O). Starting thiopropylsilicone oil SMS 022 (50g). Product yield: 47.437 g, 91%.

G-COOH-4: ^{1}H-NMR (500 MHz, chloroform-*d*, ppm) δ = 0.07 (131H, Si-CH_3), 0.61 (2H, Si-CH_2, 1.66 (2H, CH_2), 2.68 (2H, S-CH_2,1H, $CH_2C{=}O$), 2.99 (1H, $CH_2C{=}O$), 3.63 (1H, S-CHC=O). Starting thiopropylsilicone oil SMS 042 (50g). Product yield: 46.428 g, 88%.

G-COOH-14: ^{1}H-NMR (500 MHz, chloroform-*d*, ppm) δ = 0.07 (46H, Si-CH_3), 0.61 (2H, Si-CH_2, 1.66 (2H, CH_2), 2.68 (2H, S-CH_2,1H, $CH_2C{=}O$), 2.99 (1H, $CH_2C{=}O$), 3.63 (1H, S-CHC=O). Starting thiopropylsilicone oil SMS 142 (20g). Product yield: 22.002 g, 92%.

5.3.4 General Synthesis of Ionically Crosslinked Elastomers

Ionic networks were prepared simply by mixing amino-functional silicone and maleic acid silicones. The mixture was stirred until a homogeneous gel material was formed (typically, this took around 1 min). Then, the mixture was degassed in a vacuum desiccator. The elastomers were left at 60 °C for 3 days to allow the fully cure of the ionic network.

Table 5.1 Formulations for ionic crosslinked silicone elastomers.

Entry	Gemini acid silicone (g)	Amino silicone (g)	COOH/NH_x	Gel temperature (°C)	Young's modulus[a] (kPa)
1	**G-COOH-2** (1.00)	**G-NH$_x$-14** (0.12)	1:1	75	174.5
2	**G-COOH-2** (1.00)	**G-NH$_x$-4** (0.47)	1:1	73	55.9
3	**G-COOH-4** (1.00)	**G-NH$_x$-4** (0.78)	1:1	NM[b]	54.6
4	**G-COOH-14** (1.00)	**G-NH$_x$-4** (0.40)	1:1	NM	227
5	**G-COOH-2** (1.00)	**G-NH$_x$-14** (0.06)	2:1	48	37.1
6	**G-COOH-2** (1.00)	**G-NH$_x$-4** (0.24)	2:1	-[c]	Liquid
7	**G-COOH-2** (1.00)	**G-NH$_x$-14** (0.23)	1:2	-	Liquid
8	**G-COOH-2** (1.00)	**M-NH$_2$-4**(1.09)	1:1	-	Liquid
9	**G-COOH-2** (1.00)	**G-NH$_x$-4** (0.70)	1:1.5	62	56.2
10	**G-COOH-2** (1.00)	**G-NH$_x$-4** (0.95)	1:2	55	33.6
11	**G-COOH-2** (1.00)	**G-NH$_x$-14** (0.38)	1:1.5	30	13.1

[a] Young modulus was reported at the 20% strain.
[b] The measurement was not applicable for these samples.
[c] The gel temperature was lower than room temperature.

5.3.5 Preparation of Samples for Self-healing Tensile Test at Elevated Temperatures

The samples for self-healing test was prepared by enlarge the scale of Table 5.1, Entry 4. Amino-functional silicone (**G-NH$_x$-4**, 4 g, NH_x 4.6 mmol) and maleic acid modified silicone (**G-COOH-14**, 1.6 g, COOH 4.6 mmol) were mixed and degassed by the same procedure as described above. The soft gel mixture was transferred into metal dog bone molds (geometry parameters for the neck part: gauge length: ~20 mm, width: 3 mm, thickness: 4 mm) and placed into a 60 °C oven for 3 days to achieve complete cure. After tensile measurements were performed on those samples, the sample was put back into the metal mold (after ensuring the broken surfaces were in contact), at 80 °C for various time periods (0.5, 3, 8h). The tensile data is shown in Table 5.4.

5.3.6 General Synthesis of Ionic Elastomer with SiO_2 Filler

In a typical synthesis of silica-reinforced ionic elastomer (3wt% loading, Table 5.2, Entry 13), silica (Aerosil 150, 0.17 g) was first added into a polypropylene mixing cup with 4.00 g amino silicone **G-NH$_x$-4** (AMS 233, NH_x 4.6 mmol). The mixture was mixed using a planetary centrifugal mixer (FlackTek Inc., 3000 rpm, 1.5 min). **G-COOH-14** (1.6 g, COOH 4.6 mmol) was then added and mix by stirring with a spatula. The mixture was degassed in a vacuum desiccator and placed into a polytetrafluoroethylene dog bone mold (geometry parameters for the neck part: gauge length: ~45 mm, width: 3 mm, thickness: 2 mm). The samples were placed into a 60 °C oven for 3 days to ensure complete cure.

5.3.7 General Synthesis of Hydrosilylation-cured Elastomers

Base formulation soft elastomer (Vinyl-4 + SiH-5): A master batch of hydrosilylation cure base was made by mixing 30.0 g of PS-441 (H_2C=CH-

$SiMe_2(OSiMe_2)_nOSiMe_2CH{=}CH_2$, n = ~ 52, MW = 3850, vinyl 15.57 mmol) with crosslinker 22.8 g HMS 053 ($SiMe_3(OSiMeH)_x(OSiMe_2)_yOSiMe_3$, x,y = ~ 15, ~ 285, MW = 20000-25000 g/mol, SiH 15.56 mmol).

Base formulation hard elastomer (Vinyl-4 + SiH-17): A master batch of hydrosilylation cure base was made by mixing 5.0 g of PS-441 ($H_2C{=}CH$-$SiMe_2(OSiMe_2)_nOSiMe_2CH{=}CH_2$, n = ~ 52, MW = 3850, compound VINYL 2.6 mmol) with crosslinker 1.1 g HMS 151 ($SiMe_3(OSiMeH)_x(OSiMe_2)_yOSiMe_3$, x,y = ~ 4, ~ 20, MW = 1900-2000 g/mol, SiH 2.3 mmol).

A control elastomer was prepared by adding Karstedt's catalyst solution (12.5 µl diluted, concentration: 1mg/ml, 3.3×10^{-5} mmol) to the base mixture (5.0 g). No reinforcing agents were used (Table 5.2, Entry 16). The mixture was then degassed by a vacuum desiccator and heated at 60 °C overnight.

In a typical synthesis of a silica reinforced silicone elastomer (3wt% loading, Table 5.2, Entry 17), the premixed base (5.0 g) was mixed with diluted Karstedt's catalyst solution (12.5 µl, 3.3×10^{-5} mmol, concentration: 1 mg/ml in toluene). Silica (Aerosil 150, 0.15 g) was then added to the mixture and mixed using the FlackTek speedmixer (3000 rpm, 1.5 min). After degassing in a vacuum desiccator, the mixture was transferred into dog bone molds (geometry parameters for the neck part: gauge length: ~45 mm, width: 3 mm, thickness: 2 mm) and placed into a 60 °C oven overnight to achieve complete cure.

Table 5.2 Formulations for silica filled ionic crosslinked silicone elastomers and silica filled hydrosilylation cured control.

Entry	Silicone (g)		SiO_2 (g/wt%)	Karstedt's catalyst solution [a](μl)	Temperature/ Time (°C/h)
	Ionic elastomers (**G-COOH-14** + **G-NH$_x$-4**)[a]				
	G-COOH-14 (g)	**G-NH$_x$-4** (g)			
12	1.60	4.00	0/0	-	60/72
13	1.60	4.00	0.17/3	-	60/72
14	1.60	4.00	0.28/5	-	60/72
15	1.60	4.00	0.56/10	-	60/72
	Hydrosilylation cure elastomers (Vinyl-4 + SiH-5)				
16	(Vinyl-4 + SiH-5) Base (5.0)		0/0	12.5	60/18
17	(Vinyl-4 + SiH-5) Base (5.0)		0.15/3	12.5	60/18
18	(Vinyl-4 + SiH-5) Base (5.0)		0.25/5	12.5	60/18
19	(Vinyl-4 + SiH-5) Base (5.0)		0.5/10	12.5	60/18
20 [b]	(Vinyl-4 + SiH-17) Base (5.0)		0/0	12.5	60/18

[a] Karstedt's catalyst solution concentration:1 mg/ml in toluene.
[b] Those samples was too brittle to pull out from tensile dog bone mold.

5.4 Results and Discussion

Unlike aminosilicones, for which a wide variety of molecular weight and amine densities are commercially available, the range of silicone oils bearing carboxylic groups is quite limited. Shi et al. successfully synthesized carboxylic acid functionalized PDMS by modifying vinyl silicone with 3-mercaptopropionic acid though a thiol-ene reaction.[22] In our research, we attempted to avoid using low molecular weight thiol compounds due to their unpleasant odor. Therefore, dicarboxylic acid functional groups were grafted onto thiol-functionalized silicones using a thiol-Michael addition, a versatile reaction between thiols and electron deficient C=C bonds.[24] To do so, thiopropylmethylsiloxane-co-dimethylsiloxane polymers were reacted with maleic acid in the presence of excess triethylamine. The concentration of COOH groups in the prepared carboxylic acid functionalized silicones could be tuned simply by changing the concentration of thiols in the starting material. The final dicarboxylic acid concentrations along the chain ranged from 2 to 14 mol% (2 mol% **G-COOH-2**, 4 mol% **G-COOH-4**, 14 mol% **G-COOH-14**, Figure 5.1a), with the remaining monomer units being Me_2SiO. Product FT-IR spectra showed an increase in the peak intensity at 1710 cm^{-1}, consistent with the presence of succinic acid moieties. The viscosities of silicone oil to which maleic acid was grafted were significantly higher than the starting materials due to the hydrogen bonding arising from the COOH groups (Figure S5.2).

Mechanical Properties - Products as a Function of NH_x/COOH Ratio

5.4.1.1 Gemini Acid + Mono Amine 1:1 Equivalent

The ability of electrostatic or ionic interactions to form crosslinks between amino and carboxylic groups was first examined by mixing monosubstituted aminosilicones (**M-NH_2-4**) and Gemini acid silicone (**G-COOH-2**) in a 1:1 molar ratio. The product was a soft, viscous, gel-like material. As shown in Figure 5.2, the storage modulus G' of the resulting material was significantly lower than the loss modulus G". The viscosity of the soft gel (1347 Pa s, test frequency :10 rad/s, 25 °C) was much larger than the dicarboxylic acid modified silicone itself (80 Pa·s, test frequency 10 rad/s, 25 °C), consistent with the formation of ionic bonding to give ammoniumpolysiloxane carboxylates.

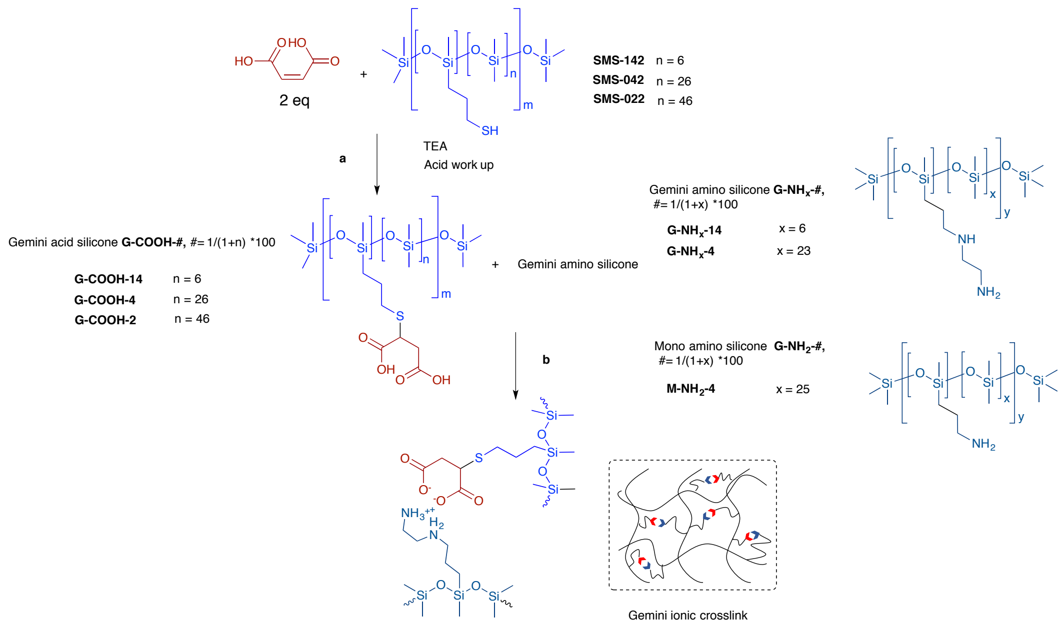

Figure 5.1 Preparation of Gemini acid silicones using thiol-Michael additions and then ionic crosslinked silicone elastomers.

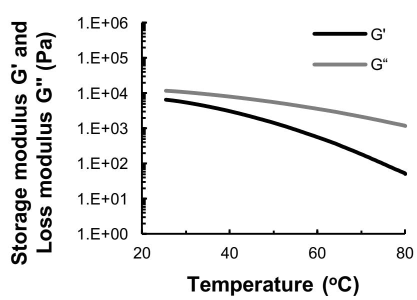

Figure 5.2 Rheology curve for **G-COOH-2** + **M-NH$_2$-4**, COOH/NH$_x$ =1:1.

5.4.1.2 Gemini Acid+ Gemini Amine 1:1 Equivalent

When initially designed, it was hypothesized that the combination of a diamine and a dicarboxylic acid – Gemini ions – would be synergistic and perform better with respect to ionic crosslinking than the same number of monofunctional amines plus difunctional acids. This expectation was shown to be correct. Without changing the total number of crosslink sites within the material, replacement of diamines with a monoamine led to a large reduction in the modulus (Table 5.1. Entry 2 vs 8, 55.9 kPa vs liquid). That is, Gemini anions plus Gemini cations provide more effective crosslinking than monofunctional ionic bonds.

5.4.1.3 Gemini Acid + Gemini Amine at Different Ratios $COOH/NH_x$

To better understand of the nature of Gemini ionic linkages in the network, ionic gels with various [COOH]:[NH_x] ratios were prepared in a competitive binding experiment. When combined at a 2:1 [COOH]:[NH_x] or 1:2 [COOH]:[NH_x] molar ratio. Two different types of linkage can exist: (1) Gemini linkage + sol molecule[25] (Figure 5.3a, c the sol molecule does not participate in the network); or, (2) single ion linkage between one COOH or NH_x group from the excess Gemini molecule (Figure 5.3b,d). Due to the existence of strong Gemini linkage in the first case, a strong, elastomeric material would be expected, while the second type of linkage should lead to a very weak gel or even a liquid.

COOH in Excess

The mixture of a 2:1 molar ratio of **G-COOH-2** and **G-NH$_x$-4** ([COOH]:[NH$_x$]= 2:1) was a viscous liquid at room temperature. The rheology study showed a higher G" over G' Figure 5.4a (typical for liquid or soft gel materials). This behavior was similar to that of the product made with **M-NH$_2$-4** (Figure 5.2), which suggests a weak monoionic linkage was established in both cases. This may due to the difference in pKa of the two COOH groups on succinic acid (pKa$_1$= 4.21, pKa$_2$= 5.41) such that the dicarboxylic acid only utilizes the more reactive acid[26] to give monoionic linkages (Figure 5.3b).

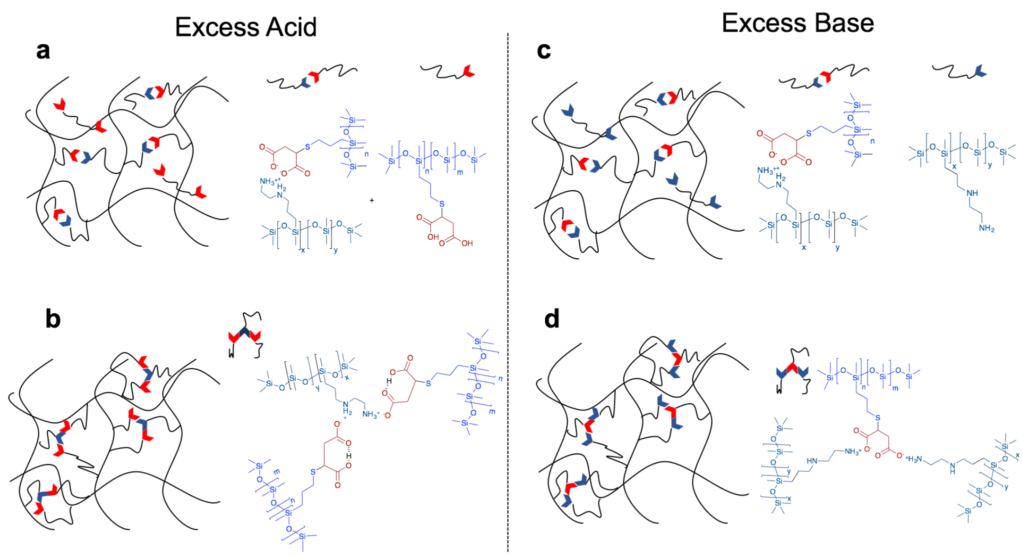

Figure 5.3 Different type of linkages could exist in the network when acid is in excess: (a) Gemini linkages with sol carboxysilicones, (b) single ionic linkages; or base is in excess: (c) Gemini linkages with sol aminoalkylsilicones, (d) single ionic linkages.

NH$_x$ in Excess

As the concentration of amines is increased, the fraction of Gemini links increases, with a maximum at a 1:1 molar ratio of COOH to NH_x. Unlike the case with excess acid, it was surprising to observe at yet higher amine concentrations that there was only a slightly decrease in Young's modulus for **G-COOH-2** + **G-NH$_x$-4** (Figure 5.5, gray line). A similar trend was observed in tensile tests (shown in Figure S5.3). For samples with even two times excess NH_x, the product was a strong, elastomeric material with a Young's modulus similar to the elastomers formed with a quantitative stoichiometric ratio (Table 5.1, Entry 10 vs 2, 33.6 kPa vs 55.9 kPa). Rheological studies further confirmed that a high storage modulus at room temperature was achieved (Figure 5.4b). This data is consistent with the efficient formation of Gemini linkages plus amine sol polymer when excess amine is present (Figure 5.3c).

In further test the hypothesis that the vicinal amine undergo preferentially protonation to form Gemini linkages (i.e., Figure 5.3c is more representative than Figure 5.3d), ionic silicone elastomers were made using amino silicones with a higher substitution degree on the silicone back bone (**G-NH$_x$-14**) (COOH: NH_x = 2:1, 1:1, 1:1.5, 1:2). In this case, the expected decrease in Young's modulus for the ionic gel (**G-COOH-2** + **G-NH$_x$-14**) was observed when amine was in excess

(Figure 5.5, black line). Thus, two regimes exist. At high backbone amine concentrations in a localized area, charge screening removes selectivity for Gemini ionic association and weak single ionic linkages lead to liquid products (Figure 5.3d); at low backbone amine concentrations, vicinal amines preferentially form Gemini linkages that, upon addition of more amine polymer lead to only minor reductions in Young' moduli by sol dilution (Figure 5.3c).

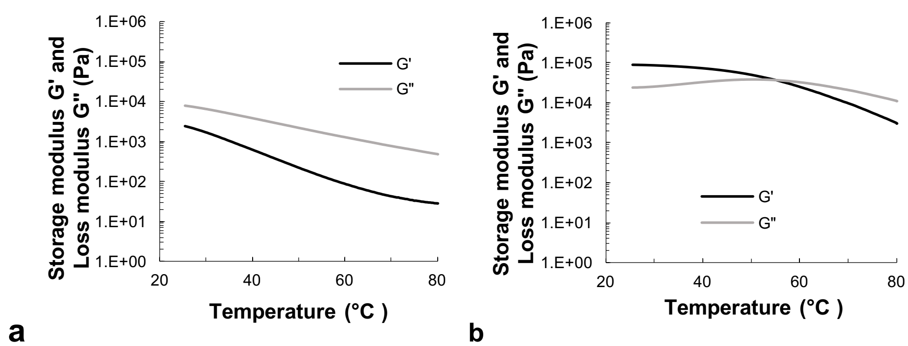

Figure 5.4 Rheology curve as a factor of temperature. (a) **G-COOH-2** + **G-NH$_x$-4**, COOH:NH$_x$ =2:1, (b) **G-COOH-2** + **G-NH$_x$-4**, COOH:NH$_x$ =1:2.

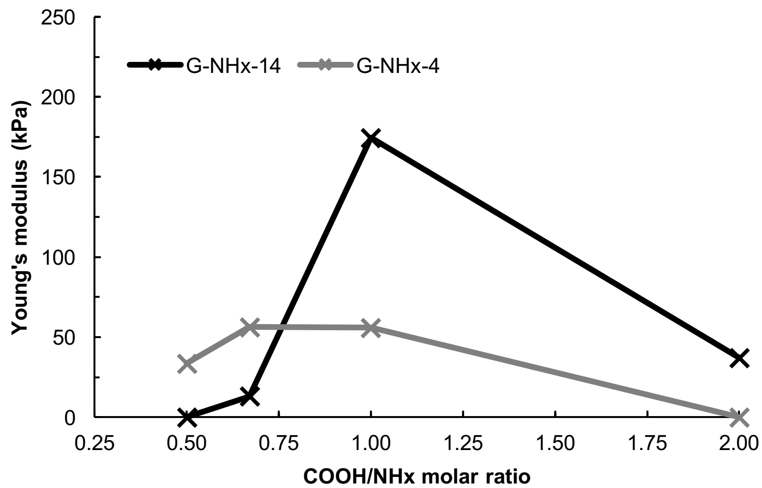

Figure 5.5 Young's modulus of **G-COOH-2** + **G-NH$_x$-14** series (black) and **G-COOH-2** + **G-NH$_x$-4** series (gray).

5.4.1.4 Effect of Crosslink Density

The mechanical properties of elastomers correlate with crosslink density.[27] The ionic gels prepared with lower ionic crosslink concentrations (**G-COOH-2** series and **G-COOH-4** series) were relatively soft (compression Young's modulus of 55.9 kPa and 54.6 kPa, respectively, Table 5.2 Entry 2 and 3). Tensile measurements for these samples were not practical. Elastomers with higher ionic crosslink densities prepared from the **G-COOH-14** series exhibited mechanical properties within a similar range as for traditional silicone thermosets, depending on how the tensile measurements were performed.

Covalently crosslinked elastomers (black solid curve, Figure 5.6) had a much higher Young modulus than its ionic counterpart with similar crosslink density (pink dashed curve), however, the ionically crosslinked elastomer exhibited much higher stretchability.

The ionic crosslinked elastomer with higher ionic concentrations (**G-COOH-14** series, Table 5.2 Entry 12-15) showed good mechanical properties and demonstrated a typically elastic curve when using a 500 mm/min tensile speed. By comparison, covalently linked silicone elastomers with similar crosslink densities, prepared using hydrosilylation cure, were too brittle for the tensile test (Table 5.2 Entry 20, Figure 5.6). Instead, covalently crosslinked PDMS controls matching the crosslink density of **G-COOH-4** series were successfully made (Entry 16, Table 5.2). Thus, the physical properties of both types of polymers are readily controlled, but using different parameters.

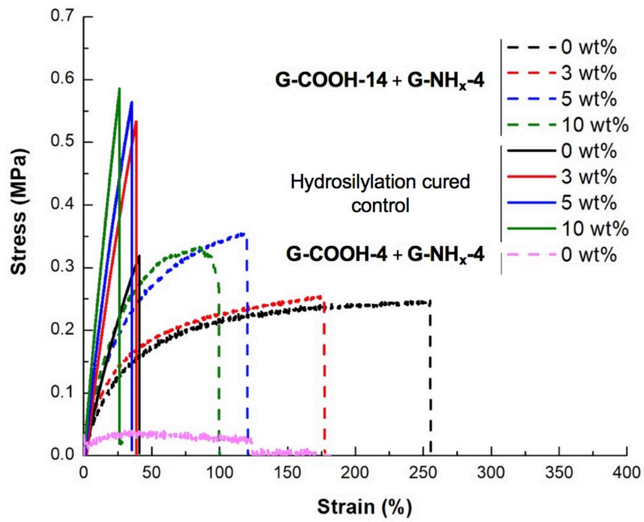

Figure 5.6 Tensile curves for PDMS elastomers with covalent linkages (hydrosilylation cure control, solid lines) and ionically linked elastomers (dashed lines). Different amounts of silica fillers (Aerosil-150) were added. The tensile speed for ionic elastomers and hydrosilylation cure elastomers were 500 mm/min and 10mm min^{-1}, respectively.

5.4.2 Improving Mechanical Properties - Silica Fillers

Unfilled, ionically crosslinked silicone materials are inherently weak. Silica is traditionally added as reinforcing agent to silicone elastomers; hydrogen bonds arise between the silanol groups on the silica surface and the oxygen atoms of the silicone backbone.[28] As shown in Figure 5.6, when hydrophilic silica (Aerosil 150) was added as reinforcing agent the Young's modulus of the silica-filled elastomers (both covalently crosslinked and ionic crosslinked elastomers) increased with increasing filler concentration accompanied, as expected, with an accompanying decrease in the elongation at break (Table 5.2). Thus, it is possible to further improve the mechanical properties of ionic crosslinked elastomer with the use of other physical bonds.

Table 5.3 Summary of mechanical properties of ionic crosslinked silicone elastomers.

Sample	SiO_2 wt%	Young modulus (MPa)	Strength at break (MPa)	Strain at Break (%)
Ionic elastomers (**G-COOH-14** + **G-NH$_x$-4**)[a]				
	0	0.65 ± 0.24	0.26 ± 0.09	197 ± 52
	3	0.62 ± 0.11	0.26 ± 0.06	191 ± 22
	5	0.77 ± 0.09	0.32 ± 0.03	124 ± 5
	10	1.04 ± 0.17	0.30 ± 0.02	74 ± 36
Ionic elastomers (**G-COOH-4** + **G-NH$_x$-4**)[a]				
	0	0.15	0.0215	124
Hydrosilylation cure elastomers (Vinyl-4 + SiH-5)[b]				
	0	0.99 ± 0.16	0.31 ± 0.01	35 ± 8
	3	1.33 ± 0.19	0.45 ± 0.12	36 ± 4
	5	1.54 ± 0.30	0.43 ± 0.18	29 ± 8
	10	2.14 ± 0.21	0.53± 0.07	26 ± 1

[a] A tensile speed of 500 mm/min was used. At 10 mm/min, the samples have high stretch ability that beyond the range of tensile tester (Figure 5.9a).
[b] A tensile speed of 10 mm/min was used. Testing hydrosilylation cured elastomers at 500mm/min would not be possible since the samples would be break within seconds.

5.4.3 Thermoplasticity

The ionically crosslinked silicone elastomers were thermally labile.[9] The thermoplasticity of the ionic elastomers was examined using a rheological temperature ramp study. The storage modulus (G’) was higher than loss modulus

(G”) at room temperature, indicating the elastomeric nature of the material. As shown in Figure 5.7, the storage modulus of the elastomer decreased (G’) with increasing temperature. At high temperature, the loss modulus (G”) was higher than the storage modulus (G’) and a liquid state was achieved. The crossover point of G’ and G” was defined as gel point.[23] As shown in Table 5.1, the gel temperature for samples with [COOH]/[NH_x]=1:1 shows the highest gel temperature (Table 5.1 Entry 1, 75 °C and Entry 2, 73 °C) due to the Gemini ionic links. The mild gel temperature indicates their re-processability can be achieved under with mild heating.

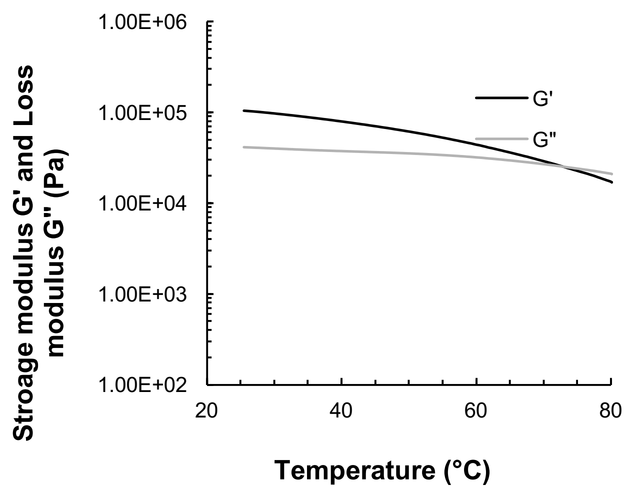

Figure 5.7 Rheology curve as a factor of temperature. (**G-COOH-2** + **G-NH_x-4**, COOH/NH_x =1:1).

To demonstrate the re-processability of the ionic silicone elastomers though thermoplastic processing, the **G-COOH-2** + **G-NH$_x$-14** elastomer was crushed into small pieces, placed into a round mold, and heated to 90 °C. After cooling to room temperature, a new elastomer formed (Figure 5.8).

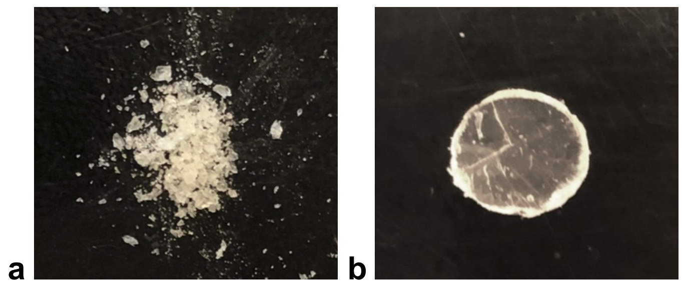

Figure 5.8 Pictures showing thermoplasticity. (a) **G-COOH-2** + **G-NH$_X$-14** elastomer was crashed into small pieces (b) The elastomer crumbs were remolded to give a new elastomer (the 90° lines on the elastomer were from a wrinkle from the Teflon sheet lined on the mold, not a crack).

5.4.4 Thermal Stability

The stability of Gemini ionically crosslinked silicones was examined by thermogravimetric analysis under either N_2 or air. As shown in Figure 5.9c, the TGA curve for **G-COOH-14** oil shows a two-stage weight loss, the first beginning at 200 °C, and the second at ~350 °C (a typical temperature for silicone degradation).[29] These data suggest that the grafted succinic acid groups undergo degradation prior to the degradation of silicone backbone. The TGA curve of the ionic silicone elastomer showed improved thermostability over the Gemini acid oil

(Figure 5.9c, red curve vs black curve). There was only a slight weight loss (< 10 wt%) below 450 °C. That is, the thermal stability of the dicarboxylic side chains was improved when the carboxylic groups were neutralized to carboxylate by the Gemini amine groups. The thermostability of the elastomer was also examined in air environment and shown to be only slightly less stable than in argon (Figure 5.9c).

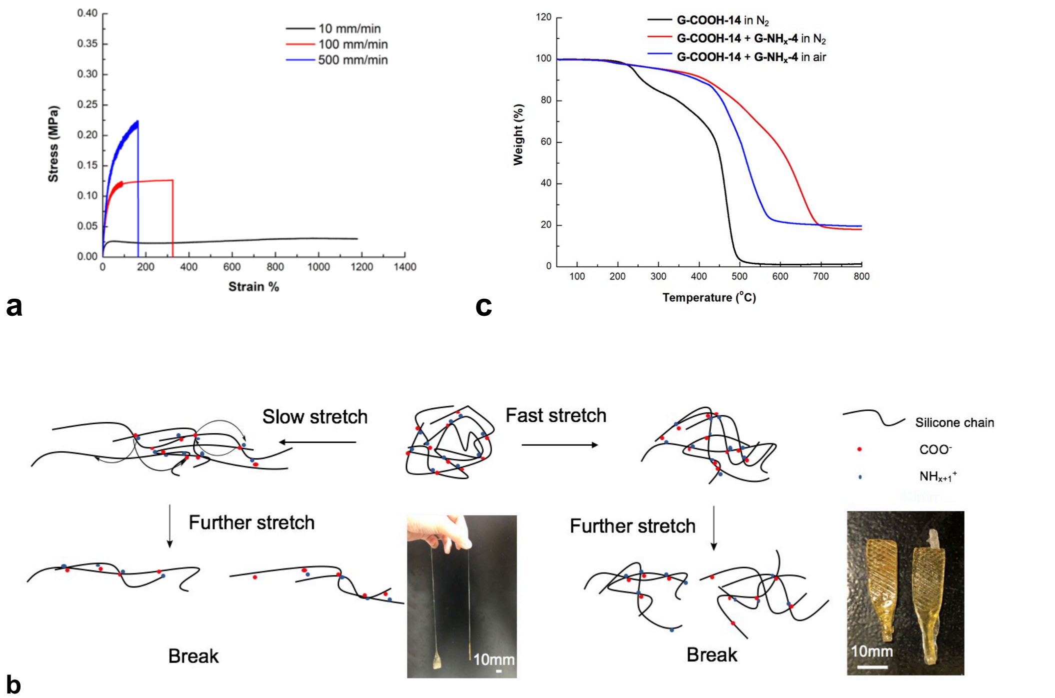

Figure 5.9 (a) Stress-strain curves for **G-COOH-14** + **G-NH$_x$-4** elastomer stretched at 10 mm/min, 100 mm/min, and 500 mm/min. The sample could not extended to break at 10mm/min speed, since the length was beyond the test limit of the instrument. (b) Schematic behavior of ionic silicone elastomer under different stretching rate. (c) TGA curves of **G-COOH-14** oil, ionic crosslinked elastomer **G-COOH-14** + **G-NH$_x$-4**, COOH:NH$_x$=1:1 elastomer.

5.4.5 Viscoelastic Properties - Self-healing

Elastomers with dynamic crosslinks may be targeted to self-healing materials, even at lower temperatures.[30] Unlike permanent covalent crosslinks, self-healing materials are networks that exhibit time-dependent mechanical properties (e.g., viscoelasticity). The association and dissociation of the reversible crosslinks allows self-healing, as the flexible polymer chains self-diffuse to the exposed faces and reconnect.[31]

Both the **G-COOH-2** and **G-COOH-4** series exhibited spontaneous self-healing at room temperature. As shown in Figure 5.10, optical microscope pictures of a freshly cut ionic elastomer were examined at different time periods. The interface completely disappeared after 24 hours for soft materials (**G-COOH-2** and **G-COOH-4** series), whereas more than 7 days was required for the harder **G-COOH-14** series to heal (Figure S5.4).

With self-healing polymers, there is typically a trade-off between self-healing and mechanical properties.[32] Higher degrees of self-healing are typically easier to achieve with materials having low mechanical strength and where the polymer chains are mobile at the interface of the elastomer body. In such cases, appropriate functional groups that exhibit dynamic covalent bonding, hydrogen bonding, ionic boing, etc. can easily combine with each other as two bodies meet. The strong elastomer prepared from **G-COOH-14** + **G-NH$_x$-4** was self-healing. The process only occurred rapidly at higher temperatures because of increased chain mobility. After only 30 minutes of heating at 80 °C, the healed parts exhibited 20% recovery of elongation at break, 60% recovery of break strength, while after healing for 8 hours 100% of the elongation and strength properties had recovered (Table 5.4).

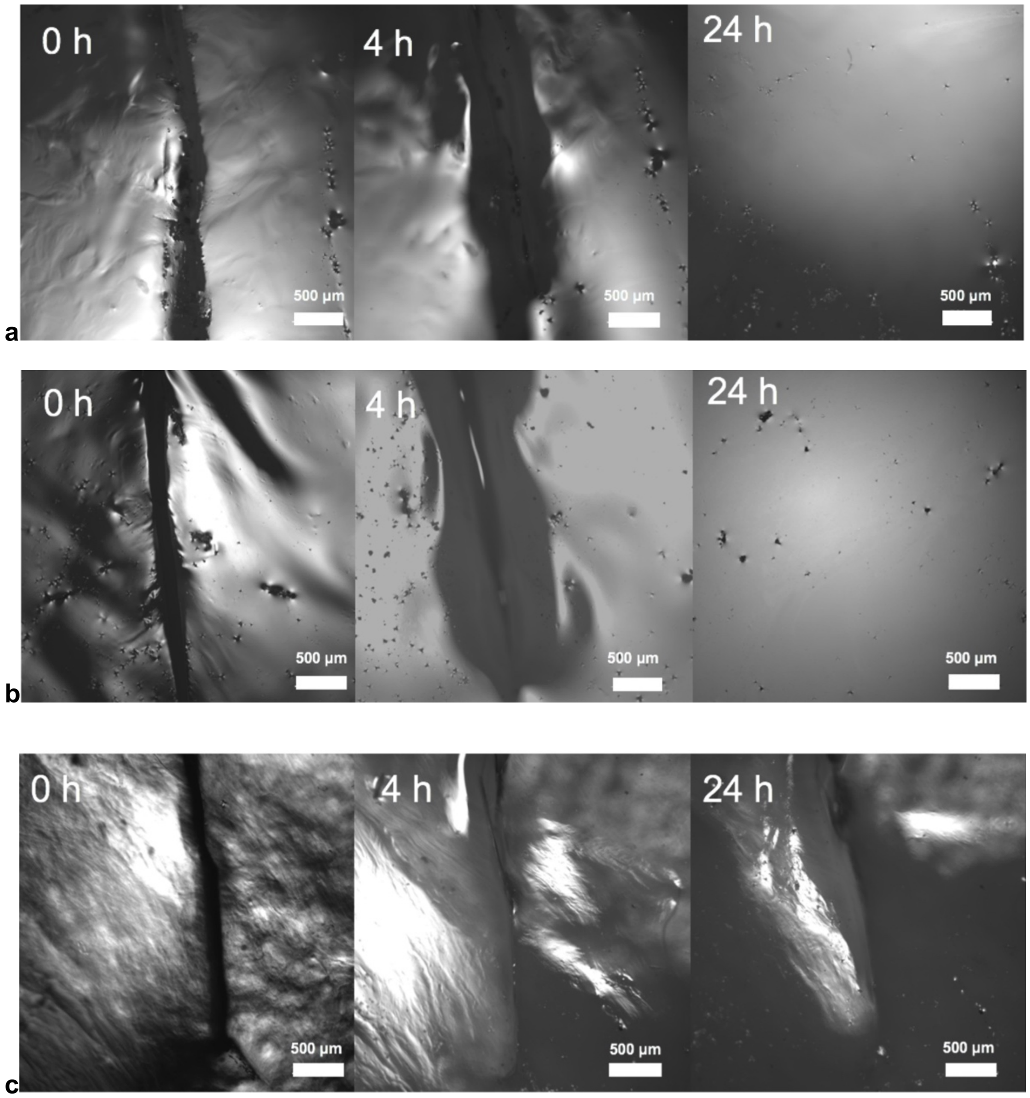

Figure 5.10 Optical microscopic images of a cut healed at room temperature. (a) **G-COOH-2** + **G-NH$_x$-4** (b) **G-COOH-4** + **G-NH$_x$-4** (c) **G-COOH-14** + **G-NH$_x$-4**.

Table 5.4 Self-healing ability of **G-COOH-14** + **G-NH$_x$-4** at 80 °C for various time periods.

Healing time (h)	Young's modulus (MPa)	Strength at break (MPa)	Strain at break (%)
Original	0.81 ± 0.01	0.31 ± 0.03	292 ± 56
0.5	0.79 ± 0.09	0.20 ± 0.01	59 ± 2
3	0.78 ± 0.10	0.37 ± 0.11	186 ± 47
8	0.55 ± 0.04	0.34 ± 0.01	314 ± 120

5.4.6 Viscoelastic Properties - Time Dependent Mechanical Properties

Elastomers cured with dynamic ionic crosslinks show the potential of having high Young's modulus as well as high stretchability because the "effective" crosslink density depends upon the experimental conditions. As noted by Leibler et al.,[33], a network of a dynamic crosslinked material shows time dependent properties (viscoelasticity). At times shorter than the lifetime of a crosslink, the networks behave as elastic rubbers, while at longer time scales, breaking only a few crosslinks allows the chain to diffuse and crosslinks to reform. The observed mechanical properties of the ionic crosslinked silicones depend on the speed of extension, due to the ability of the ionic linkages to 'hop' through the structure.[34] As shown in Figure 5.9, the elastomer shows very high extension (>1200%) when slow stretching speeds are used (10mm/min). A yield point near 30% strain was observed after the initial elastic region. After the yield point, the stress barely changes with the increasing strain (Figure 5.9a). These data are consistent with silicone chains that first untangle and stretch at the beginning of the tensile test. After that, the ionic linkages start to detach and then reform (Figure 5.9b). By contrast, at a stretching speed of 500 mm/min, the elastomer behaves more elastically, indicating the ionic linkage are acting as crosslink sites that cannot reform under the shorter timeframe.

The concept of making supramolecular silicone elastomers though "Salt-Forming Vulcanization" was first reported by Lu et al.[21] They showed the benefits of ionic linkages in a silicone environment. Their attempts to make silicone elastomers by direct mixing aminosilicones with acids only worked with an excess amount of strong acids (H_2SO_4, HNO_3) or solid organic acids (citric acid, oxalic acid) as crosslinkers and solid fillers. Handling strong acids during the material preparation can be problematic and residual acids in the product could be problematic, as they can lead to silicone depolymerization.[3] They noted in the presence of excess strong acid that the thermostability was also relatively low (<260 °C).

Skov avoided these problems, and exploited the benefits ionic linkages, by combining simple ammonium carboxylate crosslinkers within an interpenetrating network with covalently linked silicones, which led to elastomers with a some dynamism of properties and excellent mechanical strength.[19, 20]

Gemini ionic crosslinks are able to provide strong mechanical strength to elastomers and, by avoiding strong acids, remain thermally stable. The mechanical properties are readily tuned by a combination of net density of Gemini crosslinks and other monofunctional links. Viscoelastic properties provided by the Gemini linkage imbue the elastomer with excellent stretchability that, because of the nature of the ionic linkers, depends on the rate of extension. Due to the fact that no covalent network is involved, full thermal re-processability was easily achieved. The thermoplastic properties of these silicone elastomers provide a strategy to enhance silicone's sustainability.

5.5 Conclusions

Maleic acid was successfully grafted onto silicone backbones though a Michael addition pathway. Physical crosslinking between acidic (COOH) and basic (NH_x) silicones gave viscous oils or elastomers; the physical properties could be easily tuned by changing the ionic crosslink density. More importantly, the use of Gemini crosslinks provided enhanced mechanical strength compared to monofunctional ions, and led to polymers with competitive mechanical properties compared to their covalently crosslinked counterparts with lower crosslink densities. The materials have high extension at low rates of extension because of the ability of the crosslinks to 'hop.' The thermoplastic elastomers are also self-healing at room temperature for softer materials (**G-COOH-2 and G-COOH-4** series) or elevated temperature (80 °C) for more highly crosslinked materials (**G-COOH-14** series).

5.6 References

1. Goodyear, C., Improvement in India-Rubber Fabrics. *US Patent 3633* **1844**.
2. Filippidi, E.; Cristiani, T. R.; Eisenbach, C. D.; Waite, J. H.; Israelachvili, J. N.; Ahn, B. K.; Valentine, M. T., Toughening Elastomers Using Mussel-Inspired Iron-Catechol Complexes. *Science* **2017,** *358* (6362), 502.
3. Brook, M. A., Silicones. In *Silicon in Organic, Organometallic, and Polymer Chemistry*, Jhon Wiley & Sons, INC: 1999; pp 256-298.
4. Shit, S. C.; Shah, P., A Review on Silicone Rubber. *Natl. Acad. Sci. Lett.* **2013,** *36* (4), 355-365.
5. Nasresfahani, A.; Zelisko, P. M., Synthesis of a Self-healing Siloxane-based Elastomer Cross-linked via a Furan-modified Polyhedral Oligomeric Silsesquioxane: Investigation of a Thermally Reversible Silicon-based Cross-link. *Polym. Chem.* **2017,** *8* (19), 2942-2952.
6. Wittenberg, E.; Meyer, A.; Eggers, S.; Abetz, V., Hydrogen Bonding and Thermoplastic Elastomers - a Nice Couple with Temperature-Adjustable Mechanical Properties. *Soft Matter* **2018,** *14* (14), 2701-2711.
7. Prisacariu, C.; Scortanu, E.; Agapie, B., Effect of the Hydrogen Bonding on the Inelasticity of Thermoplastic Polyurethane Elastomers. *J. Ind. Eng. Chem.* **2013,** *19* (1), 113-119.
8. Park, S.-A.; Jeon, H.; Kim, H.; Shin, S.-H.; Choy, S.; Hwang, D. S.; Koo, J. M.; Jegal, J.; Hwang, S. Y.; Park, J.; Oh, D. X., Sustainable and Recyclable Super Engineering Thermoplastic from Biorenewable Monomer. *Nat. Commun.* **2019,** *10* (1), 2601.
9. Antony, P.; De, S. K., Ionic Thermoplastic Elastomers: A Review. *J. Macromol. Sci. C* **2001,** *41* (1-2), 41-77.
10. Rousseaux, D. D. J.; Drooghaag, X.; Sclavons, M.; Godard, P.; Carlier, V.; Marchand-Brynaert, J., Polypropylene Ionic Thermoplastic Elastomers: Synthesis and Properties. *Polym. Degrad. Stabil.* **2010,** *95* (3), 363-368.
11. Wang, W.; Zhang, J.; Jiang, F.; Wang, X.; Wang, Z., Reprocessable Supramolecular Thermoplastic BAB-Type Triblock Copolymer Elastomers with Enhanced Tensile Strength and Toughness via Metal-Ligand Coordination. *ACS App. Polym. Mater.* **2019,** *1* (3), 571-583.
12. Fawcett, A. S.; Brook, M. A., Thermoplastic Silicone Elastomers through Self-Association of Pendant Coumarin Groups. *Macromolecules* **2014,** *47* (5), 1656-1663.

13. Bui, R.; Brook, M. A., Dynamic Covalent Schiff-base Silicone Polymers and Elastomers. *Polymer* **2019,** *160*, 282-290.
14. Stricher, A. M.; Rinaldi, R. G.; Barrès, C.; Ganachaud, F.; Chazeau, L., How I Met Your Elastomers: from Network Topology to Mechanical Behaviours of Conventional Silicone Materials. *RSC Adv.* **2015,** *5* (66), 53713-53725.
15. Yilgör, E.; Yilgör, I., Silicone Containing Copolymers: Synthesis, Properties and Applications. *Prog. Polym. Sci.* **2014,** *39* (6), 1165-1195.
16. Liu, M.; Wang, Z.; Liu, P.; Wang, Z.; Yao, H.; Yao, X., Supramolecular Silicone Coating Capable of Strong Substrate Bonding, Readily Damage Healing, and Easy Oil Sliding. *Sci. Adv.* **2019,** *5* (11), eaaw5643.
17. Stukenbroeker, T.; Wang, W.; Winne, J. M.; Du Prez, F. E.; Nicolaÿ, R.; Leibler, L., Polydimethylsiloxane Quenchable Vitrimers. *Polym. Chem.* **2017,** *8* (43), 6590-6593.
18. Faiczak, K.; Brook, M. A.; Feinle, A., Energy-Dissipating Polymeric Silicone Surfactants. *Macromol. Rapid Comm.* **2020,** *n/a* (n/a), 2000161.
19. Madsen, F. B.; Yu, L.; Skov, A. L., Self-Healing, High-Permittivity Silicone Dielectric Elastomer. *ACS Macro Lett.* **2016,** *5* (11), 1196-1200.
20. Yu, L.; Madsen, F. B.; Hvilsted, S.; Skov, A. L., Dielectric Elastomers, with Very High Dielectric Permittivity, Based on Silicone and Ionic Interpenetrating Networks. *RSC Adv.* **2015,** *5* (61), 49739-49747.
21. Lu, H.; Feng, S., Supramolecular Silicone Elastomers with Healable and Hydrophobic Properties Crosslinked by "Salt-Forming Vulcanization". *J. Polym. Sci., Part A: Polym. Chem.* **2017,** *55* (5), 903-911.
22. Shi, J.; Zhao, N.; Yan, D.; Song, J.; Fu, W.; Li, Z., Design of a Mechanically Strong and Highly Stretchable Thermoplastic Silicone Elastomer based on Coulombic Interactions. *J. Mater. Chem. A* **2020,** *8* (12), 5943-5951.
23. Tung, C.-Y. M.; Dynes, P. J., Relationship between Viscoelastic Properties and Gelation in Thermosetting Systems. *J. Appl. Polym. Sci.* **1982,** *27* (2), 569-574.
24. Devatha P.Nair, M. P. S., Shunsuke Chatani,Tao Gong,Weixian Xi,Christopher R. Fenoli, and Christopher N. Bowman,, The Thiol-Michael Addition Click Reaction: A Powerful and Widely Used Tool in Materials Chemistry. *Chem. Mater.* **2014,** *26*, 724-744.
25. Mazurek, P.; Vudayagiri, S.; Skov, A. L., How to Tailor Fexible Silicone Elastomers with Mechanical Integrity: a Tutorial Review. *Chem. Soc. Rev.* **2019,** *48* (6), 1448-1464.

26. Hussain, S.; Pinitglang, S.; Bailey, T.; Reid, J.; Noble, M.; Resmini, M.; Thomas, E.; Greaves, R.; Verma, C.; Brocklehurst, K., Variation in the pH-dependent Pre-steady-state and Steady-state Kinetic Characteristics of Cysteine-proteinase Mechanism: Evidence for Electrostatic Modulation of Catalytic-site Function by the Neighbouring Carboxylate Anion. *Biochem. J.* **2003,** *372*, 735-46.

27. Zhao, F.; Bi, W.; Zhao, S., Influence of Crosslink Density on Mechanical Properties of Natural Rubber Vulcanizates. *J. Macromol. Sci.* **2011**, 1460-1469.

28. Bokobza, L., Elastomeric Composites. I. Silicone Composites. *J. Appl. Polym. Sci.* **2004,** *93* (5), 2095-2104.

29. Fatona, A.; Moran-Mirabal, J.; Brook, M. A., Controlling Silicone Networks using Dithioacetal Crosslinks. *Polym. Chem.* **2019,** *10* (2), 219-227.

30. Roy, N.; Bruchmann, B.; Lehn, J.-M., Dynamers: Dynamic Polymers as Self-healing Materials. *Chem. Soc. Rev.* **2015,** *44* (11), 3786-3807.

31. Yu, K.; Xin, A.; Wang, Q., Mechanics of Self-healing Polymer Networks Crosslinked by Dynamic Bonds. *J. Mech. Phys. Solids* **2018,** *121*, 409-431.

32. Hernández Santana, M.; Huete, M.; Lameda, P.; Araujo, J.; Verdejo, R.; López-Manchado, M. A., Design of a New Generation of Sustainable SBR Compounds with Good Trade-off between Mechanical Properties and Self-healing Ability. *Eur. Polym. J.* **2018,** *106*, 273-283.

33. Leibler, L.; Rubinstein, M.; Colby, R. H., Dynamics of Reversible Networks. *Macromolecules* **1991,** *24* (16), 4701-4707.

34. Miwa, Y.; Kurachi, J.; Kohbara, Y.; Kutsumizu, S., Dynamic Ionic Crosslinks Enable High Strength and Ultrastretchability in a Single Elastomer. *Commun. Chem.* **2018,** *1* (1), 5.

Supporting Information

Thermoplastic Silicone Elastomers Based on Gemini Ionic Crosslinks

Sijia Zheng, Yang Chen, Michael A. Brook*

McMaster University, Chemistry and Chemical Biology, 1280 Main Street West, Hamilton, ON, L8S 4M1, Canada

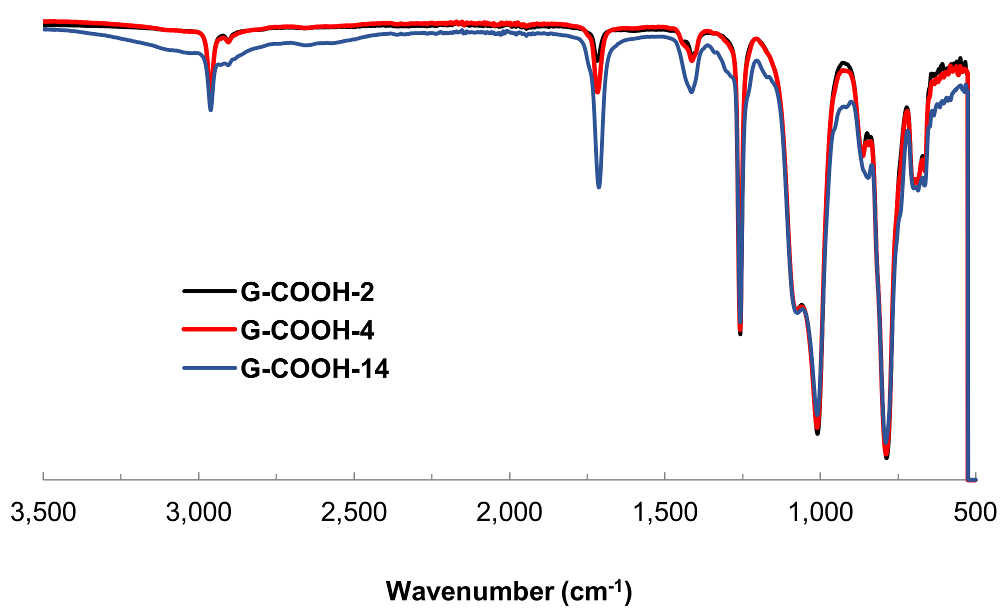

Figure S5.1 FT-IR spectra of **G-COOH-2** (black), **G-COOH-4** (rad), **G-COOH-14** (blue).

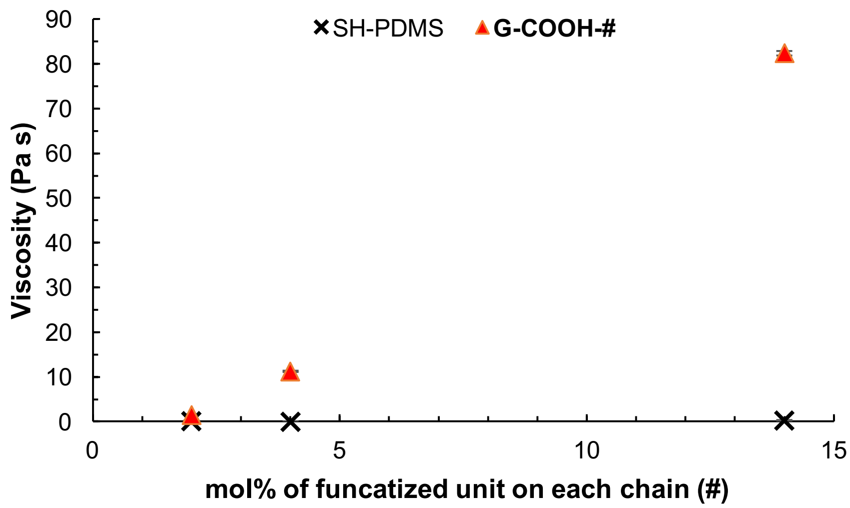

Figure S5.2 Viscosity of thioalkylsilicone oil with different thiol concentrations and maleic acid-modified silicone oil with different maleic acid graft densities.

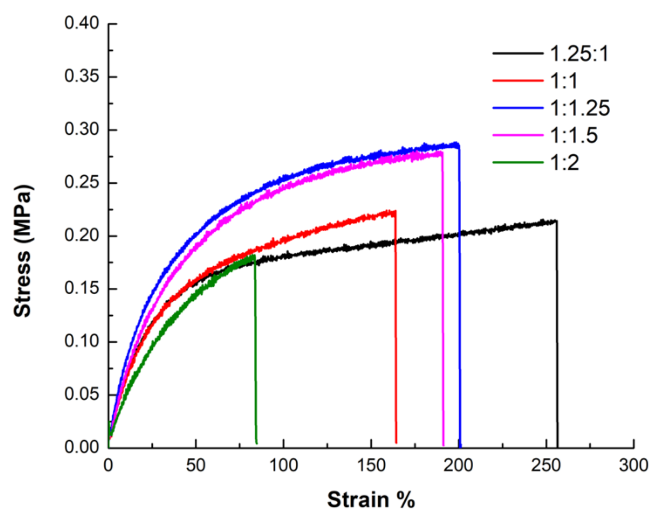

Figure S5.3 Tensile curves with different COOH/NH_x. **G-COOH-14** + **G-NH_x-4** series.

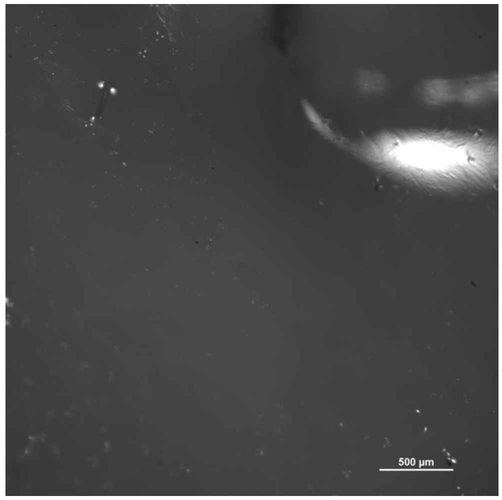

Figure S5.4 Optical microscopic images of a scratch on **G-COOH-14** + **G-NH$_x$-4** healed at room temperature for 7 days.

6 Chapter 6: General Conclusions

Silicone elastomers are important materials in industry due to their unparalleled properties when compared to their carbon-based analogues. Nowadays, those intrinsic properties are not enough. There is a requirement to develop new synthetic routes to create silicone elastomers with more interesting properties, particularly responsiveness to various triggers. This requires both unique linkages and the ability to address synthetic challenges to incorporate them for various applications. The focus of this thesis was the development of different ways to exploit sulfur chemistry in silicone elastomers. The abundance of sulfur reactions, their versatile reaction conditions, and unique linkage properties provide solutions for various kinds of research interests, as noted in the introduction.

In Chapter 2, a simple and versatile method for crosslinking silicone elastomers using the thiol-ene reaction was demonstrated. Thiopropylsilicones were reacted with vinyl terminated silicone oil with the initiation by UV light (Figure 6.1a). The ultrafast reaction rate built up the viscosity in short time (~2s) which allows their application in extrusion 3D printing processes. Various silicone structures with different hardnesses were successfully printed.

In Chapter 3, the oxidation of thiols was used to prepare silicone materials containing disulfide linkages. Based on different types of oxidant, thiopropyl-modified silicone oils were crosslinked into silicone elastomers or foams, respectively (Figure 6.1b). The overoxidation of thiol to sulfonate could be used to tune the hydrophilicity of the S-S linked silicone elastomer surface or control the hydrophilicity of the silicone backbone, leading to silicone foams with well distributed pores. In addition, we showed that S-S groups were able to undergo further oxidation with the presence of strong oxidants (Figure 6.1d). This strategy was used to tune the surface hydrophilicity of disulfide linked silicone elastomers. Furthermore, S-S bridges were found to be readily reduced back to thiols by hydrosilanes in the presence of $B(C_6F_5)_3$, which allows for the recycling of the starting oils (Figure 6.1c).

Chapter 3 demonstrated that redox reactions of disulfide bond can be used to make and then cleave silicone elastomers. In chapter 4, the reductive cleavage of disulfide bonds was extensively applied to breaking the disulfide and polysulfide linkages in synthetic rubber. Various kind of used rubber samples were successfully broken down by this method (Figure 6.1g). New elastomers could be generated by oxidizing the thiols (Figure 6.1h) or by peroxide-initiated radical polymerization

(Figure 6.1i). This method may become a powerful tool for rubber tire recycling, as the used rubber could go back to new high value products.

In Chapter 5, a novel dicarboxylic acid silicone structure was synthesized using maleic acid and thiopropylsilicones linked though a Michael addition pathway (Figure 6.1e); an ionic network was successfully created with this acid and a diamine-modified silicone (Figure 6.1f). The resulting silicones show thermoplastic properties, as well as self-healing at room temperature. The viscoelastic properties of silicones containing ionic linkages include high stretchability (~1200% strain).

Overall, sulfur reactions (thiol-ene radical reaction, thiol-Michael reaction, thiol oxidation, and disulfide reduction reactions) have proven to be a powerful tool box for silicone materials. Silicone elastomers with customized silicone structures or smart materials that can respond to redox or thermal stimuli has been demonstrated. Robust reaction conditions were used in all synthetic routes and no special requirements for N_2 protection or humidity were needed. While the method for reductive cleavage disulfide bond was first developed to creating redox responsive linkages, it was demonstrated that this could be extended further. Sulfur-crosslinked synthetic rubbers used in the automotive industry were successfully dissolved by the same method, which may have a huge impact on future tire recycling.

As one could expect, no synthetic method is perfect and there is still some restrictions to the current methods described above. Considering the importance of silicones and the extensive range of sulfur-crosslinked materials that are or can become available, it is definitely necessary to further explore the sulfur chemistry in silicone-related materials. This thesis provides an initial exploration for those who desire to work in this area. The possibilities of extending this research are promising and the benefits could be huge if the fundamental research can be applied to real industrial problems.

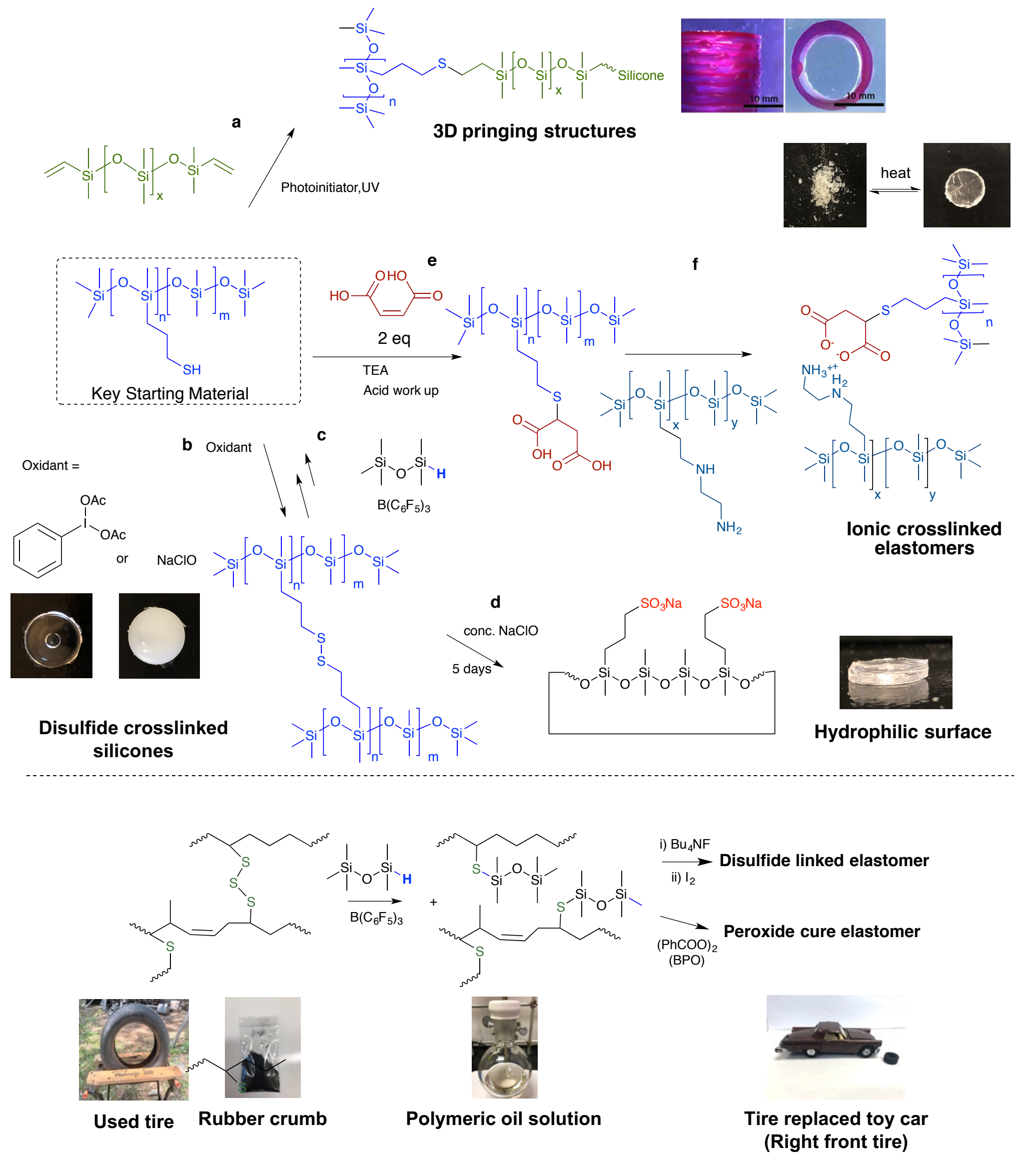

Figure 6.1 Thesis scope of using sulfur chemistry to make silicone materials.